Discrete supramolecular metal complexes: Synthesis, structures, host-guest chemistry with anions, and DNA binding properties

Anzhela Galstyan

Ph.D. Thesis submitted to the

Fakultät Chemie der Technischen Universität Dortmund, Germany

for obtaining the degree of a

Doktor der Naturwissenschaften (Dr. rer. nat.)

Ph.D. Advisor: Prof. Dr. Bernhard Lippert

Referee: Prof. Dr. Jens Müller

Submitted on: 25.11.2010

Disputation on: 17.12.2010

This work was carried out between September 2007 and Juni 2010 at the Lehrstuhl für Bioanorganische Chemie, Fachbereich Chemie, Universität Dortmund, Deutschland.

First of all I would like to express my sincere gratitude to my Ph. D. Supervisor

Prof. Dr. Bernhard Lippert

for his advice and guidance from the very early stage of this research,
as well as for giving me extraordinary experiences throughout the work.
I am also very thankful for providing me with the research facilities
and the financial support.

Acknowledgements

First and foremost, I would like to thank Prof. Dr. Jens Müller for kindly acting as referee.

During my work, I had to deal with a number of people who supported me in the most pleasing ways at various stages of my dissertation. It is my pleasure to convey my gratitude to all of them in my acknowledgment.

It has been my pleasure to work in a team with such a good atmosphere, and my sincere thanks go to all past and present members of the Lippert group, Dr. Pablo Sanz Miguel, Dr. Weizheng Shen, Sabine Siebel, Anupam Khutia, Philip von Grebe, Lu Yin, Dr. Francisca Alberti, Dr. Susana Ibáñez, Dr. Deepali Gupta, Dr. Lars Holland, Dr. Thea Welzel, Dr. Barbara Müller and Dr. Tushar van der Wijst, with whom I worked during my stay in Dortmund. Also, many thanks to Prof. Dr. Iris Oppel for helpful discussions and suggestions. Special thanks to Dr. Gabriele Trötscher-Kaus for her meticulous proof-reading of parts of my thesis and Sabine Siebel for correcting my German summary. I wish to thank Michaela Markert and Birgit Thormann for their assistance and help with administrative work.

I wish to express my heartfelt gratitude to Dr. Pablo Sanz Miguel for his contribution in the measurement and refinement of X-ray structures, without which, most of the results in this thesis would not have been possible. For determination of the X-ray structures I also thank Dr. Weizheng Shen and Prof. Dr. Eva Freisinger.

I would like to acknowledge Dr. W. Hiller, Christa Nettelbeck and Benjamin Kissel for the NMR measurements and Markus Hüffner for the determinations of elemental analyses. I wish to thank Torsten Grund and Dr. Pablo Sanz Miguel for their help with computer related problems and for keeping the computers running all the time.

It is a great pleasure to extend my thanks to Prof. Dr. Martin Engelhard, Prof. Dr. Roger S. Goody, Dr. Waltraud Hofmann-Goody, Christa Hornemann and Dr. Jutta Roetter from International Max Planck Research School Dortmund for assistance and financial support. COST action and Poniard Pharmaceuticals are also acknowledged for financial assistance.

I also wish to covey my deepest thanks to Jian Hou from Max-Plank Institute of Molecular Physiology for his guidance during DNA preparation.

I would like to express my gratitude to Prof. Dr. R. Winter for allowing me to use his laboratories, where I carried out the AFM experiments. I am especially thankful to Dr. Katrin Weise for teaching me so much about AFM and Simone Möbitz for her assistance with the measurements. I also would like to thank Dr. Weizheng Shen and Jacqueline Ksienczyk for introducing me to AFM technique from the very beginning.

I would like to thank my Bachelor students Lena Butt, Sarah Immohr, Jacqueline Wolf and Katrin Netzel for their contributions to this work and apprentice Lukas Schulte for preparation of some starting compounds.

Last but not least my love and thanks go to my mother and father for unwavering support and encouragement throughout my studies, to my sister Anna, who was always there to lift my spirits. I would especially like to thank my husband Artur. You have shared all my pains and frustrations; your love, complete understanding and belief in me are what kept me focused and driven. Finally, many thanks to my daugther Meline for her love and patience.

To my Family

Acknowledgements iii

Chapter 1 – General introduction 1

1.1 Metals in biological systems: inherent components and drugs 1

1.2 DNA and DNA binding molecules 3

1.2.1 Structure of DNA 3

1.2.2 Natural and synthetic DNA binding molecules 6

1.3 Basics of supramolecular chemistry 9

1.4 Aim of the thesis 13

Chapter 2 – Self-assembly of 2,2´-Bipyrazine-linked metallo-macrocycles 15

2.1 Background 15

2.2 Supramolecular isomerism with 2,2´-bpz and Pt(II): case of triangle - square equilibrium 18

2.2.1 Complexation of 2,2´-bpz to a Pt(II) center 18

2.2.2 Molecular square [{*cis*-Pt(NH_3)$_2$(*tttt*-bpz-*N4,N4´*)}$_4$](SO_4)$_4$ (II-1) 19

2.2.3 Molecular triangles 22

2.2.3.1 Crystal structure of BF_4⊂ *cis*-[{Pt(NH_3)$_2$(*ttt*-bpz-*N4,N4´*)}$_3$](BF_4)(SiF_6)$_2$ (II-2) 25

2.2.3.2 Crystal structure of (NO_3)(PF_6)⊂*cis*-[{Pt(NH_3)$_2$(*ccc*-bpz-*N4,N4´*)}$_3$](PF_6)$_4$ (II-3) 27

2.2.3.4 Crystal structure of NO_3⊂[{Pt(en)(*ccc*-bpz-*N4,N4´*)}$_3$](SO_4)$_2$(NO_3) (II-4) 29

2.2.4 Influence of counter anion and concentration on triangle-square equilibrium 31

2.2.5 Building block for molecular architechture: 2,2´-bpz as monotopic ligand 32

2.2.5.1 Crystal structure of *cis*-[Pt(NH_3)$_2$(bpz-*N4*)$_2$](NO_3)$_2$ (II-5) 34

2.2.5.2. Reactions of "corner stone" *cis*-[Pt(NH_3)$_2$(bpz)$_2$](NO_3)$_2$ (II-5) 35

2.3 Molecular Vases 38

2.3.1 Synthesis and spectroscopic characterization of [{(NH_3)$_2$Pt(*N4,N4'*-bpz-*N1,N1'*)Pd(en)}$_3$]$^{12+}$ with NO_3^- (II-6), SO_4^{2-} (II-7) and NO_3^--PF_6^- (II-8) as counter anions 38

2.3.2 Crystal structures of molecular vases 39

2.3.2.1 Crystal structure of {(NO_3)$_2$⊂[(NH_3)$_2$Pt(bpz)Pd(en)]$_3$}(NO_3)$_{10}$ (II-6) 40

2.3.2.2 Crystal structure of {SO_4⊂[(NH_3)$_2$Pt(bpz)Pd(en)]$_3$}(SO_4)$_5$ (II-7) 42

2.3.2.3 Preliminary crystal structure of {PF_6⊂[(NH_3)$_2$Pt(bpz)Pd(en)]$_3$}(PF_6)$_{10}$(NO_3) (II-8) ... 44

2.3.3 Building blocks for extended structures (towards deeper cavities) 45

2.3.3.1 Mononuclear chelates [Pd(2,2'-bpz)(*o*-pda)]$(NO_3)_2$ (II-9) and [Pd(*o*-pda)$_2$]$(NO_3)_2$ (II-10) 46
2.3.3.2 Mononuclear chelate [Pd(2,2'-bpz)(bipzp)]$(NO_3)_2$ (II-11) 49
2.3.3.2 Mononuclear chelate [Pd(2,2'-bpz)(dpk·H_2O)]$(NO_3)_2$ (II-12) 50
2.3.4 Coordination behavior of mononuclear complexes 53
2.3.4.1 Synthesis of a molecular vase {[$(NH_3)_2$Pt(bpz)Pd(*o*-pda)]$_3$}$(NO_3)_{12}$ (II-13) 53
2.3.4.2 Reactions of $[Pd(en)(bpz)]^{2+}$ with $AgNO_3$ and $AgPF_6$ 53
2.3.4.3 Crystal structure of discrete trinuclear [{Pd(en)(2,2´-bpz)}$_2$Ag]$(NO_3)_5$ (II-14) 55
2.3.4.4 Crystal structure of [Pd(en)(bpz)]$(PF_6)_2$ (II-15) 56
2.3.4.5 Reacting [Pd(2,2'-bpz)(bipzp)]$(NO_3)_2$ (II-11) with $AgNO_3$ and $CuSO_4$ 57
2.3.4.6 Crystal structure of *ht*-[Pd(bipzp)$_2$][Ag$(NO_3)_3(H_2O)$] (II-16) 57
2.3.4.6 Crystal structure of [Cu(2,2´-bpz)$(H_2O)_2SO_4$] (II-17) 59
2.4. Molecular architectures of Pt_3 triangle with Cu(II) 60
2.4.1 Crystal structure of molecular "paddle-wheel" {[(en)Pt(bpz)]$_6$ $Cu_4(H_2O)_6$}$(NO_3)_{20}$ (II-18) 60
2.4.2 Crystal structure of molecular capsule [(en)Pt(2,2´-bpz)Cu(NO_3) (H_2O)]$_3(NO_3)_6$·[Cu$(NO_3)_3(H_2O)$][Cu$(NO_3)_3(H_2O)_2$][Cu$(NO_3)_2(H_2O)_3$]1.5H_2O (II-19) .. 64
2.5. Coordination polymers: 1D chain and 2D network 68
2.5.1 Crystal strucure of {[$(enPt)_3(bpz)_3Cd_2(H_2O)_7$][Cd$(H_2O)_6$]$(SO_4)_6$}$_n$ (II-20) 68
2.5.2 Crystal structure of {[$(NH_3)_2$Pt(bpz)]$_3$Ag $(SiF_6)_3(BF_4)$}$_n$ (II-21) 71
2.5.3 Preliminary crystal structure of {[$(NH_3)_2$Pt(bpz)]$_3$Ag $(SO_4)_{3.5}$}$_n$ (II-22) 73
2.6 Conclusions 73
Chapter 3 – Complexes of Pt(II) and Pd(II) containing terminal and bridging cyanido ligands 75
3.1 Background 75
3.2 Towards molecular squares 76
3.2.1 Synthesis and NMR spectroscopic studies 76
3.2.2 IR spectra 80
3.2.3 X-ray crystal structures 81
3.2.3.1 Characterization of Pd(en)$(CN)_2$ (III-1) 81
3.2.3.2 Characterization of [$(en)_2$Pt][Pt$(CN)_4$] (III-2a) 83
3.2.3.3 Molecular squares [M(en)$(CN)]_4(NO_3)_4$ M = Pd^{II} (III-4) and Pt^{II} (III-5) 84
3.2.3.4 Crystal structure of the [Pd(en)(bpy)](SO_4) · 3H_2O (III-7) 86

3.3 Interactions with anions and nucleic acids 87
3.3.1 Interactions with anions 87
3.3.1.1. Characterization of $[Pt(en)(\mu\text{-}CN)]_4(C_8H_4O_4)_2 \cdot 10H_2O$ (III-5a) 88
3.3.2 Interactions with nucleic acid components 90
3.3.2.1. Characterization of *trans*-$[Pd(1\text{-}MeC\text{-}N3)(CN)I_2](1\text{-}MeC)(1\text{-}MeCH)\cdot 2H_2O$ (III-8) 91
3.4 Conclusions 92

Chapter 4 – Coordination of cyanopyridine to Pt(II) and Pd(II) centers and subsequent hydrolysis. Formation of novel hexanuclear square 93
4.1 Cyanopyridine ligands and their hydrolysis 93
4.2 Bis-(4-CNpy) and -(3-CNpy) complexes of Pt(II) and Pd(II) 95
4.2.1 Synthesis and NMR spectroscopic studies 95
4.2.2 IR spectra 97
4.2.3 X-ray crystal structures 97
4.2.3.1 Crystal structure of $[(en)Pt(4\text{-}CNpy)_2](NO_3)_2$ (IV-1) 98
4.2.3.2 Crystal structure of $[(en)Pt(3\text{-}C(O)NH_2py)_2](NO_3)_2$ (IV-2) 99
4.2.3.3 Crystal structure of $[(en)Pd(4\text{-}C(O)NH_2py)_2](SO_4)$ (IV-3) 100
4.2.3.2 Crystal structure of $[(en)Pd(3\text{-}C(O)NH_2py)_2](ClO_4)_2$ (IV-4) 102
4.3 Towards structures of higher complexity 104
4.3.1. Synthesis and characterization of $[\{(en)Pt\}_6(4\text{-}C(O)NHpy)_4(PF_6)](NO_3)_7$ (IV-5) 104
4.3.2. Characterization of $[(en)Pd(4\text{-}C(O)NH_2py)(NO_3)](NO_3)$ (IV-6) 107
4.4 Conclusions 109

Chapter 5 – Dependance of aqua ligand basicity from substituent (*L*) in complexes of type *trans*-$[Pt(NH_3)_2(L)(H_2O)]^{2+}$ 110
5.1 Background 110
5.2 Platin-triamine complexes 111
5.2.1 Preparation of complexes 113
5.2.2 X-ray crystal structures of *trans*-$[(NH_3)_2Pt(2\text{-}pic)Cl](NO_3)$ (V-1), *trans*-$[(NH_3)_2Pt(2\text{-}pic)_2](NO_3)_2$ (V-11) and *cis*-$[(NH_3)_2Pt(2\text{-}pic)Cl](NO_3)$ (V-12) 115
5.2.3 pK_a values of complexes obtained 117
5.2.4 Solvation of *trans*-$[(NH_3)_2Pt(2\text{-}pic)Cl](NO_3)$ (V-1) in DMF and DMSO 121
5.3 Complexes of *trans*-$[(NH_3)_2Pt(L)Cl](NO_3)$ containing S-donor ligands *L*. 123

5.3.1 Preparation of the complexes 124
5.3.2 Crystal structure of {*trans*-[PtCl(CH_3-*S*-CH_3)(NH_3)$_2$](NO_3)}$_2$ · *trans*-[$PtCl_2(NH_3)_2$] (V-13a) 124
5.3.3 pK_a values of the aqua complexes 125
5.4 Conclusions 126
Chapter 6 – Anion complexation by cyclic hosts 127
6.1 Background 127
6.2 Triangular $[\{a_2Pt\}_3(bpz)_3]^{6+}$ hosts 127
6.3 Anion binding by tetranuclear $[\{a_2Pt\}_4(bpz)_4]^{8+}$ host 132
6.4 Anion binding by $[\{a_2Pt\}_3\{a'_2Pd\}_3(bpz)_3]^{12+}$ hosts 133
6.5 Polycyclic architectures as anion hosts 139
6.6 Conclusions 141
Chapter 7 – Studies of metal complex-DNA interactions using AFM 142
7.1 Background 142
7.2 Studies on DNA-metal complex interactions 143
7.2.1 DNA imaging 143
7.3.3 Imaging of metallocomplex-DNA adducts 146
7.4 Conclusions 149
Chapter 8 – Experimental section 150
8.1 Instrumentation and methods 150
8.1.1 NMR spectroscopy 150
8.1.2 IR spectroscopy 150
8.1.3 Elemental analysis 150
8.1.4 X-Ray crystallography 150
8.1.5 DNA isolation 151
8.1.6 Atomic Force Microscopy (AFM) 152
8.1.7 pK_a value determination 152
8.1.8 Association constant determination for host-guest interactions 153
8.2 General work descriptions 154
8.2.1 Starting materials 154

8.2.2 Synthesis of compounds 155
8.2.2.1 Synthesis of [{*cis*-Pt(NH_3)$_2$(*tttt*-bpz-*N4,N4´*)}$_4$](SO_4)$_4$ (II-1) 155
8.2.2.2 Synthesis of BF_4⊂ *cis*-[{Pt(NH_3)$_2$(*ttt*-bpz-*N4,N4´*)}$_3$](BF_4)(SiF_6)$_2$ (II-2) 155
8.2.2.3 Synthesis of (NO_3)(PF_6)⊂*cis*-[{Pt(NH_3)$_2$(*ccc*-bpz-*N4,N4´*)}$_3$](PF_6)$_4$ (II-3) 155
8.2.2.4 Synthesis of NO_3⊂[{Pt(en)(*ccc*-bpz-*N4,N4´*)}$_3$](SO_4)$_2$(NO_3) (II-4) 155
8.2.2.5 Synthesis of *cis*-[Pt(NH_3)$_2$(bpz-*N4*)$_2$](NO_3)$_2$ (II-5) 156
8.2.2.6 Synthesis of [{(NH_3)$_2$Pt(*N4,N4'*-bpz-*N1,N1'*)Pd(en)}$_3$](NO_3)$_{12}$ (II-6) and [{(NH_3)$_2$Pt(*N4,N4'*-bpz-*N1,N1'*)Pd(en)}$_3$](SO_4)$_6$ (II-7) 156
8.2.2.7 Synthesis of [{(NH_3)$_2$Pt(*N4,N4'*-bpz-*N1,N1'*)Pd(en)}$_3$](NO_3)(PF_6)$_{11}$ (II-8) 157
8.2.2.8 Synthesis of [Pd(2,2'-bpz)(*o*-pda)](NO_3)$_2$ (II-9) 157
8.2.2.9 Synthesis of [Pd(*o*-pda)$_2$](NO_3)$_2$ (II-10) 158
8.2.2.10 Synthesis of [Pd(2,2'-bpz)(bipzp)](NO_3)$_2$ (II-11) 158
8.2.2.11 Synthesis of [Pd(2,2'-bpz)(dpk·H_2O)](NO_3)$_2$ (II-12) 158
8.2.2.12 Synthesis of {[(NH_3)$_2$Pt(bpz)Pd(*o*-pda)]$_3$}(NO_3)$_{12}$ (II-13) 159
8.2.2.13 Synthesis of [{Pd(en)(2,2´-bpz)}$_2$Ag](NO_3)$_5$ (II-14) 159
8.2.2.14 Synthesis of [Pd(en)(2,2´-bpz)](PF_6)$_2$ (II-15) 160
8.2.2.15 Synthesis of {[Pd(en)(2,2´-bpz) Ag](PF_6)$_3$}$_n$ (II-15a) 160
8.2.2.16 Synthesis of *ht*-[Pd(bipzp)$_2$][Ag(NO_3)$_3$(H_2O)] (II-16) 160
8.2.2.17 Synthesis of [Cu(2,2´-bpz)(H_2O)$_2$$SO_4$] (II-17) 160
8.2.2.18 Synthesis of {[enPt(bpz)]$_6$$Cu_4$($H_2O$)$_6$}($NO_3$)$_{20}$ (II-18) and [(en)Pt(2,2´-bpz)Cu(NO_3)(H_2O)]$_3$(NO_3)$_6$·[Cu(NO_3)$_3$(H_2O)]·[Cu(NO_3)$_3$(H_2O)$_2$]· [Cu(NO_3)$_2$(H_2O)$_3$]·1.5H_2O (II-19) 161
8.2.2.19 Synthesis of {[(enPt)$_3$(bpz)$_3$$Cd_2$($H_2O$)$_7$][Cd($H_2O$)$_6$]($SO_4$)$_6$}$_n$ (II-20) 161
8.2.2.20 Synthesis of {[(NH_3)$_2$Pt(bpz)]$_3$Ag (SiF_6)$_3$(BF_4)}$_n$ (II-21) 161
8.2.2.21 Synthesis of {[(NH_3)$_2$Pt(bpz)]$_3$Ag (SO_4)$_{3.5}$}$_n$ (II-22) 161
8.2.2.22 Synthesis of Pd(en)(CN)$_2$ (III-1) 162
8.2.2.23 Synthesis of Pt(en)(CN)$_2$ (III-2) and [Pt(en)$_2$][Pt(CN)$_4$] (III-2a) 162
8.2.2.24 Synthesis of *trans*-Pt(ma)$_2$(CN)$_2$ (III-3) 162
8.2.2.25 Synthesis of [Pd(en)(CN)]$_4$(NO_3)$_4$ (III-4) 163
8.2.2.26 Synthesis of [Pt(en)(CN)]$_4$(NO_3)$_4$ (III-5) 163
8.2.2.27 Synthesis of [Pt(en)(CN)]$_4$($C_8H_4O_4$)$_2$ · 10H_2O (III-5a) 163
8.2.2.28 Synthesis of [Pd_4(bpy)$_2$(en)$_2$(CN)$_4$](NO_3)$_4$ · H_2O (III-6) 163
8.2.2.29 Synthesis of [Pd(bpy)(en)](SO_4)·3H_2O (III-7) 164
8.2.2.30 Synthesis of *trans*-[Pd(1-MeC-*N*3)(CN)I_2][(1-MeC)(1-MeCH)] · 2H_2O (III-8) 164
8.2.2.31 Synthesis of [(en)Pt(4-CNpy)$_2$](NO_3)$_2$ (IV-1) 164
8.2.2.32 Synthesis of [(en)Pt(3-C(O)NH_2py)$_2$](NO_3)$_2$ (IV-2) 165

8.2.2.33 Synthesis of [(en)Pd(4-C(O)NH_2py)$_2$](SO_4) (IV-3) 165
8.2.2.34 Synthesis of [(en)Pd(3-C(O)NH_2py)$_2$](ClO_4)$_2$ (IV-4) 165
8.2.2.35 Synthesis of [{(en)Pt}$_6$(4-C(O)NH_2py)$_4$(PF_6)](NO_3)$_7$ (IV-5) 166
8.2.2.36 Synthesis of [(en)Pd(4-C(O)NH_2py)(NO_3)](NO_3) (IV-6) 166
8.2.2.37 Synthesis of *trans*-[(NH_3)$_2$Pt(2-pic)Cl](NO_3) (V-1) 166
8.2.2.38 Synthesis of *trans*-[(NH_3)$_2$Pt(py)Cl]Cl (V-3) 167
8.2.2.39 Synthesis of *trans*-[(NH_3)$_2$Pt(4-Clpy)Cl]Cl (V-4) 167
8.2.2.40 Synthesis of *trans*-[(NH_3)$_2$Pt(2-Clpy)Cl]Cl (V-6) 167
8.2.2.41 Synthesis of *trans*-[(NH_3)$_2$Pt(3,5-DiMeAn)Cl]NO_3 (V-9) 167
8.2.2.42 Synthesis of *trans*-[(NH_3)$_2$Pt(2-pic)$_2$](NO_3)$_2$ (V-10) 168
8.2.2.43 Synthesis of *cis*-[(NH_3)$_2$Pt(2-pic)Cl]Cl (V-11) 168
8.2.2.44 ^{1}H NMR chemical shifts of *trans*-[(NH_3)$_2$Pt(L)Cl]$^+$complexes not isolated in pure form: 168
8.2.2.45 Synthesis of *trans*-[(NH_3)$_2$Pt(Me_2SO)Cl](NO_3) (V-12) 169
8.2.2.46 Synthesis of *trans*-[(NH_3)$_2$Pt(Me_2S)Cl](NO_3) (V-13) 169

Appendix I – List of compounds isolated or studied in solution 170

Appendix II – Abbreviations 172

Summary 174

Zusammenfasung 180

References 186

Chapter 1 – General introduction

1.1 Metals in biological systems: inherent components and drugs

Bioinorganic chemistry, which initially focused on exploring the function of metals in biological systems, has developed to a widespread and still growing field of chemistry, which finds applications in the medical, pharmaceutical, agricultural, biotechnological and environmental industries. Only through a thorough understanding of the structural and functional roles of metals in biological processes will the design and application of metal containing compounds be possible. In the past decades it has become evident that metals play diverse roles. Some metals occur naturally in the biological systems and are significant for the biological activity (Table 1.1), others have been used to probe and explore biological functions or to treat a variety of diseases. For all of them reactivity depends on features such as concentration, oxidation state, chemical speciation *etc.*

Table 1.1 Role of transition and main group metals in biological systems.

Metal	Function
Main group	Alkaline - *charge neutralization, structure stabilization, osmotic balance* Alkaline earth - *structure regulation, enzyme activation, messengers*
Transition	*electron transfer, redox catalysis, oxygen transport*

Most abundant monovalent ions (K^+, Na^+) initially were considered not to have a significant role but mainly to serve to neutralize anionic phosphates of nucleic acids. However, later studies predicted that these monovalent cations have an influence on DNA structure, such as AT-tract bending and changes in the minor-groove width[1] or stabilization of G-quartet structures.[2] Irregular coordination geometries of these metals makes it often difficult to identify them in crystal structures of nucleic acids. The hybrid – solvent model proposed by Williams and coworkers,[3] based on the elegant model of Manning, explains this phenomenon. In this model, a concentrated cloud of mobile and hydrated monovalent cations distributes around DNA, and solvent sites that were previously considered as pure water, are in fact partially occupied by alkali metal ions. Generally, divalent cations have a greater

tendency to polarize and orientent water molecules. In contrast, the Mg^{2+} ion can be readily identified by its characteristic octahedral geometry. The behaviour of Ca^{2+} ions is similar to Mg^{2+}, although the solvation shell is less well defined. Whereas Ca^{2+} takes part in muscle construction, signal transduction pathway, blood coagulation and is the material of bones and teeth are composed of, the role of Mg is mainly associated with the stabilization and activation of enzymes and energy transfer (hydrolysis of ATP to ADP).[4]

Living organisms store and transport transition metals because they are inherent components of metalloproteins and cofactors.[5] Among the transition metals, iron, zinc, copper and cobalt are the most abundant elements in the organism. Iron participates in processes like oxygen transport, energy production, nitrogen reduction *etc.* The role of zinc is both structural and catalytic, although much of the zinc has no known function. Well known is that zinc is present in nucleic acid binding proteins, where the number of zinc atoms could reach eleven.[6] Cobalt is an essential trace element and his biochemical impact is related to Vitamin B_{12} and similar co-enzymes. Currently a large number of copper containing proteins have been isolated. In some instances copper participates in reactions which are characteristic of iron, *e. g.* reversible binding of dioxygen by haemoglobin (Fe) and hemocyanine (Cu). Concentrations of nearly all metals are extremely regulated and deficiency or overload of metals in the body leads to disfunction, disease, or death of the organism.

Metallodrugs containing essential as well as non-essential and even toxic metals have been used as pharmaceutics for a long time. For instance, gold salts have been used to treat arthritis,[7] lithium salt as mood stabilizing agents[8] and an arsenic compound was for many years the standard treatment for syphilis. Without any doubt the leading metal containing drug is cisplatin, discovered by Rosenberg in 1960s.[9] This discovery initiated renewed interest in platinum research and considerable effort is being devoted to the development of "second and third generation" Pt-based drugs. Since then thousands of analogues have been proposed and tested. Among these, carboplatin, oxaliplatin, nedaplatin and lobaplatin were found to be the most successful, with fewer toxic side effects and/or activity against a broader rage of types of cancer. In recent years, non-platinum compounds were also found to show anticancer activity.[10] Among them ruthenium (II)-arene complexes were proposed to have another mode of action than cisplatin[11] and could be effective alternatives. Metal-based agents also found an application in imaging of different organs and studies of their function. For instance, technetium-99m and other short-living isotopes are used as radiopharmaceuticals in disease

diagnosis as well as treatment. In magnetic resonance imaging (MRI) gadolinium compounds are usually used as contrast agents.

Numerous examples of metal complexes, which are already in clinical use and cover a broad range of application, motivate further studies for new metallodrugs. They could be useful as metal-mediated antibiotics, antibacterial, antiviral, antiparasitic agents and anticancer compounds.

1.2 DNA and DNA binding molecules

1.2.1 Structure of DNA

DNA is the most important biopolymer. Its biological role is the capability to hold information needed for life and evolution. These messages are held in distinct regions of DNA called genes, and are the basis for the synthesis of proteins, which occurs in a complex process where *m*-RNA, *t*-RNA and ribosomes are also involved.

The main building blocks of DNA are only four – the nucleosides deoxyadenosine, deoxyguanosine, deoxycytidine, and deoxythymidine. Purine or pyrimidine bases, sugar and phosphate groups produce nucleotides. The deoxyribose sugars are joined at both the 3'-hydroxyl and 5'-hydroxyl groups to phosphate groups, thus making "phosphodiester" bonds, connecting subunits and resulting in the formation of the polymeric DNA backbone. Two DNA strands form a helical spiral, where hydrogen bonding between two complementary bases forces the DNA backbone to twist. π–π stacking of aromatic bases (3.4 Å) gives additional stability to the double helix (Figure 1.1).

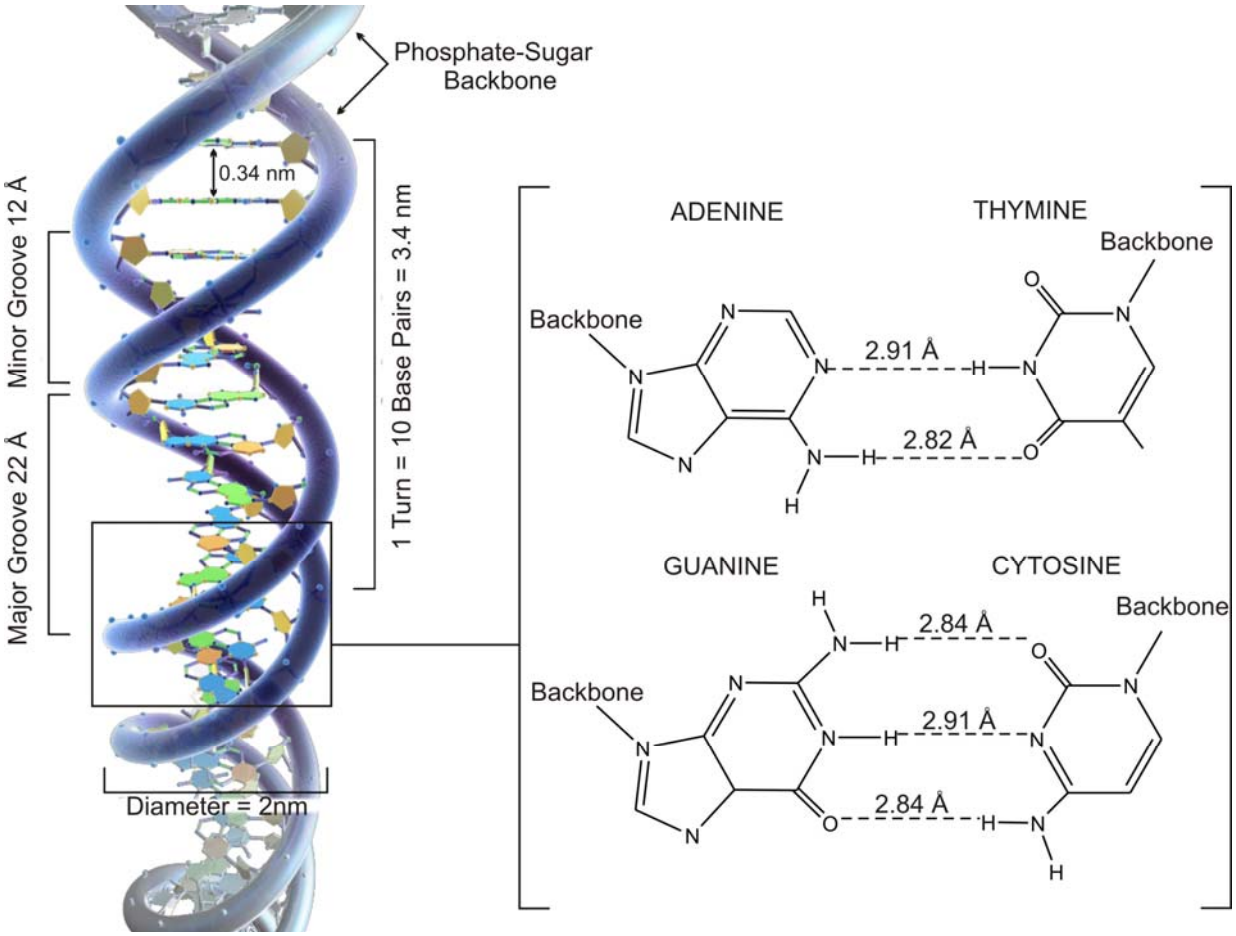

Figure 1.1 Helical shape of DNA with structural details[i]

Watson and Crick first suggested this helical structure of DNA in 1953.[12] Prior to its discovery, a number of initial and key studies have already been done in this field. Many scientists made significant contribution in this historic breakthrough. In 1865, Gregor Mendel, based on his genetic descriptions of pea plants, proposed that "factors" (later called genes) were responsible for inheritance. Shortly afterwards, in 1868, the Swiss doctor Friedrich Miescher, when trying to find out the chemical composition of leucocytes, noticed a precipitate of an unknown substance and isolated this white, slightly acidic chemical "nuclein". However, the structure of nucleic acids became known only by the late 1940s. Because of their diversity for a long time proteins were thought to be the carriers of genetic information. In 1944, Oswald Avery proved that DNA was the hereditary substance. By comparing DNA of different species, in 1949 Erwin Chargaff reported that the proportion of each base varies from one species to another, but the amount of adenine is always equal to the amount of thymine and the amount of guanine is always equal to the amount of cytosine. This

[i] Part of the picture was taken from www.wikipedia.org

biochemical evidence for the nucleotide base-pairing is known as Chargaff's rule.[13] Probably the most essential role regarding the discovery of the structure of the "molecule of life" belongs to Rosalind Franklin. Together with Maurice Wilkins, she obtained good crystallographic data showing that DNA has a double-helical shape.

Besides the classical double helical structure of B-DNA, secondary DNA structures are believed to be significant in diverse biological processes.[14] Changes in environmental conditions, protein binding and superhelical tension are possible reasons for the formation of alternative DNA structures. Transition to shorter and more compact, but still right-handed A-DNA has been found in complexes of DNA with certain proteins[15] and enzymes.[16] Moreover, low water content, the presence of organic solvents or high salt concentrations can promote the formation of this alternative structure. The presence of mono- and polyvalent cations contributes to the formation of elongated, left-handed Z-DNA. However, the main driving force for Z-DNA formation is DNA supercoiling.

Bases of DNA have still hydrogen bond donor and acceptor groups available, which could be involved in base triad formation. In the triplex structures recognition of the third strand occurs through the major groove by formation of Hoogsteen or reversed Hoogsteen-type hydrogen bonds. Alternative DNA structures like three-way and four-way junctions are important in DNA recombination, repair and cell development. The structure of four-way junction was proposed by R. Holliday in 1964 as a structural model, by which genetic information could be exchanged, subsequently named after him. In the last few years its structure has been confirmed by X–ray crystallography (Figure 1.2).[17]

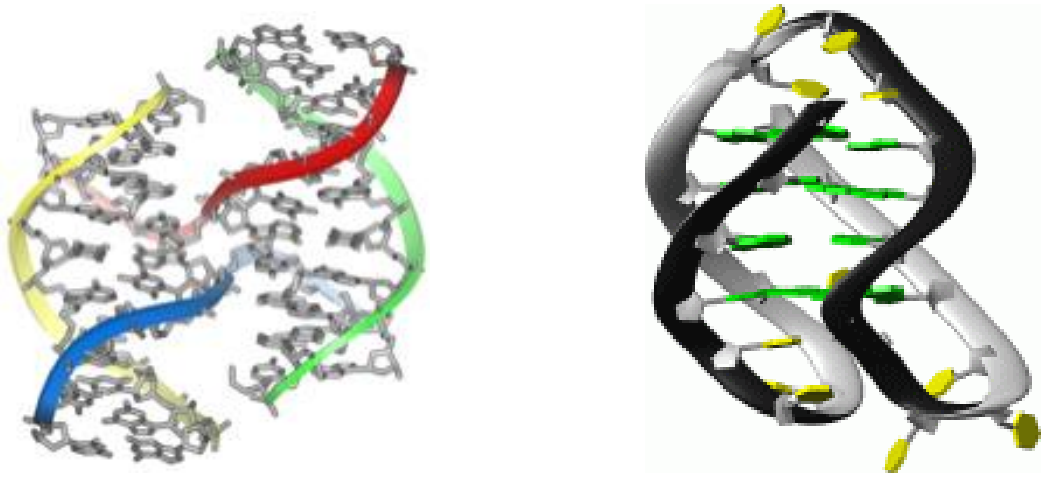

(a) (b)

Figure 1.2 Structures of Holliday junction[18] (a) and one of several possible G-quadruplex stuctures[19] (b).

Spectroscopic and X-ray diffraction studies showed that G-rich sequences of repetitive non-coding DNA in the ends of linear chromosomes form four-stranded structures stabilized by hydrogen bonded G-quartets and K^+ ions. These "strands of the time" play an important role since the length of the telomere serves as a biological clock: after each cell division the telomere shortens, finally leading to cell death. Telomerase is an enzyme that adds telomere to the end of the chromosome and it is expressed in ~80 – 90% of all cancers analyzed. Consequently, much attention has recently been focused on the stabilization of quadruplex structures and the inhibition of telomerase activity. A similar DNA structures could also occur in certain regions of continuous DNA sequences, for example in gene promoter regions.

1.2.2 Natural and synthetic DNA binding molecules

Interactions of DNA with natural molecules can be either independent of the base sequence or highly sequence-dependent. An example of non-precise DNA-protein interaction is DNA binding to histones, which results in the compact packing of DNA in the cell nucleus.[20] On the other hand, in the biological systems specific regulatory proteins, such as transcription factors are able to bind selectively to the promoter regions of DNA and are responsible for transcriptional activation of genes in a cell-cycle and controlled gene expression (central dogma in molecular biology). Another example of specific binding is the interaction of DNA with restriction enzymes and telomerase that modify DNA at specific sites. DNA-binding proteins contain, among others, domains like Zn finger, leucine zipper, helix-turn-helix motifs *etc.* and often bind to the major groove of DNA, due to the larger size and more hydrogen bonding possibilities.

Synthetic DNA binding molecules, especially those with high affinity and sequence specificity could serve as probes to understand the notable diversity of functions of the DNA double helix or serve as drugs to treat diseases more specifically, since action of the drug at the DNA level is expected to be more efficient than at the protein level. These drugs are able to break off replication and/or transcription processes and in doing so, influence delivery of genetic information or biological processes such as recombination or repair. Information obtained from the *Human Genome Project* will open new possibilities for individual treatment, where genomics and pharmacology together could make their contribution to the development of new specific DNA binding pharmaceuticals.

DNA binding molecules can be divided into two groups: those which form covalent bonds and those which interact non-covalently (Figure 1.3).

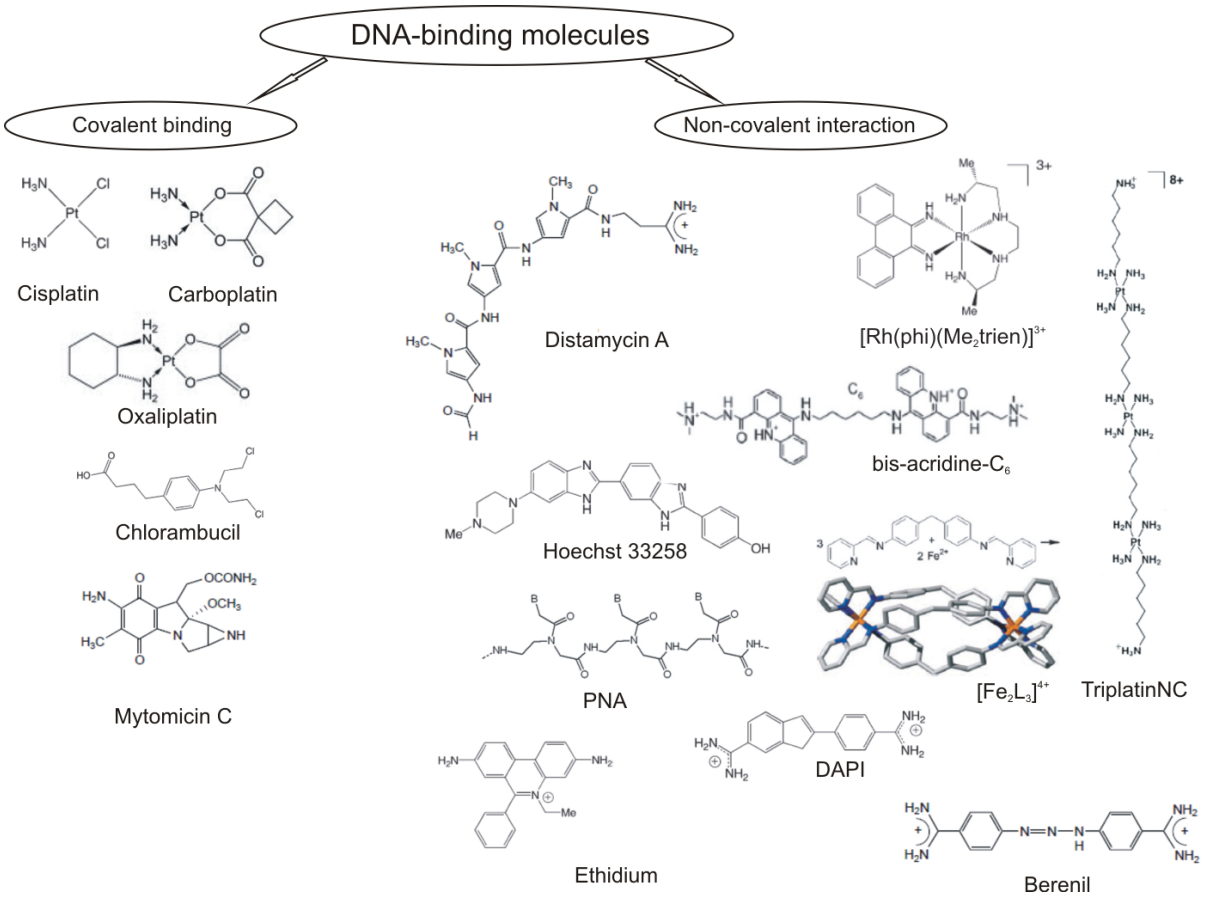

Figure 1.3 Chemical structures of some DNA binding molecules.

Alkylating agents derived from aniline mustard[21] (chlorambucil, mitomycin C) or cisplatin[22] and its analogues have antitumor properties, due to their ability to form covalent interstrand cross-links in cellular DNA. Covalent binding is not reversible and kinks introduced in DNA lead to apoptosis.

Non-covalent DNA binding can be classified as binding to the sugar-phosphate backbone, groove binding and intercalation. Substituting labile chlorides of reactive Pt(II) compounds with inert ammine or amine ligands prevents Pt-DNA adduct formation. As has been recently shown by Farrell and Williams,[23] the trinuclear platinum(II) compound TriplatinNC: $[\{trans\text{-}Pt(NH_3)_2\,(NH_2(CH_2)_6(NH_3^+)\}_2\text{-}\mu\text{-}\{trans\text{-}Pt(NH_3)_2\text{-}(NH_2(CH_2)_6NH_2)_2\}]^{8+}$ shows selectivity for phosphate oxygens, forming "Phosphate Clamps" through amine-phosphate-ammine hydrogen bonds.

Driving forces for groove binding are hydrogen bonding, electrostatic and van der Waals interactions. Most DNA-binding drugs, synthetic or natural and being small in size, are known to bind to the minor groove of the duplex DNA, with notable preference for AT-rich regions. The design ideas of artificial groove binding molecules are gained from examination of natural binding molecules like Distamycin A. Other well known DNA minor groove binders 4,6-diamidine-2-phenylindole (DAPI), berenil, netropsin, Hoechst 33258 and many others find wide applications in medicine. All these molecules have similar structural properties: they contain more than one aromatic ring and usually have a positive charge at the ends of the molecule.

Recognition of the major groove is mainly achieved by oligonucleotides or PNAs which are able to form a triple helix with the targeted ds-DNA sequence (antigene strategy). However, in the same manner they are also capable to target single-stranded messenger RNA (antisense strategy).[24] As has been shown by M. Hannon and co-workers, a metallosupramolecular cylinder obtained from three imine-based ligands and two Fe^{2+} ions binds to the major groove of ds-DNA and induces intra-molecular coiling.[25]

It is well established that a variety of small molecules with a flat shape containing aromatic moieties have the possibility to intercalate between the base pairs, inducing strong structural perturbations. Additional to other non-covalent interactions, π-π stacking between drugs and two adjacent base pairs of the DNA double helix stabilizes this binding mode, first proposed by Lerman in 1961.[26] Well known DNA intercalators are ethidium bromide, proflavine, doxorubicin, acridine orange *etc*. Metal complexes which are planar (d^8 square-planar geometry) or contain extended aromatic ligands as fragments of the molecule (d^6 octahedral geometry), are also able to intercalate. Several platinum complexes containing bipyridine, terpyridine or phenanthroline moieties were found to show antitumor activity due to their ability to intercalate.[27] Barton *et al* have studied the interaction of the metallo-intercalator Δ-α-$[Rh\{(R,R)\text{-}Me_2trien\}(phi)]^{3+}$ with DNA.[28] As the crystal structure shows the complex is selectively bound to the major groove of the sequence 5′-TGCA-3′. Combination of molecules with different binding affinities, *e. g.* intercalators with minor-grove binders or covalent binders, seems to be promising for the development of drugs or as tools in molecular biology.

The discovery of novel types of DNA motifs provides additional specific targets for drug binding and is a possibility to influence precise biological function.[29] Small molecules have been described that target higher order DNA structures such as G quadruplexes[30] and,

more recently, three-way and four-way junctions. Many classical DNA-intercalators are also able to stabilize G_4 structures by end-stacking. However, also non-planar molecules are able to bind to the telomere sequences. For instance, being known as a minor groove-binder, Distamycin A has also been shown to interact with two opposite sides of quadruplex DNA structures in a 4:1 ratio.[31] Another interesting example is the interaction of a chiral supramolecular complex with a G-quadruplex DNA.[32] As these authors show, the P enantiomer of the complex is able to convert an antiparallel G_4 structure into a hybrid one. Crystallographic studies show that a $[Fe_2L_3]^{4+}$ triple helicate binds to the central cavity of a three way junction.[33] Recognition of a Holliday junction has been achieved with the six-carbon-linked bis-acridine derivative.[34]

1.3 Basics of supramolecular chemistry

Supramolecular chemistry has been recognized as research area only after chemists began to consider the role that non-covalent bonds can play. The main feature of supramolecular chemistry is organisation of complex, well-defined structures from small molecules via a self–assembly process.[35] Non-covalent interactions involved in these processes make *supermolecules* from molecules, which have significantly different chemical and physical properties.[36] The strength of non-covalent forces range from 5 – 350 kJ mol^{-1} (Figure 1.4).

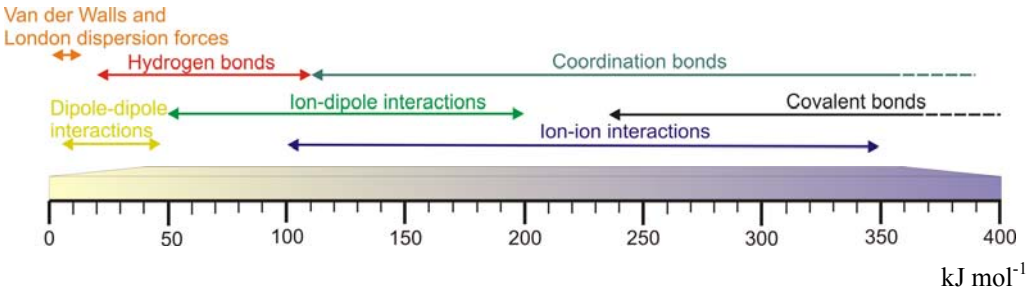

Figure 1.4 Range of non-covalent intermolecular interactions involved in the formation of supramolecular architectures.

Careful observation of living organisms shows that biological systems consist of supramolecular structures. Emil Fischer's "lock and key" description of interactions between biological entities[37] shows nicely how complementary subunits join together by weak forces,

generating stable systems. Self-assembly processes of various kinds of molecules leading to formation of complex biological structures (lipid bilayers, viral capsids, the DNA double helix, and the tertiary and quaternary structure of proteins*)*, as well as self-repairing and self-controlling are common in biological systems.

The term supramolecular chemistry has significantly broadened over time and now unites different scientific disciplines, such as inorganic, organic and physical chemistry, material science, biology, medicine *etc*. This discipline provides an opportunity to create organized systems that are interesting for a variety of applications, such as phase transfer, drug design and delivery, separation of mixtures, molecular sensors, switches and molecular machinery, as well as catalysts. A huge number of compounds, obtained by supramolecular chemists and a large amount of chemical knowledge have gathered during the last 50 years.

To obtain entities of higher complexity than molecules themselves by the self-assembly process, two main criteria should be met: (i) Molecules should contain complementary functionalities – appropriate geometrical and electronic structure and (ii) necessary reaction conditions should be provided. The reversibility of non-covalent bonds allows the system to equilibrate, thereby generating single or diverse products. The latter occurs in systems where the obtained products are close in energy of formation and none of the structures is thermodynamically favored. Rates of the dynamic exchange processes depend on many factors, such as

- metal center (if coordination bonds are used for construction)
- flexibility of the ligand
- presence of template molecules
- concentration
- temperature of reaction medium
- solvent polarity, *etc.*

Each of these factors affects the outcome and can be used to control the reaction. The most frequently used strategy for goal-seeking synthesis is the directional-bonding approach, which makes possible the construction of discrete molecular species in nanoscale and in many cases gives the possibility to predict size and shape of the molecules.[38] This is particularly true, when hydrogen bonding or metal coordination is used in the self-assembly process, not only because the bonds are relatively strong, but also because they have directionality, which is helpful for the rational design. The number of possible combinations can be reduced by

applying pre-organized building blocks, where the coordination sphere of metal ion is well-defined and multidentate ligands have fewer binding modes. Another popular strategy is the use of a template molecule, forcing the units to get aggregated in a uniform way.[39] In multicomponent systems reversible reactions enable exchange between building blocks. These reorganisation processes provoke formation of *dynamic combinatorial libraries* (DCL),[40] where the amounts of the individual species depend on their thermodynamic stabilities.

Supramolecular isomers, can be classified as follows: structural, conformational, catenane and optical.[41] Competition between thermodynamic and kinetic factors can explain this phenomenon to some extent.[42]

Heterocyclic ligands containing soft nitrogen atoms in combination with transition metals are predominantly used for the construction of the large and complex architectures.[43] Numerous examples incorporating *N,N′*-bidentate ligands in supramolecular architecture are now available in literature. From the geometric shapes accessible through the directional bonding approach, squares have been the most widely reported. One of the first tetranuclear squares was synthesized by Fujita *et al*.[44] After the initial stage had been set, Stang *et. al.*[45] prepared charged, macrocyclic, tetranuclear Pt(II) and Pd(II) molecular boxes in high yields. Since then, many other research groups use end-capped metal components and organic ligands to construct molecules of different shapes and properties.

One of the most exciting feature of supramolecular structures is their ability to include neutral and charged molecules as guests in the void space. Crown ethers, discovered by Pedersen in 1967,[46] have the ability to serve as hosts for binding inorganic and organic guests, especially cationic ones. The synthesis of host-guest inclusion compounds has attracted much attention and currently numerous different host frameworks are known which are able to change properties and reactivity of guest molecules.[47] Molecular cages are an important group of such compounds and could serve as nanoscale reaction vessels. Rebek *et al.* discovered that the cylindrical host capsule formed from suitably functionalized organic molecules with directed hydrogen-bonding groups, encapsulates a variety of small molecules and has received much attention.[48] Fujita *et al*. reported the synthesis of molecular cage compounds with large cavities. These structures have attracted great interest due to their ability to act as functional molecular flasks. It has been nicely demonstrated in a number of reports, that cage compounds are able to influence the rate of formation and regio- and stereoselectivity of different reactions.[45]

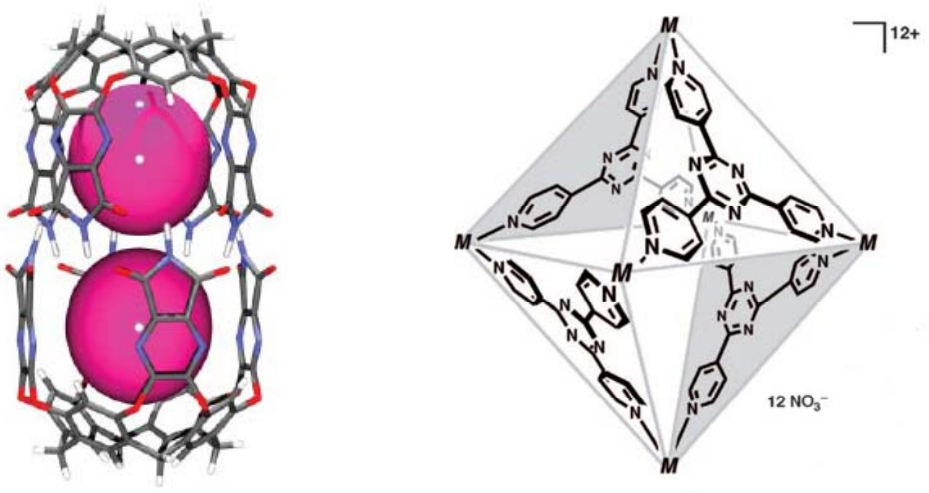

(a) (b)

Figure 1.5 Examples of cage compounds: cylindrical capsule of Rebek and co-workers (a) and octahedral coordination cage of Fujita and co-workers (b)

Many concepts of supramolecular chemistry are applicable for the formation of coordination polymers. In the area of materials chemistry nano- and microscale superstructures called also MOFs (*M*etal *O*rganic *F*ramework) find applications due to their porosity and ability to absorb guest molecules. Although, compared to inorganic zeolites, metal-ligand bonds are often weak, MOFs provide unique opportunities to include properties such as chirality and tailored pore size.

Supramolecular chemistry provides an opportunity to create structures in nanoscale with large cavities, which makes them applicable for host-guest chemistry. Anion recognition and sensing have been a major subject of recent research due to their involvement in biological topics (activity of enzymes, transport of hormones, protein synthesis, DNA regulation) as well as environmental subjects (capture and removal of pollutants).[49,50]

Among many other recognition fragments such as electrostatic attraction, hydrogen bonding, Lewis acid/base interactions *etc.,* anion-π interactions are relatively unexplored, since electron density of aromatic ring is expected to interact repulsively with anions. However, initial calculations made by Dougherty,[51] Besnard[52], Alkorta[53] and co-workers demonstrate that in complexes between electron-deficient aromatic rings and H_2O, HCN, and HF molecules the negative end of the dipole is directed toward the center of the ring. Now numerous theoretical studies confirm the presence of attractive forces between anions and π-acidic aromatic rings.[54] A careful examination of numerous crystal structures also reveals this type of interaction in the solid state.[55]

The behavior of anions in aqueous solution is highly dependent on their hydration energies. They cover a large range of values and increase with charge of the anion and decrease with the size of it ($\Delta G_h \sim -Z^2/r$, where Z is charge and r is thermochemical radius). Different strategies like incorporation of transition metal centers or hydrogen bond donor groups into the receptors are usually utilized in order to increase the receptor's binding affinity for a specific anion.

Anions can also play an active role in the self-assembly processes of supramolecular architectures by acting as templates.

1.4 Aim of the thesis

Within the large field of supramolecular chemistry, discrete (as opposed to polymeric) constructs derived from metal ions and di- or multitopic ligands play important roles. Among these, the synthesis of designed constructs, their characterization and their potential applications in such diverse areas such as host-guest chemistry, sensing, catalysis, or medicine represent major challenges.

This thesis is primarily concerned with issues along these lines: Firstly, generation of (preferably cyclic) complexes derived from ligands and square-planar Pt^{II} and Pd^{II} entities. Employed was a series of ligands (Figure 1.6) such as 2,2´-bipyrazine (2,2´-bpz), cyanide (CN^-), 4-cyanopyridine (4-CNpy), 3-cyanopyridine (3-CNpy), and the hydrolysis products of the two latter ones, namely isonicotineamide (3-$CO(NH_2)$py) and nicotineamide (4-$CO(NH_2)$py), respectively.

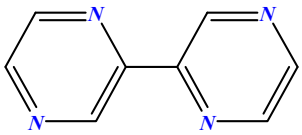

2,2´-bipyrazine
(2,2´-bpz)

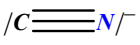

Cyanide

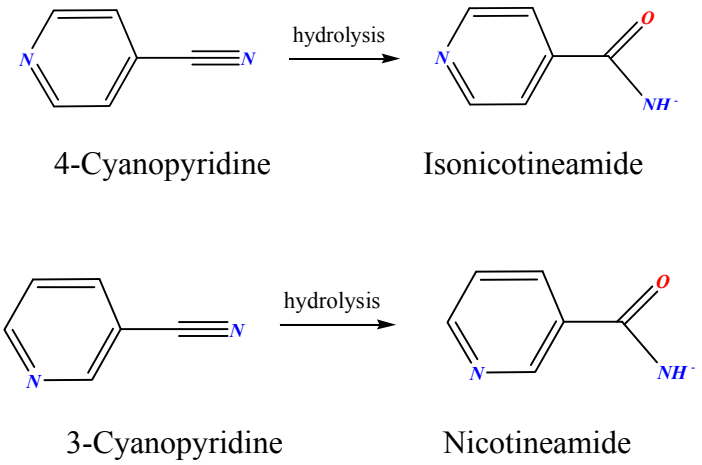

Figure 1.6 List of ligands used in this thesis.

The usefulness of the 2,2´-bpz ligand for the generation of 2D– and 3D–molecular triangles has previously been proven in our group.[63,69,70,71,72] Concerning the metal entities employed in the synthesis of these constructs, they were square-planar metal entities of type *cis*-Ma_2 (with M = Pt^{II} and/or Pd^{II}; a = am(m)ine or a_2 = chelating diamine).

Secondly, the systematic study of host-guest chemistry of cationic, metal containing constructs with anions. Although also previously observed in our group, the full scope of principles of anion complexation by cyclic 2,2´-bpz complexes was still unexplored.

Thirdly, the extension of supramolecular C_3-symmetric vases to discrete constructs of larger dimensions via labile transition metal ions. Here it was the idea to cross-link substitutionally inert Pt/Pd cycles by transition metal ions to generate larger entities, which, in principle, might be useful as "molecular flasks" in the future.

Finally, it was of interest – in particular with regard to biological and medicinal aspects – how such (cationic) metal-ligand constructs might affect DNA structure (and eventually function). It was clear at the outset of this work that at most preliminary results may be obtained here.

Although originally not planed, another objective had caught our attention during the course of this dissertation, namely the question as to how aqua group acidities in mixed-ligand complexes of Pt^{II} are influenced by co-ligands. Therefore, a systematic study on the effect of a ligand *L* in complexes of type *trans*-$[Pt(NH_3)_2(L)(H_2O)]^{2+}$ on the pK_a value of the water ligand was carried out.

Chapter 2 – Self-assembly of 2,2´-Bipyrazine-linked metallo-macrocycles

2.1 Background

The reversibility of a coordination bond in metal mediated self-assembly reactions provide systems with the opportunity to "correct mistakes" and form products with low overall free energy. The thermodynamics of the process promote formation of discrete oligomeric structures rather than of smaller aggregates or polymeric network. Depending on the reaction conditions, the combination of a *cis*-blocked square planar metal center with a linear bridging ligand has shown to form molecular squares and triangles in most cases (Scheme 2.1).

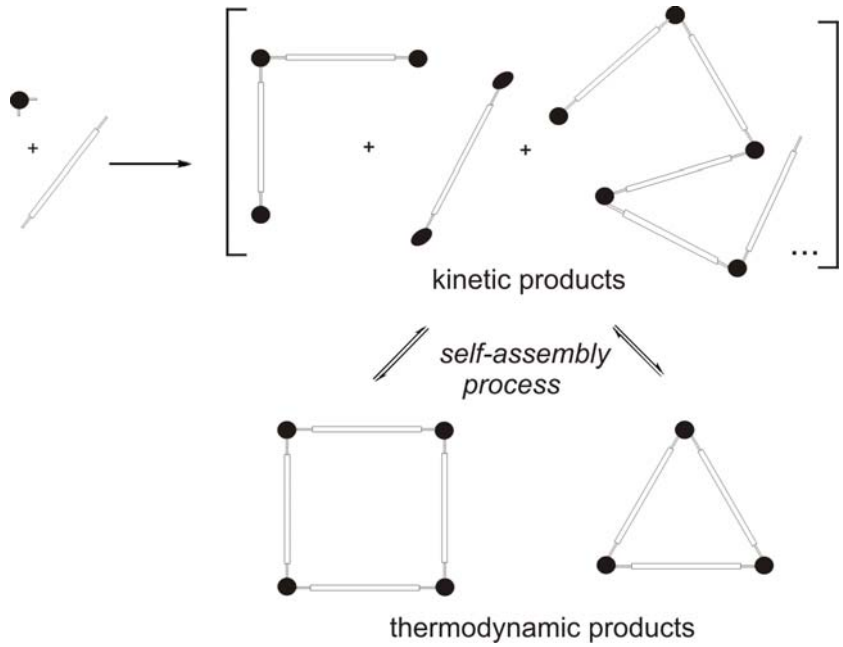

Scheme 2.1 Schematic representation of the self-assembly process between a *cis*-blocked square planar metal center and a linear bidentante ligand.

The equilibrium between metallosupramolecular squares and triangles is one of the simplest examples of dynamic processes existing between cyclic oligomers. It has recently been extensively studied using symmetrical[56] as well as nonsymmetrical[57] ambidentate ligands. Structural topologies of metal based supramolecules, among other factors, could be highly influenced by anions present in the solution.[58] For instance, the influence of the

different anions on the triangle-square equilibrium has been studied by Stang *et al*.[59] They were able to achieve anion-induced crystallization of both products in high yields.

A combination of entropic (ΔS^o) and enthalpic (ΔH^o) factors regulates the process and contributes to the reduction of Gibbs free energy (ΔG^o).[60] The standard-state free energy equation can be written as follows (T is temperature in Kelvin).

$$\Delta G^o = \Delta H^o - T\Delta S^o$$

The tendency to generate a square is driven by enthalpy, because a square is less strained than a triangle. Alternatively, entropy benefits when triangles are formed from the squares, as the number of particles increases in agreement with Le Chatelier's principle.

In the present chapter self-assembly processes of 2,2'-bipyrazine (2,2´-bpz) with square-planar *cis*-$[Pt(a)_2(H_2O)_2]X$ corners (a = NH_3 or a_2 = en), where X= NO_3^-, BF_4^- and SO_4^{2-}, will be reported. As will be shown, it is possible to crystallize one of two species by the predetermined choice of the appropriate anion. Moreover, NMR experiments are discussed which allow to obtain quantitative data on triangle-square equilibria. In this system, both the square and two different conformers of triangular species have been characterized by X-ray crystallography. The "corner stone" *cis*-$[Pt(NH_3)_2(bpz)_2](NO_3)_2$ has also been prepared and characterized by means of X-ray diffraction, revealing a new monodentante binding mode of 2,2´-bpz. Subsequently it was shown that triangular species could be used as synthons for the construction of larger systems – molecular vases, "paddle wheel", capsule, 1D and 2D polymeric structures – which have been obtained applying Pd^{II}, Cu^{II}, Ag^{I} and Cd^{II} ions. The resulting macrocycles contain cavities, which are useful for ion and/or molecule recognition.

Containing four nitrogen atoms in the structure, the 2,2´-bpz ligand belongs to the group of *N*-donor ligands particularly useful in supramolecular chemistry. An important structural feature of 2,2´-bpz is its flexibility: rotation of two pyrazine rings with respect to each other enables many possibilities to bind metals (Scheme 1.1).

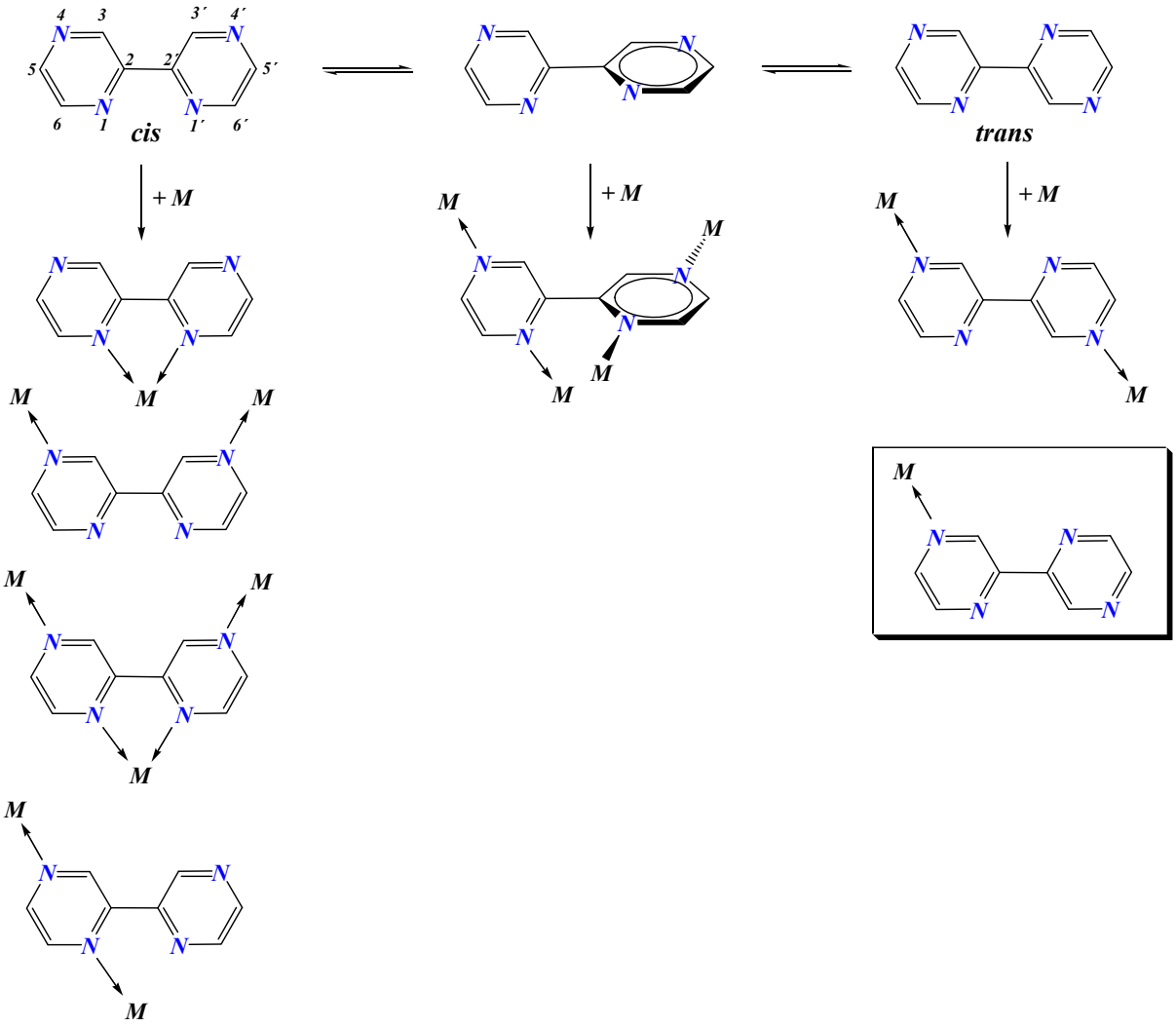

Scheme 1.1 Conformations of bpz (top) and principal metal binding patterns (below). A novel metal binding pattern (boxed-in) is reported, among others, in this work.

2,2′-bpz has been obtained from pyrazinecarboxylic acid in two steps, involving formation of the copper complex and pyrolysis of the later in a glass tube.[61] Different conformers of 2,2′-bpz are not distinguishable in the ^{1}H NMR spectra at RT (ΔE = 5.4 kcal/mol).[62] The doublet at 9.35 ppm is assigned to H3,H3′ protons, while H6,H6′ protons show a doublet at 8.75 ppm and H5,H5′ protons a doublet-of-doublets at 8.79 ppm. Both H3,H3′ and H6,H6′ signals are coupled to the H5,H5′ signal with the coupling constants having values of $^{4}J_{3,5}$ = 1.4 Hz and $^{3}J_{5,6}$ = 2.6 Hz respectively.

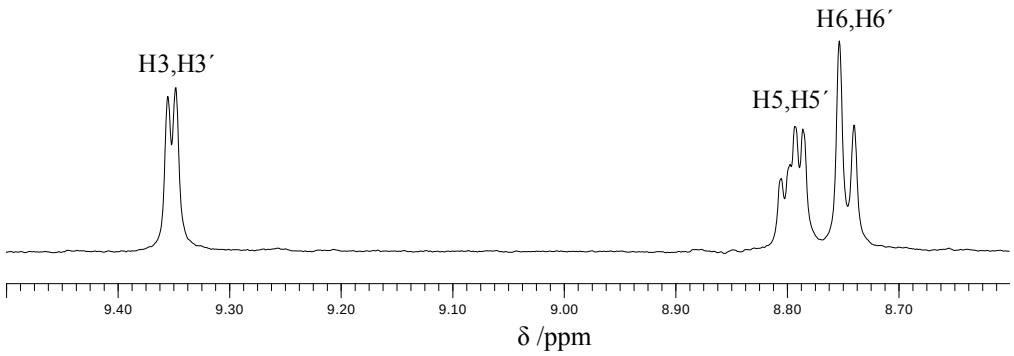

Figure 2.1 Aromatic region of ^{1}H NMR spectrum of 2,2'-bpz in D_2O (200 MHz, pD 5.6).

In contrast to D_2O, signals attributed to the H5,H5´ and H6,H6´ proton are not distinguishable in organic solvents like DMSO-d_6 and CD_3Cl. The ^{1}H NMR spectrum of 2,2´-bpz dissolved in DMSO-d_6 shows resonances at 9.51ppm (H3,H3´) and 8.81ppm (H5,H5´; H6,H6´) and in CD_3Cl at 9.57ppm (H3,H3´) and 8.63ppm (H5,H5´; H6,H6´).

2.2 Supramolecular isomerism with 2,2´-bpz and Pt(II): case of triangle - square equilibrium

2.2.1 Complexation of 2,2´-bpz to a Pt(II) center

^{1}H NMR studies on the reaction of *cis*-$[Pt(NH_3)_2(H_2O)_2]^{2+}$ with 2,2´-bpz in 1:1 stoichiometry were carried out at different temperatures in order to get a deeper insight into the self-assembly process (Figure 2.2). The downfield shift of the signals compared to free ligand is characteristic of the metal-ligand complexation. Results show that when the reaction is carried out at RT, in addition to molecular triangle and square (identified by isolated species) also minor amounts of unknown species are formed (marked with * in the spectra). Although structural features are unclear as yet, formation of the structures where bpz ligand adopts different conformations, could be possible.

When *cis*-$[Pt(NH_3)_2(H_2O)_2]^{2+}$ is allowed to react with 2,2'-bpz at 45^{o}C, after 1d no formation of side products is observed. Increasing the temperature to 100^{o}C does not cause any significant changes. A higher temperature only affects the amounts of products formed: the equilibrium shifts towards formation of the triangle.

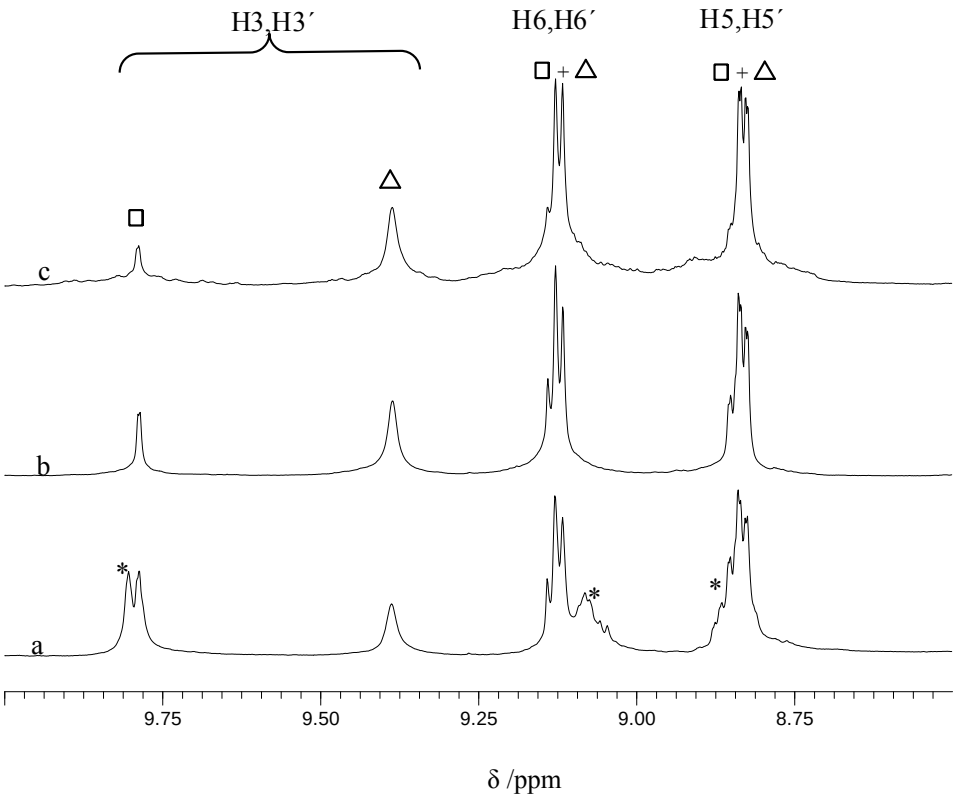

Figure 2.2 Typical ^{1}H NMR spectra of reaction mixture of *cis*-$[Pt(NH_3)_2(H_2O)_2]^{2+}$ with 2,2'-bpz in 1:1 stoichiometry (300 MHz, pD 3 - 4) reaction carried out 1d at a) RT, b) 45°C and c) 100°C. Resonances marked □ and Δ correspond to tetranuclear and trinuclear species, * denotes unidentified species.

While a lower temperature favors the kinetic product, higher temperature promotes formation of the thermodynamically favored species. Hence, by controlling the reaction temperature, it is possible to influence the equilibrium. From the reactions carried out at 45°C, one tetramer and two triangles with different counterions have been isolated and fully characterized.

2.2.2 Molecular square [{*cis*-Pt(NH$_3$)$_2$(*tttt*-bpz-*N4,N4´*)}$_4$](SO$_4$)$_4$ (II-1)

According to the directional bonding approach, combination of a 90° metal acceptor with a linear ligand is expected to yield a metallo-supramolecular square. Indeed, a tetranuclear complex of general formula $[Pt_4bpz_4]^{8+}$ has been prepared by reacting *cis*-$[Pt(NH_3)_2(H_2O)_2](SO_4)$ with bpz in a 1:1 ratio. The ^{1}H NMR spectrum of the isolated substance in D_2O (Figure 2.3) shows a set of 2,2´-bpz signals of nearly identical intensities. This observation suggests that the two aromatic rings of the linker are equivalent.

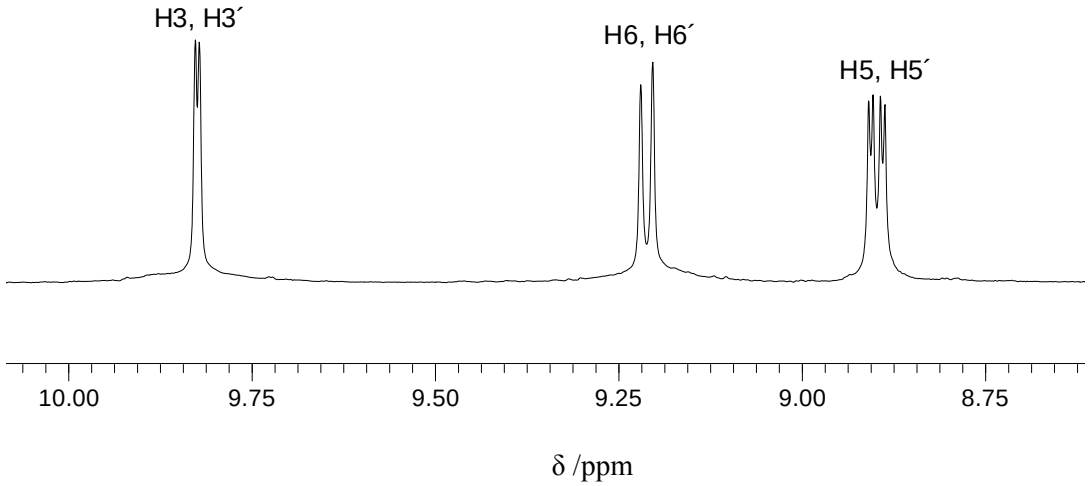

Figure 2.3 Aromatic region of the ^{1}H NMR spectrum in D_2O (200 MHz, pD = 6.3) of [{*cis*-$Pt(NH_3)_2$(*tttt*-bpz-*N4,N4´*)}$_4$]$(SO_4)_4$ (**II-1**).

Doublets at 9.82 and 9.21 ppm are attributed to the H3,H3´ and H6,H6´ protons, respectively, and the doublet-of-doublet at 8.90 ppm to the H5,H5´protons of 2,2´-bpz. Coupling constants are $^{3}J_{3,5}$ = 1 Hz and $^{3}J_{5,6}$ = 3.4 Hz. H3,H3´ and H6,H6´ resonances of 2,2´-bpz are shifted downfield from those of the free ligand by Δδ = 0.47 and 0.46 ppm.

Single crystals of **II-1** were successfully isolated from water solution during one week at 4^{o}C. X-ray analysis proved the formation of the molecular square, which consists of a tetranuclear Pt_4 core with bridging 2,2´-bpz ligands via N4,N4´nitrogens atoms (Figure 2.4). Preference of Pt(II) for N4,N4´ nitrogens and the formation of the kinetic product, rather than the thermodynamically more stabile chelate (through binding via N1,N1´) under the same reaction conditions, was shown before.[63]

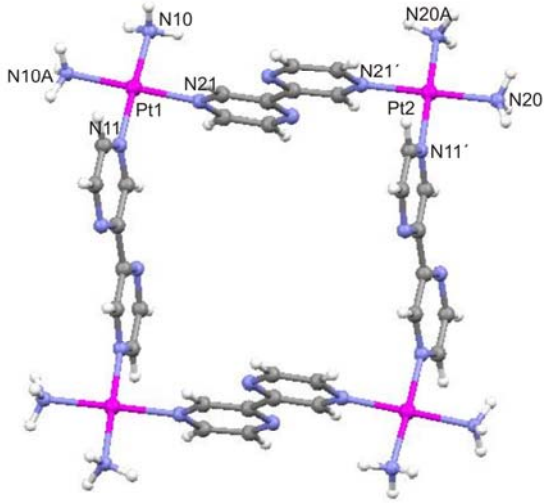

Figure 2.4 Molecular structure of *cis*-[{$Pt(NH_3)_2$(*tttt*-bpz-*N4,N4´*)}$_4$]$^{8+}$ cation (**II-1**) with numbering of relevant atoms.

The Pt(II) coordination geometry is close to ideal square-planar. Selected interatomic distances and angles are shown in Table 2.1. The average Pt-N bond length is 2.03 Å. All four 2,2´-bpz ligands are in *trans* orientation (indicated as *tttt*-bpz in the formula). The sequence of *trans*-bpz ligands in the cycle is (– +)(+ –)(+ –)(– +) (+ means pyridine ring higher than the metal position, while – means pyridine ring lower than the metal position).[64] Torsion angles between two pyrazine rings have values of 4.5 and 5.5° showing that two halves of the ligands are nearly coplanar. Metal-metal distances are as follows: Pt1-Pt2, 9.5938(3) Å; Pt1-Pt1, 13.6853(4) Å and Pt2-Pt2, 13.4076(4) Å.

Table 2.1 Selected bond lengths (Å) and angles (deg.) for **II-1**.

[{*cis*-Pt(NH_3)$_2$(*tttt*-bpz-*N4,N4´*)}$_4$](SO_4)$_4$ (**II-1**)			
Pt1–N21	2.004(4)	Pt2–N21´	2.019(4)
Pt1–N11	2.010(4)	Pt2–N11´	2.029(4)
Pt1–N10	2.042(4)	Pt2–N20A	2.038(4)
Pt1–N10A	2.043(4)	Pt2–N20	2.047(4)
N21–Pt1–N11	89.65(18)	N21´–Pt2–N11´	89.37(17)
N21–Pt1–N10	89.22(18)	N21´–Pt2–N20A	90.28(18)
N11–Pt1–N10A	90.71(19)	N11´–Pt2–N20	91.75(18)
N10–Pt1–N10A	90.42(19)	N20A–Pt2–N20	88.58(19)
N11–Pt1–N10	178.51(18)	N11´–Pt2–N20A	179.27(18)
N21–Pt1–N10A	179.64(19)	N21´–Pt2–N20	178.52(17)

An analysis of the crystal packing reveal stacking interactions between neighboring molecules, with alternating orientations being about 10.5 Å apart. 1D pore channels are formed, which are filled with disordered water molecules, joined via multiple hydrogen bonds.

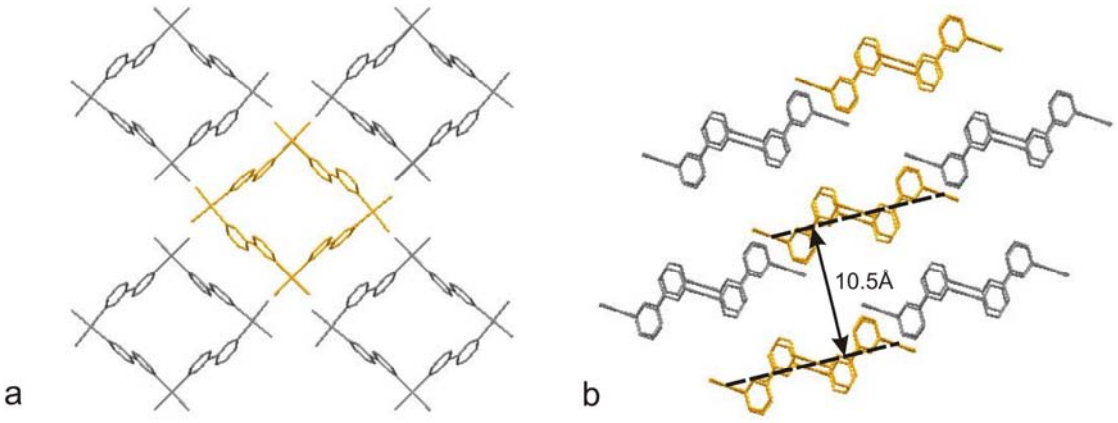

Figure 2.5 Crystal packing of cations of *cis*-[{Pt(NH_3)$_2$(*tttt*-bpz-*N4,N4´*)}$_4$](SO_4)$_4$ (**II-1**) along the a-axis (a) and anolg the b-axis (b).

The 8+ charge of the Pt_4 square is compensated by four sulfate anions, which are located outside the cavities of the tetranuclear cycle.

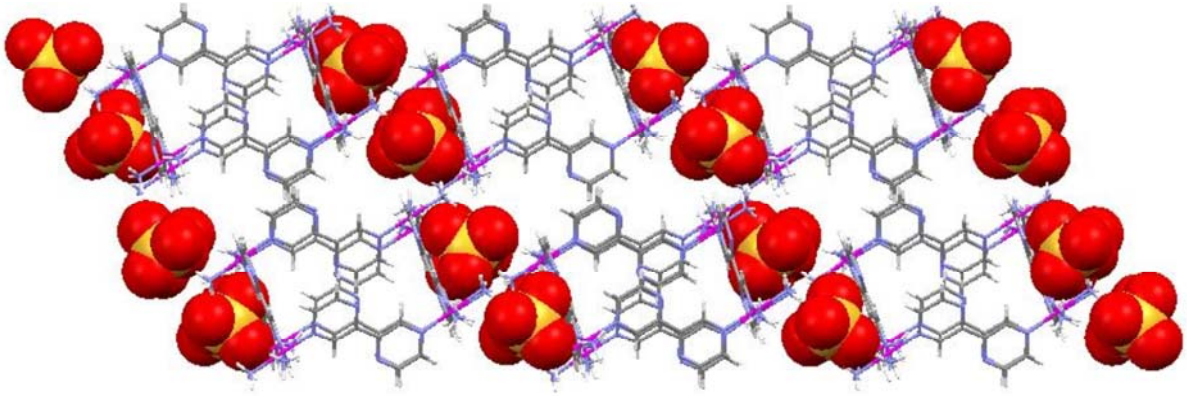

Figure 2.5 Formation of linear chains of cations and anions of **II-1** in the solid state.

The molecules are extensively laced together through hydrogen bonds between sulfate anion, NH_3 ligands of platinum (O13···N10A, 2.81 Å; O21···N10, 2.89 Å; O21···N10A, 2.92 Å; O22···N20A, 2.93 Å; O23···N10, 2.88 Å; O23···N20, 2.89 Å; O24···N20A, 2.94 Å;) and water molecules. These hydrogen bonding interactions lead to the formation of linear chains of cations and anions in alternating sequence (Figure 2.5).

2.2.3 Molecular triangles

In general, access to triangular species is achieved by using 60° bridging ligands and linear metal centers.[65] The reverse situation is usually not applicable, because metals with 60° bond angles are extremely rare. Another appreciated method is the use of flexible ligands and metal centers with 90° bond angle.[66] The unexpected formation of a triangle from two rigid subunits, namely of a ditopic platinum acceptor and pyrazine, is also known from the literature.[67] In this case, a considerable portion of the tension generated from creating the smaller species is concentrated in the Pt-N connections themselves.

In the following molecular triangles obtained by reaction of *cis*-$[Pt(a_2)(H_2O)_2]^{2+}$ with 2,2´-bpz will be discussed.

As shown in Figure 2.6, the ^1H NMR spectra of aqueous solutions of isolated $[Pt_3(bpz)_3]^{6+}$ triangles, with BF_4^-/SiF_6^{2-} (**II-2**) and NO_3^-/PF_6^- (**II-3**) as counter anions, indicate the presence of symmetric species in both cases. As can be seen, different anions influence the

proton resonances of the 2,2´-bpz. The H3,H3´ protons of the 2,2´-bpz are the most affected ones. The broad singlet at 9.32 ppm for **II-2** is downfield shifted by 0.07 ppm in comparison to the analoguous complex **II-3,** which occurs at 9.25 ppm. H5,H5´ and H6,H6´ protons are less affected and give doublets at 9.13 – 9.14 ppm, whereas the ill-resolved doublet-of-doublets at 8.83 ppm ($^3J_{5,6}$ = 3 Hz for **II-2)** and 8.85 ppm with ($^3J_{5,6}$ = 3.3 Hz for **II-3)** differ a bit more.

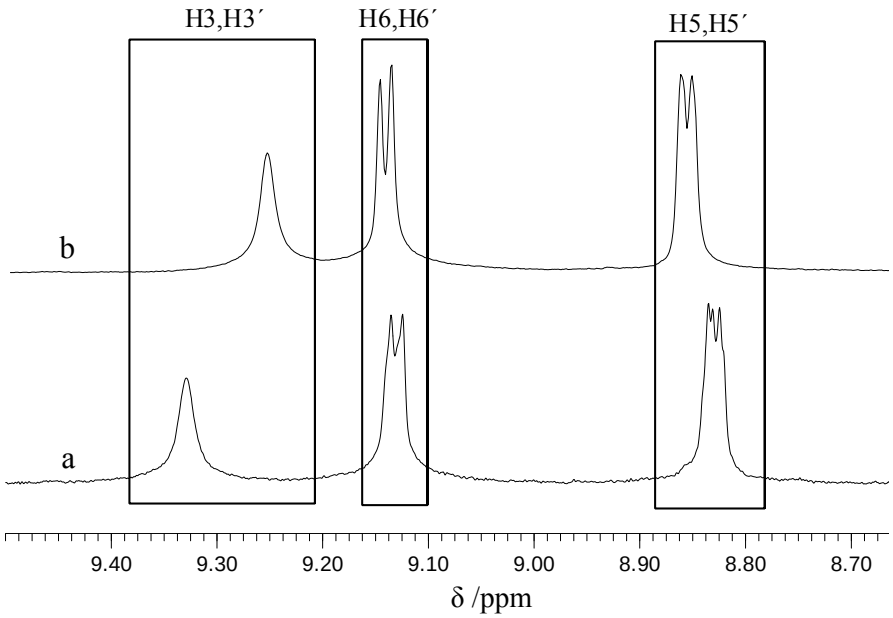

Figure 2.6 ^{1}H NMR spectra (aromatic region) of the complexes **II-2** (a) and **II-3** (b).

$NO_3\subset[\{Pt(en)(ccc\text{-bpz-}N4,N4')\}_3](SO_4)_2(NO_3)$ (**II-4**) has been obtained from an incomplete anion exchange process of the previously described NO_3^- salt of the $[(a_2Pt)_3bpz_3]^{6+}$ triangle (a_2 = ethylenediamine).[63] The ^{1}H NMR spectrum of the compound obtained gives resonances at 9.37 ppm (s, H3,H3´) and doublets ($^3J_{5,6}$ = 3 Hz) at 9.15 ppm (H6,H6´) and 8.87 ppm (H5,H5´). The resonances of partly exchanged cation **II-4** are in between those of the pure NO_3^- -salt and the completely exchanged SO_4^{2-} -salt (Figure 2.7).

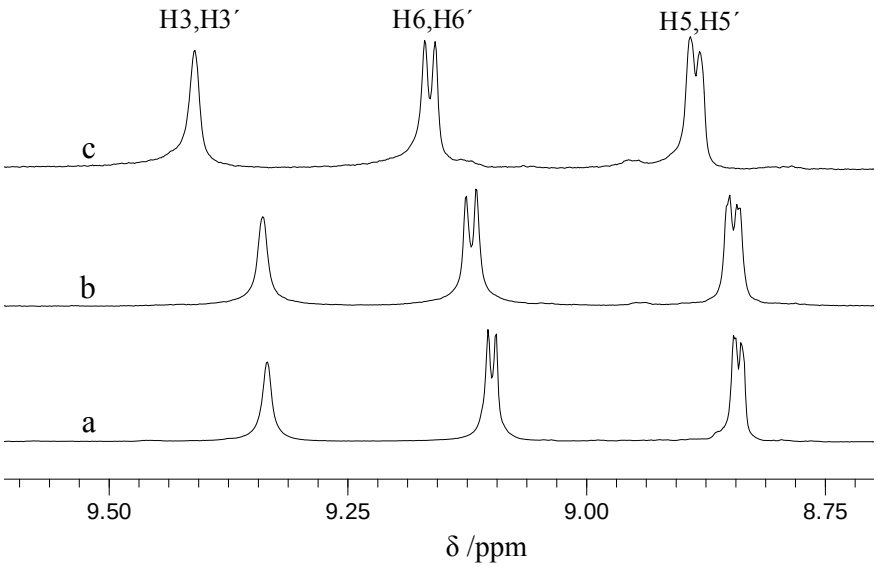

Figure 2.7 Lowfield section of ^{1}H NMR spectra (D_2O, 300 MHz, pD = 6.2) of a) $(NO_3)_6$-salt, b) partially exchanged (($(NO_3)x(SO_4)y$-salt and c) fully exchanged $(SO_4)_3$-salt.

For compound **II-2,** formation of SiF_6^{2-} anions in aqueous solution has been observed. Handling of **II-2** in a glass apparatus causes hydrolysis of the BF_4^- anions and formation of SiF_6^{2-} according to the following reaction cascade:

$$BF_4^- + H_2O \rightarrow F^- + B(OH)F_3^- + H^+$$
$$B(OH)F_3^- + H_2O \rightarrow F^- + B(OH)_2F_2^- + H^+$$
$$\cdots\cdots$$
$$6F^- + SiO_2 + 4\ H^+ \rightarrow SiF_6^{2-} + 2H_2O$$

^{19}F NMR studies were carried out to follow this process (Figure 2.8). The ^{19}F resonances consist of a singlet at 134 ppm due to coupling of the ^{19}F and ^{29}Si nuclei with ^{1}J(F-Si) = 144 Hz, and of two singlets with a ratio of 1:4 at around 155.5 ppm. The appearance of two singlets is the result of coupling of ^{19}F with ^{11}B (I=3/2) and ^{10}B (I=3). Spectra taken after two months indicate that nearly half of the BF_4^- anions have exchanged to give SiF_6^{2-}. Keeping the solution for an additionally four months shows that the ratio of peaks is 1(BF_4^-) : 2.5 (SiF_6^{2-}). Generation of SiF_6^{2-} anions from BF_4^- and glass in water is a known phenomenon.[68]

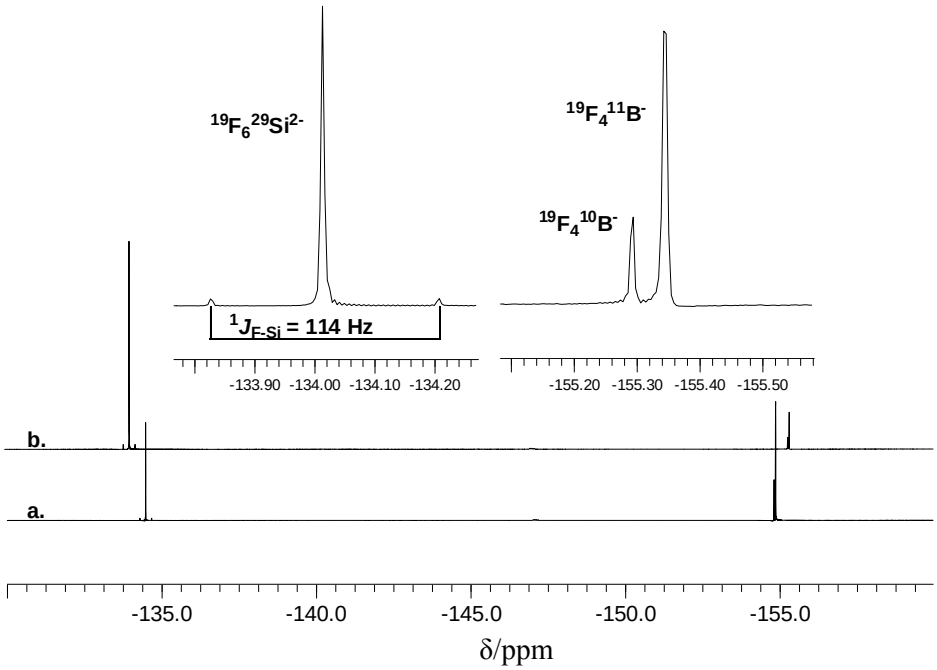

Figure 2.8 ^{19}F NMR spectra of **II-2** recorded in D_2O (300 MHz, pD = 3.2) 2 months after dissolving (a), 6 months after dissolving **II-2** (b).

X-ray structurally characterized compounds are: $BF_4\subset$*cis*-[{Pt(NH_3)$_2$(*ttt*-bpz-*N4,N4´*)}$_3$](BF_4)(SiF_6)$_2$ (**II-2**), $PF_6\subset$*cis*-[{Pt(NH_3)$_2$(*ccc*-bpz-*N4,N4´*)}$_3$](PF_6)$_5$(NO_3) (**II-3**) and $NO_3\subset$[{Pt(en)(*ccc*-bpz-*N4,N4´*)}$_3$](SO_4)$_2$(NO_3) (**II-4**) (with *ccc*-bpz representing a cyclic structure in which all three 2,2´-bpz ligands adopt *cis* orientations and *ttt*-bpz defining a cycle with the three 2,2´-bpz ligands being in *trans* orientations).

2.2.3.1 Crystal structure of $BF_4\subset$ *cis*-[{Pt(NH_3)$_2$(*ttt*-bpz-*N4,N4´*)}$_3$](BF_4)(SiF_6)$_2$ (II-2)

The X-ray analysis of **II-2** shows that the three 2,2´-bpz ligands adopt *trans* orientations and are nearly perpendicular to the Pt_3 plane (Figure 2.7). The angles around the Pt centers are between 88.0° and 91.9° (Table 2.2) and differ only slightly from the ideal 90°. This indicates that flexibility of the ligand is significant for the formation of this triangular species. Pt-Pt-Pt angles range from 59.9° to 60.2°, hence are likewise close to ideal 60° angles for a triangle. The intramolecular Pt···Pt distances are as follows: Pt1···Pt2, 9.4461(7) Å; Pt2···Pt3, 9.4523(5) Å and Pt3···Pt1, 9.4742(7) Å.

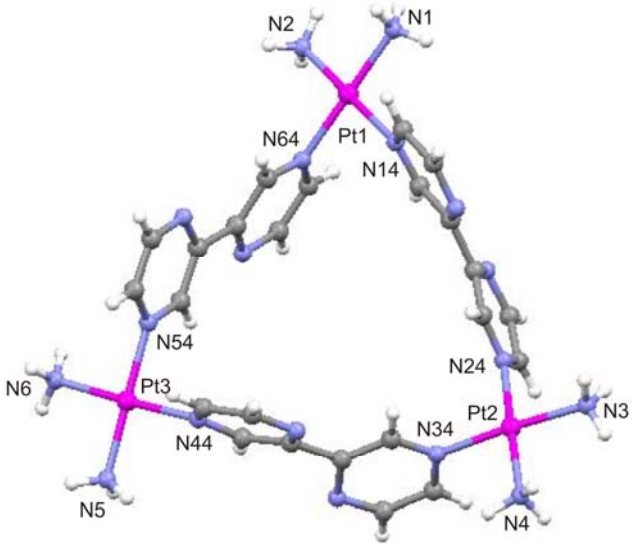

Figure 2.9 View of *cis*-[{Pt(NH$_3$)$_2$(*ttt*-bpz-*N4,N4´*)}$_3$]$^{6+}$ cation (**II-2**) with numbering scheme of relevant atoms.

Table 2.2 Selected bond lengths (Å) and angles (deg.) for **II-2.**

BF$_4$ ⊂ *cis*-[{Pt(NH$_3$)$_2$(*ttt*-bpz-*N4,N4´*)}$_3$](BF$_4$)(SiF$_6$)$_2$ (**II-2**)			
Pt1–N1	2.031(10)	Pt3–N5	2.012(8)
Pt1–N2	2.010(8)	Pt3–N6	2.024(8)
Pt1–N64	2.029(8)	Pt3–N44	2.022(8)
Pt1–N14	2.030(8)	Pt3–N54	2.013(9)
Pt2–N3	2.024(9)	Pt1–Pt2	9.4461(7)
Pt2–N4	2.028(10)	Pt2–Pt3	9.4523(5)
Pt2–N24	1.988(9)	Pt1–Pt3	9.4742(7)
Pt2–N34	2.029(8)		
N2–Pt1–N14	90.1(4)	N5–Pt3–N44	91.3(3)
N64–Pt1–N14	89.9(3)	N54–Pt3–N44	88.0(3)
N2–Pt1–N1	89.5(4)	N5–Pt3–N6	90.8(3)
N64–Pt1–N1	90.5(4)	N54–Pt3–N5	89.8(4)
N2vPt1–N64	179.1(4)	N5–Pt3–N54	179.2(3)
N14–Pt1–N1	179.3(4)	N44–Pt3–N6	177.4(4)
N24–Pt2–N3	91.2(4)	Pt1–Pt2–Pt3	60.17
N3–Pt2–N4	88.2(4)	Pt2–Pt1–Pt3	59.95
N24–Pt2–N34	91.9(3)	Pt1–Pt3–Pt2	59.88
N4–Pt2–N34	88.7(4)		
N24–Pt2–N4	178.4(4)		
N3–Pt2–N34	176.3(4)		

The crystal structure analysis of complex **II-3** reveals that the two halves of 2,2´-bpz ligands are twisted with respect to each other by 28.7^o, 16.9^o and 34.6^o for ligands crosslinking the Pt1···Pt2, Pt1···Pt3 and Pt2···Pt3 centers. Further examination of the crystal

packing motif reveals π···π stacking interaction of 2,2´-bpz with the neighbor molecule with a contact distance of 3.5 Å (Figure 2.10).

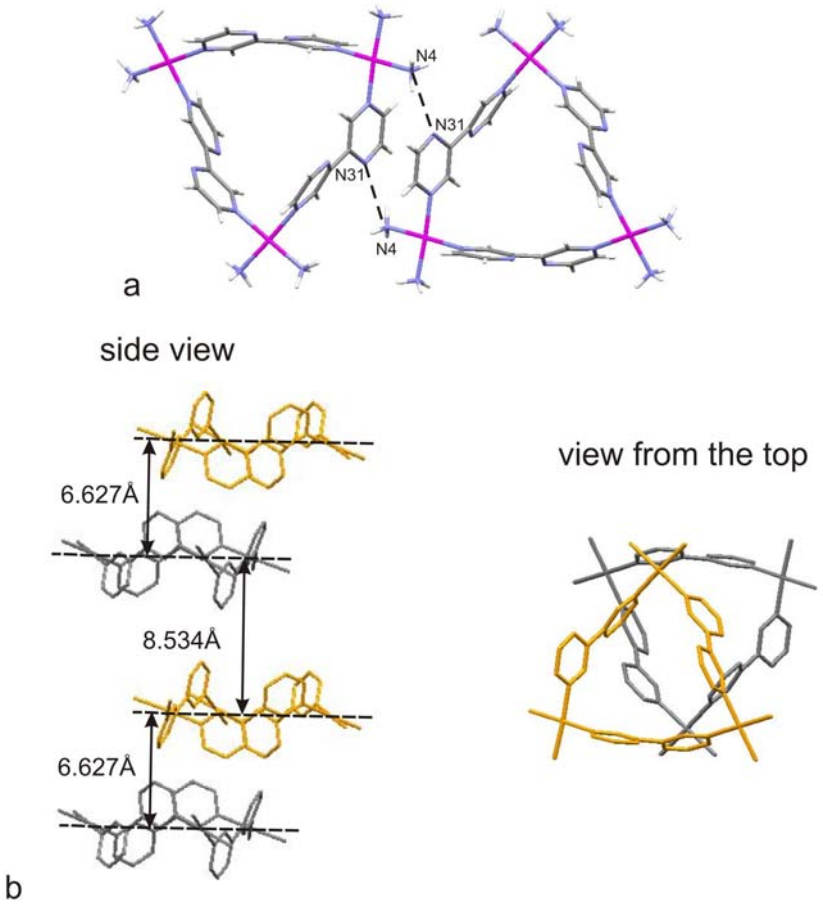

Figure 2.10 Hydrogen bonding interactions between two molecules of **II-2** (a) and stacking of **II-2** into columns (b) (side view and view from the top).

In addition, hydrogen bonds between uncoordinated nitrogen atoms of bpz and hydrogen atoms of ammonia ligands of the neighboring molecule with distances of 3.08 Å are found in the structure. The triangles stack in columns with $Pt_3\cdots Pt_3$ interplane distances of *ca.* 6.63 and *ca.* 8.53 Å. The counteranions are positioned between the planes, with one BF_4^- anion encapsulated in the cavity. (Host-guest interactions are discussed in more detail in Chapter 6.)

2.2.3.2 Crystal structure of $(NO_3)(PF_6)\subset$*cis*-[{Pt$(NH_3)_2$(*ccc*-bpz-*N4,N4´*)}$_3$]$(PF_6)_4$ (II-3)

As can be seen from the crystal structure (Figure 2.9), the 2,2´-bpz ligands link adjacent Pt atoms via N4,N4´ nitrogens, with N(pz)-Pt-N(pz) angles ranging from 88.6° to

91.4°. Pt···Pt interatomic distances in **II-3** are significantly shorter than in **II-2** and have the following values: Pt1···Pt2, 7.8179(12) Å; Pt2···Pt3, 8.0911(14) Å and Pt3···Pt1, 7.9604(13) Å. All three 2,2′-bpz ligands are oriented above the Pt_3 plane. The internal angles of the triangle are 58.3°, 60.0° and 61.7°, and thus are comparable to those observed in Pt_3 complex described above. Selected bond lengths and angles are reported in the Table 2.3.

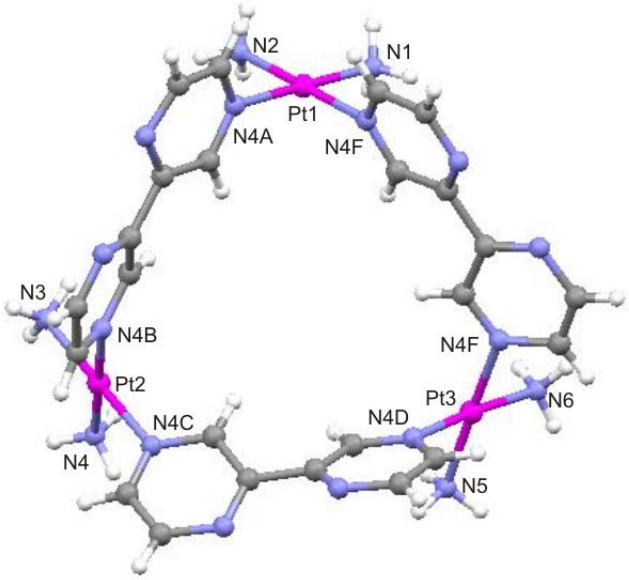

Figure 2.11 Crystal structure of *cis*-[{Pt$(NH_3)_2$(*ccc*-bpz-*N4,N4′*)}$_3$]$^{6+}$ (**II-3**) with numbering scheme of relevant atoms.

The pyrazine rings are tilted with respect to each other by 18.4° (pzA-pzB), 31.7° (pzC-pzD) and 25.4° (pzE-pzF). The cavity generated by the all-*cis* conformer of the triangle hosts both a PF_6^- and a NO_3^- anion.

Table 2.3 Selected bond lengths (Å) and angles (deg.) for **II-3**.

(NO_3)(PF_6)⊂*cis*-[{Pt$(NH_3)_2$(*ccc*-bpz-*N4,N4′*)}$_3$](PF_6)$_4$ (**II-3**)			
Pt1–N4A	2.002(16)	Pt3–N4D	1.97(2)
Pt1–N1	2.011(19)	Pt3–N6	1.98(3)
Pt1–N4F	2.011(15)	Pt3–N4E	2.019(18)
Pt1–N2	2.058(17)	Pt3–N5	2.057(18)
Pt2–N4C	2.016(16)	Pt1–Pt2	7.8179(12)
Pt2–N3	2.025(15)	Pt2–Pt3	8.0911(14)
Pt2–N4	2.036(17)	Pt1–Pt3	7.9604(13)
Pt2–N4B	2.044(17)		
N4A–Pt1–N1	179.5(8)	N4D–Pt3–N6	174.9(9)
N4A–Pt1–N4F	91.4(7)	N4D–Pt3–N4E	90.4(7)

N1–Pt1–N4F	88.2(8)	N6–Pt3–N4E	89.4(8)
N4A–Pt1–N2	89.2(7)	N4D–Pt3–N5	89.0(8)
N1–Pt1–N2	91.3(8)	N6–Pt3–N5	91.0(9)
N4F–Pt1–N2	179.1(7)	N4E–Pt3–N5	177.4(8)
N4C–Pt2–N3	178.6(7)	Pt1–Pt2–Pt3	60.02
N4C–Pt2–N4	93.1(7)	Pt2–Pt1–Pt3	61.69
N3–Pt2–N4	88.3(7)	Pt1–Pt3–Pt2	54.29
N4C–Pt2–N4B	88.6(7)		
N3–Pt2–N4B	90.0(7)		
N4–Pt2–N4B	178.3(7)		

In the solid state molecular triangles of **II-3** are arranged into infinite columns, with $Pt_3\cdots Pt_3$ interplane distances of *ca.* 4.78 and *ca.* 9.28 Å.

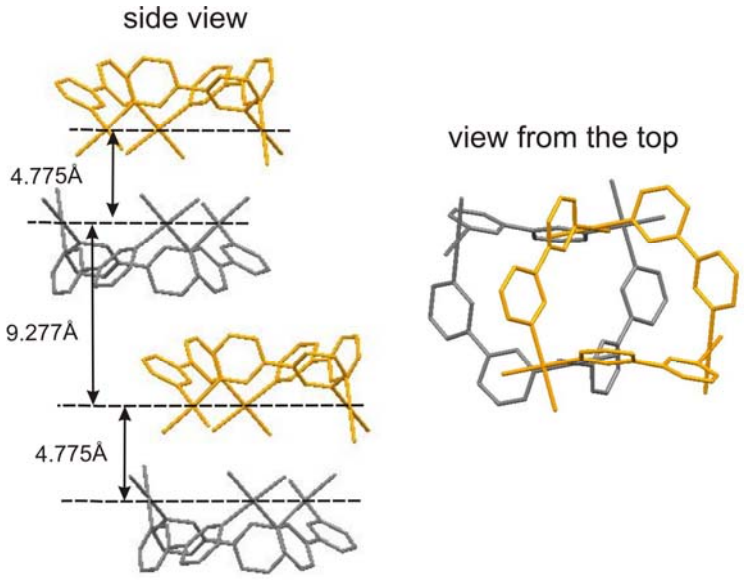

Figure 2.12 Crystal packing of cations of **II-3**, showing two different views

2.2.3.4 Crystal structure of $NO_3\subset[\{Pt(en)(ccc\text{-}bpz\text{-}N4,N4')\}_3](SO_4)_2(NO_3)$ (II-4)

The crystal structure of **II-4** indicates, as expected, the presence of a triangular triplatinum unit. Each Pt atom is bridged by a 2,2′-bpz ligand in all-*cis* conformation. One NO_3^- anion is entrapped inside the cavity. In contrast to other triangular species, two of six pyrazine rings are almost perpendicular to the Pt_3 plane (84.5 and 84.7°), and the cavity is somewhat narrower than in the similar all-*cis* conformer **II-3**. The average N(pz)–Pt–N(pz) angle is 90.3°.

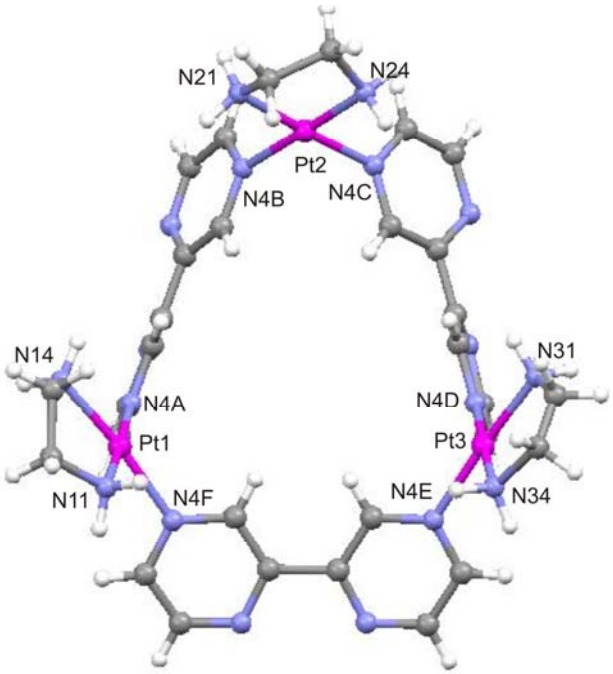

Figure 2.13 Crystal structure of $[\{Pt(en)(ccc\text{-bpz-}N4,N4')\}_3]^{6+}$ (**II-4**) with numbering scheme of relevant atoms (anions are omitted for the clarity)

The intramolecular Pt···Pt distances are as follows: Pt1···Pt2, 7.9598(5) Å; Pt2···Pt3, 7.9112(5) Å and Pt3···Pt1, 7.7887(5) Å, with the latter being slightly shorter than the two former.

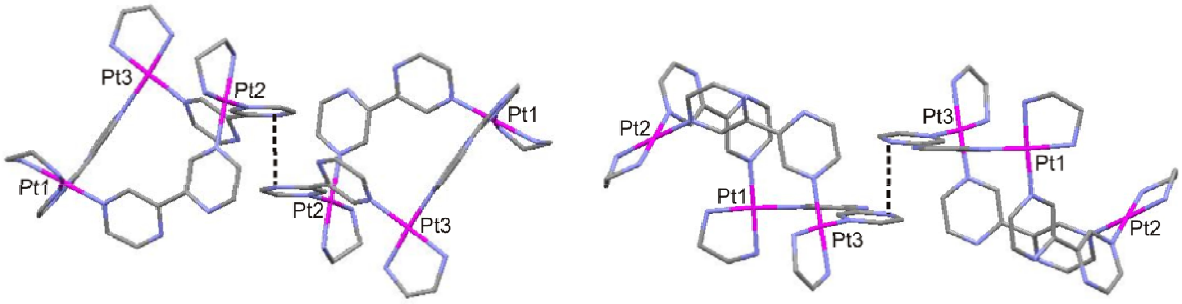

Figure 2.14 Details of π-π staking interactions between two neighbouring molecules.

Pairs of cations of **II-4** are arranged in a way as to allow stacking of the pyrazine rings, with the shortest centroid-plane distances being *ca.* 3.30 and 3.22 Å.

Table 2.4 Selected bond lengths (Å) and angles (deg.) for **II-4**.

$NO_3 \subset [\{Pt(en)(ccc\text{-bpz-}N4,N4')\}_3](SO_4)_2(NO_3)$ (**II-4**)			
Pt1–N11	2.008(7)	Pt1-N4A	2.024(7)
Pt1–N14	2.021(6)	Pt1-N4F	2.039(6)
Pt2–N21	2.018(7)	Pt2-N4B	2.022(6)
Pt2–N24	2.017(6)	Pt2-N4C	2.012(6)
Pt3–N31	2.034(7)	Pt3-N4D	2.029(7)
Pt3–N34	2.030(8)	Pt3-N4E	2.018(7)
N11–Pt1–N14	84.1(3)	N4C-Pt2-N4B	88.7(2)
N11–Pt1–N4A	177.6(3)	N21-Pt2-N4B	94.8(3)
N14–Pt1–N4A	93.6(3)	N24-Pt2-N4B	178.9(3)
N11–Pt1–N4F	91.2(3)	N4E-Pt3-N4D	90.9(3)
N14–Pt1–N4F	173.8(3)	N4E-Pt3-N34	91.3(3)
N4A–Pt1–N4F	91.2(3)	N4D-Pt3-N34	177.7(3)
N4C–Pt2–N21	176.5(2)	N4E-Pt3-N31	175.5(3)
N4C–Pt2–N24	92.4(2)	N4D-Pt3-N31	93.4(3)
N21–Pt2–N24	84.1(3)	N34-Pt3-N31	84.4(3)

2.2.4 Influence of counter anion and concentration on triangle-square equilibrium

H5,H5´ and H6,H6´ protons of the 2,2´-bpz ligands of triangles and square overlap in the aromatic region, but the H3,H3´ protons next to the coordinated nitrogen at around 9.3 ppm (triangle) and 9.8 ppm (quartet) give rise to well separated, characteristic resonances. The assignment is supported by the ^{1}H NMR spectra of isolated single crystals. The ratios of the integrated intensities of these signals provide a measure for the amounts of triangle and square formed.

In order to test, whether the anion present in solution would have an influence on the relative amounts of square and triangle, NMR-scale reactions have been carried out using different silver salts ($AgNO_3$, $AgBF_4$ and Ag_2SO_4) in the initial step of Cisplatin activation. Reactions have been carried out at identical concentrations of Cisplatin and at identical temperature (45^{o}C) in order to avoid other effects that can influence the triangle-square equilibrium. On the basis of the changes in the relative peak intensities between the H3,H3´ signals corresponding to square and triangle, relative amounts of components have been calculated.

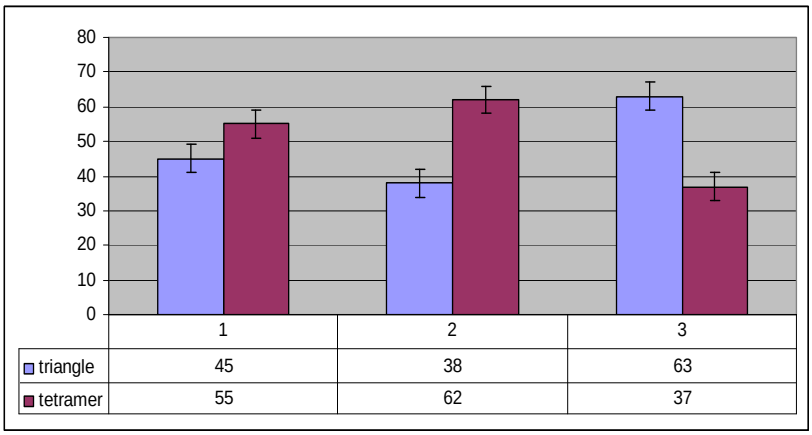

Diagram 2.1 Relative amounts of triangle and tetramer formed (%) in the presence of 1) NO_3^-, 2) SO_4^{2-}, and 3) BF_4^- anions.

As can be seen from the Diagram 2.1, when NO_3^- is present in solution, amounts of square and triangle are nearly equal. In the case of SO_4^{2-}, the tetramer dominates, and in the case of BF_4^- the situation is reversed.

It was also found that the ratio between square and triangle is concentration dependant. Thus an increase of the concentrations in reacting components from 0.5 M to 1.5 M, increases the amount of the tetramer by *ca.* 8% for the NO_3^- -salt and *ca.* 9% for the SO_4^{2-}-salt.

2.2.5 Building block for molecular architecture: 2,2´-bpz as monotopic ligand

NMR scale reactions of *cis*-$[Pt(NH_3)_2(H_2O)_2]^{2+}$ with 2,2´-bpz in 1:2 stoichiometry produce complicated spectra, which become more simple when the reactions are carried out in more dilute solutions with the ratio of components being 1:4. Reaction carried out on a preparative scale yielded *cis*-$[Pt(NH_3)_2(bpz\text{-}N4)_2](NO_3)_2$ (**II-5**). This compound has been isolated and characterized by means of ^1H NMR spectroscopy, X-ray crystal structure analysis and elemental analysis. Formation of analogous complexes containing $enPt^{II}$, *trans*-$(NH_3)_2Pt^{II}$ and *trans*-$(CH_3NH_2)_2Pt^{II}$ metal moieties have also been monitored by NMR spectroscopy. These building units could in principle enable the formation of large molecular systems, with extended inner and outer surfaces (Scheme 2.3).

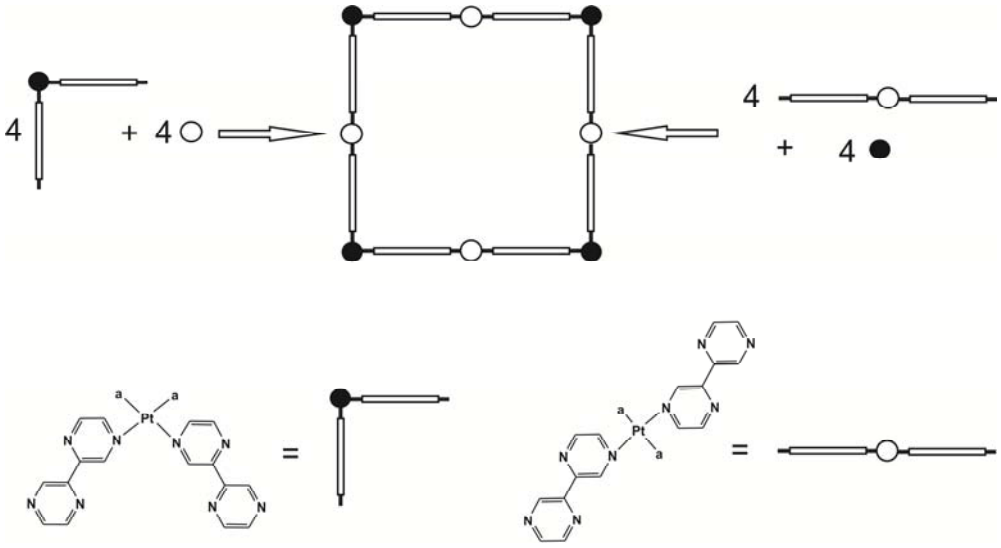

Scheme 2.3 Schematic representation of the formation of an octanuclear molecular square.

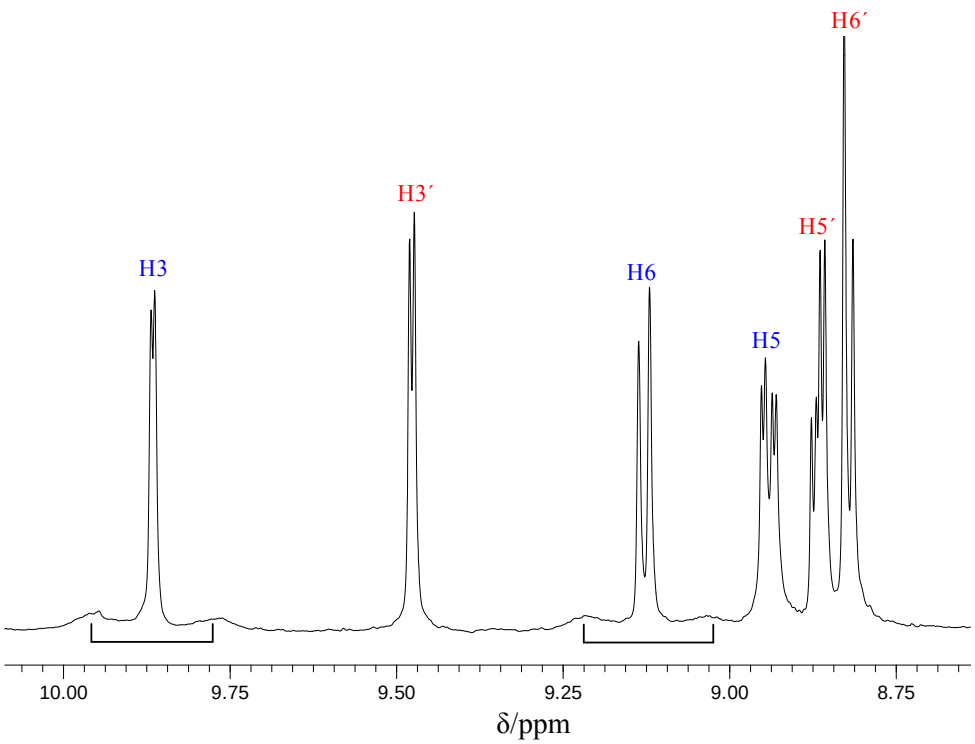

Figure 2.15 Aromatic region of the ^{1}H NMR spectrum of *cis*-[Pt(NH$_3$)$_2$(bpz-*N4*)$_2$](NO$_3$)$_2$ (**II-5**) (D$_2$O, 300 MHz, pD = 5.8).

The coordination of 2,2´-bpz to the Pt center is evident from the ^{1}H NMR spectrum, which clearly reveals a downfield shift of the protons of one of the pyrazine rings and results in a doubling of signals. The spectrum consists of six sharp peaks for two sets of non-equivalent pyrazine rings. The resonances for the protons at the 3 and 6 positions of the

coordinated pyrazine ring display ^{195}Pt satellites due to ^{3}J coupling, with coupling constants of 37 Hz (H3) and 41 Hz (H6). For H5 platinum satellites are not detectable because of overlap with other signals, but its presence was clearly detectable when the proton signal was observed with ^{195}Pt broad-band decoupling. The ^{1}H resonances of the coordinated pyrazine ring are shifted downfield in comparison to free ligand and occur at 9.87 ppm (d, H3, $^{4}J_{3,5}$ = 1.1 Hz), 9.13 ppm (d, H6, $^{3}J_{6,5}$ = 3.3 Hz) and 8.94 ppm (dd, H5, $^{4}J_{5,3}$ = 1.1 Hz and $^{3}J_{5,6}$ = 3.3 Hz), respectively. Proton signals of the non-coordinated pyrazine ring are not much affected by metal coordination and occur at 9.48 ppm (d, H3´, $^{4}J_{3',5'}$ = 1.4 Hz), 8.86 ppm (dd, H5´, $^{4}J_{5',3'}$ = 1.4 Hz and $^{3}J_{5',6'}$ = 2.6 Hz) and 8.82 ppm (d, H6´, $^{3}J_{6',5'}$ = 2.6 Hz).The coupling constants and the COSY NMR experiment permit an accurate assignment of proton signals.

2.2.5.1 Crystal structure of *cis*-[Pt(NH$_3$)$_2$(bpz-*N4*)$_2$](NO$_3$)$_2$ (II-5)

In the crystal structure of **II-5,** the Pt atom adopts square-planar coordination geometry with two ammine and two ligands coordinated to it. (Figure 2.16). Pt binding is through the N4 nitrogen of the 2,2´-bpz, which acts as a monodentate ligand and adopts a *trans* conformations of the two pyrazine (pz) entites.

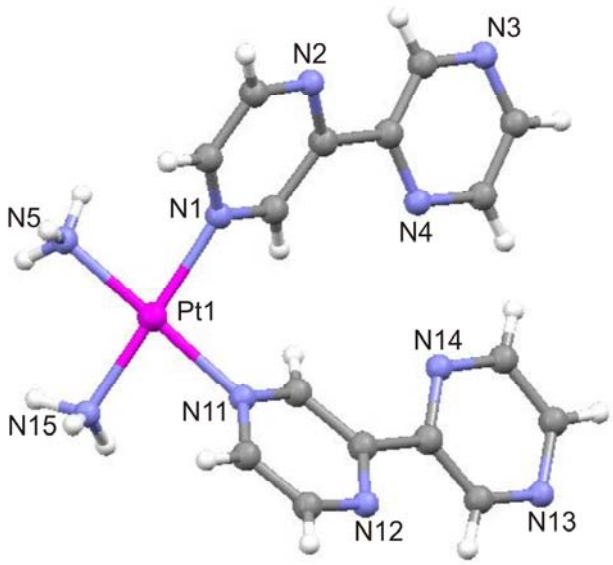

Figure 2.16 Cation structure of *cis*-[Pt(NH$_3$)$_2$(bpz-*N4*)$_2$]$^{2+}$ (**II-5**) with atom numbering scheme. Note that the atom numbering scheme does not conform to the usual one.

Table 2.5 Selected bond lengths (Å) and angles (deg.) for **II-5**.

cis-[Pt(NH$_3$)$_2$(bpz-*N4*)$_2$] (**II-4**)			
Pt1–N1	2.053(10)	N15-Pt1-N5	90.8(4)
Pt1–N5	2.011(10)	N15-Pt1-N1	179.2(4)
Pt1–N11	2.058(11)	N5-Pt1-N1	90.0(4)
Pt1-N15	1,983(11)	N1-Pt1-N11	89.3(4)
		N15-Pt1-N11	90.0(4)
		N5-Pt1-N11	179.2(4)

The pz planes are tilted with respect to the PtN$_4$ plane with angles of 52.8^o and 53.0^o. Twist angles between two halves of 2,2´-bpz rigs are of 24.5^o and 24.1^o are. The tendency of aromatic moieties of **II-5** to stack leads to formation of infinite columnar assemblies in the solid state. The distance of face-to-face stacking is *ca*. 3.22 Å.

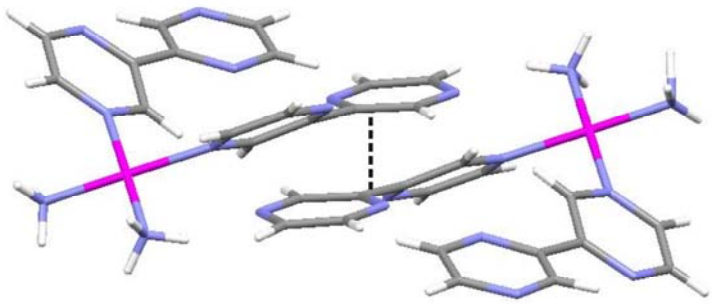

Figure 2.17 Details of π-π staking interactions between neighbouring molecules of **II-5**.

A concentration-dependant ^{1}H NMR experiment was carried out in order to obtain information about π-π stacking interactions in solution. As expected, 2,2´-bpz resonances of the non-coordinating rings (H3´ > H5´ > H6´), are involved in intermolecular stacking interactions, displaying slight upfield shifts (Δδ 0.04 – 0.02 ppm) with increasing concentrations. The other resonances remain virtually unchanged.

2.2.5.2. Reactions of "corner stone" *cis*-[Pt(NH$_3$)$_2$(bpz)$_2$](NO$_3$)$_2$ (II-5)

Reactions of the "corner stone" *cis*-[Pt(NH$_3$)$_2$(bpz)$_2$](NO$_3$)$_2$ (**II-5**) with *cis* and *trans* blocked Pt^{II} or Pd^{II} centers have been studied by ^{1}H NMR spectroscopy, giving the following findings:

a) *cis*-Pt^{II}(NH$_3$)$_2$: The ^{1}H NMR spectrum of a reaction mixture agrees with the presence of two major components in the solution: triangle and tetramer, and

thus is very similar to the one obtained from the reaction of *cis*-$Pt^{II}(NH_3)_2$ with bpz. This confirms the dynamic nature of the system.

b) $enPt^{II}$: Reaction of *cis*-$[Pt(NH_3)_2(bpz)_2](NO_3)_2$ with $enPt^{II}$ is found to form the tetramer in an initial step. In the product formed, the Pt centers alternatively have en ligands and *cis*-diammine ligands, respectively. A spectrum taken after 2d (RT) contains multiple signals. The existence of the known trianglular $[(enPtbpz\text{-}N4,N4')_3](NO_3)_6$ species suggests that dissociation into components and reassociation into closed cycles occurs continuously during this reaction and different combinations are possible.

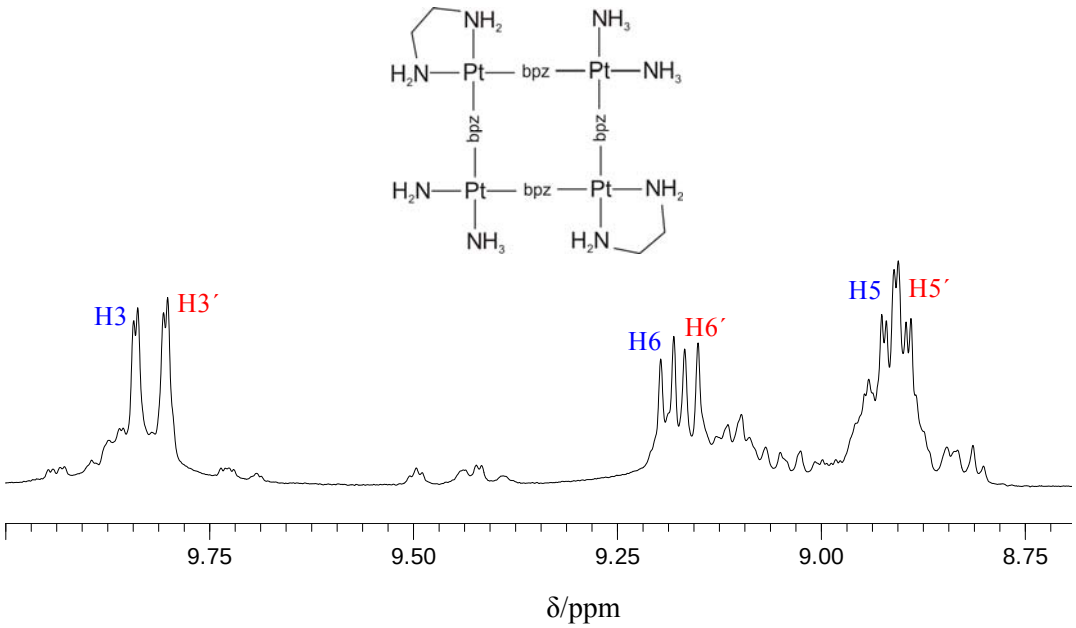

Figure 2.18 Aromatic region of the ^1H NMR spectra of the reaction between **II-5** and $[enPt(H_2O)_2]^{2+}$ after 1d at RT.

c) $enPd^{II}$: From ^1H NMR spectra, taken directly after mixing the components in a 1:1 ratio, it is evident that $enPd^{II}$ coordinates to the N1,N1´position of one of the 2,2´-bpz ligands. The intensities of the new peaks gradually decrease with time. Simultaneously peaks corresponding to $[Pd(en)(bpz)]^{2+}$ increase. Addition of a second equivalent of $enPd^{II}$ does not cause any significant changes.

d) *trans*-$Pt(NH_3)_2^{II}$: The presence of multiple signals at the beginning of the reaction suggests that the multicomponent system is not able to self-assemble. Prolonged heating leads to a broadening of peaks and formation of an insoluble light-yellow precipitate. Most likely polymeric compounds are formed. Reaction of *trans*-$[Pt(NH_3)_2(bpz)_2]^{2+}$ with *cis*-$[(NH_3)_2Pt(H_2O)_2]^{2+}$ seems to follow the same reaction pathway.

2.3 Molecular Vases

Complexes possessing deep molecular cavities are of great interest because of their ability to host neutral and charged molecules. The molecular triangles described above still contain uncoordinated nitrogen atoms at the N1,N1´ positions, which could be used to extend the structure by coordinating additional metals to them. For instance, molecular vases containing six $[enM]^{II}$ units (M = Pd^{II} or Pt^{II}) interconnected via three 2,2´-bpz ligands have been prepared and structurally characterized previously.[69] Encapsulation of anions was found to be typical for this type of compounds. The cations formed upon coordination of $enPd^{II}$ to the triangular *cis*-$[\{Pt(NH_3)_2(bpz\text{-}N4,N4')\}_3]^{6+}$ species led to the formation of structurally related molecular vases. Three of them with different counter anions have been isolated and characterized crystallographically. The volume of the cavity can be effectively enlarged upon coordination of metal entities bearing aromatic rings. Thus, attempts were made to obtain molecular vases with deeper cavities by using Pd^{II} species bearing aromatic ligands such as *o*-phenylenediamine (pda), dipyridylketon (dpk) and bis(pyrazol-1-yl)propane (bipzp).

2.3.1 Synthesis and spectroscopic characterization of $[\{(NH_3)_2Pt(N4,N4'\text{-}bpz\text{-}N1,N1')Pd(en)\}_3]^{12+}$ with NO_3^- (II-6), SO_4^{2-} (II-7) and NO_3^--PF_6^- (II-8) as counter anions

The syntheses of molecular vases were accomplished in two steps. In the first step triangular species have been obtained by reacting *cis*-$[Pt(NH_3)_2(H_2O)_2]^{2+}$ with bpz in 1:1 ratio. Taking into consideration that higher temperature promotes formation of entropy-favored triangles, reactions were carried out at 80°C. In the second step, upon coordination of $enPd^{II}$ to the N1,N1´positions of bpz ligands, the desired molecular vases were formed. Reactions leading to the Pt_3Pd_3 vases were accompanied by the color change from pale-orange to dark red-brownish. The stoichiometry of Pt_3Pd_3 creates a framework charge of +12, which is balanced by twelve NO_3^- anions for the compound **II-6**, six SO_4^{2-} anions for the compound **II-7,** and one NO_3^- and eleven PF_6^- for the compound **II-8**.

The ^1H NMR data for the complexes have been obtained by dissolving the respective crystals in D_2O and are summarized in Table 2.6. ^1H NMR spectra consist of three characteristic peaks which are compatible with the presence of highly symmetrical structures

and are indicative of a single product being present in solution. As expected, 2,2´-bpz signals of the Pt_3Pd_3 vases are downfield shifted with respect to the triangular species **II-2** and **II-3**.

Table 2.6 ^{1}H NMR data for the compounds **II-6**, **II-7** and **II-8** (D_2O, 300 MHz, pD = 5.9 – 6.4)

Proton	**II-6**	**II-7**	**II-8**
CH_2	s, 2.97	s, 2.96	s, 2.95
H5,H5´	d, 8.82 $^3J_{5,6}$ = 3.9 Hz	d, 8.81 $^3J_{5,6}$ = 3.9 Hz	d, 8.80 $^3J_{5,6}$ = 3.9 Hz
H6,H6´	d, 9.82 $^3J_{5,6}$ = 3.9 Hz	9.81 $^3J_{5,6}$ = 3.9 Hz	9.80 $^3J_{5,6}$ = 3.9 Hz
H3,H3´	s, 10.64	s, 10.88	s, 10.61

2.3.2 Crystal structures of molecular vases

The molecular structures of **II-7, II-8** and **II-9** have been determined by X-ray diffraction studies, which confirmed the proposed composition. 2,2´-bpz behaves as μ_2-bridging ligand to coordinate to Pt(II) centers through N4,N4´nitrogen atoms and as a chelating ligand for Pd(II) centers (Figure 2.19).

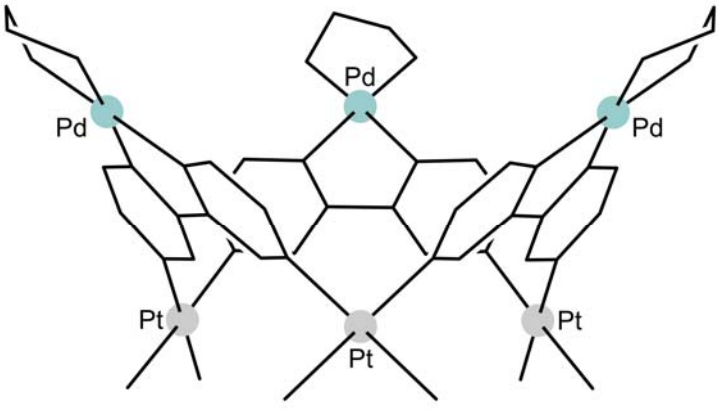

Figure 2.19 View of hexanuclear cation $\{[(NH_3)_2Pt(bpz)Pd(en)]_3\}^{12+}$.

Three Pt atoms form an equilateral triangle at the bottom of the vase and three Pd atoms from a triangle on top of it. Pt-Pt and Pd-Pd distances for **II-6** and **II-7** are compiled in the Table 2.7.

Table 2.7 Selected bond lengths (Å) and angles (deg.) for **II-6a**, **II-6b** (asymmetric unit of **II-6** contains two independent cations) and **II-7**.

$\{[(NH_3)_2Pt(bpz)Pd(en)]_3\}^{12+}$	**II-6a**	**II-6b**	**II-7**
Pt1-Pt2	7.9513(10)		8.0002(6)
Pt1-Pt3	7.8086(10)		7.9593(6)
Pt2-Pt3	7.6886(8)		7.9409(6)
Pt4-Pt5		7.7800(9)	
Pt4-Pt6		8.0011(10)	
Pt5-Pt6		8.0170(11)	
Pd1-Pd2	9.3070(23)		9.6933(13)
Pd1-Pd3	10.2409(22)		9.7769(13
Pd2-Pd3	9.5353(20)		9.2835(14)
Pd4-Pd5		8.5675(22)	
Pd4-Pd6		9.2660(24)	
Pd5-Pd6		8.8993(20)	

With respect to platinum and palladium geometries, no significant differences could be seen. Detailed structural features of these molecular vases are discussed below, whereas anion binding properties of them are summarized in Chapter 6.

2.3.2.1 Crystal structure of $\{(NO_3)_2\subset[(NH_3)_2Pt(bpz)Pd(en)]_3\}(NO_3)_{10}$ (II-6)

The asymmetric unit of the title compound contains two independent Pt_3Pd_3 cations: **II-6a** and **II-6b**, as depicted in Figure 2.20. In both structures the pyrazine rings of the 2,2´-bpz ligands are nearly coplanar with torsion angles of pz(A)-pz(B) = 8.0°, pz(C)-pz(D) = 1.8°, pz(E)-pz(F) = 1.4°, pz(G)-pz(H) = 6.7°, pz(J)-pz(I) = 5.5°, pz(K)-pz(L) = 9.6°.

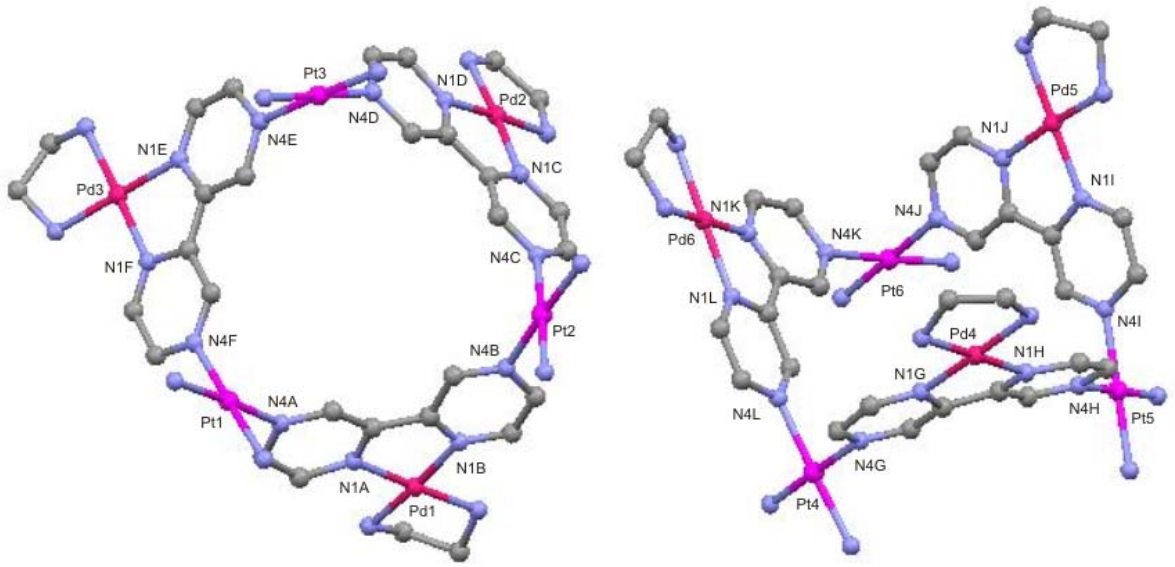

Figure 2.20 Molecular structures of two independent $\{(NO_3)_2\subset[(NH_3)_2Pt(bpz)Pd(en)]_3\}(NO_3)_{10}$ (**II-6a** and **II6b**) with numbering of relevant atoms. Hydrogen atoms are omitted for clarity.

The bond distances around Pt and Pd centers are around 2 Å (Table 2.8). The square-planar geometries of Pd(II) are distorted with N-Pd-N angles ranging from 79.6° to 99.5°, whereas N-Pt-N angles range from 87.2° to 92.9°.

Table 2.8. Selected bond lengths (Å) and angles (deg.) for **II-6**.

$\{(NO_3)_2\subset[(NH_3)_2Pt(bpz)Pd(en)]_3\}(NO_3)_{10}$ (**II-6**)			
Pt1-N4F	2.023(15)	Pd1-N1B	2.022(13)
Pt1-N4A	2.035(14)	Pd1-N1A	2.034(15)
Pt2-N4B	2.003(14)	Pd2-N1D	2.012(14)
Pt2-N4C	2.014(15)	Pd2-N1C	2.014(14)
Pt3-N4D	2.020(13)	Pd3-N1E	2.022(14)
Pt3-N4E	2.021(16)	Pd3-N1F	2.025(14)
Pt4-N4L	2.030(13)	Pd4-N1G	2.017(14
Pt4-N4G	2.045(14)	Pd4-N1H	2.040(15)
Pt5-N4H	2.030(13)	Pd5-N1I	1.987(13)
Pt5-N4I	2.040(14)	Pd5-N1J	2.012(13)
Pt6-N4J	2.001(14)	Pd6-N1L	2.011(14)
Pt6-N4K	2.072(13)	Pd6-N1K	2.012(13)
N4F-Pt1-N4A	91.7(6)	N1B-Pd1-N1A	80.6(6)
N4B-Pt2-N4C	91.2(6)	N1D-Pd2-N1C	80.0(6)
N4D-Pt3-N4E	90.6(6)	N1E-Pd3-N1F	80.8(6)
N4L-Pt4-N4G	89.5(6)	N1G-Pd4-N1H	80.4(6)
N4H-Pt5-N4I	89.1(6)	N4I-Pd5-N4I	80.0(5)
N4J-Pt6-N4K	89.2(6)	N4L-Pd6-N4K	79.6(6)

Two neighboring molecules are oriented in a way to form a container structure with a Pd1-Pd1 distance of *ca*. 6.3 Å (Figure 2.21). Intermolecular hydrogen-bond contacts occur among the ammine ligand, nitrate anions and water molecules.

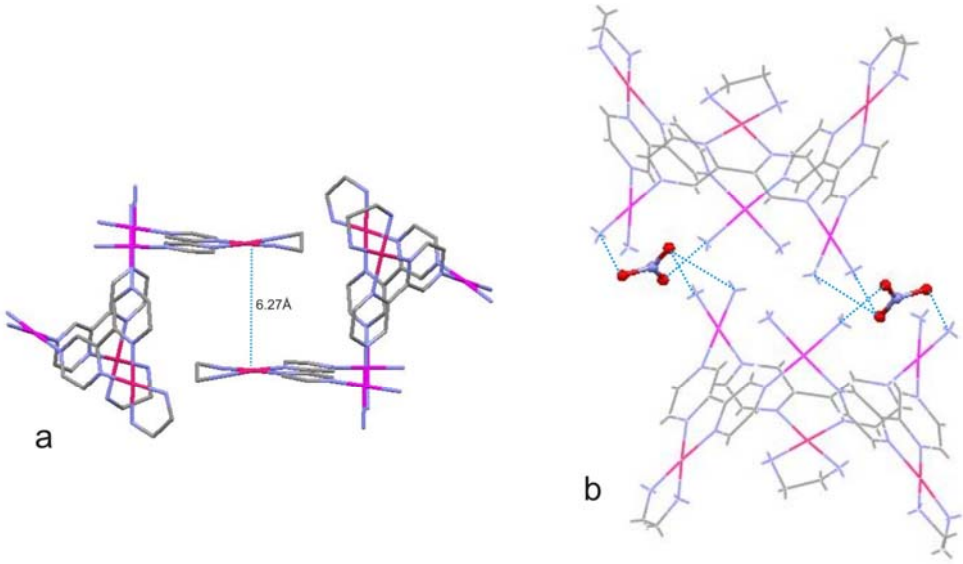

Figure 2.21 View of centrosymmetric pair of cations **II-6** (a) and hydrogen bonding interactions between cations and nitrate anions (b).

2.3.2.2 Crystal structure of $\{SO_4 \subset [(NH_3)_2Pt(bpz)Pd(en)]_3\}(SO_4)_5$ (II-7)

The sulfate salt of the molecular Pt_3Pd_3 vase has been obtained in the similar way as **II-6,** applying Ag_2SO_4 in the initial step of Cisplatin activation. The cation geometry is very similar to that of **II-6** (Figure 2.22). Selected bond lengths and angles are summarized in Table 2.9. Twist angles between two pyrazine rings are following: pz(1)-pz(2) = 3.5^o, pz(3)-pz(4) = 4.4^o, pz(5)-pz(6) = 1.2^o.

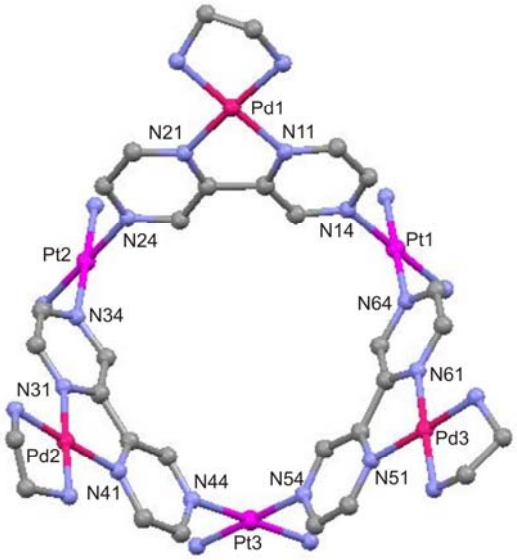

Figure 2.22 Molecular structure of cation of $\{SO_4\subset[(NH_3)_2Pt(bpz)Pd(en)]_3\}(SO_4)_5$ (**II-7**) with numbering scheme. Hydrogen atoms are omitted for clarity.

Table 2.9 Selected bond lengths (Å) and angles (deg.) for **II-7**.

$\{SO_4\subset[(NH_3)_2Pt(bpz)Pd(en)]_3\}(SO_4)_5$ (**II-7**)			
Pt1-N14	2.001(9)	Pd1-N21	1.992(10)
Pt1-N64	2.030(9)	Pd1-N11	2.012(9)
Pt2-N34	2.013(99	Pd2-N31	2.010(9)
Pt2-N24	2.022(9)	Pd2-N41	2.020(11)
Pt3-N54	2.038(10)	Pd3N61	2.017(10)
Pt3-N44	2.053(11)	Pd3-N51	2.030(10)
N14-Pt1-N64	89.3(4)	N21-Pd1-N11	80.9(4)
N34-Pt2-N24	91.3(4)	N31-Pd2-N41	80.5(4)
N54-Pt3-N44	89.4(4)	N61-Pd3-N51	80.4(4)

Similar to **II-6** two molecules of **II-7** form a container structure in the solid state. Pd3-Pd3 distances are in this case slightly longer and equal to *ca.* 7.5Å (Figure 2.23, a). In the very similar way, two molecules of **II-7** are connected via hydrogen bonds through SO_4^{2-} anions (Figure 2.23, b).

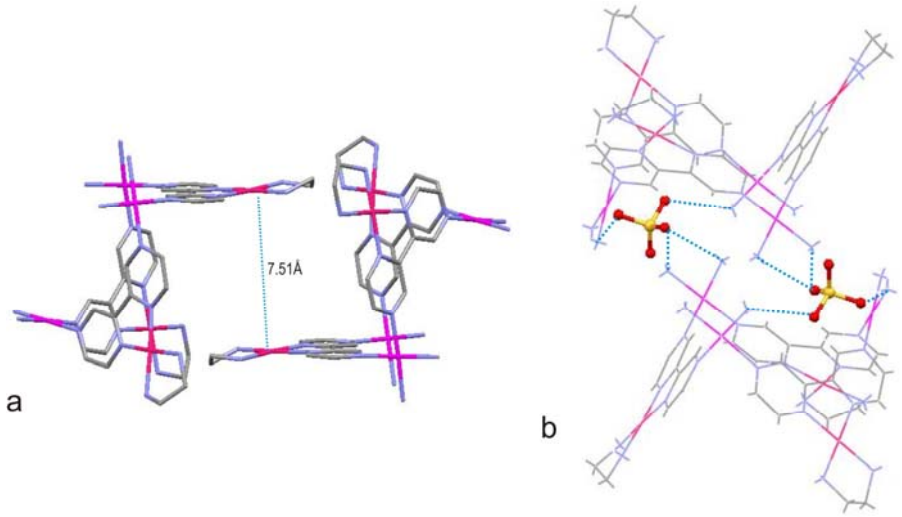

Figure 2.23 View of centrosymmetric pair of cations **II-7** (a) and hydrogen bonding interactions between cations and sulfate anions (b).

2.3.2.3 Preliminary crystal structure of $\{PF_6\subset[(NH_3)_2Pt(bpz)Pd(en)]_3\}(PF_6)_{10}(NO_3)$ (II-8)

Single crystals of a mixed NO_3^--PF_6^--salt of the molecular Pt_3Pd_3 vase have been obtained by dissolving **II-7** in water and recrystallising it in the presence of an excess $NaNO_3$ and NH_4PF_6. Molecular structure of $\{PF_6\subset[(NH_3)_2Pt(bpz)Pd(en)]_3\}(PF_6)_{10}(NO_3)$ (**II-8**) is similar to those of **II-6** and **II-7**.

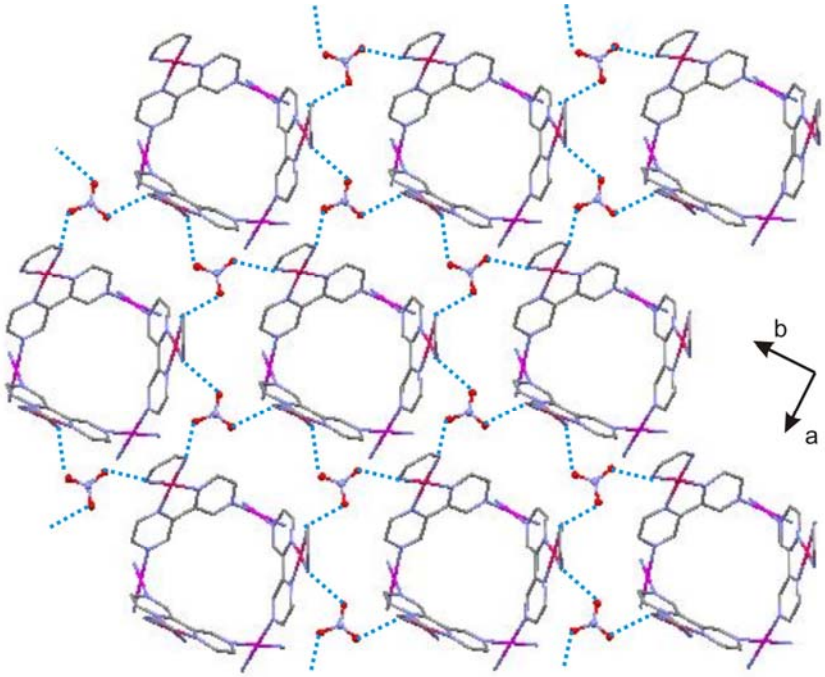

Figure 2.24 Hydrogen bonding interactions between cations of **II-8** and nitrate anions resulting in the formation of 2D layers in solid state.

The crystal structure of **II-8** shows a packing pattern that differs from that of the previous two cases, with 2D layers formed by the hydrogen bonding between amine groups of ethylenediamine ligand and NO_3^- anions (Figure 2.24). 2D layers assemble along a and along b axis.

2.3.3 Building blocks for extended structures (towards deeper cavities)

The hexanuclear vases described above have been prepared starting from Pt3 triangles. Analogous structure could also be obtained by bridging three mononuclear $[(L1)M1(2,2'\text{-bpz})]^{2+}$ entities via three $[(L2)M2(H_2O)]^{2+}$ ions. Using this method several combination (L1 = L2 = en, M1 and M2 Pt(II) or Pd(II)) have been prepared and structurally characterized.[70] The two synthetic routes are shown in Scheme 2.4.

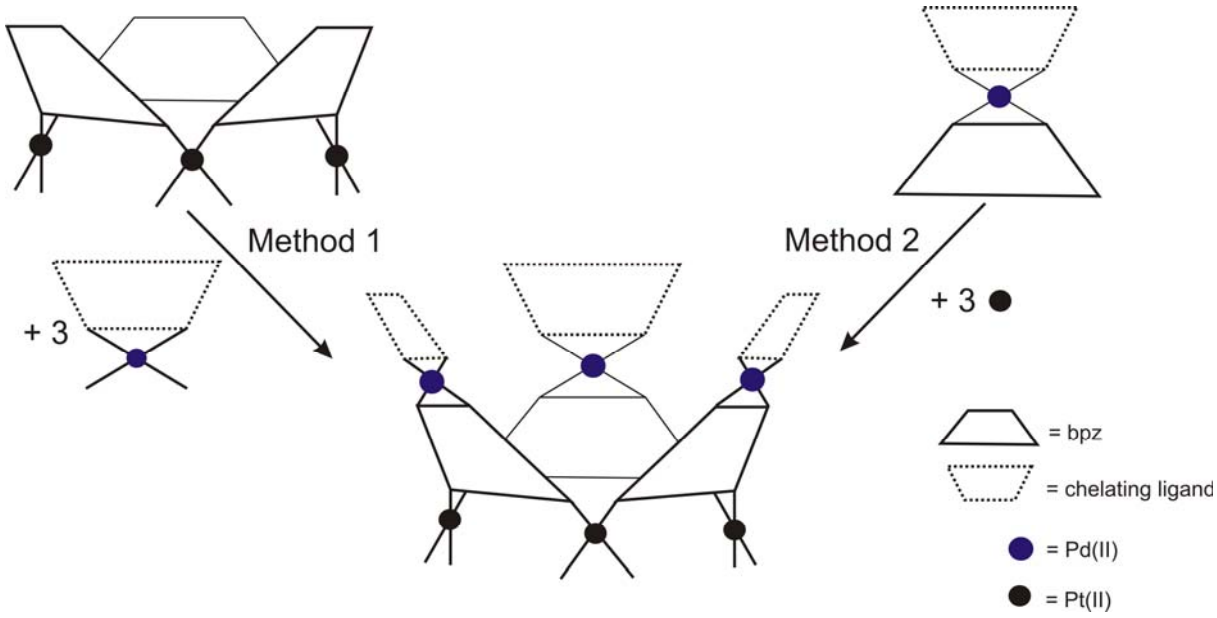

Scheme 2.4 A schematic representation of the formation of the molecular vase using two strategies.

With the aim to obtain molecular vases with deeper cavities using method 2, mononuclear species $[(L1)M1(2,2'\text{-bpz})]^{2+}$, where L1 is *o*-phenylenediamine (*o*-pda), dipyridylketon (dpk) or bis(pyrazol-1-yl)propane (bipzp), have been prepared and structurally characterized. Besides, these mononuclear species have still available N4,N4´ coordination sites which could be used to obtain higher order structures. For instance, combination of

$[Pd(en)(2,2'\text{-bpz})]^{2+}$ with *trans*-$[Pt(NH_3)_2(H_2O)_2]^{2+}$ yielded a flat triangle with Pd(II) at the corners and Pt(II) in the middle of the sides of the triangle.[71] With $AgClO_4$, mononuclear $[Pd(en)(2,2'\text{-bpz})]^{2+}$ cations arrange into an infinite loop architecture (meso helix).[72]

2.3.3.1 Mononuclear chelates $[Pd(2,2'\text{-bpz})(o\text{-pda})](NO_3)_2$ (II-9) and $[Pd(o\text{-pda})_2](NO_3)_2$ (II-10)

The complex **II-9** could be obtained by two ways: a) reacting $[(o\text{-pda})Pd(H_2O)_2]^{2+}$ with 2,2'-bpz at RT, for 1d or b) reacting $[(2,2'\text{-bpz})Pd(H_2O)_2]^{2+}$ with *o*-pda under similar conditions. In both cases the ^{1}H NMR spectra show formation of symmetrical species. Peaks corresponding to *o*-pda and 2,2'-bpz ligands are downfield shifted as a consequence of palladium complexation and occur at 9.85 ppm (d, H3, $^4J_{3,5}$ = 1.2 Hz), 9.17 ppm (d, H6, $^3J_{6,5}$ = 3.3 Hz) and 8.69 ppm (dd, H5, $^4J_{5,3}$ = 1.2 Hz, $^3J_{6,5}$ = 3.2 Hz) for the 2,2'-bpz, as well as at 7.36 ppm (m, H3´ and H4´) for the *o*-pda ligand.

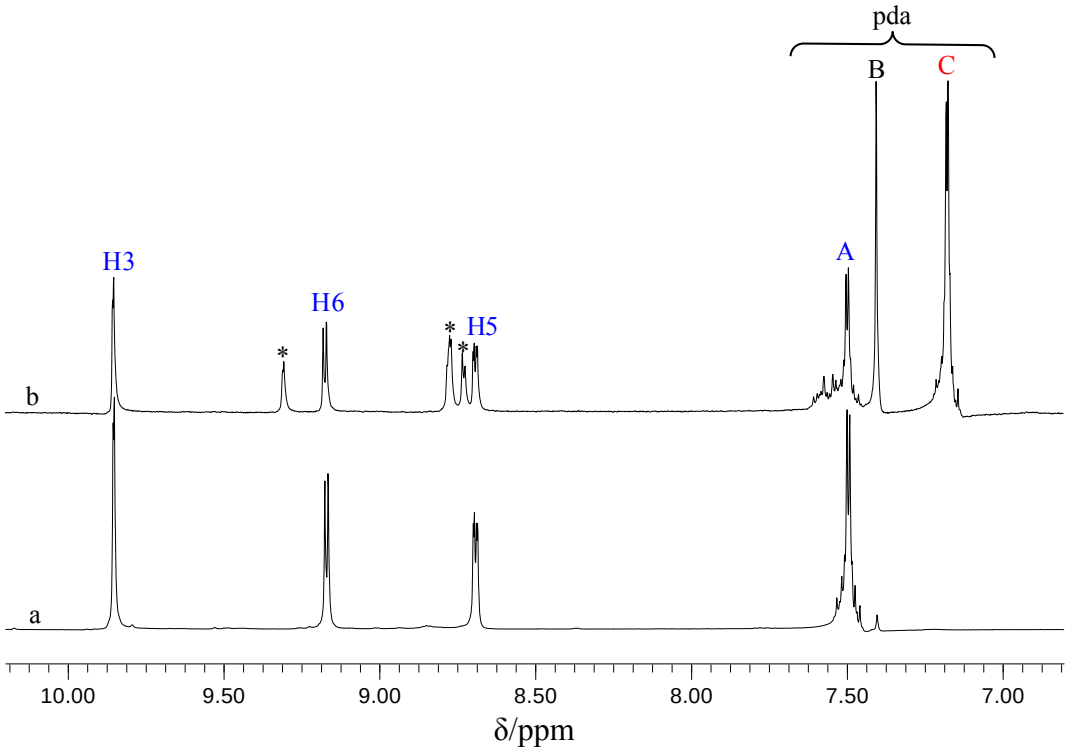

Figure 2.25 ^{1}H NMR spectra (D_2O, 300 MHz) of reaction of $[(o\text{-pda})Pd(H_2O)_2]^{2+}$ with 2,2´-bpz (a) and reaction of $[(2,2'\text{-bpz})Pd(H_2O)_2]^{2+}$ with *o*-pda (b).

In the ^{1}H NMR spectra of the reaction mixture carried out in the second way, several additional peaks are present (Figure 2.25, b). The peaks at 9.31, 8.77 and 8.72 ppm are

assigned to the free 2,2'-bpz. The singlet at 7.40 ppm (marked B in the spectra) is due non-exchaned NH_2 protons and finally, the doublet at 7.17 ppm (marked C in specrum (b)) is assigned to $[Pd(o\text{-pda})_2](NO_3)_2$ (**II-10**).

The molecular structure of **II-9** consists of discrete mononuclear units, with 2,2'-bpz and *o*-pda ligands chelated to the Pd1 center. The complexation of Pd(II) to the N1,N1´ rather than to N4,N4´ nitrogens of 2,2'-bpz was shown before[63] and is due to faster reaction kinetics of Pd(II) and consequently due to formation of a thermodynamically more stabile product. The small bite-angle of ligands results in a distortion of the square-planar geometry around Pd1 (N-Pd-N angles range from 81.1° to 98.1°). Selected bond distances and angles are given in Table 2.11.

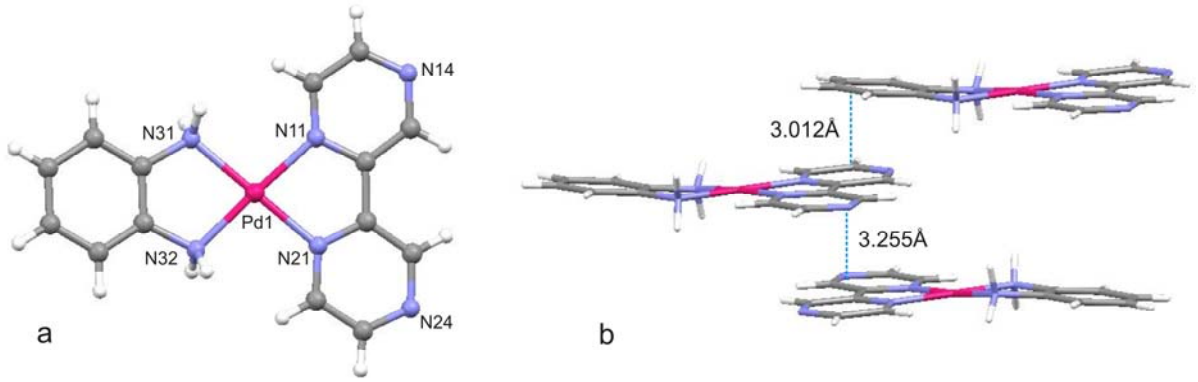

Figure 2.26 Cation structure of $[Pd(2,2'\text{-bpz})(pda)]^{2+}$ (**II-9**) with atomic numbering scheme (a) and π-π stacking interactions between neighbouring molecules (b).

In the solid state intermolecular stacking of 2,2´-bpz and *o*-pda ligands is evident, with ring centroid – plane separations of 3.01 Å and 3.26 Å, suggesting significant π–π interactions.

Several modes of decomposition of complexes containing *o*-pda ligand are known from the literature.[73,74] 2,3-diaminophenazine is a common product of the oxidation of *o*-phenylenediamine in the presence of transition metal ions.[75] Furthermore, these complexes are unstable in alkaline solution. As was shown, they are very sensitive towards oxidation to give strongly colored *o*-benzoquinonediimine complexes.[76]

From a NMR-scale reaction carried out by the second way, small amounts of dark-red crystals were isolated. Single-crystal X-ray diffraction analysis showed it to be a mononuclear Pd(II) complex bearing two *o*-pda ligands. The structure of the cation is shown in Figure 2.27.

Values of Pd-N bond distances and N-Pd-N angles are similar to those observed in the complex **II-9** (Table 2.10).

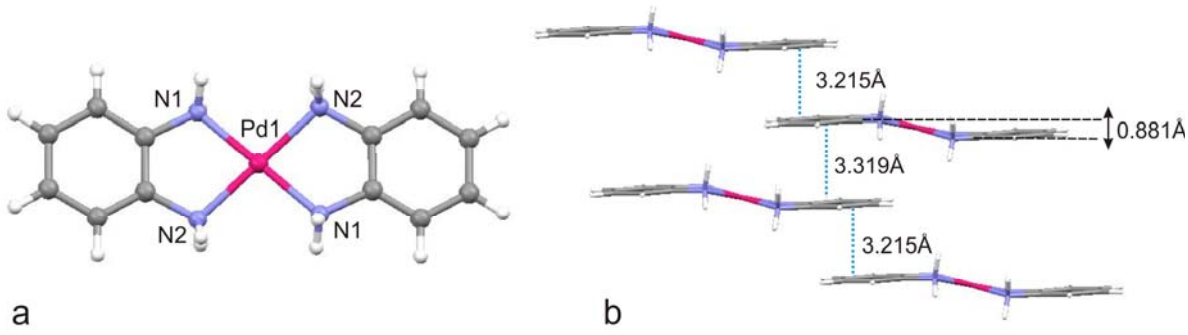

Figure 2.27 Molecular structure of $[Pd(o\text{-pda})_2]^{2+}$ (**II-10**) with atomic numbering scheme (a) and π-π stacking interactions between neighboring molecules (b).

In the solid state **II-10** exhibits similar π–π interactions within columns of *o*-pda units, with centroid – plane separations of 3.22 Å and 3.32 Å. The two chelated *o*-pda ligands are not coplanar. Rather, they are oriented in parallel planes above and below the Pd center with an interplane distance of *ca.* 1 Å and make an angle of 16.1° with the PdN_4 coordination plane.

Table 2.10 Selected bond lengths (Å) and angles (deg.) for **II-9** and **II-10**.

$[Pd(2,2'\text{-bpz})(o\text{-pda})](NO_3)_2$ (**II-9**)			
Pd1-N11	2.017(2)	N11-Pd1-N31	96.82(8)
Pd1-N31	2.018(2)	N11-Pd1-N32	175.98(8)
Pd1-N32	2.021(2)	N31-Pd1-N32	83.97(8)
Pd1-N21	2.023(2)	N11-Pd1-N21	81.09(8)
		N31-Pd1-N21	177.90(8)
		N32-Pd1-N21	98.12(8)
$[Pd(o\text{-pda})_2](NO_3)_2$ (**II-10**)			
Pd1-N1	2.027(2)	N1-Pd1-N1	180.00(8)
Pd1-N2	2.026(2)	N2-Pd1-N1	83.94(8)
		N1-Pd1-N2	96.06(8)

Structural and spectroscopic features of similar complexes containing substituted *o*-phenylenediamine ligands and divalent transition metal ion (Ni, Pt, Pd) reveal that as a result of redox reactions in air in a presence of a base, the electronic structure of the resulting compounds are best described as singlet diradicals: $[M^{II}(L)_2]$ S = 0 (L = N,N-coordinated π radical anion).[77]

2.3.3.2 Mononuclear chelate [Pd(2,2'-bpz)(bipzp)]$(NO_3)_2$ (II-11)

Reaction of equimolar amounts of $[(bipzp)Pd(H_2O)_2]^{2+}$ with 2,2´-bpz at RT, for 1d yields mononuclear chelate $[Pd(2,2'\text{-bpz})(bipzp)](NO_3)_2$ (**II-11**).

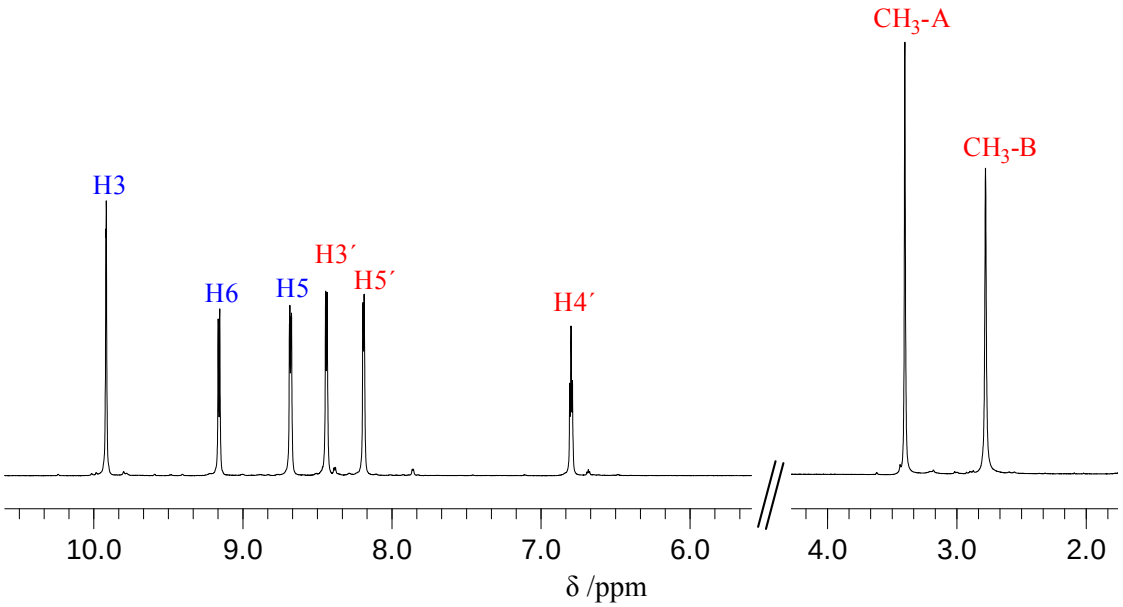

Figure 2.28 ^{1}H NMR spectrum (D_2O, 300 MHz) of $[Pd(2,2'\text{-bpz})(bipzp)](NO_3)_2$ (**II-11**).

The ^{1}H NMR spectrum of the isolated compound (Figure 2.28) displays three characteristic peaks for the 2,2´-bpz ligand, which occur at 9.92 ppm (d, H3, $^3J_{3,5}$ = 0.9 Hz), 9.16 ppm (d, H6, $^3J_{6,5}$ = 3.3 Hz) and 8.68 ppm (dd, H5, $^4J_{5,3}$ = 0.9 Hz, $^3J_{6,5}$ = 3.3 Hz). The bipzp ligand displays peaks at 8.44 ppm (d, H3´, $^3J_{3,4}$ = 2.7 Hz), 8.19 ppm (d, H5´, $^3J_{5,4}$ = 2.4 Hz) and 6.80 ppm (dd, H4´) in the aromatic region and two singlets at 3.40 ppm and 2.78 ppm in the aliphatic region for methylene protons. The doubling of methyl resonances is due to non-equivalent environments of the two groups.

The complex crystallizes with three molecules of water. A perspective view of **II-11** with the atom numbering scheme is given in Figure 2.29, and selected bond lengths and angles are listed in Table 2.11. Similar to the previous case, Pd is coordinated to N1,N1´ nitrogens of 2,2´-bpz. The distortion in the square planar geometry can be seen in the values of the bond angles around the metal. Thus, N-Pd-N angles are in between 80.3° and 97.4°.

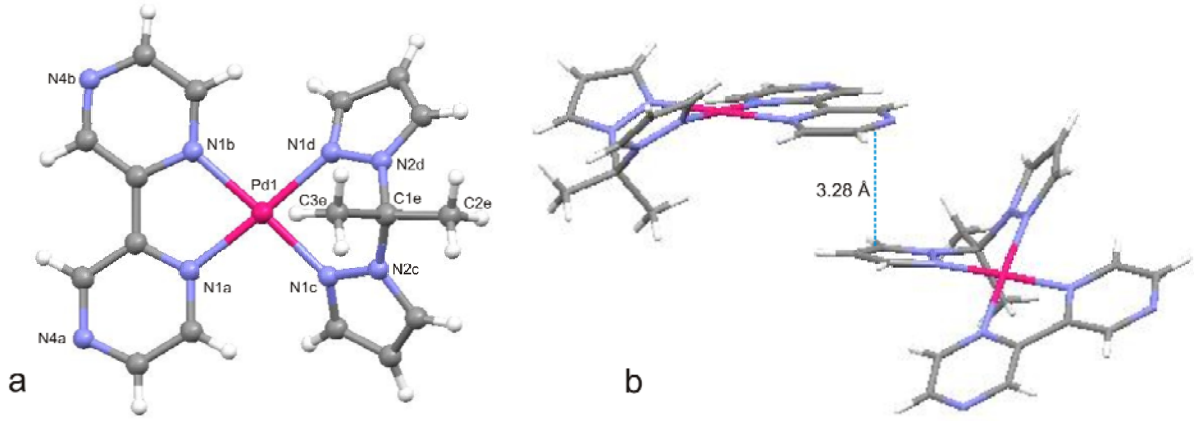

Figure 2.29 Cation structure of $[Pd(2,2'\text{-bpz})(bipzp)]^{2+}$ (**II-11**) with atomic numbering scheme (a) and π-π stacking between two neighboring molecules in the crystal lattice (b).

While the two pyrazine rings of 2,2´-bpz are nearly coplanar (pz(A)-pz(B) = 5.7°), the dihedral angle between two pyrazole rings is 118.7° and is consequently larger than expected for the sp^3 hybridized C(1e) atom. The proton of one of the two methyl groups of the 2,2'-bis(pyrazol-1-yl)propane ligand interacts with the metal center with a C(3e) ···Pd1 distance of 3.21 Å, while the other one is pointing out to the opposite direction. This non-equivalence of two methyl groups is consistent with the ^{1}H NMR spectrum.

Table 2.11 Selected bond lengths (Å) and angles (deg.) for **II-11**.

$[Pd(2,2'\text{-bpz})(bipzp)](NO_3)_2$ (**II-11**)			
Pd1-N1D	2.000(3)	N1D-Pd1-N1C	85.00(14)
Pd1-N1C	2.003(3)	N1D-Pd1-N1A	177.58(14)
Pd1-N1A	2.017(3)	N1C-Pd1-N1A	97.42(14)
Pd1-N1B	2.027(3)	N1D-Pd1-N1B	97.29(14)
		N1C-Pd1-N1B	177.71(14)
		N1A-Pd1-N1B	80.29(14)

2.3.3.2 Mononuclear chelate $[Pd(2,2'\text{-bpz})(dpk\cdot H_2O)](NO_3)_2$ (II-12)

The mononuclear Pd complex containing the dpk·H_2O ligand has been prepared analogously to the previous complexes.

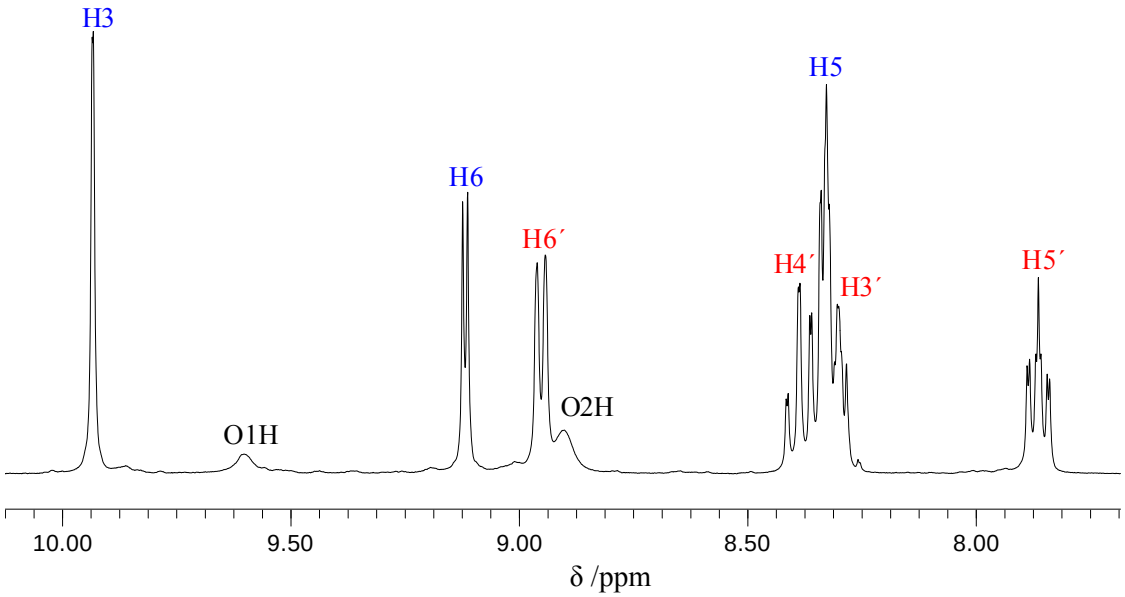

Figure 2.30 ^{1}H NMR spectra (D_2O, 300 MHz) of [Pd(2,2'-bpz)(dpk·H_2O)](NO_3)$_2$ (**II-12**).

In the ^{1}H NMR spectrum of **II-12,** H3 and H6 proton signals of bpz appear at 9.93 ppm (d, H3, $^{3}J_{3.5}$ = 0.6 Hz) and 9.12 ppm (d, H6, $^{3}J_{6,5}$ = 3.3 Hz). The signal corresponding to H5 protons overlaps with the H3´proton signals of the dpk ligand and appears as a multiplet at *ca.* 8.33 ppm. Other signals corresponding to pyridine ring of dpk appear at 8.95 ppm (d, H6´, ^{3}J = 5.4 Hz), 8.39 ppm (dd, H4´, ^{3}J = 7.8 Hz and ^{4}J = 1.5 Hz) and 7.86 ppm (ddd, H5´,^{3}J = 7.5 Hz; ^{3}J = 6 Hz; ^{4}J = 1.8 Hz). Addition of nucleophiles such as water to the dpk ligand is known to give its hydrated *gem*-diol form dpk·H_2O.[78] Low intensity peaks of OH groups appear at 9.60 ppm (s, O1H) and 8.90 ppm (s, O2H).

As in the case of the *o*-pda ligand, the symmetrization reaction takes place during the synthesis of **II-12**. Previously described[79] crystals of [Pd(dpk)$_2$]$^{2+}$ have been formed within 1d at RT, whereas crystals of **II-12** have been obtained after *ca.* one week.

A view of the cation is depicted in Figure 2.31 and some selected bond angles and distanced are listed in Table 2.12.

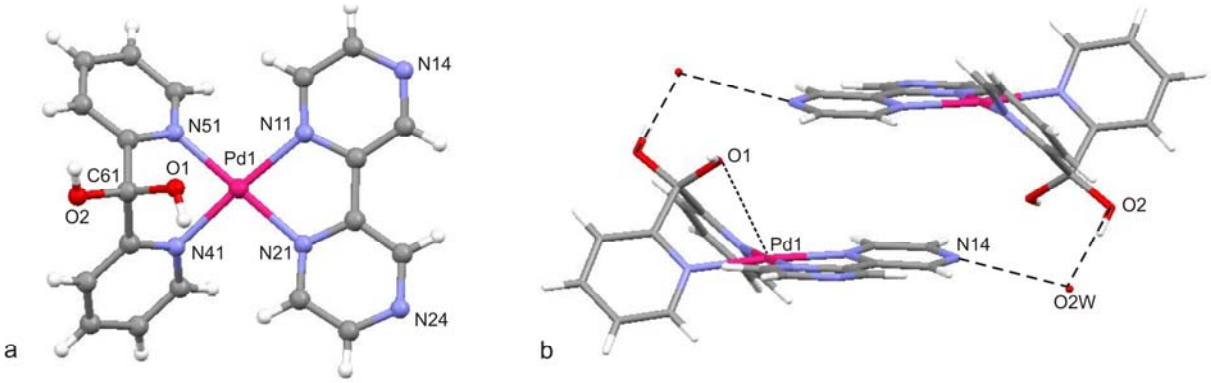

Figure 2.31 Cation structure of $[Pd(2,2'\text{-bpz})(dpk\cdot H_2O)]^{2+}$(**II-12**) with atom numbering scheme (a) and hydrogen bonding interactions between two molecules (b).

Pd-N distances are in the normal range, but the coordination geometry of Pd shows a considerable distortion as evidenced by chelate bite angles N21-Pd1-N11 of 80.4° and N41-Pd1-N51 of 83.3°. Two pyridine rings of $dpk\cdot H_2O$ form an angle of 105.1°, which is slightly smaller than the ideal tetrahedral angle 109.4°, which is a consequence of the conversion of the sp^2 hybridized C atom in $dpk\cdot H_2O$ to sp^3 in $dpk\cdot H_2O$. Inspection of the structure reveals hydrogen bonding interactions between two neighboring molecules. These exist between one hydroxo group of dpk, the nitrogen atom of bpz and a water molecule with the following distances: N14···O2W, 2.95 Å and O2···O2W, 2.74 Å. There is a short contact (2.73 Å) between the second oxygen atom of dpk and Pd1, which is in agreement with the ^{1}H NMR spectrum.

Table 2.12 Selected bond lengths (Å) and angles (deg.) for **II-12**.

$[Pd(2,2'\text{-bpz})(dpk\cdot H_2O)](NO_3)_2\cdot$(**II-12**)			
Pd1-N51	2.017(3)	N51-Pd1-N41	83.32(12)
Pd1-N41	2.021(3)	N51-Pd1-N21	178.10(14)
Pd1-N21	2.022(3)	N41-Pd1-N21	97.42(13)
Pd1-N11	2.034(3)	N51-Pd1-N11	98.99(12)
O1-C61	1.395(5)	N41-Pd1-N11	175.47(13)
O2-C61	1.387(4)	N21-Pd1-N11	80.39(13)

2.3.4 Coordination behavior of mononuclear complexes

2.3.4.1 Synthesis of a molecular vase $\{[(NH_3)_2Pt(bpz)Pd(o\text{-pda})]_3\}(NO_3)_{12}$ (II-13)

Method 1 and method 2 (Scheme 2.4) have been used for the construction of the molecular vase $\{[(NH_3)_2Pt(bpz)Pd(o\text{-pda})]_3\}^{12+}$. NMR scale reaction between $[Pt_3(bpz)_3]^{6+}$ triangle and $[(o\text{-pda})Pd(H_2O)_2]^{2+}$ in 1:1.5 stoichiometry shows formation of the desired molecular vase. ^{1}H NMR spectra reveal downfield shifted 2,2´-bpz signals at 10.77 ppm (s, H3,H3), 9.97 ppm (d, H6,H6´, $^3J_{6,5}$ = 3.9 Hz) and 9.02 ppm (d, H5,H5´, $^3J_{6,5}$ = 3.6 Hz), indicative of the coordination of Pd(II) to the N1,N1´positions of the 2,2´-bpz. The peak for the *o*-pda ligand appear at 7.43 ppm for NH protons and 7.47 – 7.52 ppm for aromatic ring.

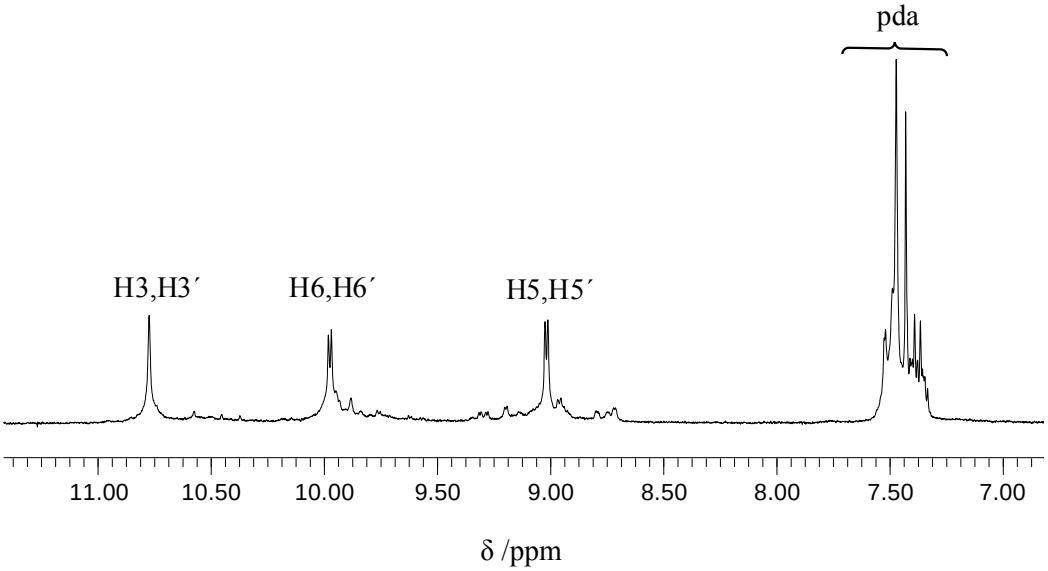

Figure 2.32 ^{1}H NMR spectrum (D_2O, 300 MHz) of $\{[(NH_3)_2Pt(bpz)Pd(o\text{-pda})]_3\}(NO_3)_{12}$ (**II-13**).

Attempt to obtain the molecular vase by Method 2 was not successful. The ^{1}H NMR spectrum of products formed displays multiple signals. Probably due to the prolonged reaction time required for formation of the Pt(II) triangle, the mononuclear complex [Pd(2,2'-bpz)(*o*-pda)]$(NO_3)_2$ decomposes to some extent, resulting in the formation of a mixture.

2.3.4.2 Reactions of $[Pd(en)(bpz)]^{2+}$ with $AgNO_3$ and $AgPF_6$

In order to fully understand the coordination behavior of mononuclear complexes, reaction between $[Pd(en)(bpz)]^{2+}$ with $AgNO_3$ and $AgPF_6$ salts have been studied. The role

that counter ion can play in the formation of supramolecular metal coordination compounds and in particular those of Ag^{+},[80] is well known. As have been shown in our group before, $[Pd(en)(2,2´\text{-bpz})]^{2+}$ and $AgClO_4$ arrange into an infinite loop structure ("meso-helix") of Pd,Ag stoichiometry.[72] Here, the influence of NO_3^- and PF_6^- anions on the formation of the structure have been studied.

The mononuclear Pd complex was prepared as previously described.[63] Crystals of $[\{Pd(en)(2,2´\text{-bpz})\}_2Ag](NO_3)_5$ (**II-14**) were obtained upon addition of $AgNO_3$ to an aqueous solution of $[Pd(en)(2,2´\text{-bpz})](NO_3)_2$ in 1:1 ratio and subsequent crystallization. Even at high concentration of silver salt only formation of trinuclear **II-14** has been observed under the conditions applied. For the formation of the corresponding PF_6-salt, $[Pd(en)(2,2´\text{-bpz})](NO_3)_2$ was first converted to the PF_6^--salt by passing its aqueous solution over an anion exchange column conditioned with KPF_6. Slow evaporation of the solution at RT resulted in the formation of crystalline $[Pd(en)(2,2´\text{-bpz})](PF_6)_2$ (**II-15**). Upon cocrystallization of **II-15** with $AgPF_6$ in 1:1 ratio, small light yellow crystals were isolated, which were, however, not suitable for X-ray analysis. The composition of the resulting microcrystalline product was established by elemental analysis, revealing a $\{[Pd(en)(2,2´\text{-bpz})\ Ag](PF_6)_3\}_n$ (**II-15a**) composition.

Because Ag-N(bpz) bonds are labile in solution, the ^{1}H NMR spectrum of the resulting mixed-metal complexes displays only peaks corresponding to the mononuclear Pd complex. They occur at 9.78 ppm (s, H3,H3´), 9.10 ppm (d, H6,H6´, $^3J_{6,5}$ = 3 Hz), 8.59 ppm (d, H5,H5´, $^3J_{6,5}$ = 2.7 Hz) for 2,2´-bpz and at 3.05 ppm (s, CH_2) for ethylenediamine ligand.

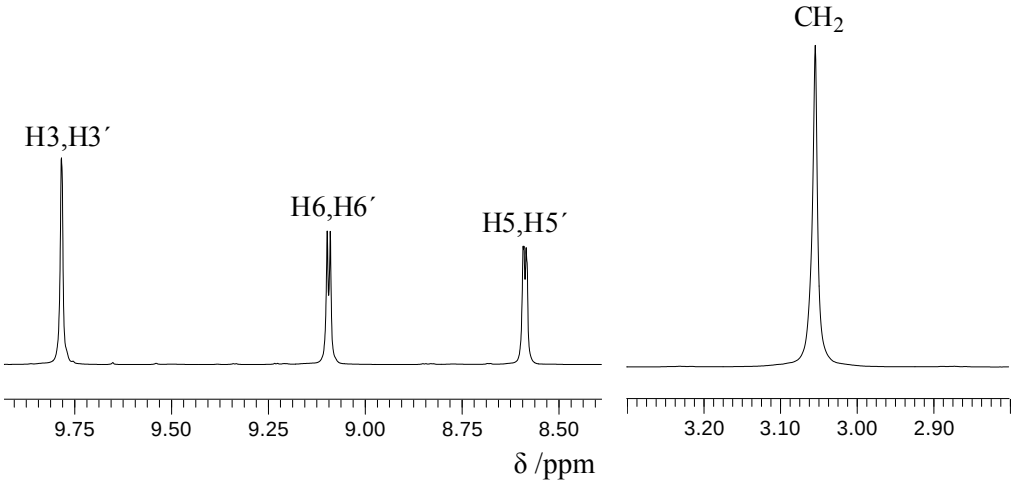

Figure 2.33 ^{1}H NMR spectrum (D_2O, 300 MHz) of $[Pd(en)(2,2´\text{-bpz})](PF_6)_2$ (**II-15**).

2.3.4.3 Crystal structure of discrete trinuclear [{Pd(en)(2,2′-bpz)}$_2$Ag](NO$_3$)$_5$ (II-14)

The projection of the molecule with the atomic numbering scheme is presented in Figure 2.34 and the relevant bond distances and bond angles are listed in Table 2.13. The square-planar paladium(II) atom is chelated by ethylenediamine ligand and 2,2′-bpz at N1,N1′ positions. Two such units are linked via Ag^+ ion being coordinated at N4 positions of the 2,2′-bpz. The coordination geometry about Ag^+ is linear (N1-Ag-N3 = 176.7°), and the two Pd(en)(2,2′-bpz) entities adopt a *head-tail* orientation. The N4′ position of the ligand is uncoordinated.

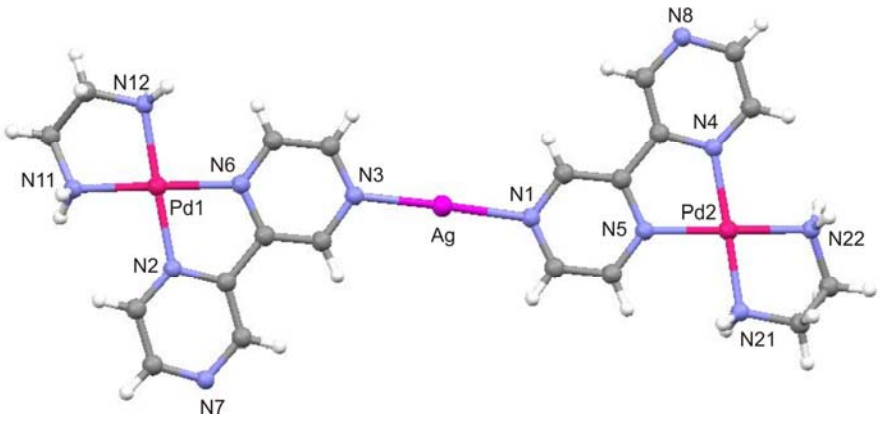

Figure 2.34 Cation structure of [{Pd(en)(2,2′-bpz)}$_2$Ag]$^{5+}$ (**II-14**) with atom numbering scheme. Note that the atom numbering scheme does not conform to the usual one.

Distances between metal centers are as follows: Pd1···Ag1, 6.9760(21) Å; Pd2···Ag1, 6.9831(21) Å; Pd1···Pd2, 13.9581(42) Å. Metal cations of **II-14** are arranged in form of interpenetrated parallel layers. Weak interactions between nitrate anions and uncoordinated nitrogens of 2,2′-bpz are present in the solid state (Ag1···O33, 2.73 Å; Ag1···O41, 2.77 Å; Ag1···N7, 2.97 Å; Ag1···N8, 2.90 Å).

Table 2.13 Selected bond lengths (Å) and angles (deg.) for **II-14**.

[{Pd(en)(2,2′-bpz)}$_2$Ag](NO$_3$)$_5$(**II-14**)			
Ag1-N1	2.215(2)	N1-Ag1-N3	176.70(14)
Ag1-N3	2.217(2)	N12-Pd1-N2	178.18(8)
Pd1-N12	2.0162(18)	N12-Pd1-N6	97.68(8)
Pd1-N2	2.0252(18)	N2-Pd1-N6	80.55(8)
Pd1-N6	2.029(2)	N12-Pd1-N11	83.24(8)
Pd1-N11	2.037(2)	N2-Pd1-N11	98.51(8)
Pd2-N4	2.0162(18)	N6-Pd1-N11	178.1(2)
Pd2-N21	2.0202(18)	N4-Pd2-N11	176.76(12)

Pd2-N5	2.030(2)	N4-Pd2-N5	80.77(7)
Pd2-N22	2.033(2)	N21-Pd2-N5	97.18(8)
		N4-Pd2-N22	98.95(8)
		N21-Pd2-N22	83.21(8)
		N5-Pd2-N22	177.1(2)

2.3.4.4 Crystal structure of $[Pd(en)(bpz)](PF_6)_2$ (II-15)

Figure 2.35 shows the cation $[Pd(en)(2,2´\text{-bpz})]^{2+}$ with its atomic numbering scheme. Relevant bond lengths and angles are summarized in Table 2.14. The X-ray structure determination reveals that complex **II-15** has a structure in which the 2,2´-bpz ring planes are located approximately in the Pd coordination plane (dihedral angle between pz units is very small pz(1)-pz(2) = 6.1°). In the solid state molecules are joined through hydrogen bonds between the amine protons of the ethylenediamine ligand and uncoordinated N4,N4´nitrogen atoms of 2,2´-bpz (N1···N24, 3.08 Å; N1···N14, 2.93 Å), leading to the formation of infinite chains.

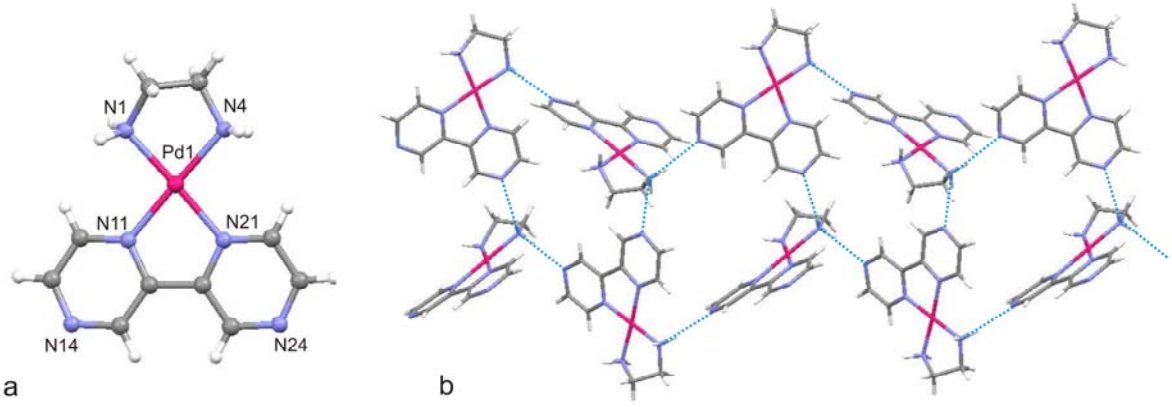

Figure 2.35 Cation structure of $[Pd(en)(2,2´\text{-bpz})](PF_6)_2$ (**II-15**) with atom numbering scheme (a) and section of the chain formed in solid state (b).

Table 2.14 Selected bond lengths (Å) and angles (deg.) for **II-15**.

$[Pd(en)(2,2´\text{-bpz})](PF_6)_2$(**II-15**)			
Pd1-N21	2.012(3)	N21-Pd1-N11	80.98(11)
Pd1-N11	2.020(3)	N21-Pd1-N4	97.48(11)
Pd1-N4	2.024(3)	N11-Pd1-N4	176.43(11)
Pd1-N1	2.027(3)	N21-Pd1-N1	178.82(11)
		N11-Pd1-N1	97.92(11)
		N4-Pd1-N1	83.60(11)

2.3.4.5 Reacting [Pd(2,2'-bpz)(bipzp)]$(NO_3)_2$ (II-11) with $AgNO_3$ and $CuSO_4$

Attempts were made to cocrystallize [Pd(2,2'-bpz)(bipzp)]$(NO_3)_2$ (**II-11**) with $AgNO_3$ and $CuSO_4$. In both instances, decomposition of the starting mononuclear complex has been observed. The ^{1}H NMR spectrum of yellow crystals isolated from the solution containing [Pd(2,2'-bpz)(bipzp)]$(NO_3)_2$ and Ag^+ ions shows only peaks corresponding to bipzp ligand (Figure 36).

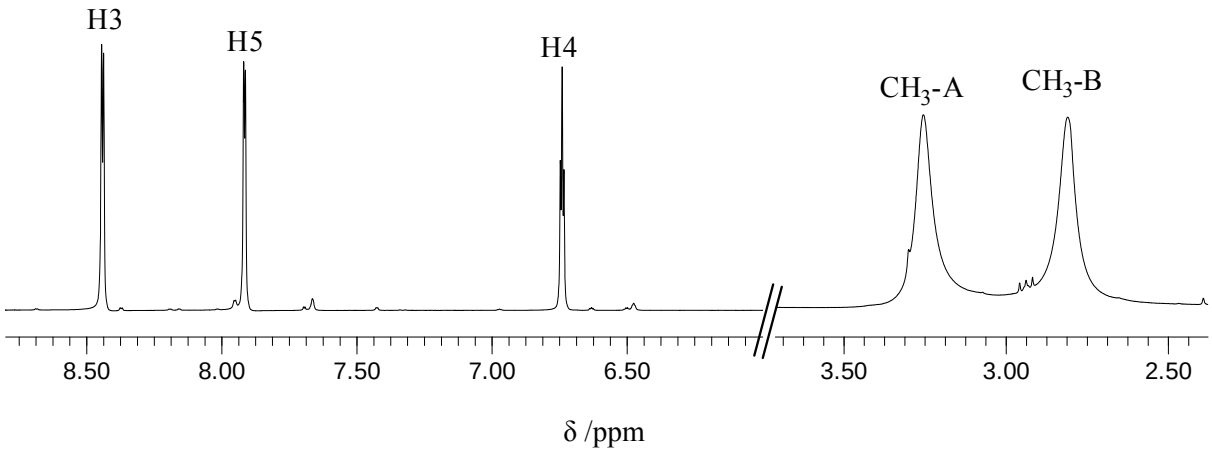

Figure 2.36 ^{1}H NMR spectrum (D_2O, 300 MHz) of *ht*-[Pd(bipzp)$_2$][Ag$(NO_3)_3(H_2O)$].

It displays peaks at 8.43 ppm (d, H3, $^3J_{3,4}$ = 2.8 Hz), 7.91 ppm (d, H5, $^3J_{5,4}$ = 2.4 Hz) and 6.73 ppm (dd, H4, $^3J_{5,4}$ = 2.4 Hz, $^3J_{3,4}$ = 2.6 Hz) in the aromatic region and two singlets at 3.25 ppm and 2.80 ppm in the aliphatic region for methylene protons. The doubling of methyl resonances is, as in the case of **II-11,** due to non-equivalent environments of the two groups.

Cocrystalization of $CuSO_4$ with [Pd(2,2'-bpz)(bipzp)]$(NO_3)_2$ (**II-11**) led to formation of blue crystals in 13% yield. Crystal structure analysis reveals formation of [Cu(2,2´-bpz)$(H_2O)_2SO_4$]. The ^{1}H NMR spectrum of the isolated product shows only broad bands as a result of the presence of paramagnetic Cu^{2+} ions.

2.3.4.6 Crystal structure of *ht*-[Pd(bipzp)$_2$][Ag$(NO_3)_3(H_2O)$] (II-16)

The solid state structure of **II-16** consists of cationic *ht*-[Pd(bipzp)$_2$]$^{2+}$ and anionic [Ag$(NO_3)_3(H_2O)$]$^{2-}$ moieties (Figure 2.37). Selected bond lengths and angles are listed in Table 2.16. Palladium center adopts the characteristic square-planar geometry with N-Pd-N angles ranging from 87.1^o to 93.4^o.

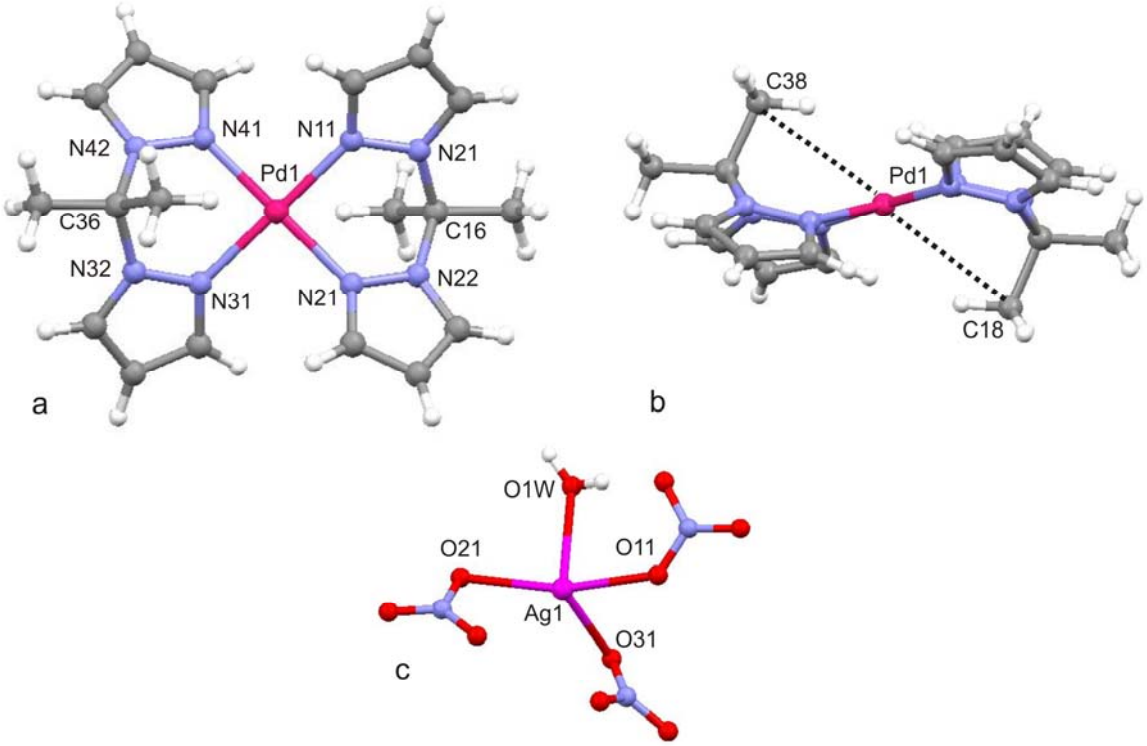

Figure 2.37 Cation structure of *ht*-$[Pd(bipzp)_2]^{2+}$ (**II-16**) with atom numbering scheme top view (a), side view (b) and coordination geometry of Ag^+ (c).

Two bipzp ligands are arranged in a *head*-to-*tail* orientation with respect to the Pd coordination plane. Angles between two pyrazole rings are *ca.* 105.9° and 107.0°. One methyl group from each ligand points towards Pd center with a distance of *ca.* 3.27 Å each. The coordination geometry about silver in **II-16** is distorted tetrahedral (Figure 2.37, c). In consist of three nitrate anions with Ag-O distances ranging from 2.33 to 2.53 Å and one water molecule with Ag-O1W equal to *ca.* 2.63 Å.

Table 2.15 Selected bond lengths (Å) and angles (deg.) for **II-16**.

ht-$[Pd(bipzp)_2][Ag(NO_3)_3(H_2O)]$ (**II-16**)			
Pd1-N11	1.981(3)	N11-Pd1-N41	92.14(13)
Pd1-N41	1.990(2)	N11-Pd1-N21	87.10(13)
Pd1-N21	1.996(2)	N41-Pd1-N21	178.48(13)
Pd1-N31	2.000(3)	N11-Pd1-N31	178.48(11)
Ag1-O31	2.528(3)	N41-Pd1-N31	87.36(13)
Ag1-O21	2.333(3)	N21-Pd1-N31	93.44(13)
Ag1-O11	2.392(3)	O21-Ag1-O11	150.77(8)
		O21-Ag1-O31	121.53(10)
		O11-Ag1-O31	86.96(9)

2.3.4.6 Crystal structure of [Cu(2,2´-bpz)$(H_2O)_2SO_4$] (II-17)

Crystal structure of [Cu(2,2´-bpz)SO_4] shows that coordination environment of Cu^{2+} ion consist of two nitrogen atoms from 2,2´-bpz (Cu1-N11; 2.00 Å), two oxygen atoms from sulfate anion (Cu1-O11; 2.38 Å) and two oxygen atoms from coordinated water molecules (Cu1-O; 1.95 Å). Coordination to the 2,2´-bpz occurs via N1,N1´ positions. Formed units are internally bridged through sulfate anions leading to the formation of 1D layer in solid state.

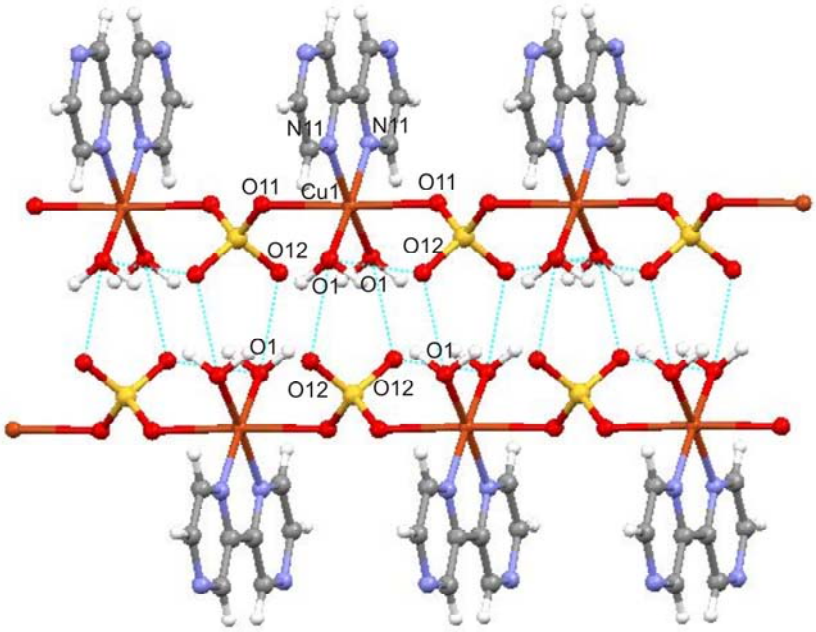

Figure 2.38 Section of the chain of [Cu(2,2´-bpz)$(H_2O)_2SO_4$] (**II-17**) formed in solid state.

Table 2.16 Selected bond lengths (Å) and angles (deg.) for **II-17**.

[Cu(2,2´-bpz)$(H_2O)_2SO_4$] (**II-17**)			
Cu1-O1	1.949(6)	O1-Cu1-O1	95.5(3)
Cu1-N11	2.002(7)	O1-Cu1-N11	91.8(3)
Cu1-O11	2.377(6)	N11-Cu1-N11	80.8(4)
		O1-Cu1-O11	88.5(2)
		N11-Cu1-O11	88.2(3)
		O1-Cu1-O11	88.5(2)
		O11-Cu1-O11	177.6(3)

Neighboring layers are bridged by hydrogen bonds between the coordinated water molecule and sulfate anion (O1···O12, 2.65 Å).

2.4. Molecular architectures of Pt_3 triangle with Cu(II)

Having a $3d^9$ outer sphere electronic configuration and flexible coordination environment, the Cu(II) ion forms complexes of different topologies. Most characteristic are octahedral and square pyramidal and to a smaller extent square-planar and trigonal bipyramidal geometries. The use of Cu(II) ions in crystal engineering and supramolecular chemistry leads to formation of polymeric[81] as well as discrete[82] structures.

$[Pt_3(bpz)_3]$ triangular species have six uncoordinated nitrogen atoms (N1,N1´) and could therefore serve as building blocks for the construction of multicomponent system. As has previously been shown this strategy proved to be promising.[70] In the course of our investigations on the self assembly process of $[\{(en)Pt(2,2´\text{-bpz-}N4,N4´)\}_3]^{6+}$ with Cu^{2+} ions in 1:3 ratio, green crystals have been isolated, which were found to be a mixture of two (or more) components. The products formed are in dynamic interconversion and crystallization of either species could be promoted by several factors such as crystal packing, template effects *etc.* The ^1H NMR spectrum of this mixture shows broad singlets, as a consequence of the presence of paramagnetic Cu^{2+} ions interacting with the 2,2´-bpz ligands.

2.4.1 Crystal structure of molecular "paddle-wheel" $\{[(en)Pt(bpz)]_6Cu_4(H_2O)_6\}(NO_3)_{20}$ (II-18)

One of the complexes characterized crystallographically is a complex of composition $\{[(en)Pt(bpz)]_6Cu_4(H_2O)_6\}^{20+}$ (**II-18**). The way of its formation is depicted in the Scheme 2.5.

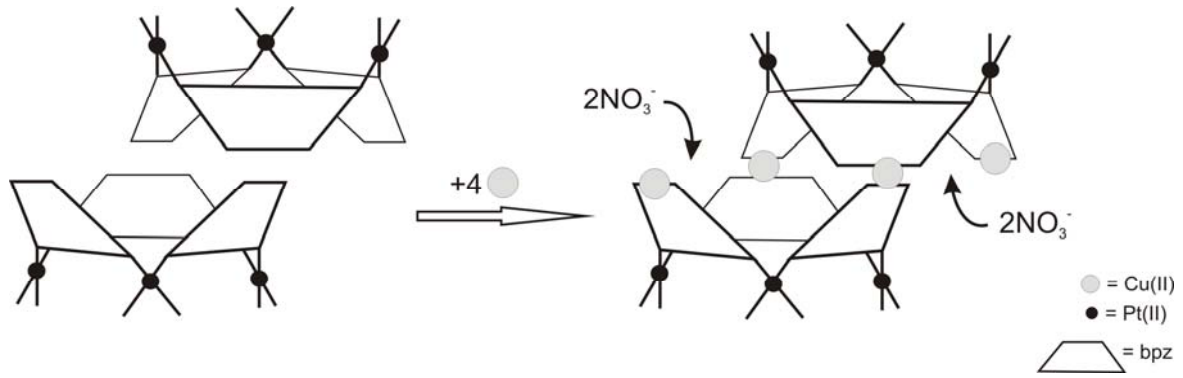

Scheme 2.5 A schematic representation of the formation of "paddle-wheel" **II-18**.

The crystal structure of **II-18** is composed of $[Pt_3(bpz)_3]^{3+}$ triangles interconnected via two Cu^{2+} ions, which are coordinated to the two nitrogen atoms of chelating 2,2´-bpz ligand from each triangle. Two other Cu^{2+} ions are coordinated to the available N4,N4´ nitrogens of 2,2´-bpz at the terminal sides of the structure.

A view of the decanuclear cation **II-18** with numbering scheme is shown in Figure 2.39. It has a paddle-wheel structure. Pt-N bond lengths are in the normal range. Due to the small bite-angle of the enthylenediamine ligand, the geometry at the platinum center is distorted square-planar, with angles ranging from 82.2° to 94.3°.

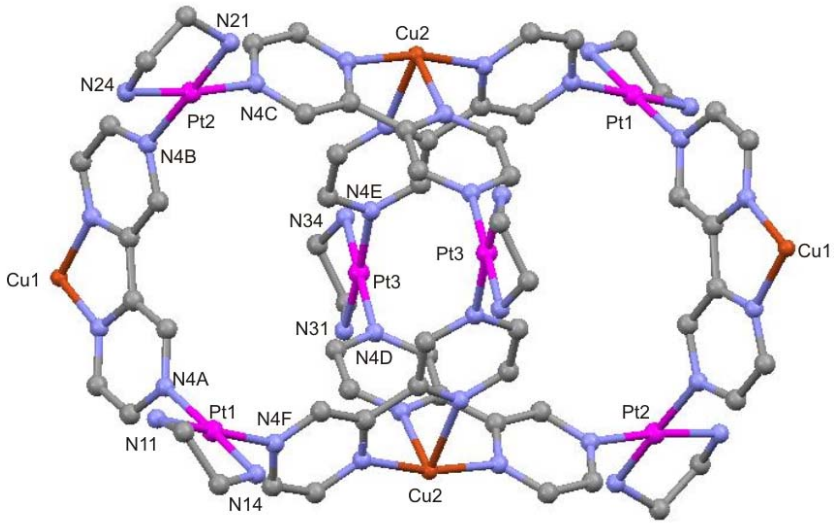

Figure 2.39 Molecular structure of **II-18** with numbering of relevant atom (hydrogen atoms, anions and water molecules omitted for clarity).

The coordination geometries around the two copper ions are distorted octahedral, with CuN_2O_4 and CuN_4O_2 environments (Figure 2.40).

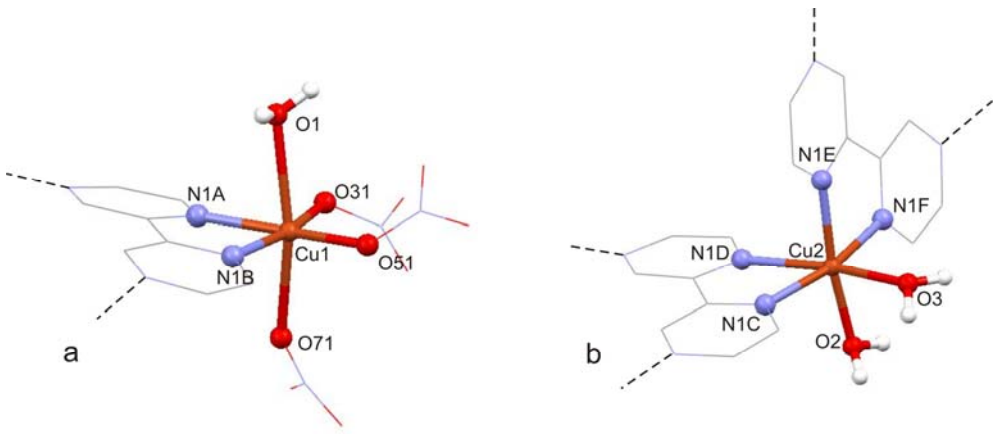

Figure 2.40 Different coordination geometries of the copper atoms in the complex **II-18.**

Two nitrogen atoms of the 2,2´-bpz ligand (N1A and N1B), a water molecule (O1) and oxygen atoms from nitrate anions (O31, O51 and O71) build the surroundings of a terminal Cu1 center (Figure 2.40, a). The coordinated water molecule exhibits a slightly longer distance (2.44Å) than the oxygen atom of the counter ion in *trans* position to it (Cu1···O71, 2.34Å). Other Cu–O and Cu–N distances are in the range of 2 Å (Table 2.17). The bridging six-coordinated Cu2 ion is bonded to the N1,N1´ positions of two bidentate 2,2´-bpz ligands (N1C, N1D, N1E and N1F) and to two water oxygens (O2 and O3) (Figure 2.40, b). The length order of the bond distances around Cu2 is Cu2-N1E ≈ Cu2-O2 > Cu2-N1F ≈ Cu2-N1D ≈ Cu2-N1C ≈ Cu2-O3. Elongated axial contacts in both cases are the result of the Jahn-Teller effect, which is common in six-coordinated copper complexes. Cu-donor atom angles fall in the range of 80.2° – 103.7° for terminal Cu1 and 75.2° – 97.8° for bridging Cu2 atoms.

Table 2.17 Selected bond lengths (Å) and angles (deg.) for **II-18**.

$\{[enPt(bpz)]_6Cu_4(H_2O)_6\}(NO_3)_{20}$ (**II-18**)			
Pt1-N11	2.008(8)	N4C-Pt2-N24	174.0(4)
Pt1-N14	2.009(8)	N4B-Pt2-N24	93.1(4)
Pt1-N4A	2.019(9)	N34-Pt3-N4E	93.2(4)
Pt1-N4F	2.023(9)	N34-Pt3-N31	82.8(4)
Pt2-N21	2.019(8)	N4E-Pt3-N31	175.7(4)
Pt2-N4C	2.024(9)	N34-Pt3-N4D	176.6(3)
Pt2-N4B	2.030(9)	N4E-Pt3-N4D	89.8(3)
Pt2-N24	2.050(9)	N31-Pt3-N4D	94.3(4)
Pt3-N34	1.999(9)	O31-Cu1-O51	103.7(6)
Pt3-N4E	2.013(8)	O31-Cu1-N1A	88.0(4)
Pt3-N31	2.022(9)	O51-Cu1-N1A	167.5(6)
Pt3-N4D	2.028(9)	O31-Cu1-N1B	168.2(4)
Cu1-O31	1.938(12)	O51-Cu1-N1B	88.0(6)
Cu1-O51	1.948(18)	N1A-Cu1-N1B	80.2(4)
Cu1-N1A	2.010(9)	O31-Cu1-O71	86.5(4)
Cu1-N1B	2.021(9)	O51-Cu1-O71	99.0(4)
Cu1-O71	2.342(9)	N1A-Cu1-O71	85.9(3)
Cu1-O1	2.442(9)	N1B-Cu1-O71	93.4(3)
Cu2-O3	1.947(8)	O3-Cu2-N1C	93.7(3)
Cu2-N1C	2.026(9)	O3-Cu2-N1D	172.3(3)
Cu2-N1D	2.037(9)	N1C-Cu2-N1D	79.8(3)
Cu2-N1F	2.070(8)	O3-Cu2-N1F	92.2(3)

Cu2-O2	2.264(8)	N1C-Cu2-N1F	168.0(4)
Cu2-N1E	2.319(9)	N1D-Cu2-N1F	94.9(3)
		O3-Cu2-O2	87.0(3)
N11-Pt1-N14	83.6(4)	N1C-Cu2-O2	97.8(3)
N11-Pt1-N4A	92.9(4)	N1D-Cu2-O2	89.8(3)
N14-Pt1-N4A	176.5(4)	N1F-Cu2-O2	93.0(3)
N11-Pt1-N4F	175.4(4)	O3-Cu2-N1E	92.9(3)
N4A-Pt1-N4F	91.1(4)	N1C-Cu2-N1E	94.0(3)
N21-Pt2-N4C	92.5(4)	N1F-Cu2-N1E	75.2(3)
N21-Pt2-N4B	176.0(4)	N1D-Cu2-N1E	91.7(3)
N4C-Pt2-N4B	91.4(3)	O2-Cu2-N1E	168.2(3)
N21-Pt2-N24	83.1(4)		

The cationic charge of the complex is neutralized by twenty NO_3^- anions, four of which are encapsulated in the two halves of the paddle wheel (Chapter 6). Neighboring molecules of **II-18** are linked together through hydrogen bonds to form a one-dimensional chain along b-axis. These bonds occur between a coordinated nitrate anion of one molecule and a coordinated water molecule of a second molecule with the distance of 2,87 Å (O1···O53), as well as between a coordinated nitrate anion of the first cation and amine ligand of second cation with the following distances 3.05 Å (O72···N34) and 2.93 Å (O73···N34) (Figure 2.41).

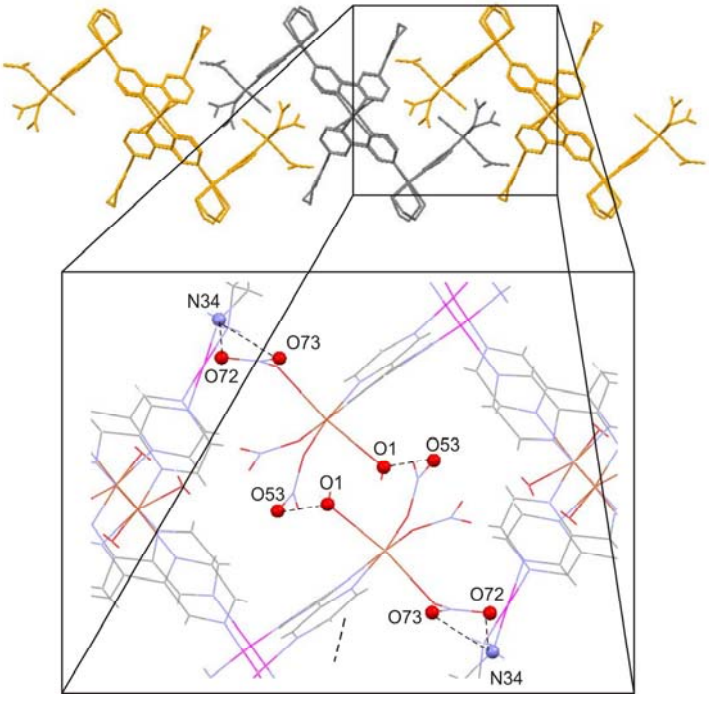

Figure 2.41 Formation of linear chains of compound **II-18** with details of hydrogen bonding between neighboring cations.

2.4.2 Crystal structure of molecular capsule $[(en)Pt(2,2´\text{-}bpz)Cu(NO_3)(H_2O)]_3(NO_3)_6\cdot[Cu(NO_3)_3(H_2O)][Cu(NO_3)_3(H_2O)_2][Cu(NO_3)_2(H_2O)_3]1.5H_2O$ (II-19)

The second complex characterized crystallographically is a container compound formed from two Pt_3 triangles and six Cu^{2+} ions coordinated to the N1,N1´ positions of 2,2´-bpz. Two Pt_3Cu_3 cup shaped units are arranged face-to-face to each other, forming a capsular cavity (Scheme 2.6).

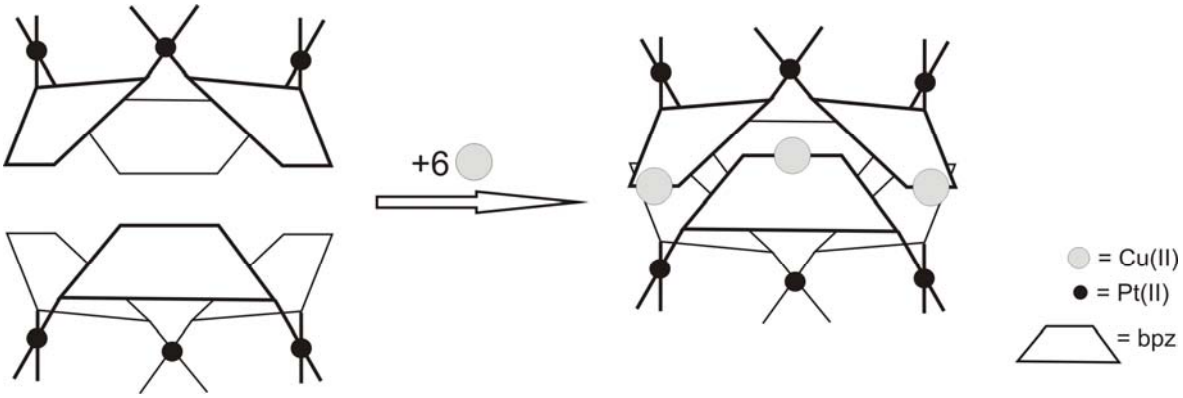

Scheme 2.6 A schematic representation of the formation of molecular capsule **II-19**.

The relative orientation of two Pt_3Cu_3 cup shaped units, with numbering scheme of the cation, is shown in the Figure 2.42 and selected bond lengths and angles are summarized in Table 2.18. Pt(II) centers have their typical coordination geometries. Metal-to-metal distances are similar to other hexanuclar species and have the following values: Pt1···Pt2, 7.7444(10) Å; Pt2···Pt3, 7.7891(11) Å; Pt1···Pt3, 7.9527(8) Å; Cu1···Cu2, 9.9048(31) Å; Cu2···Cu3, 10.2427(37) Å; Cu1···Cu3, 10.2832(37) Å.

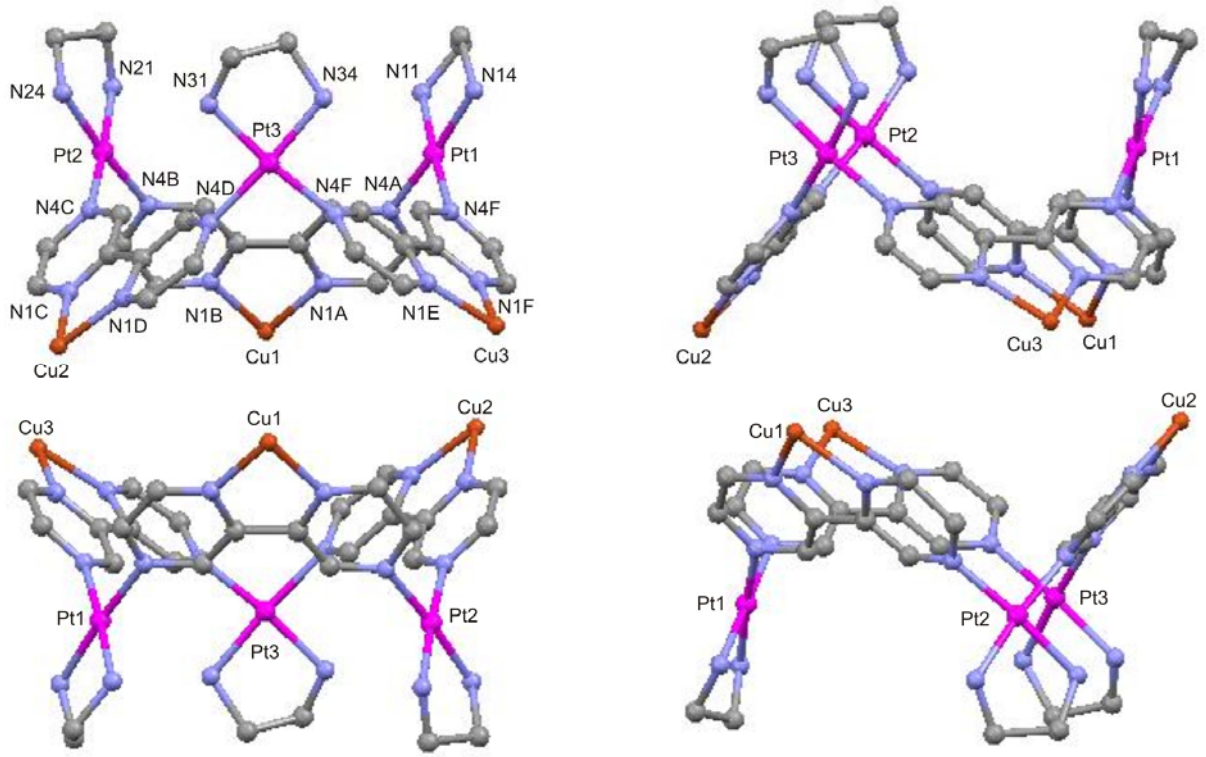

Figure 2.42 Two different views of two Pt_3Cu_3 cup shaped units showing relative orientations of the cations.

Table 2.18 Selected bond lengths (Å) and angles (deg.) for **II-19**.

$[(en)Pt(2,2´\text{-}bpz)Cu(NO_3)\ (H_2O)]_3(NO_3)_6 \cdot [Cu(NO_3)_3(H_2O)] \cdot [Cu(NO_3)_3(H_2O)_2] \cdot [Cu(NO_3)_2(H_2O)_3] \cdot 1.5H_2O$ (**II-19**)			
Pt1-N4A	1.981(14)	Cu4-O43	1.993(17)
Pt1-N11	1.988(14)	Cu4-O42	2.00(2)
Pt1-N4F	2.015(14)	Cu4-O62	2.083(13)
Pt1-N14	2.055(14)	Cu4-O4	2.382(19)
Pt2-N21	2.006(15)	Cu4-O53	2.39(3)
Pt2-N4B	2.011(15)		
Pt2-N4C	2.011(16)	N4A-Pt1-N11	92.4(6)
Pt2-N24	2.013(12)	N4A-Pt-N4F	91.2(6)
Pt3-N4E	2.023(14)	N11-Pt1-N4F	176.3(6)
Pt3-N31	2.031(14)	N4A-Pt1-N14	175.5(6)
Pt3-N34	2.046(17)	N11-Pt1-N14	84.9(6)
Pt3-N4D	2.049(16)	N4F-Pt1-N14	91.6(5)
Cu1-O11	2.005(19)	N21-Pt2-N4B	92.0(6)
Cu1-N1A	2.011(16)	N21-Pt2-N4C	174.1(6)
Cu1-N1B	2.054(13)	N4B-Pt2-N4C	93.9(5)

Cu1-O21	2.16(3)	N21-Pt2-N24	84.5(6)
Cu1-O23	2.26(3)	N4B-Pt2-N24	175.1(6)
Cu1-O51	2.44(2)	N4C-Pt2-N24	89.6(6)
Cu2-O3	1.942(19)	N4E-Pt3-N31	173.9(6)
Cu2-O31	1.970(19)	N4E-Pt3-N34	91.9(6)
Cu2-N1C	2.022(14)	N31-Pt3-N34	82.1(6)
Cu2-N1D	2.031(15)	N4E-Pt3-N4D	92.6(6)
Cu2-O61	2.280(13)	N31-Pt3-N4D	93.4(6)
Cu3-O1	1.946(19)	N34-Pt3-N4D	175.5(6)
Cu3-N1F	2.004(14)	N1A-Cu1-N1B	81.2(6)
Cu3-N1E	2.007(14)	O21-Cu1-O23	62.7(5)
Cu3-O2	2.014(18)	N1A-Cu1-O21	160.5(7)
Cu3-O112	2.31(2)	N1C-Cu2-N1D	81.7(6)
Cu3-O41	2.41(2)	N1F-Cu3-N1E	81.3(6)

Additionally two Cu^{2+} ions and six NO_3^- anions are located inside the cavity. The structure is stabilized by a network of Cu^{2+} ions coordinated to the Pt_3 triangular core and those hosted inside the cavity (Figure 2.43, a), and thus can be defined as guest-induced assembly. The coordination environments of Cu^{2+} ions are depicted in Figure 2.43.

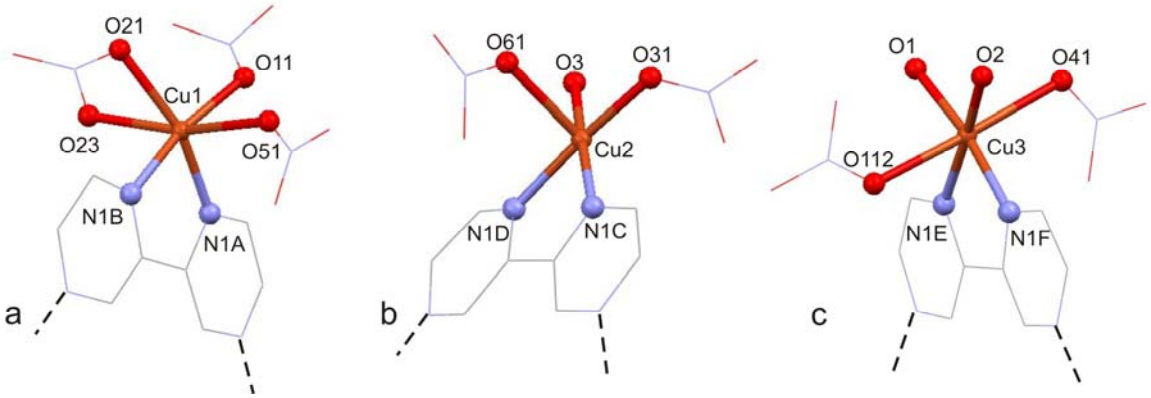

Figure 2.43 Coordination geometries of the copper atoms coordinated to the Pt_3 triangular core in the complex **II-19**.

The Cu1, Cu2 and Cu3 centers are each chelated by the N1,N1´ positions of a 2,2´-bpz ligand, but each of them has a different coordination environment. The hexacoordinate Cu1 center is composed of a CuN_2O_4 unit (Figure 2.43, a), where N-donor sites belong to a 2,2´-bpz ligand, while the remaining positions being occupied by oxygen atoms of three nitrate ions. Two nitrate anions, one water molecule and 2,2´-bpz build the CuN_2O_3 coordination geometry of Cu2 center (Figure 2.43, b). The Cu3 site, apart from being chelated by 2,2-bpz,

is coordinated to oxygen atoms of two nitrates and two water molecules (Figure 2.43, c). As previously discussed, the Cu(II) ions are strongly Jahn-Teller distorted, which suggests *trans* tetragonal distortion of metal center with two (Cu1 and Cu3) or one (Cu2) long and four short metal-ligand bond distances. Cu-N bonds lengths are in the range of 2.00 – 2.05 Å. Equatorial Cu-O distances were found to be below 2.02Å. Cu-O distances in the axial coordination sites are significantly longer and lie between 2.26 and 2.44 Å. The Cu1-O21 bond length (2.16 Å) is in-between these two values, which is probably because equatorial oriented O21 atom and axial oriented O23 atom belong to the same NO_3^- anion. The Cu4 center (Figure 2.44, a) is coordinated to three NO_3^- anions and a water molecule in a CuO_5 environment, bridging all Cu centers together (Figure 2.44).

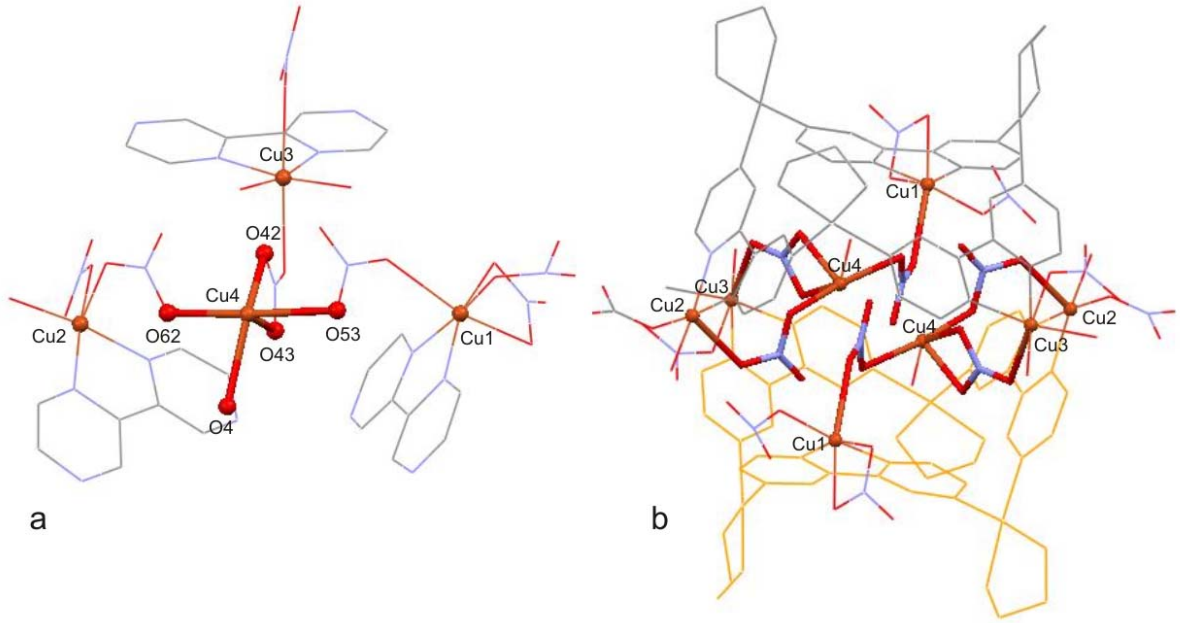

Figure 2.44 Coordination geometry of Cu4 atom (a) and formation of dimeric capsule supported by network formed by 8 Cu^{2+} ions and 6 NO_3^- anions (b).

The capsules are further associated through hydrogen bonding between external Cu^{2+} ions, nitrate anions, amine ligands and water molecules.

2.5. Coordination polymers: 1D chain and 2D network

The construction of hollow, porous network structures has recently become a rapidly growing area of research, because of the interest to obtain new functional materials.[83] Anion/guest exchange,[84] catalysis[85] and gas storage[86] are only few examples of the potential applications. The most efficient approach for construction of such type of a molecular system is self-assembly. Metal ions with octahedral coordination geometries and diverse polydentate organic ligands are widely used to construct metal-organic frameworks (MOFs).[87] In this part of the chapter the synthesis of one-dimensional (1D) and two-dimensional (2D) molecular networks composed of $[(a_2Pt)_3bpz_3]^{6+}$ units and Cd^{2+} or Ag^{+} ions is reported.

Polymeric $\{[((en)Pt)_3(bpz)_3Cd_2(H_2O)_7][Cd(H_2O)_6](SO_4)_6\}_n$ (**II-20**) has been obtained by reacting $[\{Pt(en)(ccc\text{-bpz-N4,N4´})\}_3]^{6+}$ with 1.5 equivalent of $CdSO_4$ at 45°C for 1d. The silver complexes have been prepared by cocrystalization of $[\{Pt(NH_3)_2(bpz\text{-N4,N4´})\}_3]^{6+}$ with one equivalent of $AgBF_4$ (**II-21**) or $AgSO_4$ (**II-22**). ^1H NMR spectra of all isolated compounds show that the resonances of the molecular triangle are not affected by the presence of Cd^{2+} or Ag^{+} ions. Due to the lability of M-N bonds, these complexes dissociate into components in aqueous media and reassociate only in the solid state. In the solid state the cavities of triangular Pt vases are filled with anions (see Chapter 6).

2.5.1 Crystal strucure of $\{[(enPt)_3(bpz)_3Cd_2(H_2O)_7][Cd(H_2O)_6](SO_4)_6\}_n$ (II-20)

The X-ray diffraction analysis of **II-20** indicates that, similar to other hexanuclear complexes, Cd^{2+} ions are coordinated to N1,N1´positions of *cis* oriented bpz ligands. A view of the structural unit of **II-20**, together with its numbering scheme is depicted in Figure 2.45. The torsion angle between pz(E)-pz(F) is 16.2° and thus is significantly larger than in between pz(A)-pz(B) (1.5°), pz(C)-pz(D) (2.6°). The geometry of the Pt_3 triangle is very similar to the previously described Pt_3Pd_3 species. Selected structural features are compiled in Table 2.19.

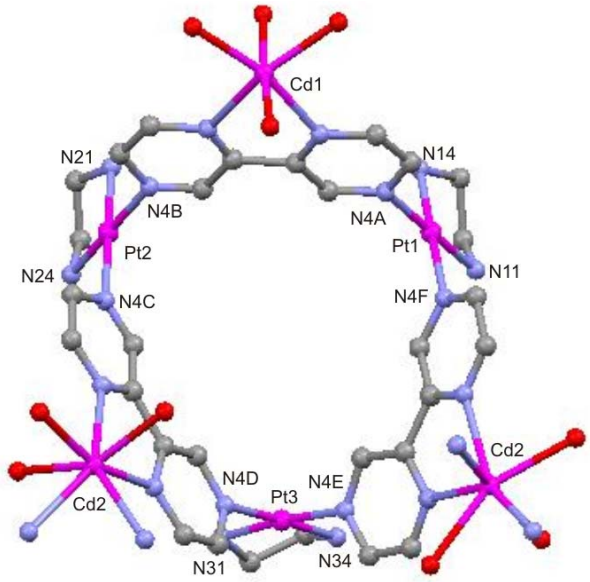

Figure 2.45 Section of molecular structure of hexanuclear cation $\{[(enPt)_3(bpz)_3Cd_2(H_2O)_7][Cd(H_2O)_6](SO_4)_6\}_n$ (**II-20**) unit with numbering scheme of relevant atoms.

Table 2.19 Selected bond lengths (Å) and angles (deg.) for **II-20**.

$\{[(en)_2Pt(bpz)]_3[Cd(H_2O)_3][Cd(H_2O)_4](SO_4)_6\ [Cd(H_2O)_6]\}_n$ (**II-20**)			
Pt1-N11	2.00(3)	Cd1-O3A	2.18(3)
Pt1-N4F	2.01(3)	Cd1-O4A	2.20(3)
Pt1-N4A	2.02(3)	Cd1-O2A	2.21(2)
Pt1-N14	2.03(3)	Cd1-O1A	2.28(3)
Pt2-N21	2.01(3)	Cd1-N1A	2.32(3)
Pt2-N4C	2.03(3)	Cd1-N1B	2.43(3)
Pt2-N24	2.04(3)	Cd2-O3B	2.28(3)
Pt2-N4B	2.04(3)	Cd2-O1B	2.32(3)
Pt3-N31	2.03(3)	Cd2-N1C	2.37(3)
Pt3-N4E	2.03(3)	Cd2-N1D	2.40(3)
Pt3-N34	2.04(3)	Cd2-N1E	2.41(3)
Pt3-N4D	2.05(3)	Cd2-O2B	2.43(3)
		Cd2-N1F	2.45(3)
N11-Pt1-N4F	91.8(11)	N4E-Pt3-N34	93.1(11)
N11-Pt1-N4A	177.5(12)	N31-Pt3-N4D	95.2(11)
N4F-Pt1-N4A	90.7(11)	N4E-Pt3-N4D	88.2(11)
N11-Pt1-N14	84.7(12)	N34-Pt3-N4D	178.3(11)
N2F-Pt1-N14	176.4(11)		
N4A-Pt1-N14	92.8(12)	N1A-Cd1-N1B	68.3(10)
N21-Pt2-N4C	176.6(12)	N1C-Cd2-N1D	69.4(10)
N21-Pt2-N24	84.0(11)	N1C-Cd2-N1E	144.4(10)
N4C-Pt2-N24	92.8(11)	N1D-Cd2-N1E	122.6(10)
N21-Pt2-N4B	93.1(11)	N1C-Cd2-N1F	146.2(10)
N4C-Pt2-N4B	90.0(11)	N1D-Cd2-N1F	86.6(10)
N24-Pt2-N4B	176.1(11)	N1E-Cd2-N1F	68.8(9)

N31-Pt3-N4E	174.5(13)
N31-Pt3-N34	83.5(11)

In **II-20** Pt_3 triangles are linked by Cd^{2+} ions coordinated to two 2,2´-bpz ligands of neighboring cations to generate a 1D zigzag chains long the a-axis (Figure 2.46) This gives rise to metal-metal distances of Pt1···Pt2, 7.6108(18) Å; Pt1···Pt3, 7.7407(17) Å; Pt2···Pt3, 7.9716(20) Å; Cd1···Cd2, 10.0499(39) Å and 11.0824(44) Å; Cd2···Cd2, 9.3333(40) Å.

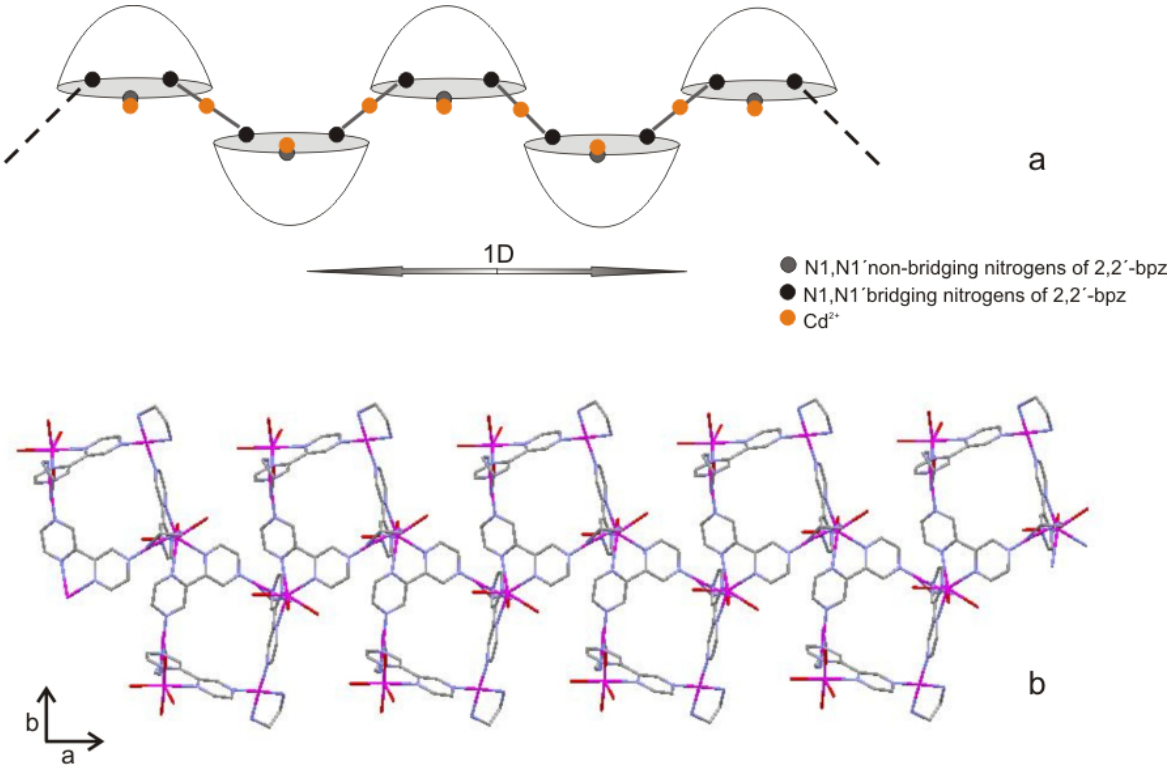

Figure 2.46 Schematic representation (a) and crystal structure (b) of the one-dimensional infinite network formed by Pt_3 triangles and Cd(II) ions.

Furthermore, the adjacent chains are interconnected through hydrogen bonds between sulfate anions, amine ligands, and water molecules.

Compound **II-20** contains three crystallographically independent Cd(II) ions in different coordination environments (Figure 2.47). Cd1 is in an octahedral CdN_2O_4 environment, being coordinated to N1,N1´ positions of 2,2´-bpz and four aqua oxygen atoms, with Cd-O distances between 2.18 and 2.28 Å and Cd-N distances between 2.32 and 2.43 Å. Angles between coordinated atoms vary from 86.1 and 96.0°.

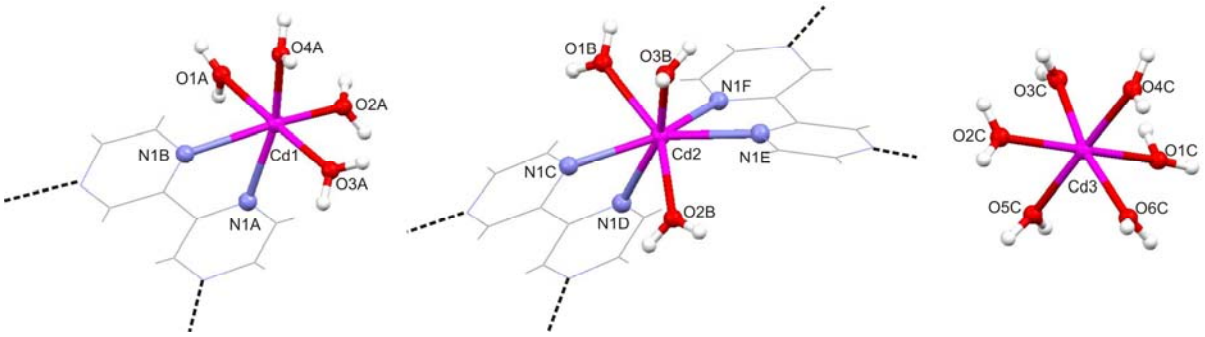

Figure 2.47 Different coordination geometries of the cadmium atoms in the complex **II-20.**

The Cd2 ions possess a seven coordinated (distorted pentagonal bipyramidal) geometry, being coordinated to the four nitrogens of two 2,2´-bpz ligands and three water molecules in the CdN_4O_3 unit. Average Cd2-N and Cd2-O distances are 2.41 Å and 2.34 Å, whereas average angles are in between 68.8° and 92.8°. Only six water molecules are coordinated to the Cd3 center, resulting in octahedral coordination sphere. Cd3-O distances range from 2.23 to 2.30 Å and O-Cd3-O angles from 82.3 to 92.6°.

2.5.2 Crystal structure of $\{[(NH_3)_2Pt(bpz)]_3Ag\ (SiF_6)_3(BF_4)\}_n$ (II-21)

From an aqueous solution containing the molecular Pt_3 triangle as BF_4^- salt and Ag^+ ions, yellow crystals were obtained within 2d at 4°C. They were identified as polymeric $\{[(NH_3)_2Pt(bpz)]_3Ag\ (SiF_6)_3(BF_4)\}_n$ (**II-21**) by single crystal X-ray analysis. The molecular unit, together with the atomic labelling system, is shown in Figure 2.48 and bond lengths and angles are summarized in Table 2.20. Pt···Pt distances are as follows: Pt1···Pt2, 7.8372(10) Å; Pt1···Pt3, 7.7998(8) Å and Pt2···Pt3, 7.7939(11) Å. The geometry of Pt is not unusual with bond lengths of *ca.* 2 Å and angles are close to ideal 90°.

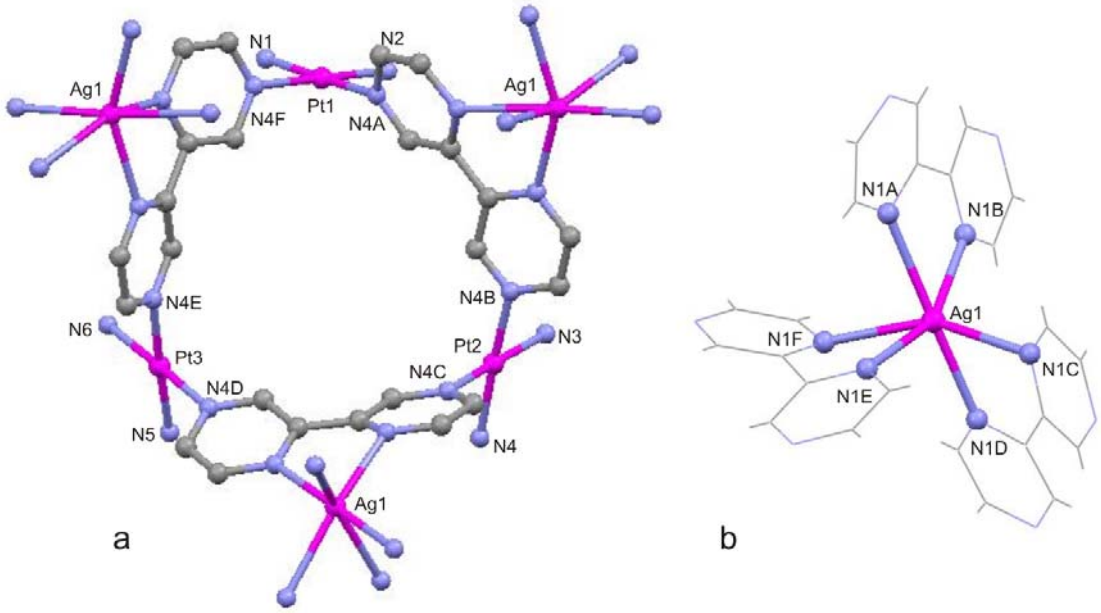

Figure 2.48 Details of polymeric structure of $\{[(NH_3)_2Pt(bpz)]_3Ag_3\ (SiF_6)_3(BF_4)\}$: section depicting the Pt_3Ag_3 vase (a) and the environment of the Ag^+ ion (b).

A two-dimensional framework is formed through the linkage of molecular triangles through silver ions. The Ag-Ag distances of in **II-21** are 10.4289(18) Å, 10.6156(16) Å and 10.7577(18) Å. Each Ag ion in the title complex is surrounded by three chelating 2,2´-bpz ligands to achieve a distorted octahedral AgN_6 coordination geometry. The Ag-N bond lengths range from 2.38 Å to 2.54 Å, and angles around Ag1 from 66.4° to 96.9°.

Table 2.20 Selected bond lengths (Å) and angles (deg.) for **II-21**.

$\{[(NH_3)_2Pt(bpz)]_3Ag\ (SiF_6)_3(BF_4)\}_n$ (**II-21**)			
Pt1-N2	1.990(13)	Ag1-N1B	2.378(11)
Pt1-N4F	2.011(11)	Ag1-N1D	2.411(12)
Pt1-N4A	2.015(9)	Ag1-N1F	2.427(13)
Pt1-N1	2.043(10)	Ag1-N1C	2.473(13)
Pt2-N3	1.993(15)	Ag1-N1E	2.514(10)
Pt2-N4C	2.003(16)	Ag1-N1A	2.535(12)
Pt2-N4	2.045(13)		
Pt2-N4B	2.008(10)	N1A-Ag1-N1B	66.4(3)
Pt3-N4E	2.003(9)	N1C-Ag1-N1D	68.0(4)
Pt3-N4D	2.020(10)	N1E-Ag1-N1F	67.2(4)
Pt3-N6	2.031(11)		
Pt3-N5	2.034(13)		
N2-Pt1-N4F	178.4(5)	N3-Pt2-N4	91.8(6)
N2-Pt1-N4A	89.9(5)	N4C-Pt2-N4	92.1(6)
N4F-Pt1-N4A	91.6(4)	N4B-Pt2-N4	177.6(8)
N2-Pt1-N1	90.5(6)	N4E-Pt3-N4D	90.7(4)
N4F-Pt1-N1			
	88.1(5)	N4E-Pt3-N6	88.4(5)

N4A-Pt1-N1	178.0(4)	N4D-Pt3-N6	177.6(6)
N3-Pt2-N4C	173.8(8)	N4E-Pt3-N5	177.3(6)
N3-Pt2-N4B	87.2(5)	N4D-Pt3-N5	89.8(5)
N4C-Pt2-N4B	88.6(5)	N6-Pt3-N5	91.2(6)

A 2D porous network, constructed by the bridged Pt_3 trinuclear units, expands along the c and b directions, as shown in Figure 2.49.

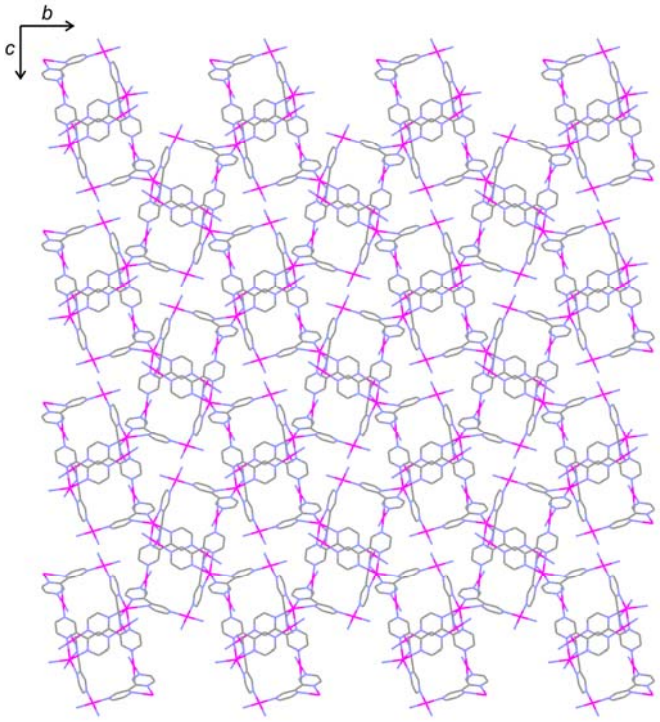

Figure 2.49 2D layer of **II-21** along b/c axis.

2.5.3 Preliminary crystal structure of $\{[(NH_3)_2Pt(bpz)]_3Ag\ (SO_4)_{3.5}\}_n$ (II-22)

A preliminary crystal structure analysis of **II-22** shows that its molecular skeleton has a very similar structure as **II-21**. Pt···Pt distances are in the rage of 7.48 – 7.87Å and Ag···Ag distances are 10.74 – 10.88Å. 2D layers of **II-22** are again arranged along b and c axis as in the previous case.

2.6 Conclusions

In the present chapter the synthesis and characterization of discrete and infinite structures composed of different metal centers and 2,2´-bpz ligand have been described. A tetranuclear complex $[\{cis\text{-}Pt(NH_3)_2(tttt\text{-}bpz\text{-}N4,N4')\}_4](SO_4)_4$ (**II-1**) and three trinuclear complexes $BF_4\subset cis\text{-}[\{Pt(NH_3)_2(ttt\text{-}bpz\text{-}N4,N4')\}_3](BF_4)(SiF_6)_2$ (**II-2**), $PF_6\subset cis$-

[{Pt(NH_3)$_2$(*ccc*-bpz-*N4,N4´*)}$_3$](PF_6)$_5$(NO_3) (**II-3**) and NO_3⊂[{Pt(en)(*ccc*-bpz-*N4,N4´*)}$_3$](SO_4)$_2$(NO_3) (**II-4**) were isolated and characterized crystallographically. The influence of temperature, anions and concentration on the triangle-square equilibrium was studied. *cis*-[Pt(NH_3)$_2$(bpz-*N4*)$_2$](NO_3)$_2$·3H_2O (**II-5**), bearing two 2,2´-bpz ligands per metal center, has been isolated and characterized as well, showing that the 2,2´-bpz ligand can also be bonded to the metal center in a monofunctional way.

Moreover, molecular triangles [(en)Pt(bpz)]$_3^{6+}$ and [(NH_3)$_2$Pt(bpz)]$_3^{6+}$ were utilized for the synthesis of mixed-metal complexes. By coordination of [(en)Pd]$^{2+}$ to the free N1,N1´positions of the 2,2´-bpz ligands of [(NH_3)$_2$Pt(bpz)]$_3^{6+}$, different salts (NO_3^-/**II-6**, SO_4^{2-}/**II-7**, NO_3^- and PF_6^-/**II-8**) of molecular vases were obtained. Their molecular structures were authenticated by single crystal X-ray diffraction analyses, showing formation of mixed-metal Pt_3Pd_3 complexes. In order to extend the cavities of molecular vases, mononuclear complexes based on 2,2´-bpz ligand of types [Pd(2,2'-bpz)(*o*-pda)](NO_3)$_2$ (**II-9**), [Pd(2,2'-bpz)(bipzp)](NO_3)$_2$ (**II-11**) and [Pd(2,2'-bpz)(bipzp)](NO_3)$_2$ (**II-12**) were prepared as building blocks. Studies of the coordination behavior of [Pd(2,2'-bpz)(bipzp)](NO_3)$_2$ (**II-11**) reveal that in case Ag^+ was used as bridging metal, symmetrization occurs. *ht*-[Pd(bipzp)$_2$][Ag(NO_3)$_3$(H_2O)] (**II-16**) was isolated from the mixture and crystallographically characterized. When $CuSO_4$ was applied, formation of polymeric [Cu(2,2´-bpz)(H_2O)$_2$$SO_4$] (**II-17**) was observed.

Cocrystalizatiion of Cu(NO_3)$_2$ with [(en)Pt(bpz)]$_3$(NO_3)$_6$ led to the formation of green crystals. The results of the crystallographic study reveal, that two types of mixed Pt/Cu complexes were formed: "paddle wheel" {[enPt(bpz)]$_6$Cu$_4$(H_2O)$_6$}(NO_3)$_{20}$ (**II-18**) and molecular capsule [(en)Pt(2,2´-bpz)Cu(NO_3) (H_2O)]$_3$(NO_3)$_6$·[Cu(NO_3)$_3$(H_2O)] · [Cu(NO_3)$_3$(H_2O)$_2$] · [Cu(NO_3)$_2$(H_2O)$_3$]· 1.5H_2O (**II-19**). While in **II-18** molecular triangles are connected via two Cu^{2+} ions, formation of **II-19** was supported by encapsulated two Cu^{2+} ions and six nitrate anions.

And, finally, Cd^{2+} and Ag^+ were used to generate 1D {[(enPt)$_3$(bpz)$_3$Cd$_2$(H_2O)$_7$][Cd(H_2O)$_6$](SO_4)$_6$}$_n$ (**II-20**) and two 2D coordination networks {[(NH_3)$_2$Pt(bpz)]$_3$Ag(SiF_6)$_3$(BF_4)}$_n$ (**II-21**) and {[(NH_3)$_2$Pt(bpz)]$_3$Ag (SO_4)$_{3.5}$}$_n$ (**II-22**).

Chapter 3 – Complexes of Pt(II) and Pd(II) containing terminal and bridging cyanido ligands

3.1 Background

The evidence that in most cancer cells telomerase activity is overexpressed, has generated an interest in the design and preparation of substances able to target telomerase or telomeres for chemotherapy. One of the strategies is the stabilization of G-quadruplex (G_4) DNA sequences at the end of the telomeres.[88] The planar surface of G_4 structures suggests that molecules having a planar geometry could act as effective G_4-binders. Indeed, in recent years many planar organic[89] and inorganic[90] molecules have demonstrated promising anticancer properties.

Due to its linear shape and the ability to form planar skeletons, the use of cyanido ligand to bridge square planar metal centers appeared particularly suitable for this purpose. In this chapter the synthesis and characterization of (en)Pt(II) and (en)Pd(II) complexes containing terminal as well as bridging cyanido ligands are described. The main focus of this work was on cyclic metal complexes containing CN^- ligand.

Cyanide is one of the ligands having a long history in coordination chemistry,[91] first discovered by a Berlin painter in 1704. By mixing solutions of $[Fe(H_2O)_6]^{3+}$ and $[Fe(CN)_6]^{4-}$ he had obtained a compound having an intense blue colour, which was later found to be a mixed valence cyanido-bridged complex known as Prussian blue, $Fe^{III}_4[Fe^{II}(CN)_6]_3$. The chemistry of μ-CN complexes has been intensively studied in recent years, since M-CN-M´ bridges enable, for example, metal-to-metal charge transfer and are suitable for the synthesis of materials with magnetic properties[92] or light harvesting devices.[93] The various metal ion binding patterns (Scheme 3.1) make possible the formation of complexes having diverse topologies. Yet, the most frequent binding mode of the cyanido ligand is linear.

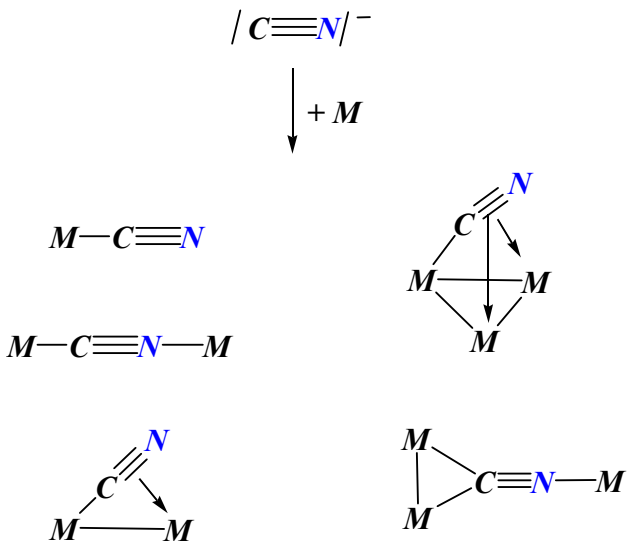

Scheme 3.1 Possible metal binding patterns of cyanido ligands.

The literature on discrete CN-bridged Pd(II) and Pt(II) complexes characterized crystallographically is rather small. Among these, molecules of different topologies are known. For instance, a CN-bridged cyclic Pd trimer had been prepared by removing one CN from $Pd(dppe)(CN)_2$.[94] However, the relative orientation of the three CN groups within the cycle is not clear. Mixed metal CN-briged squares of type Pt_2Pd_2 have been described by Forniés *et al*.[95] Che *et.al.* report a rare example of a Pt_6 macrocycle, bridged through CN ligands.[96]

3.2 Towards molecular squares

3.2.1 Synthesis and NMR spectroscopic studies

To avoid formation of polymeric structures, coordination sides of the Pt(II) and Pd(II) were minimized by blocking them, using the chelating ethylendiamine ligand. Theoretically, combination of CN^- with equimolar amount of $[enM(H_2O)_2]^{2+}$ could lead to the formation of a mixture of different linkage isomers (Scheme 3.2).

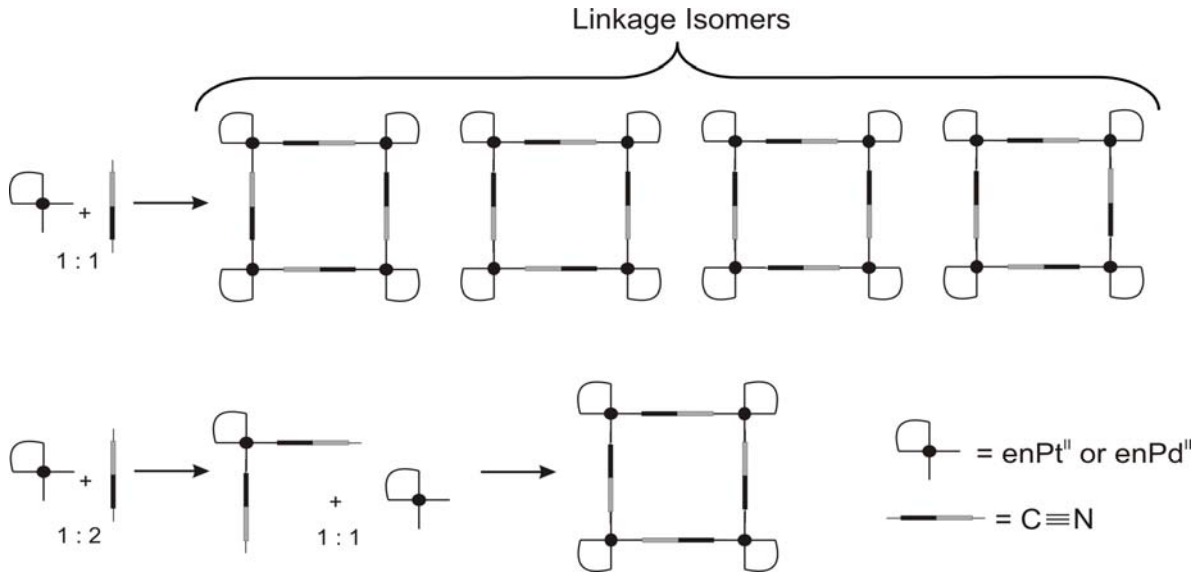

Scheme 3.2 Formation of linkage isomers when reacting $[enM(H_2O)_2]^{2+}$ with one equiv. of CN^- (top) and illustration of stepwise construction leading only to a single isomer (bottom).

In order to reduce the structural variety of compounds, the advantage of a stepwise construction has been used by starting from a *cis*-$M(a)_2(CN)_2$ species and reacting it subsequently with $[M(a)_2(H_2O)_2]^{2+}$ ($M = Pt^{II}$ and/or Pd^{II}).

Complex $Pd(en)(CN)_2$ (**III-1**) has been prepared by the reaction of $enPdCl_2$ with AgCN in 1:2 molar ratio. The ^1H NMR spectrum of the isolated product displays a singlet at 2.80 ppm for the CH_2 protons of the ethylendiamine ligand (Figure 3.1, a).

Reaction of $enPtCl_2$ with two equivalents of AgCN was followed by ^1H NMR spectroscopy. The singlet at 2.65 ppm with $^3J(^{195}Pt\text{-}^1H) = 40$ Hz was assigned to $Pt(en)(CN)_2$ (**III-2**) and the singlet at 2.78 ppm with $^3J(^{195}Pt\text{-}^1H) = 32$ Hz was assigned to $[Pt(en)_2][Pt(CN)_4]$ (**III-2a**), as confirmed by the ^1H NMR spectrum of an isolated and crystallographically characterized species of **III-2a**.

The potential building block *trans*-$Pt(ma)_2(CN)_2$ (**III-3**) has also been prepared in a similar manner. The ^1H NMR spectrum of an isolated sample shows a singlet for the methyl group of the methylamine ligand which occurs at 2.57 ppm and has ^{195}Pt satellites of $^3J(^{195}Pt\text{-}^1H) = 53$ Hz.

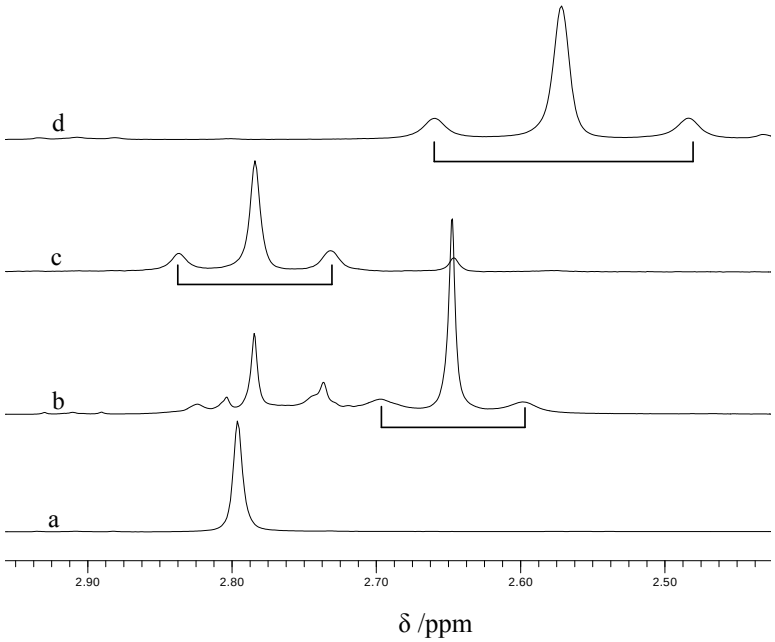

Figure 3.1 ^{1}H NMR spectra (D_2O, 300 MHz) of a) $Pd(en)(CN)_2$ (**III-1**), b) spectra obtained upon mixing $Pt(en)Cl_2$ and AgCN in 1:2 ratio and mixing at 45°C for 1d, c) $[Pt(en)_2][Pt(CN)_4]$ (**III-2a**), d) *trans*-$Pt(ma)_2(CN)_2$ (**III-3**).

$Pd(en)(CN)_2$ and $Pt(en)(CN)_2$ species have been used for the construction of molecular squares by establishing coordinative bonds between the nitrogen atom of the cyanide groups and a second metal cation. A comparison of the ^{1}H NMR signals of $Pd(en)(CN)_2$ (2.80 ppm) and $[Pd(en)(D_2O)_2]^{2+}$ (2.62 ppm) with those of the product formed reveals that the signals corresponding to the cyclic complex are slightly shifted.

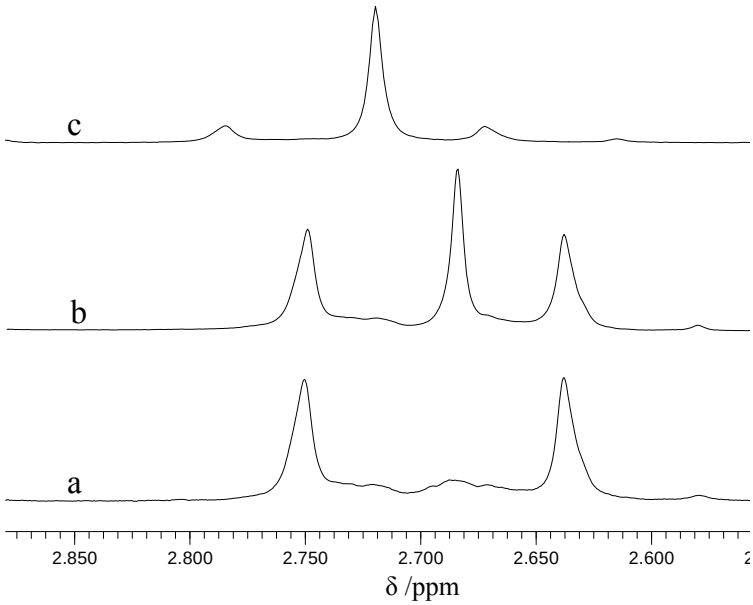

Figure 3.2 ^{1}H NMR spectra (D_2O, 300 MHz) of $[Pd(en)(CN)]_4(NO_3)_4$ (**III-4**) a) immediately after dissolving the crystals, b) after 4d at RT and c) after 1d at 60°C.

The ^{1}H NMR spectrum of a freshly prepared solution of the cyclic tetramer **III-4**, obtained by dissolving crystals of **III-4** in D_2O and recording the ^{1}H NMR spectrum immediately afterwards, shows two CH_2 resonances in 1:1-ratio at 2.63 and 2.75 ppm. Presence of two signals of identical intensities clearly indicates the differences in coordination environments of the metal centers. Upon aging of the solution (3 – 4 d, RT), a new peak at 2.68 ppm appears. Further heating of the solution at 45°C for 3d does not cause significant changes. However, an increase in temperature (60°C, 1d) leads to a new signal at 2.72 ppm, possibly due to a rearrangement process or due to decomposition. A symmetrization according to following equation could account for the presence of a single en-resonance (due to $[Pd(en)_2]^{2+}$) in the ^{1}H NMR spectrum:

$$[Pd(en)(CN)]_4(NO_3)_4 \xrightarrow{H_2O} [Pd(en)_2](NO_3)_2 + [Pd(en)_2]\,[Pd(CN)_4] + [Pd(H_2O)_4](NO_3)_2$$

The fact that in the analogous Pt-system, a $[Pt(en)_2][Pt(CN)_4]$ species has been isolated as a side product , makes such a proposal reasonable.

The corresponding Pt complex **III-5** has two singlets of identical intensities at 2.54 ($^3J(^{195}Pt\text{-}^1H)$ = 36 Hz) and 2.71 ppm ($^3J(^{195}Pt\text{-}^1H)$ = 29 Hz). These peaks are assigned analogously to the proton signals of ethylenediamine ligand of PtN_4 and PtN_2C_2 centers. In comparison to the Pd analogue, **III-5** is stable: no significant changes of the spectrum are observed after 3 days of heating at 80°C.

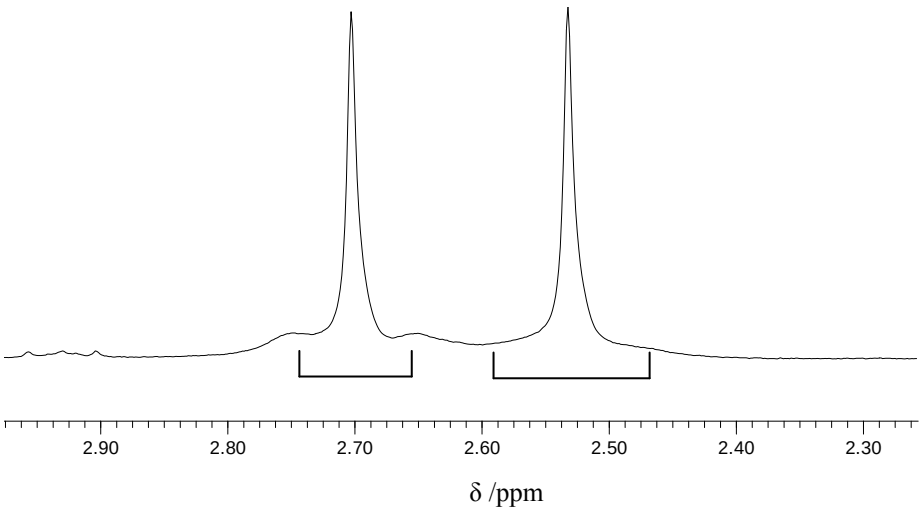

Figure 3.3 ^{1}H NMR spectra (D_2O, 300 MHz) of $[Pt(en)(CN)]_4(NO_3)_4$ (**III-5**).

Since incorporation of aromatic rings would probably provide better interactions with G-quartets, an attempt was made to obtain complex containing (bpy)Pd(II) by the reaction of $[(bpy)Pd(H_2O)_2]^{2+}$ with $Pd(en)(CN)_2$, using methanol or water as solvent. However, the product isolated from methanolic solution was not soluble in water and common organic solvents, which hampered its full characterization. Elemental analysis suggests formation of a species of composition $[Pd(bpy)(en)(CN)_2(NO_3)_2]\cdot H_2O$ (**III-6**). Attempt to crystallise it by dissolving **III-6** in concentrated NH_4OH and by slow evaporation of NH_3, results in the formation of very thin needles, which were not suitable for X-ray measurement. This unusual procedure had previously been used to crystallize another discrete cyanido-bridged compound, $[\{Cu(bpy)(H_2O)Pt(CN)_4\}_2]$, which has a similar molecular skeleton.[97] If this reaction is carried out in water, it leads to the formation of a gel. The phenomenon of gelation generally may be understood as a form of arrested or partial crystallisation.[98] From the more diluted solution containing SO_4^{2-} ions, a crystalline compound has been isolated in 11% yield. It proved to be $[Pd(bpy)(en)](SO_4)\cdot 3H_2O$ (**III-7**).

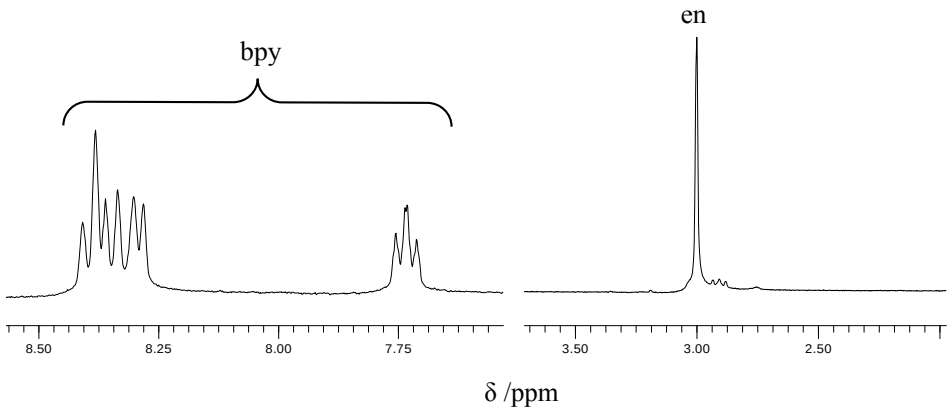

Figure 3.4 ^{1}H NMR spectrum (D_2O, 300 MHz) of $[Pd(en)(bpy)](SO_4)\ 3H_2O$ (**III-7**).

The ^{1}H NMR spectrum of **III-7** shows bpy signals in the aromatic region (dd, H5,H5′, 7.74 ppm and m, H3,H3′, H4,H4′, H6,H6′, 8.28 – 8.41 ppm) and a peak corresponding to the en ligand (s, CH_2, 3.00 ppm) (Figure 3.4).

3.2.2 IR spectra

Infrared spectra of the complexes containing cyanido ligand are very informative, since it is possible to differentiate bridging and terminal cyanido groups on the basis of their

differences in their ν(CN) modes. Thus the bridging cyanido ligand generally leads to a shift to *higher* wavenumbers of ν(CN) (about 5–25 cm^{-1}), opposite to the halogeno- and carbonyl-bridged complexes. The IR spectra of the complexes synthesized were measured as KBr pellets. The relevant IR absorption data are presented in Table 3.1.

Table 3.1 Vibrational frequences of ν(CN) in the various compounds

	III-1	**III-2a**	**III-3**	**III-4**	**III-5**	**III-6**
υ(CN) $[cm]^{-1}$	2145, 2135	2123	2125	2190	2192	2190

The IR spectrum of **III-1** shows two characteristic sharp bands for ν(CN) at 2135 and 2145 cm^{-1}, for IR active *sym* and *asym* stretches (C_{2v} symmetry), which confirms *cis* geometry of the compound. In contrast, the *trans* isomer **III-3** has only one characteristic band at 2125 cm^{-1} ($D_{\infty h}$ point group). The IR spectrum of the **III-2a** shows a poorly resolved doublet centered at 2123 cm^{-1}. The two bands of $Pd(en)(CN)_2$ are replaced by a single ν(CN) band of $[Pd(en)\mu\text{-}CN]_4^{4+}$(**III-4**) at 2190 cm^{-1}. The 2192 cm^{-1} band observed in the spectrum of **III-5** is also attributed to a bridging cyanide vibration. Compound **III-6** has a sharp IR band at 2190 cm^{-1}, consistent with the presence of bridging cyanide. However, its structure is unknown at present.

3.2.3 X-ray crystal structures

3.2.3.1 Characterization of $Pd(en)(CN)_2$ (III-1)

Single crystals of $Pd(en)(CN)_2$ have been obtained from aqueous solution during one week at 4°C. The X-ray diffraction study shows that the two cyanido ligands are coordinated to the metal center trough their carbon atoms. Pd is in a distorted square planar coordination environment, with a small bite angle of ethylenediamine (N11-Pd1-N14, 83.10°). Pd-N distances are in the normal range (Table 3.1).

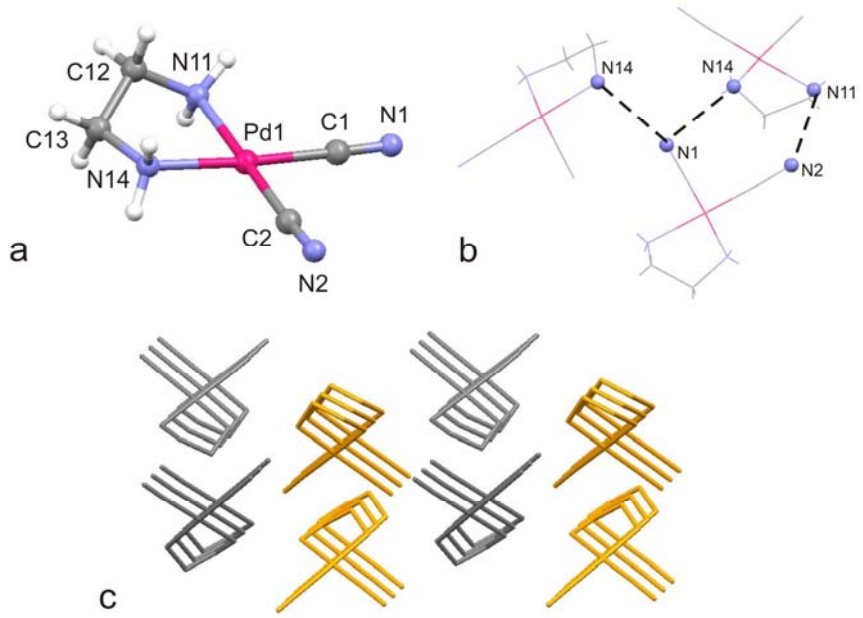

Figure 3.5 a) Molecular structure of **III-1** with atomic numbering scheme, b) hydrogen bonding pattern and c) crystal packing.

As shown in the Figure 3c, the crystal packing of $Pd(en)(CN)_2$ leads to columnar stacking of monomeric units along the c-axis. In the solid state the layers are packed in such a way that two neighboring molecules from each layer make a dihedral angle of *ca.* 90°, with Pd···Pd distances of *ca.* 5.31 Å. $Pd(en)(CN)_2$ entities are interconnected through intramolecular hydrogen bonds (N1···N14, 3.04 Å; N1···N14, 2.99 Å; N2···N11, 3.09 Å) (Figure 3b).

Table 3.2 Selected bond lengths (Å) and angles (deg.) for **III-1**

$Pd(en)(CN)_2$ (**III-1**)			
Pd1-N11	2.069(2)	C1-Pd1-C2	88.71(10
Pd1-N14	2.062(2)	C1-Pd1-N14	176.56(11)
Pd1-C1	1.948(3)	C2-Pd1-N14	93.91(10)
Pd1-C2	1.964(3)	C1-Pd1-N11	94.13(9)
C1-N1	1.144(3)	C2-Pd1-N11	175.25(10)
C2-N2	1.133(3)	N14-Pd1-N11	83.10(8)
		N1-C1-Pd1	178.5(3)
		N2-C2-Pd1	175.3(3)

3.2.3.2 Characterization of $[(en)_2Pt][Pt(CN)_4]$ (III-2a)

The Pt analogue of **III-1** has been characterized only by means of NMR spectroscopy. Upon crystallization of the reaction mixture, only single crystals of a side product have been isolated in low yield. As the X-ray crystal structure reveals, a salt of composition $[(en)_2Pt][Pt(CN)_4]$ (**III-2**) has formed. The platinum coordination geometries show no unusual structural features (Table 3.1).

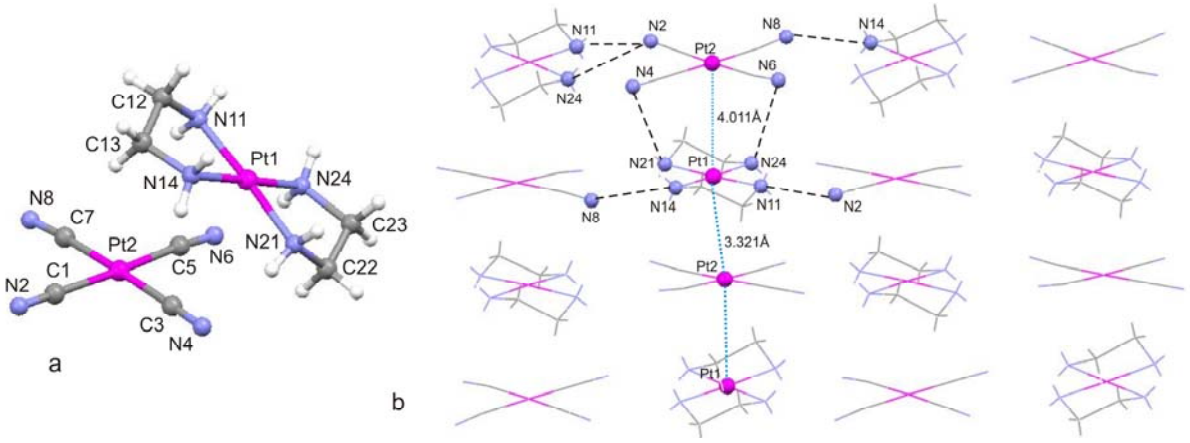

Figure 3.6 a) Crystal structure of $[(en)_2Pt][Pt(CN)_2]$ (**III-2**) with atom numbering scheme and b) crystal packing of **III-2** indicating extensive intermolecular hydrogen bonding.

Table 3.3 Selected bond lengths (Å) and angles (deg.) for **III-2.**

$[(en)_2Pt][Pt(CN)_4]$ (**III-2**)			
Pt1-N24	2.03(2)	N24-Pt1-N11	97.7(9)
Pt1-N11	2.04(2)	N24-Pt1-N14	178.5(10)
Pt1-N14	2.04(3)	N11-Pt1-N14	81.9(10)
Pt1-N21	2.06(2)	N24-Pt1-N21	83.1(9)
Pt2-C7	1.95(3)	N11-Pt1-N21	177.7(10)
Pt2-C5	1.99(3)	N14-Pt1-N21	97.3(10)
Pt2-C3	1.99(3)	C7-Pt2-C5	89.4(13)
Pt2-C1	2.02(3)	C7-Pt2-C3	177.2(13)
		C5-Pt2-C3	93.3(12)
		C7-Pt2-C1	87.0(12)
		C5-Pt2-C1	176.4(11)
		C3-Pt2-C1	90.3(12)

The important feature of this structure is the occurrence of parallel chains, with an arrangement similar to the known Magnus green salt,[99] where planar cations of $[Pt(NH_3)_4]^{2+}$ and $[PtCl_4]^{2-}$ anions form chains with Pt···Pt distances of ca. 3.25 Å. The polymeric chains of

III-2a are oriented along the b-axis. In addition to ionic interactions, the components of this complex are held together by multiple hydrogen bonds. They occur between NH_2 groups of ethylenediamine ligands and nitrogen atoms of the cyanide ligands (N4···N21, 2.99 Å; N6···N24, 2.99 Å; N2···N11, 2.97 Å; N2···N24, 3.01 Å; N8···N14, 2.90 Å). Pt···Pt distances within the chain are ca. 3.32 Å and 4.01 Å.

3.2.3.3 Molecular squares $[M(en)(CN)]_4(NO_3)_4$ M = Pd^{II} (III-4) and Pt^{II} (III-5)

$[Pd(en)(CN)]_4(NO_3)_4$ (**III-4**) and $[Pt(en)(CN)]_4(NO_3)_4$ (**III-5**) have been crystallized from water solution at RT within several hours and within one week, respectively. X-ray diffraction of these crystals reveals the formation of [2+2]-type discrete molecular squares. Figure 3.7 shows a view of the molecular squares obtained and Table 3.3 summarizes selected bond lengths and angles.

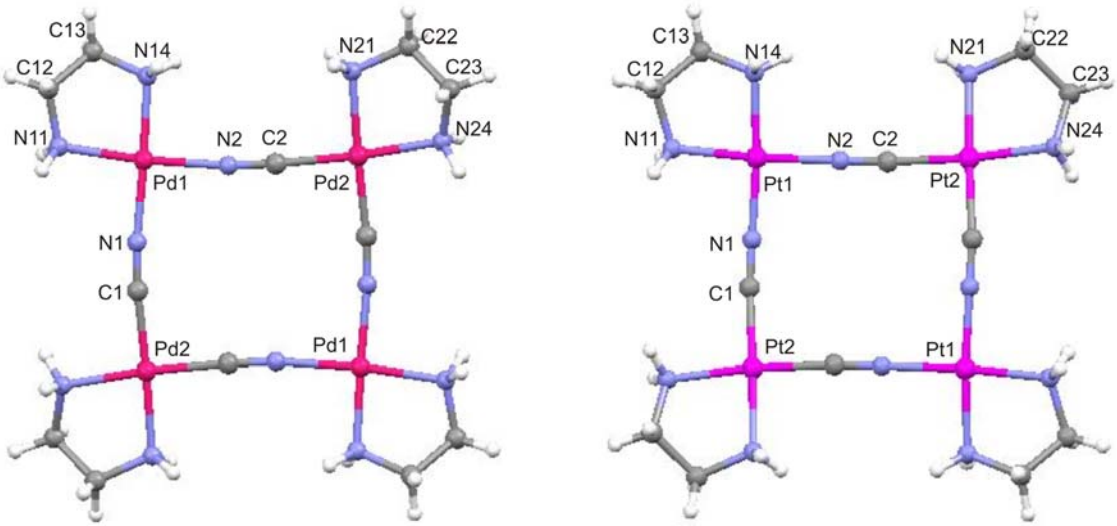

Figure 3.7 Cation structures of $[Pd(en)(CN)]_4(NO_3)_4$ (**III-4**) and $[Pt(en)(CN)]_4(NO_3)_4$ (**III-5**) with numbering scheme.

The structures of Pd and Pt-tetranuclear macrocycles are isomorphous. The values of intramolecular Pd···Pd distances (5.0835(7) and 5.0826(8) Å) are in the same range as Pt···Pt distances (5.0413(7) and 5.0661(7) Å). The bond angles of M2-M1-M2 and M1-M2-M1 for **III-4** are 90.73° and 89.27°, and those for **III-5** are 90.7° and 89.3°. These values are close to ideal 90° and thus true squares have been generated.

Table 3.3 Selected bond lengths (Å) and angles (deg.) for **III-4** and **III-5**.

$[Pd(en)(CN)]_4(NO_3)_4$ (**III-4**)		$[Pt(en)(CN)]_4(NO_3)_4$ (**III-5**)	
Pd1-N11	2.008(6)	Pt1-N11	2.036(9)
Pd1-N14	2.042(6)	Pt1-N14	2.049(9)
Pd1-N1	2.007(8)	Pt1-N1	1.978(10)
Pd1-N2	1.992(7)	Pt1-N2	2.000(13)
Pd2-N21	2.054(6)	Pt2-N21	2.061(9)
Pd2-N24	2.026(6)	Pt2-N24	2.054(9)
Pd1-C1	1.957(7)	Pt1-C1	1.986(10)
Pd1-C2	1.965(6)	Pt1-C2	1.945(12)
C1-N1	1.133(10)	C1-N1	1.129(13)
C2-N2	1.146(10)	C2-N2	1.127(13)
N1-Pd1-N2	91.0(3)	N1-Pt1-N2	91.5(4)
N1-Pd1-N11	91.2(3)	N1-Pt1-N11	92.3(4)
N2-Pd1-N11	177.7(3)	N2-Pt1-N11	175.8(4)
N1-Pd1-N14	174.7(3)	N1-Pt1-N14	175.1(4)
N2-Pd1-N14	94.1(3)	N2-Pt1-N14	92.9(4)
N11-Pd1-N14	83.7(3)	N11-Pt1-N14	83.4(4)
C2-Pd2-C1	90.0(3)	C2-Pt2-C1	90.1(4)
C2-Pd2-N24	178.0(2)	C2-Pt2-N21	91.7(4)
C1-Pd2-N21	92.0(3)	C1-Pt2-N21	177.3(4)
C2-Pd2-N24	94.4(3)	C2-Pt2-N24	174.9(4)
C1-Pd2-N24	94.4(3)	C1-Pt2-N24	94.8(4)
N21-Pd2-N24	83.7(2)	N21-Pt2-N24	83.4(4)

The observed C–N bond distances in **III-4** are the same as the corresponding bond distances in $enPd(CN)_2$ (**III-1**) and thus the coordination of the cyanide nitrogen to the Pd^{2+} center did not cause any significant changes in the bond lengths. The angles Pd-N ≡ C and Pd-C ≡ N range from 173.7(3) to 176.6(3)°. In the corresponding Pt complex, two unit are almost linear (Pt1-N2-C2, 176.0(11)° and Pt2-C2-N2, 176.3(10)°), but the two others are slightly bent (Pt1-N1-C1, 173.9(13)° and Pt2-C1-N1, 167.5(12)°).

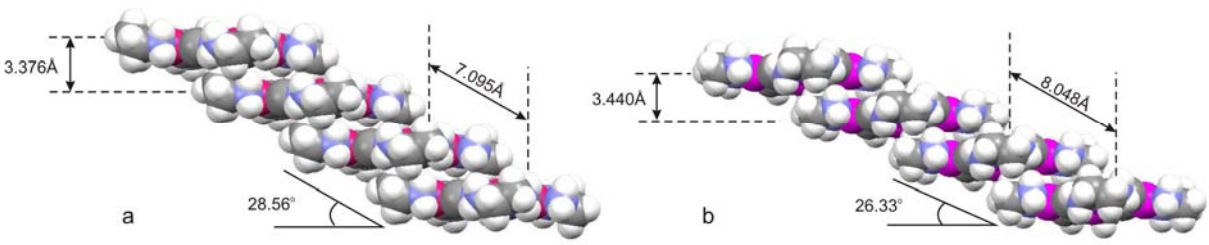

Figure 3.8 Crystal packing of **III-4** (a) and **III-5** (b), indicating formation of "stairs" in solid state.

In the three-dimensional packing of **III-4** and **III-5** the molecules are arranged in the form of stacked sheets (**III-4** along the a-axis and **III-5** along the b-axis), with interlayer separations of 3.38 and 3.44 Å, respectively (Figure 3.8). The M_4 centroid – centroid distance in the **III-4** is about 1 Å shorter than in **III-5** and thus Pt_4 "stairs" are less inclined (26.3°) than those of Pd_4 (28.6°). Adjacent layers are interconnected and alternatively stabilized by hydrogen bonding between NO_3^-, NH_2 groups of ethylendiamine ligands, and water molecules.

3.2.3.4 Crystal structure of the $[Pd(en)(bpy)](SO_4) \cdot 3H_2O$ (III-7)

The single crystal X-ray structure of $[Pd(en)(bpy)](SO_4) \cdot 3H_2O$ reveals a planar metal center with a distorted square-planar geometry (Figure 3.9). Deviations of angles around the Pd atom from ideal 90° are the result of the small bite angle of the chelating 2,2´-bipyridine and ethylenediamine ligands. Distances within the cation are normal.

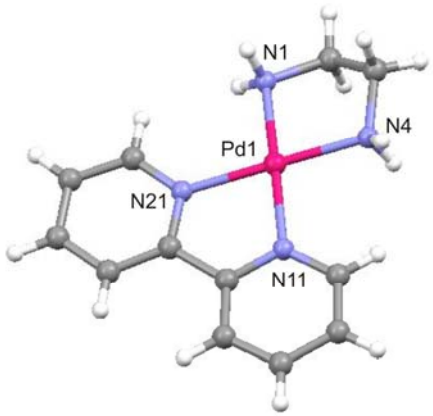

Figure 3.9 $[Pd(en)(bpy)]^{2+}$ cation (**III-7**) with numbering scheme of relevant atoms.

Table 3.4 Selected bond lengths (Å) and angles (deg.) for **III-7**.

$[Pd(en)(bpy)](SO_4)$ (**III-7**)			
Pd1-N11	2.011(7)	N11-Pd1-N21	81.3(3)
Pd1-N21	2.018(6)	N11-Pd1-N1	177.9(3)
Pd1-N1	2.021(7)	N21-Pd1-N1	97.9(3)
Pd1-N4	2.027(6)	N11-Pd1-N4	96.9(3)
		N21-Pd1-N4	177.0(3)
		N1-Pd1-N4	84.0(3)

There are π-π interactions between the bipyridine moieties of adjacent cations, with distances of less than 3.5 Å. As a result, the cations are grouped as linear stacks (Figure 3.10).

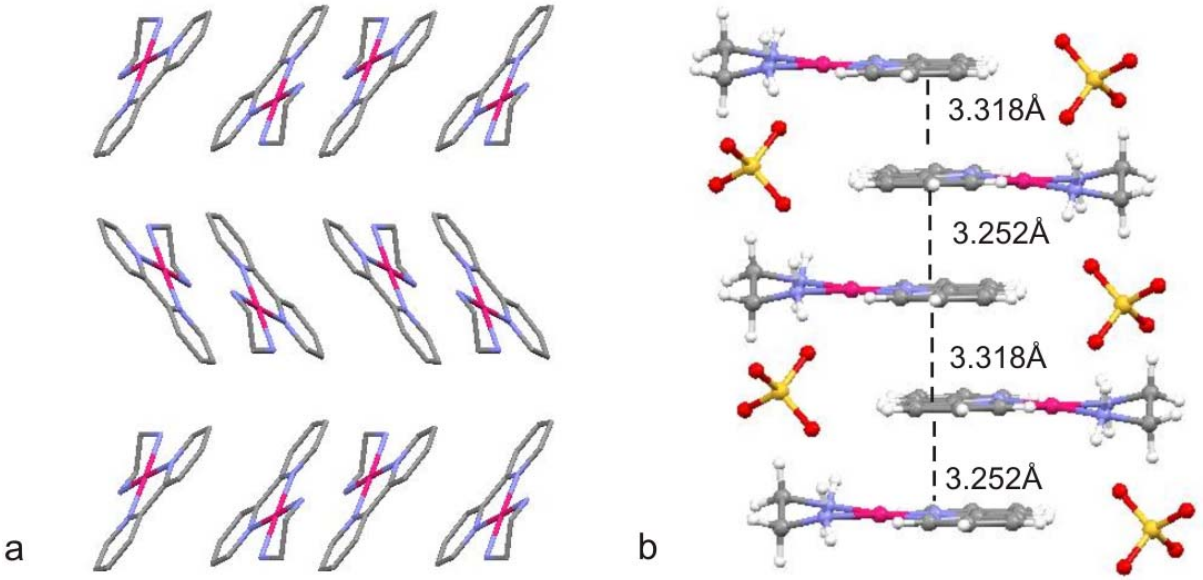

Figure 3.10 Packing arrangement of **III-7** in the crystal structure along a-axis (a) and π-π stacking interactions between neighboring cations along b-axis (b).

Sulfate anions are inserted between two en ligands via hydrogen-bonds. Additionally, cations are linked together through hydrogen bonds involving water molecules. The main hydrogen bonding distances in the crystal packing of **III-7** are: N1···O1w, 2.863(11) Å; N1···O11, 2.826(11) Å; N4···O12, 2.878(9) Å; N4···O13, 2.913(10) Å; O11···O2w, 2.946(10) Å; O13···O2w, 2.733(9) Å; O14···O1w, 2.669(10) Å.

3.3 Interactions with anions and nucleic acids

3.3.1 Interactions with anions

Host-guest interactions between **III-5** and F^-, Cl^- and SO_4^{2-} anions were investigated by ^1H NMR spectroscopy in D_2O by adding increasing amounts of the corresponding sodium salts. Evidence for weak interactions in solution comes from the minor downfield shifts ($\Delta\delta$ < 0.1 ppm) of proton resonances of the Pt_4 square (Table 3.5).

Table 3.5 Chemical shifts of **III-5** upon addition of F^-, Cl^- and SO_4^{2-} anions

Ratio **III-5**:anion	F^-		Cl^-		SO_4^{2-}	
	δ (H1) [ppm]	δ (H2) [ppm]	δ (H1) [ppm]	δ (H2) [ppm]	δ (H1) [ppm]	δ (H2) [ppm]
1:1	2.705	2.534	2.696	2.525	2.732	2.564
1:2	2.708	2.537	2.702	2.531	2.756	2.585
1:4	2.715	2.545	2.712	2.542	2.772	2.6
1:6	2.722	2.552	2.718	2.549	2.783	2.611
1:10	2.727	2.557	2.735	2.562	2.791	2.619
1:20	2.733	2.563	2.762	2.591	2.807	2.633
1:45	2.734	2.564	2.787	2.616	2.815	2.64

Since no strong host-quest interactions are observed for either case, further studies have not been performed. Attempts to study the interaction between **III-5** and the terephthalate anion were not successful, since after the ratio of Pt_4/terephthalate reached 1:3, precipitation and/or crystallization occurs. Crystals obtained from a NMR sample revealed a composition of $\{[Pt(en)(CN)]_4\}(C_8H_4O_4)_2 \cdot 10H_2O$ (**III-5a**).

3.3.1.1. Characterization of $[Pt(en)(\mu\text{-}CN)]_4(C_8H_4O_4)_2 \cdot 10H_2O$ (III-5a)

The molecular structure of the cation of **III-5a** is virtually identical with that of **III-5**, with nearly identical bond lengths and angles (Table 3.6).

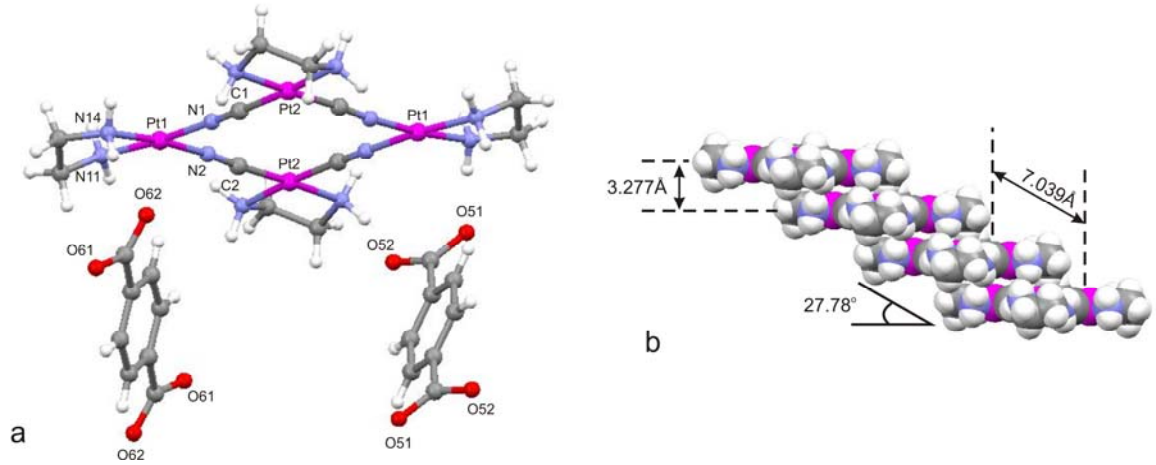

Figure 3.11 Molecular structure of $[Pt(en)(\mu\text{-}CN)]_4(C_8H_4O_4)_2$ (**III-5a**) with numbering scheme of relevant atoms (a) and crystal packing of **III-5a** (b)**,** indicating formation of "stairs" in the solid state.

Terephthalate anions are non-planar, with tilt angles between the carboxy and the phenyl planes being 17.5° and 33.8°. They are involved in hydrogen bonding interactions between anionic carboxylates and the amine ligands of the macrocycle (N11···O61, 2.95 Å; N14···O62 2.84 Å; N14···O51, 2.82 Å; N21···O52, 2.72 Å; N24···O62, 3.01 Å).

Table 3.6 Selected bond lengths (Å) and angles (deg.) for **III-5a**

$[Pt(en)(\mu\text{-}CN)]_4(C_8H_4O_4)_2$ (**III-5a**)			
Pt1-N11	2.030(11)	N1-Pt1-N2	91.4(5)
Pt1-N14	2.041(11)	N1-Pt1-N11	174.0(5)
Pt1-N1	1.966(12)	N2-Pt1-N11	94.1(5)
Pt1-N2	1.948(12)	N1-Pt1-N14	90.8(5)
Pt2-N21	2.051(11)	N2-Pt1-N14	175.0(5)
Pt2-N24	2.037(11)	N11-Pt1-N14	83.4(4)
Pt1-C1	1.937(14)	C2-Pt2-C1	90.0(6)
Pt1-C1	1.923(15)	C2-Pt2-N21	176.8(5)
C1-N1	1.168(16)	C1-Pt2-N21	93.1(5)
C2-N2	1.176(17)	C2-Pt2-N24	93.8(5)
		C1-Pt2-N24	175.9(5)
		N21-Pt2-N24	83.1(5)

The packing of ions of **III-5a** is also very similar to that of **III-5**. The distance between stacked Pt_4 squares is ca. 3.28 Å. The M_4 centroid – centroid distance in **III-5a** is ca. 7.04Å and thus ≈ 1 Å shorter the in **III-5.** Pt_4 "stairs" are inclined by 27.8°.

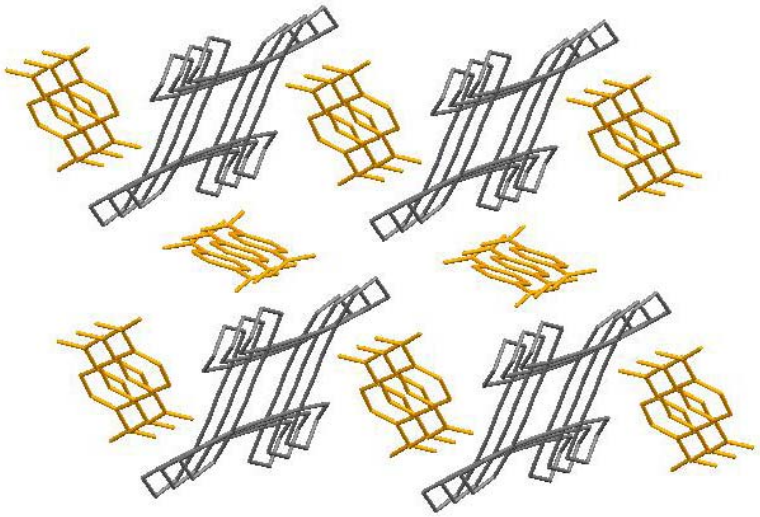

Figure 3.12 Packing arrangement of **III-5a** in the crystal structure

Pt_4 squares and terephthalate anions are packed in parallel chains and appear in fully ordered array. Similar packing patterns, albeit with smaller distances between parallel chains of the Pt_4 and Pd_4 squares and nitrate anions, are observed in **III-4** and **III-5**.

3.3.2 Interactions with nucleic acid components

The aim of this investigation was to find out whether positively charged cyanido-bridged squares interact with nucleobase aggregates (quartets, base pairs). To validate the character of interactions, preliminary solution ^{1}H-NMR experiments were carried out with the model nucleobases 1-methylcytosine (1-MeC), 1-methyluracil (1-MeUH) and 9-ethyladenine (9-EtA). For this propose **III-5** was titrated with increasing amounts of the corresponding nucleobase at pH values, where no acid-base equilibria are relevant. Chemical shifts of the **III-5** are listed in the Table 3.7. Because of low solubility, 9-methylguanine and 1-methylthymine were not applied in this study.

Table 3.7 Chemical shifts of **III-5** upon addition of 1-MeC, 1-MeUH and 9-EtA.

Ratio	1-MeC		1-MeUH		9-EtA	
III-5:nb	δ (H1) [ppm]	δ (H2) [ppm]	δ (H1) [ppm]	δ (H2) [ppm]	δ (H1) [ppm]	δ (H2) [ppm]
1:1	2.731	2.56	2.720	2.549	2.742	2.572
1:3	2.745	2.574	2.741	2.572	2.788	2.618
1:8	2.770	2.599	2.757	2.587	2.840	2.670
1:14	2.795	2.624	2.778	2.608	2.871	2.702
1:20	2.809	2.639	2.792	2.622	2.895	2.726
1:35	2.842	2.672	2.807	2.637	2.946	2.777
1:45	2.849	2.679	2.807	2.637	2.984	2.816

In the presence of a large excess of the nucleobase, *downfield* shift of the proton resonances of the Pt_4 square have been observed. Chemical shift for the pyrimidine bases are $\Delta\delta$ = 0.14 ppm (1-MeC) and 0.1 ppm (1-MeUH) for r = 1:45. The effect caused by 9-MeA was almost three times as large as with the two pyrimidine bases, namely $\Delta\delta$ = 0.28 ppm. The adenine H2 and H8 resonances shift *upfield* with increasing concentrations. In the concentration range 0.003 M – 0.105 M these shifts are $\Delta\delta$ = 0.30 ppm for H2, $\Delta\delta$ = 0.26 ppm for H8. This finding suggests a stacking interaction between 9-EtA and $[(en)Pt(CN)]_4^{4+}$.

Attempts were made to obtain cocrystals of **III-4** and **III-5** with model nucleobases. Only in one instance, namely after mixing **III-4** with [1-MeCH]I, crystals suitable for X-ray structure determination have been obtained. Unfortunately, the crystals proved not to be the expected stacked aggregate between hemiprotonated 1-MeC and **III-4**. Rather, to the above mentioned instability of the Pd_4 macrocycle and the presence of iodide, formation of [1-MeC·1-MeCH][PdI_2(CN)(1-MeC)]·$2H_2O$ (**III-8**) took place.

3.3.2.1. Characterization of *trans*-[Pd(1-MeC-*N3*)(CN)I_2](1-MeC)(1-MeCH)·$2H_2O$ (III-8)

trans-[Pd(1-MeC-*N3*)(CN)I_2](1-MeC)(1-MeCH)·$2H_2O$ (**III-8**) has been isolated as orange crystals from a solution containing [Pd(en)(CN)]$_4$(NO_3)$_4$ and an excess of [1-MeCH]I. Because of low solubility, NMR spectra could not be recorded. Compound **III-8** is composed of two subunits: anionic *trans*-[Pd(1-MeC-N3)(CN)I_2]$^-$ and cationic [(1-MeC)(1-MeCH)]$^+$ (Figure 3.13). The square-planar coordination geometry around the Pd atom consists of two *trans* oriented iodide ions, a cyanido group and 1-MeC, coordinated to Pd through its *N*3 nitrogen. The aromatic ring of 1-MeC and the Pt coordination plane are almost perpendicular to each other (∠ PtI_2NC – 1-MeC = 83.1°). In the cationic unit one neutral and one N3 protonated 1-methylcytosine bases are joined by three H-bonds, giving the typical hemiprotonated cytosine unit.

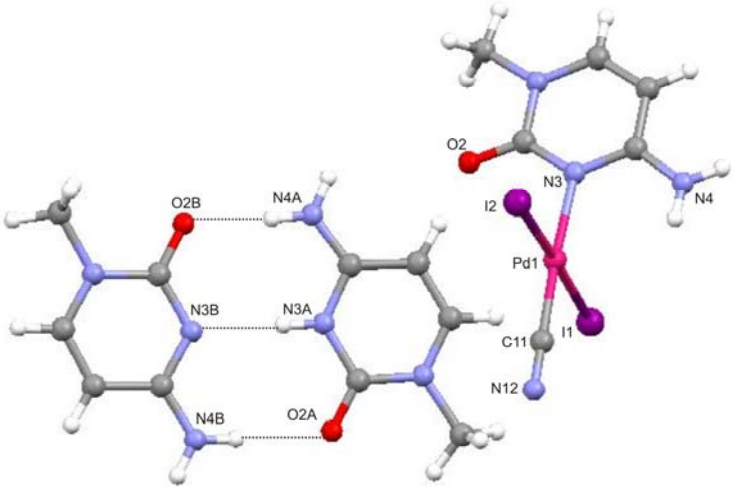

Figure 3.13 *trans*-[Pd(1-MeC-*N3*)(CN)I_2][(1-MeC)(1-MeCH)]·$2H_2O$ (**III-8**) with atomic numbering scheme.

Table 3.8 Selected bond lengths (Å) and angles (deg.) for **III-8**

trans-[Pd(1-MeC-*N3*)(CN)I_2](1-MeC)(1-MeCH) (**III-8**)			
Pd1-C11	1.939(4)	C11-Pd1-N3	176.89(18)
Pd1-N3	2.089(3)	C11-Pd1-I1	88.61(13)
Pd1-I1	2.5913(6)	N3-Pd1-I1	90.09(10)
Pd1-I2	2.5959(6)	C11-Pd1-I2	88.96(13)
		N3-Pd1-I2	92.38(10)
		I1-Pd1-I2	177.47(2)

Hydrogen bonds between the CN ligand, keto-O and amino groups of 1-MeC and water molecules lead to the formation of ordered infinite layers in the solid state. Additionally π-π stacking of [(1-MeC) $(1MeCH)^+$] moieties with a distance of 3.36Å occurs in the structure.

3.4 Conclusions

In this chapter the synthesis of CN^- bridged molecular squares and their ability to interact non-covalently with nucleobases are described. In order to prevent formation of linkage isomers, the advantage of a stepwise construction was used. Initially, upon coordination of the cyanido ligand to the $[(en)Pd(H_2O)_2]^{2+}$, $[(en)Pt(H_2O)_2]^{2+}$ and *trans*-$[(ma)_2Pt(H_2O)_2]^{2+}$, the corresponding building blocks were obtained. One of them – $Pd(en)(CN)_2$ (**III-1**) – was characterized crystallographically. An additional complication during this synthesis is the strong *trans*-effect of cyanido ligands, which promotes *trans* labilization, hence favors the formation of side products *e. g.* $[Pt(en)_2][Pt(CN)_4]$ (**III-2a**).

The self-assembly of a 90° $[(en)M(CN)_2]$ acceptor with $[(en)M(H_2O)_2]^{2+}$ donor results the designed squares, by establishing coordinative bonds between the nitrogen atom of cyanide group and a second metal cation. $[Pd(en)(CN)]_4(NO_3)_4$ (**III-4**) was found to be unstable in solution, even in the absence of nucleobases. In contrast, $[Pt(en)(CN)]_4(NO_3)_4$ (**III-5**) is stable and is suitable to study interactions with model nucleobases.

Chapter 4 – Coordination of cyanopyridine to Pt(II) and Pd(II) centers and subsequent hydrolysis. Formation of novel hexanuclear square

4.1 Cyanopyridine ligands and their hydrolysis

In the previous chapter the cyanide ligand has been used to bridge enPt(II) and enPd(II) corners. As extension of this work, 4-cyanopyridine (4-CNpy) and 3-cyanopyridine (3-CNpy) were applied as bridging ligands, with the aim to include the aromatic moiety to the skeleton and to obtain structures of larger dimensions.

Cyanopyridine ligands consist of an aromatic ring of pyridine to which a nitrile group attached in the third or fourth position. Nitrogen atoms of the pyridine rings are unprotonated over a wide pH range: pK_a of 4-CNpy is 1.9, pK_a of 3-CNpy is 1.36.[100] As shown in Scheme 4.1 these ligands have two potential coordination sites: the pyridine nitrogen (NC$_4$H$_4$CN) and the nitrogen of the nitrile group (NCpy).

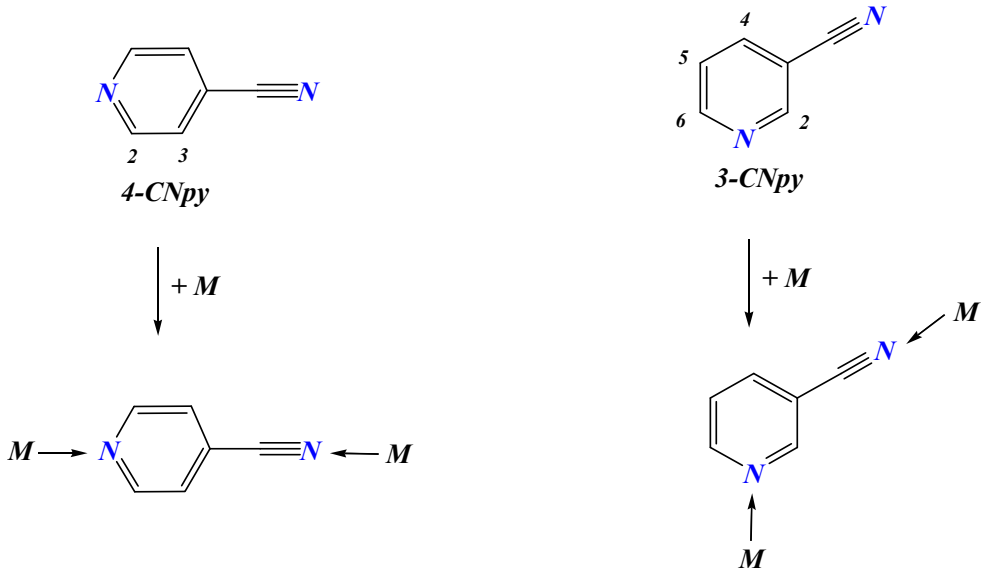

Scheme 4.1 Principal metal binding patterns of 4-cyanpyridine and 3-cyanpyridine ligands.

A series of homo- and heteronuclear, as well as mixed valence cyanopyridine-bridged complexes, containing iron, ruthenium and osmium, has previously been prepared and characterized.[101] As π-conjugated bridging units, the cyanopyridine ligands permit intramolecular electron transfer, thereby providing valuable information regarding electron exchange processes. The ligand 4-cyanopyridine has also been used to obtain coordination

compounds with ions of different transition metals, with the aim to use them as supramolecular synthons.[102]

An additional feature of interest of these ligands is the metal mediated or metal catalyzed hydrolysis. For instance, attempts to obtain a CNpy bridged complex linked to two Ru(III) centers was unsuccessful, in contrast to Ru(II), because of hydrolysis of *NC*py ligand, which led to the formation of a deprotonated pyridinecarboxamido-bridged complex.[103] Similar features have been observed in our studies.

The use of strong acid (96% H_2SO_4) or base (50% KOH/t-BuOH) for the nitrile hydrolysis leading to amides has several disadvantages. For example, uncontrolled further hydrolysis to carboxylic acid or formation of polymers can occur under the above mentioned conditions. Moreover, these harsh conditions do not permit the presence of sensitive groups in the molecules.

Hydrolysis of nitriles can also be achieved using enzymes.[104] Although nitrile hydratases are used as biocatalysts in acrylamide production, their application is limited, since they are very sensitive to the reaction conditions. A large number of metal complexes have shown to catalyze this reaction.[105] Catalyzed hydration of nitriles to their corresponding amides is one of the most important processes in the chemical and pharmaceutical industry. A widely accepted mechanism of metal catalyzed hydration of nitriles is shown in Scheme 4.2.

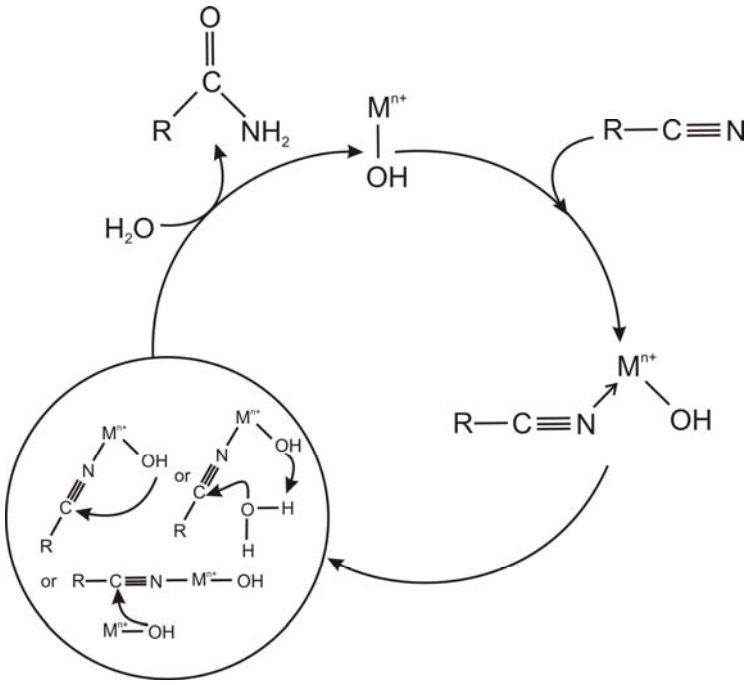

Scheme 4.2 A proposed reaction mechanism for the M-catalyzed hydration of nitriles

4.2 Bis-(4-CNpy) and -(3-CNpy) complexes of Pt(II) and Pd(II)

4.2.1 Synthesis and NMR spectroscopic studies

The compounds $[(en)M(CNpy)_2]^{2+}$ ($M = Pt^{II}$, Pd^{II}) have been prepared by reaction of the corresponding $[(en)M(H_2O)_2]^{2+}$ with 4-CNpy or 3-CNpy in H_2O. Palladium complexes have been obtained at RT, and platinum complexes have been prepared by reacting components at 40°C. The initial goal was the preparation of tetranuclear species by coordination of a second metal center to the nitrile moieties of two adjacent ligands. However, as has been found in the present study, hydrolysis of nitrile substituent occurs during the synthesis. The use of platinum or palladium metal centers as catalytic sites for hydrolysis of nitriles is known from the literature.[106]

NMR scale reactions have been carried out at different pH values to follow the process of hydrolysis. It became evident that these reactions do not proceed in a clean way; rather a complicated series of products is formed, prior to hydrolysis. The multiplicity of resonances could arise from the formation of intermediate structures, with metals coordinated to both sides of the cyanopyridine ligand and/or formation of different isomeric structures. Table 4.1 lists ^{1}H NMR resonances of free ligands and isolated complexes **IV-1** – **IV-4**.

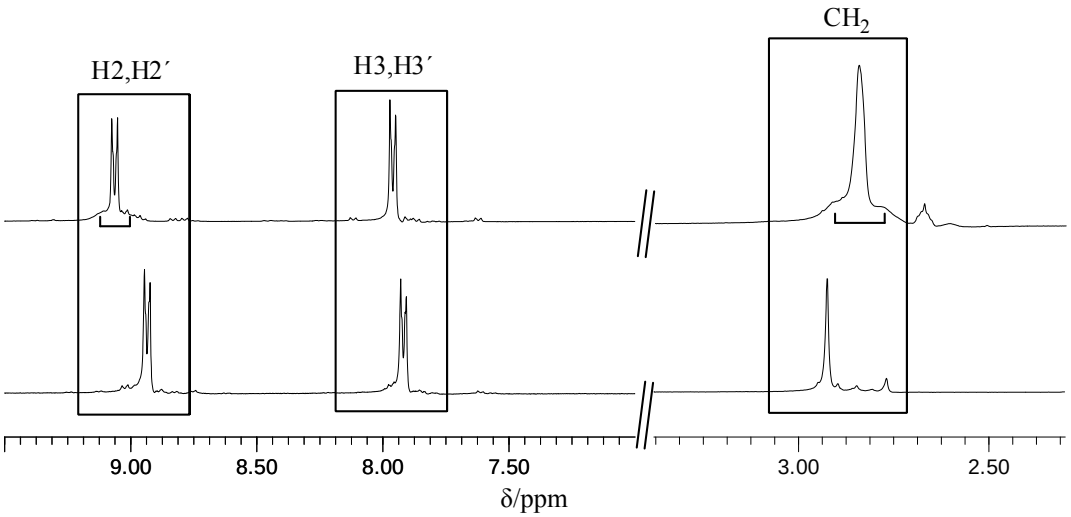

Figure 4.1 ^{1}H NMR spectra of $[(en)Pt(4\text{-}CNpy)_2](NO_3)_2$ (**IV-1**) (top) and $[(en)Pd(4\text{-}C(O)NH_2py)_2](SO_4)$ (**IV-3**) bottom.

Coordination of enPt(II) to the cyanopyridine moiety results in a downfield shift of its ^{1}H NMR signals. The complex $[(en)Pt(4\text{-}CNpy)_2](NO_3)_2$ (**IV-1**) has two pairs of protons of the pyridine moiety, which gives rise to two doublets of identical intensities with

$^3J(^{195}Pt\text{-}^1H2,^1H2')$ = 39 Hz, and a singlet corresponding to the CH_2 protons of the ethylenediamine ligand, with $^3J(^{195}Pt\text{-}^1H)$ = 34 Hz. The analogous Pd(II) complex [(en)Pd(4-$C(O)NH_2py)_2$](SO_4) (**IV-3**) been isolated as well. Its ^1H NMR spectrum is very similar, having two doublets in the aromatic region in a 1:1 ratio, and a singlet in the aliphatic region (Figure 4.1).

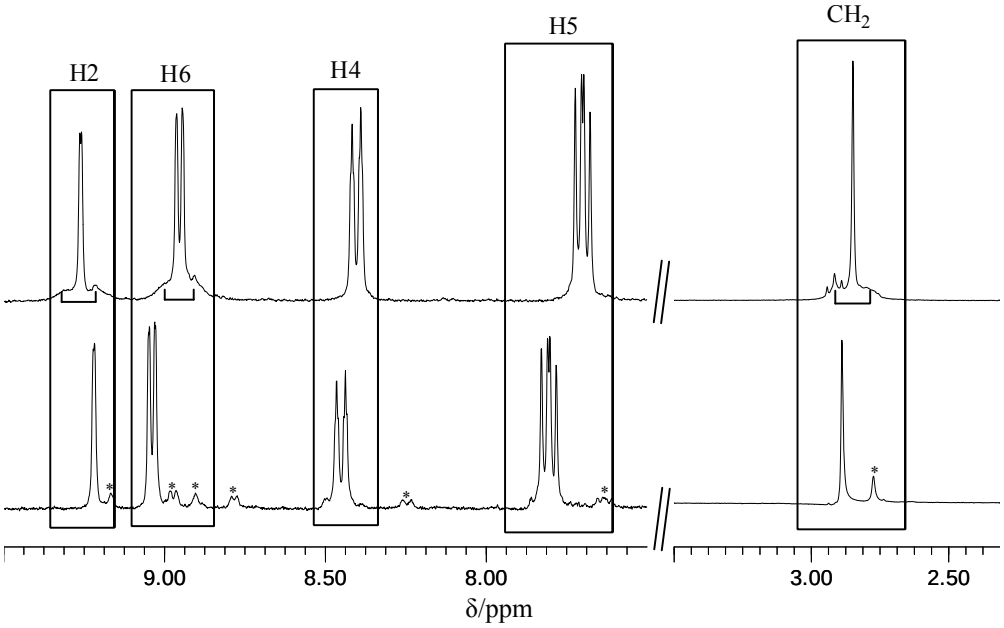

Figure 4.2 ^1H NMR spectra of [(en)Pt(3-$C(O)NH_2py)_2$]$(NO_3)_2$ (**IV-2**) (top) and [(en)Pd(3-$C(O)NH_2py)_2$]$(ClO_4)_2$ (**IV-4**) bottom (* impurities)

The ^1H NMR spectra of **IV-2** and **IV-4** in D_2O contain four sets of resonances for the $C(O)NH_2py$ ligand and one peak for the chelating en ligand. These findings are likewise consistent with the presence of a single species (Figure 4.2). For the H2, H6 and CH_2 proton signals, platinum satellites are observed, with the following coupling constants: $^3J(^{195}Pt\text{-}^1H2,^1H2')$ = 36 Hz, $^3J(^{195}Pt\text{-}^1H6,^1H6')$ = 38 Hz, and $^3J(^{195}Pt\text{-}^1H)$ = 42 Hz.

Table 4.1 ^1H NMR data of 4-CNpy, 3-CNpy and isolated metal complexes.

	H2 (H2′)	H3 (H3′)	H4	H5	H6	CH_2 (en)
4-CNpy pD = 5.8	d, 8.75 ppm ^3J = 1.8 Hz	d, 7.78 ppm ^3J = 1.8 Hz				
3-CNpy pD =6.2	d, 8.89 ppm ^3J = 0.9 Hz		dd, 8.24 ppm ^3J = 6.0 Hz ^3J = 1.0 Hz	dd 7.63 ppm ^3J = 3.9 Hz ^3J = 6.0 Hz	dd 8.78 ppm ^3J = 0.9 Hz ^3J = 3.8 Hz	

(**IV-1**) pD = 6.4	d, 9.04 ppm ^3J = 6.9 Hz	d, 7.99 ppm ^3J = 6.9 Hz				s, 2.85 ppm
(IV-2) pD = 4.6	d, 9.26 ppm ^3J = 1.5 Hz		d, 8.40 ppm ^3J = 8.1 Hz	d,d 7.70 ppm ^3J = 6.0 Hz ^3J = 8.0 Hz	d, 8.95 ^3J = 5.4 Hz	s, 2.85 ppm
(**IV-3**) pD = 5.8	d, 8.94 ppm ^3J = 6.6 Hz	d, 7.92 ppm ^3J = 6.6 Hz				s, 2.93 ppm
(**IV-4**) pD = 6.6	d, 9.21 ppm ^3J = 1.8 Hz		d, 8.40 ppm ^3J = 8.1 Hz	dd, 7.72 ppm ^3J = 8.0 Hz ^3J = 6.0 Hz	d, 8.91 ppm ^3J = 5.1 Hz	s, 2.91 ppm

4.2.2 IR spectra

Infrared spectroscopy represents a good method for analysis of hydrolyzed and unhydrolyzed species. The CN stretching vibration of 4-CNpy in **IV-1** is observed at 2242 cm^{-1} and thus is nearly identical with that of the free ligand (2243 cm^{-1}), thus clearly indicating that metal binding occurs not via the nitrile group. In the IR spectra of **IV-2**, **IV-3** and **IV-4** bands due to ν(CN) are absent. Instead strong bands corresponding to ν(CO) are observed, with wavenumbers as indicated in Table 4.2.

Table 4.2 Vibrational frequencies of $\nu_{C\equiv N}$ or $\nu_{C=O}$ in 4-CNpy, 3-CNpy and isolated metal complexes.

	4-CNPy	**3-CNPy**	**IV-1**	**IV-2**	**IV-3**	**IV-4**
υ(CN) $[cm]^{-1}$	2243	2232	2242			
υ(CO) $[cm]^{-1}$				1672	1678	1675

4.2.3 X-ray crystal structures

Crystals of all 1:2 complexes were grown at room temperature from water/methanol (1:1) solutions. In all corner units, the substituted pyridine ligands are coordinated via the pyridyl-*N* atoms to the metal ion. Individual metal centers are square-planar, displaying a N_4 coordination environment.

4.2.3.1 Crystal structure of $[(en)Pt(4\text{-}CNpy)_2](NO_3)_2$ (IV-1)

A view of the cation of **IV-1** with the atomic numbering scheme of the coordinating sites is presented in Figure 4.3, and the relevant bond distances and bond angles are listed in Table 4.3. Platinum (II) adopts square-planar coordination geometry, bearing a chelating ethylenediamine ligand, with the other two positions being occupied by two 4-CNpy ligands.

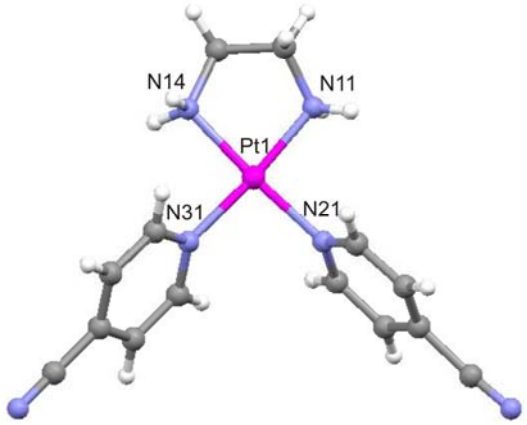

Figure 4.3 Cation structure of $[(en)Pt(4\text{-}CNpy)_2](NO_3)_2$ (**IV-1**).

Table 4.3 Selected bond lengths (Å) and angles (deg.) for **IV-1**.

$[(en)Pt(4\text{-}CNpy)_2](NO_3)_2$ (**IV-1**)			
Pt1-N11	2.021(5)	N21-Pt1-N31	90.9(2)
Pt1-N14	2.009(5)	N14-Pt1-N31	92.3(2)
Pt1-N21	2.007(6)	N14-Pt1-N11	82.9(2)
Pt1-N31	2.013(5)	N21-Pt1-N11	93.8(2)
		N21-Pt1-N14	175.9(2)
		N31-Pt1-N11	175.0(2)

One of the aromatic pyridine rings (ring 2) is almost perpendicular to the Pt coordination plane (dihedral angle of 83.9°), while the angle with the second ligand CNpy(3) is 60.4°.

The intermolecular hydrogen bonds between the NO_3^- anions, NH_2 groups of the amine moiety and water molecules (N11···O1W, 2.93 Å; O1W···O13, 2.84 Å and N14···O13, 2.93 Å) link adjacent molecules in infinite chains (Figure 4.4). Two neighboring chains are also connected by hydrogen bonding (N14···O22, 2.99 Å; O23···O1W, 2.82 Å).

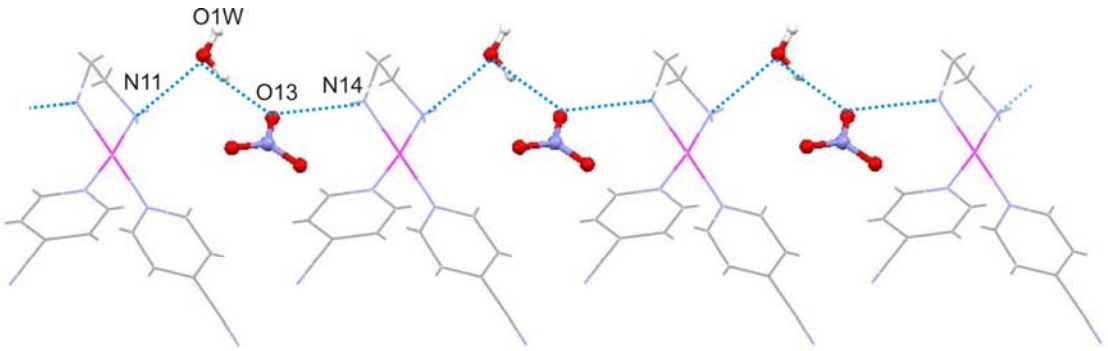

Figure 4.4 Packing arrangement of **IV-1** in the crystal structure showing formation of hydrogen bond-linked chains.

π-π interactions of 3.37 Å between the π system of the C≡ N groups and the aromatic rings of the pyridine moieties are observed in the crystal structure. Only one of the two 4-CNpy moieties from each molecule is involved in these interactions.

4.2.3.2 Crystal structure of $[(en)Pt(3\text{-}C(O)NH_2py)_2](NO_3)_2$ (IV-2)

In contrast to $[(en)Pt(4\text{-}CNpy)_2](NO_3)_2$ (**IV-1**), the complex **IV-2** crystallizes as $[(en)Pt(3\text{-}C(O)NH_2py)_2](NO_3)_2$, with the CN group of the 3-CNpy ligands hydrolysed to amide. Pt adopts the expected square-planar geometry with expected bond lengths and angles (Table 4.4).

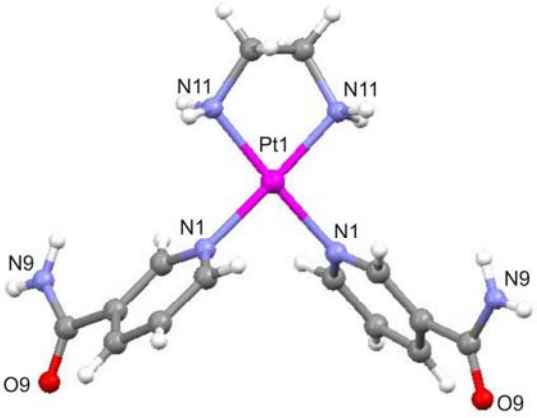

Figure 4.5 View of $[(en)Pt(3\text{-}C(O)NH_2py)_2]^{2+}$ cation (**IV-2**) with atomic numbering scheme..

Two $3\text{-}C(O)NH_2py$ ligands are mutually *head-tail* oriented in **IV-2**, with respect to the metal coordination plane, with a dihedral angle of *ca.* 81.1°.

Table 4.4 Selected bond lengths (Å) and angles (deg.) for **IV-2**.

[(en)Pt(3-C(O)NH_2py)$_2$](NO_3)$_2$ (**IV-2**)			
Pt1-N11	2.024(12)	N11-Pt1-N11	84.1(6)
Pt1-N1	2.041(12)	N11-Pt1-N1	93.4(4)
		N11-Pt1-N1	177.3(5)
		N1-Pt1-N1	89.0(6)

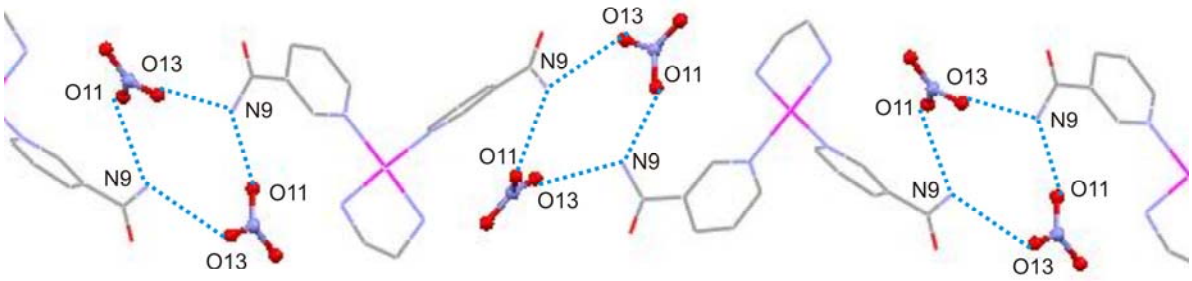

Figure 4.6 Packing arrangement of **IV-2** in the crystal structure showing formation of hydrogen bond-linked chains.

As in the previous case, hydrogen-bonded chain formation involving the anions is observed in the crystal structure (N9···O11, 2.95 Å; N9···O13, 3.02 Å) (Figure 4.6). These chains are arranged in a zigzag fashion (N11···O12, 3.05 Å).

4.2.3.3 Crystal structure of [(en)Pd(4-C(O)NH_2py)$_2$](SO_4) (IV-3)

Figure 4.7 illustrates the cation structure of [(en)Pd(4-C(O)NH_2py)$_2$](SO_4) (**IV-3**). Bond lengths and angles are given in Table 4.5 and do not show unusual features. The complex **IV-3** consists of a palladium(II)ethylenediamine unit coordinated to two isonicotinamide ligands. The dihedral angles between the Pt coordination plane and the 4-C(O)NH_2 ligands are as follows: ∠ PtN_4-4C(O)NH_2py(A) = 53.6° and ∠ PtN_4-4C(O)NH_2py(B) = 59.0°.

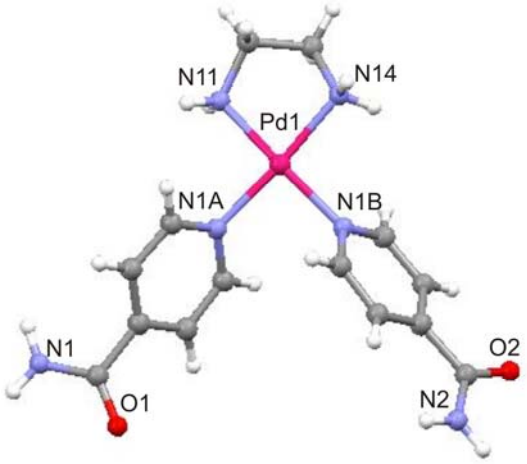

Figure 4.7 Cation structure of $[(en)Pd(4\text{-}C(O)NH_2py)_2](SO_4)$ (**IV-3**) with atomic numbering scheme.

Table 4.5 Selected bond lengths (Å) and angles (deg.) for **IV-3**.

$[(en)Pd(4\text{-}C(O)NH_2py)_2](SO_4)$ (**IV-3**)			
Pd1-N11	2.0188(19)	N11-Pd1-N1A	93.47(8)
Pd1-N1A	2.0223(19)	N1A-Pd1-N1B	88.54(8)
Pd1-N1B	2.0231(19)	N11-Pd1-N14	83.87(8)
Pd1-N14	2.0249(19)	N1B-Pd1-N14	94.56(8)
		N11-Pd1-N1B	172.40(8)
		N1A-Pd1-N14	175.52(8)

In the solid state, cations of **IV-1** extend to a 2D network in the *bc* plane (Figure 4.8). Sulfate anions and water molecules are involved in the formation of hydrogen bonds between individual cations with the following contacts: N1···O11, 2.82 Å; O1W···N11, 2.92 Å; O1W···O1, 2.91 Å; O1W···O13, 2.78 Å; N14···O14, 2.91 Å; N2···O13, 2.84 Å. Neighboring layers are interconnected via collective interactions of π-π stacks between py moieties as well as hydrogen bonding (not shown): π-π, 3.25 Å; N11···O11, 2.81 Å; N14···O13, 3.01 Å; N2···O12, 2.81 Å.

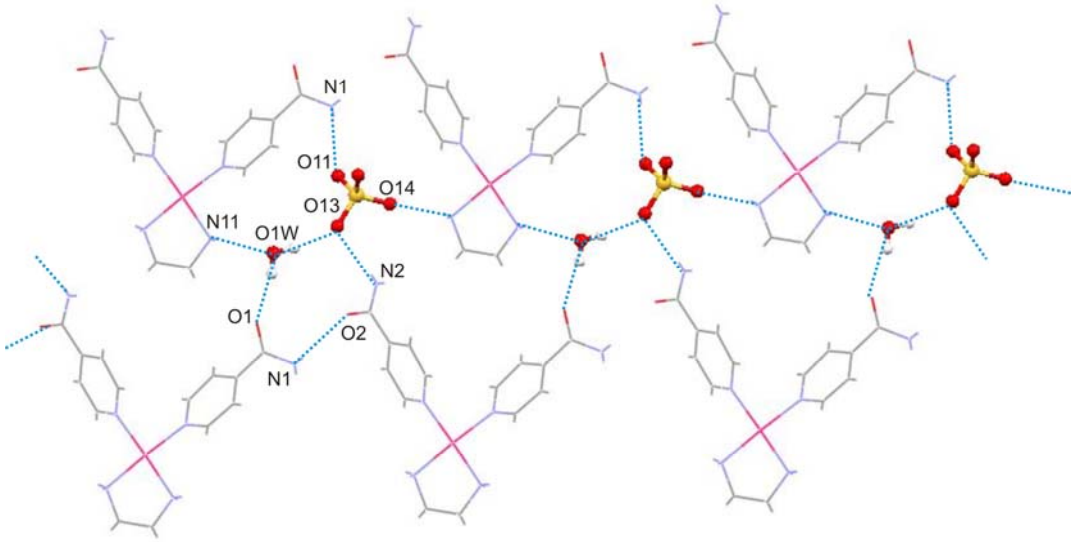

Figure 4.8 Packing arrangement of **IV-1** in the crystal structure, showing formation of hydrogen bond-linked network.

4.2.3.2 Crystal structure of $[(en)Pd(3\text{-}C(O)NH_2py)_2](ClO_4)_2$ (IV-4)

The cation structure of **IV-4** is depicted in Figure 4.9. Bond distances and angles are consistent with previously reported analogous crystal structures (Table 4.6). The 4-$C(O)NH_2$py ligands adopt a *head-head* orientation, and hence $C(O)NH_2$ groups of the nicotinamide ligands are on the same side of the Pt coordination plane. The tilt angle between the platinum coordination plane and the coordinated PtN_4-3$C(O)NH_2$py ligand is 82.8°.

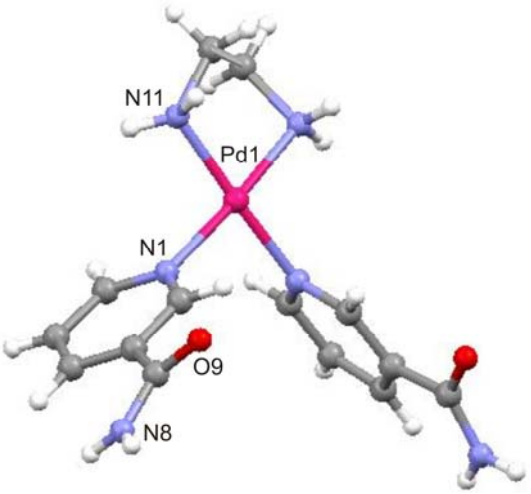

Figure 4.9 Cation structure of $[(en)Pd(3\text{-}C(O)NH_2py)_2](ClO_4)_2$ (**IV-4**) with partial atomic numbering scheme.

Table 4.6 Selected bond lengths (Å) and angles (deg.) for **IV-4**.

[(en)Pd(3-C(O)NH_2py)$_2$](ClO_4)$_2$(**IV-4**)			
Pd1-N11	2.007(4)	N11-Pd1-N11	83.7(2)
Pd1-N1	2.025(4)	N11-Pd1-N1	92.79(15)
		N1-Pd1-N1	90.7(2)
		N11-Pd1-N1	175.90(15)

A notable difference between the above described structures and **IV-4** is the presence of mirror plane in the latter. Hydrogen bonds involving amino and carbonyl groups (N11···O9, 2.80 Å) link centrosymmetricaly related cations of **IV-4** and form linear chains along the a-axis with intrachain Pd···Pd separations in the range of ca. 7.5 Å (Figure 4.10).

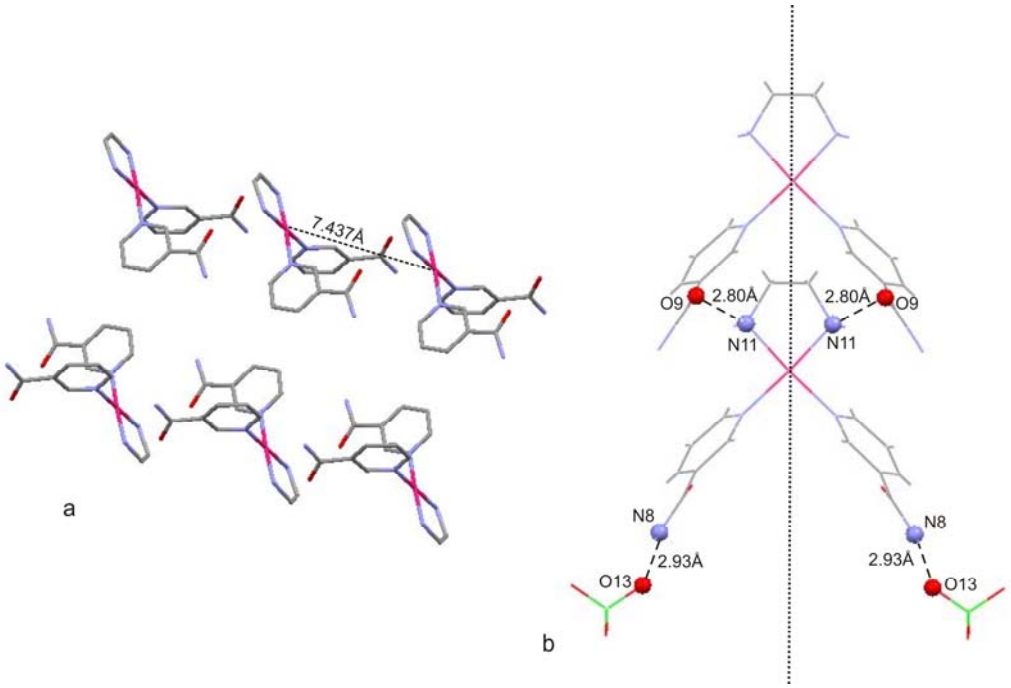

Figure 4.10 Arrangement of cations of **IV-4** showing the formation of linear Pd···Pd···Pd chains (a) and the hydrogen bonding pattern between two neighbouring cations (b).

Additionally one perchlorate anion makes hydrogen bonding contacts with the amino groups of the nicotineamide ligands: N6···O13, 2.93 Å.

4.3 Towards structures of higher complexity

Further reactions using $[(en)Pt(4\text{-}C(O)NH_2py)_2]^{2+}$ and $[(en)Pd(4\text{-}C(O)NH_2py)_2]^{2+}$ as building blocks have been initiated in an effort to obtain closed cyclic structures. Deprotonated isonicotinamide is a non-symmetrical tridentate ligand, where pyridine and amide nitrogens as well as the carbonyl group could act as metal binding sites (Scheme 4.3). Thus, the above mentioned building blocks can act as multi-bridging synthons.

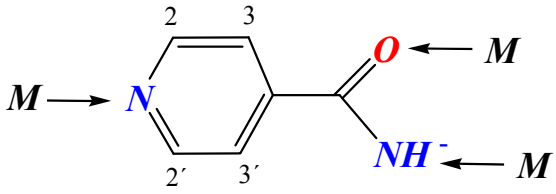

Scheme 4.3. Principal metal binding patterns of deprotonated isonicotinamide ligand.

Several amidate bridged complexes containing two Pt(II) or two Pd(II) centers are known from the literature.[107] Treatment of $[Pt(MeCN)_2Cl_2]$ with silver salts led to the formation of the first "platinum blue" as a result of hydrolysis of the acetonitrile ligand and the ability of acetamide to act as bridging ligand.[108] Ruiz and coworkers have shown that dinuclear palladium(II) hydroxo complexes can react with a variety of nitriles to yield the corresponding amidate complexes.[109] An asymmetric amidate complex, in which two $[Pd(en)]^{2+}$ units are held together by one amidate bridge and one hydroxo bridge is also known.[110] As similar binding mode has been observed in the molecular square containing Re_2(II, II) and Pt(II) at the corners bridged by isonicotinate ligands, as reported by Dunbar *et. al*.[111]

4.3.1. Synthesis and characterization of $[\{(en)Pt\}_6(4\text{-}C(O)NHpy)_4(PF_6)](NO_3)_7$ (IV-5)

The hexanuclear complex $[\{(en)Pt\}_6(4\text{-}C(O)NHpy)_4(PF_6)](NO_3)_7$ (**IV-5**) has been obtained in the reaction of $[(en)Pt(4\text{-}CNpy)_2](NO_3)_2$ (**IV-1**) with two equivalents of $[enPt(H_2O)_2]^{2+}$. The pH of the reaction medium was raised to *ca.* 10 by addition of NaOH. OH^- firstly promotes hydrolysis of nitrile and secondly assists the deprotonation of the amide group to enable metal coordination.

The ^{1}H NMR spectrum of the isolated product displays a doublet at 9.19 ppm (H2,H2´, ^{3}J = 5.1 Hz) and two superimposed doublets at ca. 8.05 ppm (H3,H3´), which are shifted downfield compared to those of the free ligand. The ^{1}H NMR resonances of the CH_2 protons of ethylenediamine are found at 3.22 ppm (Figure 4.11).

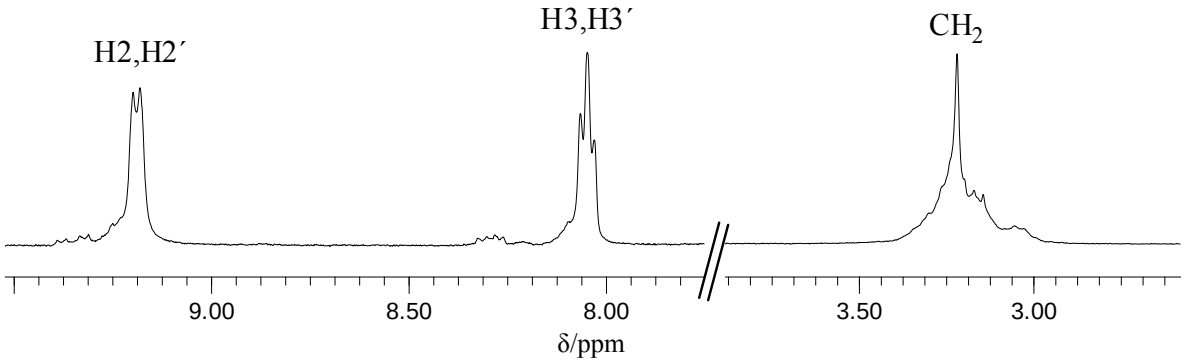

Figure 4.11. ^{1}H NMR spectrum of [{(en)Pt}$_6$(4-C(O)NHpy)$_4$(PF$_6$)](NO$_3$)$_7$ (**IV-5**).

Formation of the hexanuclear square (**IV-5**) is achieved by the combination of two different binding subunits – through pyridyl nitrogens in one corner, and two amidate ligands in the other. In principle, coordination of Pt(II) to the isonicotineamide ligand could occur in *head-head* or *head-tail* fashion, as schematically shown in Figure 4.12.

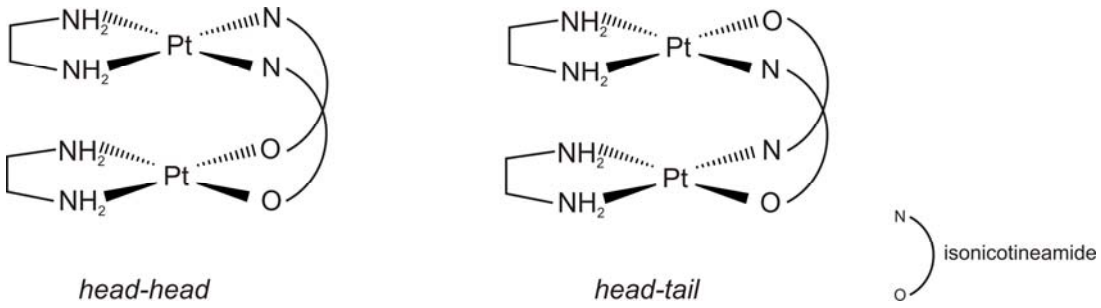

Figure 4.12 Schematic representation of *head-head* and *head-tail* orientations of isonicotinamidate ligands.

The molecular structure of complex **IV-5** (Figure 4.13) shows that in the cation two [(en)Pt]$^{2+}$ units in both corners are held together by two bridging amidate ligands in *head-head* orientation. The square-planar geometries of Pt(II) are distorted. Selected bond distances

and angles are given in Table 4.7. Pt···Pt contacts within the dinuclear corners are 3.0662(7) Å, and diagonal Pt···Pt distances are 12.2191(12) Å (Pt1···Pt2´), and 12.7354(8) Å (Pt3···Pt3´).

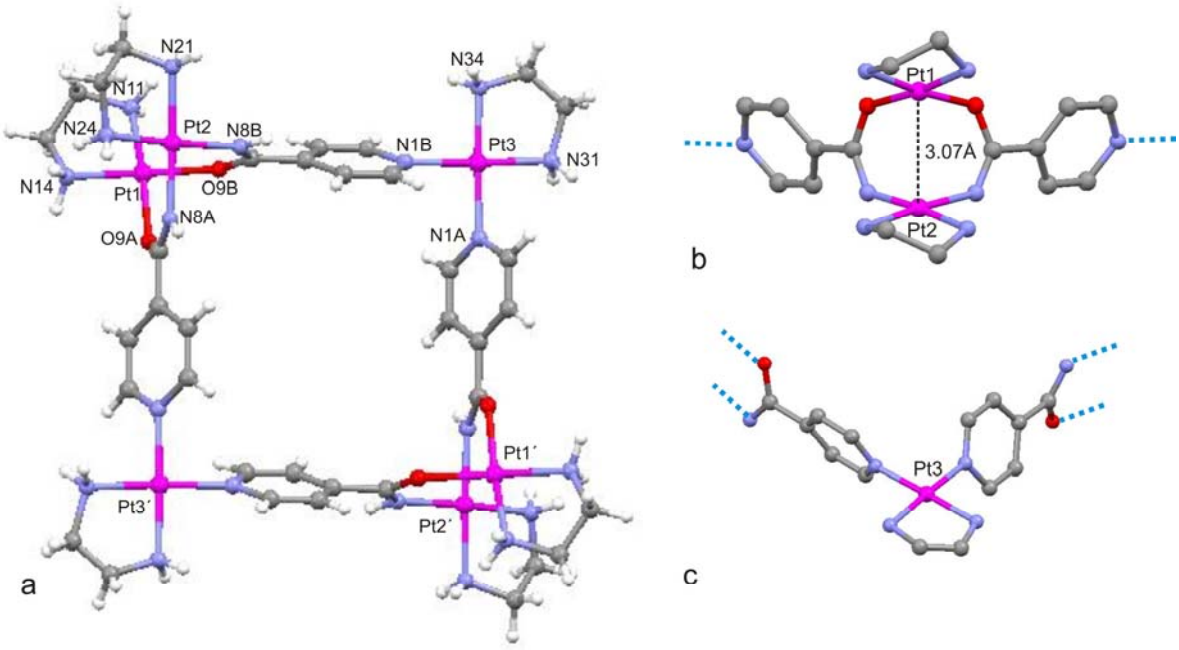

Figure 4.13 a) Molecular structure of the cation $[\{(en)Pt\}_6(4\text{-}C(O)NHpy)_4]^{8+}$ (**IV-5**) with the important atoms labeled b) and c) perspective views of corners of the square.

Table 4.7 Selected bond lengths (Å) and angles (deg.) for **IV-5**.

$[\{(en)Pt\}_6(4\text{-}C(O)NHpy)_4(PF_6)](NO_3)_7$ (**IV-5**)			
Pt1-N14	2.004(9)	N14-Pt1-O9A	92.4(4)
Pt1-O9A	2.007(7)	N14-Pt1-N11	83.3(4)
Pt1-N11	2.008(8)	O9A-Pt1-N11	174.2(4)
Pt1-O9B	2.025(6)	N14-Pt1-O9B	174.2(3)
Pt2-N8B	2.005(9)	O9A-Pt1-O9B	90.2(3)
Pt2-N8A	2.006(8)	N11-Pt1-O9B	93.8(4)
Pt2-N21	2.034(9)	N8B-Pt2-N8A	90.6(4)
Pt2-N24	2.044(9)	N8B-Pt2-N21	93.5(4)
Pt1-Pt2	3.0662(7)	N8A-Pt2-N21	175.1(4)
Pt3-N1A	2.014(9)	N8B-Pt2-N24	174.8(4)
Pt3-N1B	2.021(9)	N8A-Pt2-N24	92.7(4)
Pt3-N34	2.023(9)	N21-Pt2-N24	83.1(4)
Pt3-N31	2.032(9)	N1A-Pt3-N1B	89.2(4)
Pt1-Pt2	3.0662(7)	N1A-Pt3-N34	177.7(4)
		N1B-Pt3-N34	93.1(4)
		N1A-Pt3-N31	93.5(4)
		N1B-Pt3-N31	177.2(4)
		N34-Pt3-N31	84.2(4)

In the solid state cations of the **IV-5** are connected through hydrogen bonding between amine groups, carboxy groups, nitrate anions, and water molecules. The crystal structure of **IV-5** demonstrates that a PF_6^- anion is located centrally in the host cavity. The shortest Pt···F contact is 4.81 Å (Figure 4.14).

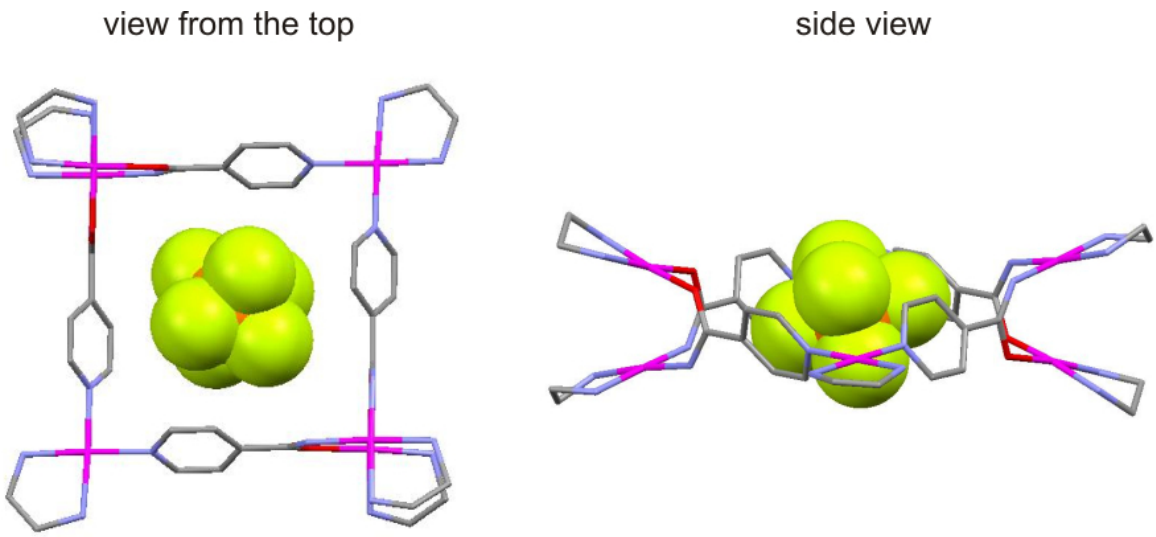

Figure 4.14 Location of PF_6^- anion within the hexanuclear square **IV-5**.

4.3.2. Characterization of [(en)Pd(4-C(O)NH$_2$py)(NO$_3$)](NO$_3$) (IV-6)

Reaction of $[(en)Pd(4\text{-}C(O)NH_2py)_2]^{2+}$ with one equivalent of $[enPd(H_2O)_2]^{2+}$ for one day at RT and pH ≈ 3 yielded a crystalline product, which was characterized as [(en)Pd(4-C(O)NH$_2$py)(NO$_3$)](NO$_3$) (**IV-6**). It is to be noted that the ^{1}H NMR spectrum of a sample of **IV-6** is not consistent with the composition according to X-ray analysis, because the en resonances have an intensity too high to account for a 1:1 stoichiometry.

X-ray diffraction studies reveal, that crystals grown from water have the composition [(en)Pd(4-C(O)NH$_2$py)(NO$_3$)](NO$_3$) (**IV-6**) (Figure 4.16).

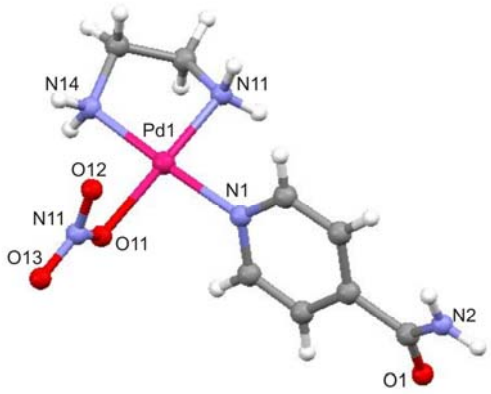

Figure 4.16 Cation structures of [(en)Pd(4-C(O)NH_2py)(NO_3)](NO_3) (**IV-6**) with atomic numbering scheme.

The coordination sphere of Pd in **IV-6** is built by NH_2 groups of a chelating ethylendiamine ligand (N11 and N14), one 4-C(O)NH_2py molecule (N1) and by an oxygen atom (O11) of coordinated nitrate ion. The 4C(O)NH_2py ligand is tilted with respect to the platin coordination plane by 61.1°.

Table 4.8 Selected bond lengths (Å) and angles (deg.) for **IV-6**.

[(en)Pd(4-C(O)NH_2py)(NO_3)](NO_3) (**IV-6**)			
Pd1-N11	1.986(2)	N11-Pd1-N1	92.16(10)
Pd1-N1	2.013(3)	N11-Pd1-N14	84.15(10)
Pd1-N14	2.03(2)	N1-Pd-O11	89.96(10)
Pd1-O11	2.058(2)	N14-Pd-O11	93.39(10)
		N1-Pd1-N14	175.00(11)
		N11-Pd1-O11	93.39(10)

The formation of layers of dimers linked by an one-dimensional hydrogen bond network is found in the solid state (N11···O23, 3.06 Å; N11···O21, 3.04 Å; N11···O22, 2.91 Å; N2···O22, 3.06 Å; N2···O21, 2.98 Å; N2···O1W, 2.87 Å). Two sandwiched layers are linked via hydrogen-bonding through water molecule located in the interlayer space (O1W···O1W, 2.86 Å) (Figure 4.17).

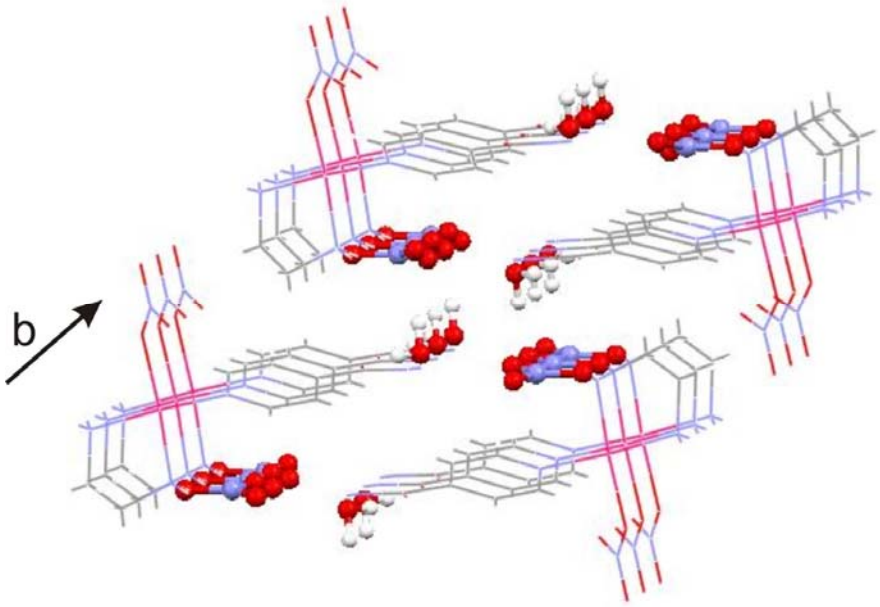

Figure 4.17 Packing arrangements of **IV-6** in the crystal structure.

4.4 Conclusions

In this chapter (en)Pt(II) and (en)Pd(II) complexes of 4-CNpy, 3-CNpy ligands have been applied with the aim to obtain discrete supramolecular aggregates. The results demonstrate that metal mediated or metal catalyzed hydrolysis of ligands occurs under the conditions applied. All four corners (**IV-1 – IV-4**) of the proposed squares have been prepared and crystallographically characterized. Only in one crystal structure, namely in $[(en)Pt(4\text{-}CNpy)_2](NO_3)_2$ (**IV-1**), is the CN group of 4-CNpy ligand not hydrolysed to amide. In all other instances metal centers have been converted to nicotinamide or isoninotinamide ligands, respectively.

A hexanuclear square $[\{(en)Pt\}_6(4\text{-}C(O)NHpy)_4(PF_6)](NO_3)_7$ (**IV-5**) has been successfully prepared in basic medium. The same reaction carried out under acidic conditions using $[(en)Pd(4\text{-}C(O)NH_2py)_2](NO_3)_2$ and $[(en)Pd(H_2O)_2](NO_3)_2$ results in formation of a mixture of products. One of these has been characterized crystallographically found to have the composition $[(en)Pd(4\text{-}C(O)NH_2py)(NO_3)](NO_3)$ (**IV-6**).

Chapter 5 – Dependence of aqua ligand basicity from substituent (*L*) in complexes of type *trans*-$[Pt(NH_3)_2(L)(H_2O)]^{2+}$

5.1 Background

Nearly one third of enzymes contain metals ions, which are responsible for their activity. Metals can play diverse roles in catalytic processes like binding and orientation of substrates, red-ox reactions, acid-base catalysis, electrostatic stabilization etc. After the discovery of dual character of RNA molecules in the 1970s in Cech's[112] and Altman's[113] labs, role of metal ion in ribozyme active sites has become a major subject of studies, since beside their structural role they are significant for catalytic processes in some cases.[114] Making parallels between these two types of enzymes it is reasonable to propose that M(OH)L*x* species could play a similarly important role in catalysis of ribozymes as they do in the metalloproteins.[115] Ribozymes are active in the presence of a variety of metal ions. They could be directly involved in the catalytic mechanism or bound to other ligands, change their p*K*a values, and thereby play an essential role. However, only complexes having p*K*a values near 7 have the potential to participate in acid-base chemistry at physiological pH. Figure 5.1 demonstrates a role which metal aqua species could play in general acid-base catalysed cleavage of phosphodiester bonds. Besides acting as Lewis acid or base as shown in Figure 5.1, positively charged complexes are also able to stabilise a negative charge in the transition state.

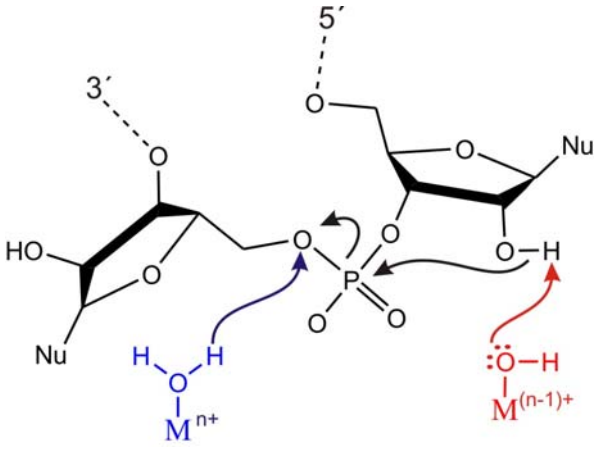

Figure 5.1 Schematic representation of acid-base catalyzed hydrolysis of a phosphodiester bond by a metal aqua species showing proton transfer for stabilization of nucleophilic oxygen and activation of the oxoanion group.

No positively charged nucleotide functional groups are expected to be available at neutral pH. Acid-base properties become meaningful for nucleic acids only when pK_a values are shifted to near-physiological pH. As numerous studies show, one of the reasons for the alteration of pK_a values is metal coordination.[116] For instance, coordination of metal to guanine N*7* and N*1*, adenine N*6* and cytosine N*4* shifts nucleobase pK_a values to 7 ± 2.[117]

Importantly, the acidity of coordinated water molecule depends on many factors, such as charge of the metal, solvent and changes in solvation shell, ligand field around the metal *etc*. The ability of a coordinated ligand to change the electron density at a metal has been studied for a long time. In square-planar four coordinate complexes of type *trans* – [Pt $(a)_2$ L_1L_2] the relative strength of the M – L_1 bond is dependant of the nature of L_2; in literature this phenomenon is known as *ground state trans-effect*. Ligands having a strong trans influence which stabilize a transition state of substitution reactions, generally termed as *kinetic trans-effect*.

Determination and understanding the factors that can influance p*K*a values of platinum complexes become relevant since these may have an influence on transport of cytostatic platinum drugs in biological fluids and/or drug receptor binding. The activity of these drugs in biological fluids is highly dependant of the existence of aqua or hydroxo species.

Could p*K*a values of Pt^{II} complexes be electronically tuned by modifying the nature of the ligand *trans* to the aqua/hydroxo substituent? The present study has been conducted in search of an answer to the above question and was focused on the complexes of the type *trans*-$[Pt(NH_3)_2(L)(H_2O)]^{2+}$, where *L* is substituted pyridine, aniline, methylamine, DMSO and DMS. Previous studies done in our group show that pK_a values of coordinated water molecule is variable in *cis* isomers (4.8 – 7), but relatively constant in *trans* isomers (5.2 ± 0.1).[118] Correlation of p*K*a values of monoaqua cations of the complexes obtained with p*K*a values of ligands confirms that there is a small, yet noticeable influence of the latter on aqua group acidity in *trans* complexes.

5.2 Platin-triamine complexes

Variation of pK_a values in Pt triamine complexes is influenced by the character of the ligand *trans* to the aqua group. The simplest triamine complex $[Pt(NH_3)_3(H_2O)]^{2+}$ has a pK_a value equal to 6.4. Substitution of NH_3 by primary amines does not change pK_a value

significantly *e. g.* for $[(dien)Pt(H_2O)]^{2+}$ the pK_a value is 6.24.[119] The influence of RNH_2 type of ligands on the electron density of the metal center is only through the σ bond (ligand → Pt). The situation is different when aromatic amines are coordinated to the metal center. Pyridine and its derivatives have six π orbitals, three of which are filled (bonding orbitals). The other three empty antibonding orbitals are capable to accept electron density from the metal giving rise to π-backbonding (Pt → ligand).[120] Van Eldik *et al*. have characterized a series of compounds containing between one to three pyridine ligands in different position (Figure 5.2).[121]

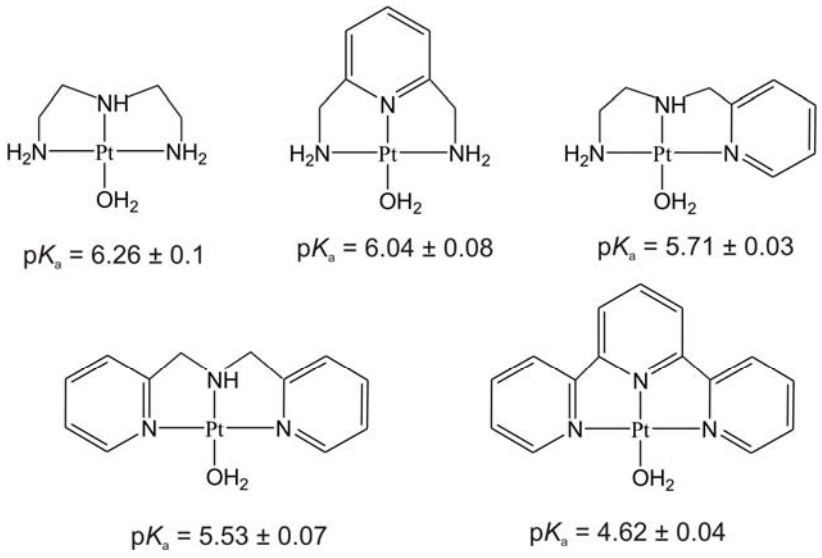

Figure 5.2 Monofunctional Pt(II) complexes with tridentate ligands studied by van Eldik *et al.*

pK_a values of the aqua ligands in these complexes drop with increasing number of aromatic substituents. Back-donation into the empty π* orbitals of the in-plane aryl ligands ($d_{yz} \rightarrow \pi^*$) has a contribution on pK_a values of the coordinated water molecule. By increasing the electrophilicity of the metal center, it stabilizes the electron rich hydroxo form, hence makes the aqua ligand more acidic.

Helpful information on the type of orbitals involved in the Pt-*L* (*L* = pyridine derivatives) bonding can be obtained from relative orientation of the pyridine ring in the platinum complexes. When pyridine ligand is not "fixed", additional factors should be considered as a consequence of free rotation of the ligand. Dihedral angles in the similar

complexes without ortho substituents are in-between 45 – 60° [122] and, because of steric demand, are particularly large when the pyridine ligands have substituents in the 2 and/or the 6 position (70 – 90°). Although it is not appreciable, $d_{xy} \rightarrow \pi^*$ back donation could occur, when the pyridine ligand is perpendicular to the Pt coordination plane. Additional interactions between the coligands of the metal become possible and, as has been shown, can have an influence on the pK_a value of the complexes, for instance, through formation of hydrogen bonds between coordinated H_2O or NH_3 ligands.[118]

5.2.1 Preparation of complexes

The platinum-triamine complexes were prepared by using one of the two general reaction methods: In method a) the reactive monoaqua intermediate was prepared from *trans*-$Pt(NH_3)_2ICl$ by treatment with 1 eq. $AgNO_3$. Later on the aqua ligand was replaced by the nucleophilic Am ligand, yielding the desired complex. In method b) *trans*-$Pt(NH_3)_2Cl_2$ and the selected Am ligand were heated in water at 50–60°C during 1–3 days to assist Cl^- substitution.[123] Although starting compounds were applied in 1:1 ratio, formation of 1:2 complexes occurs as well. Complexes **V-2**, **V-5**, **V-7** and **V-9** could not been isolated as pure compounds and were contaminated with 1:2 products. In case of the 2-pic ligand, after isolation of the 1:1 complex, *trans*-$[(NH_3)_2Pt(2\text{-pic})_2](NO_3)_2$ has been also isolated and fully characterized.

Reaction of *cis*-$[Pt(NH_3)_2Cl(NO_3)]^+$ with 2-pic in DMF and subsequent crystallization led to the formation of a product which, according to ^1H NMR spectroscopy, was the *trans* isomer. *Cis* → *trans* isomerisations of square planar Pt complexes are known from literature.[124] However, in these cases, the complexes contain ligands with a high *trans* effect and/or DMSO is used as a solvent. Mechanism and factors influencing the isomerisation of *cis*-$[Pt(NH_3)_2Cl(2\text{-pic})]^+$ have not been further investigated in the present study.

As examples, ^1H NMR spectra for compounds **V-1**, **V-11** and **V-12** are shown in Figure 5.2. Proton resonances of 2-pic ligand were observed as dd for H_3 and H_6 (^3J (^1H–^1H) = 7.5–8 Hz) and as ddd for H_4 and H_5 (^4J (^1H-^1H) ≈ 1.6 Hz). The assignment of the H_6 protons was confirmed by the presence of ^{195}Pt satellites. The values of ^3J (^{195}Pt–^1H) are dependant of the nature of the ligand in *trans* location: for **V-1** ^3J is 46 Hz (with Cl^- in *trans* position) and 36 Hz and 32 Hz for **V-11** and **V-12,** respectively (*N*-donor ligands in *trans* position).

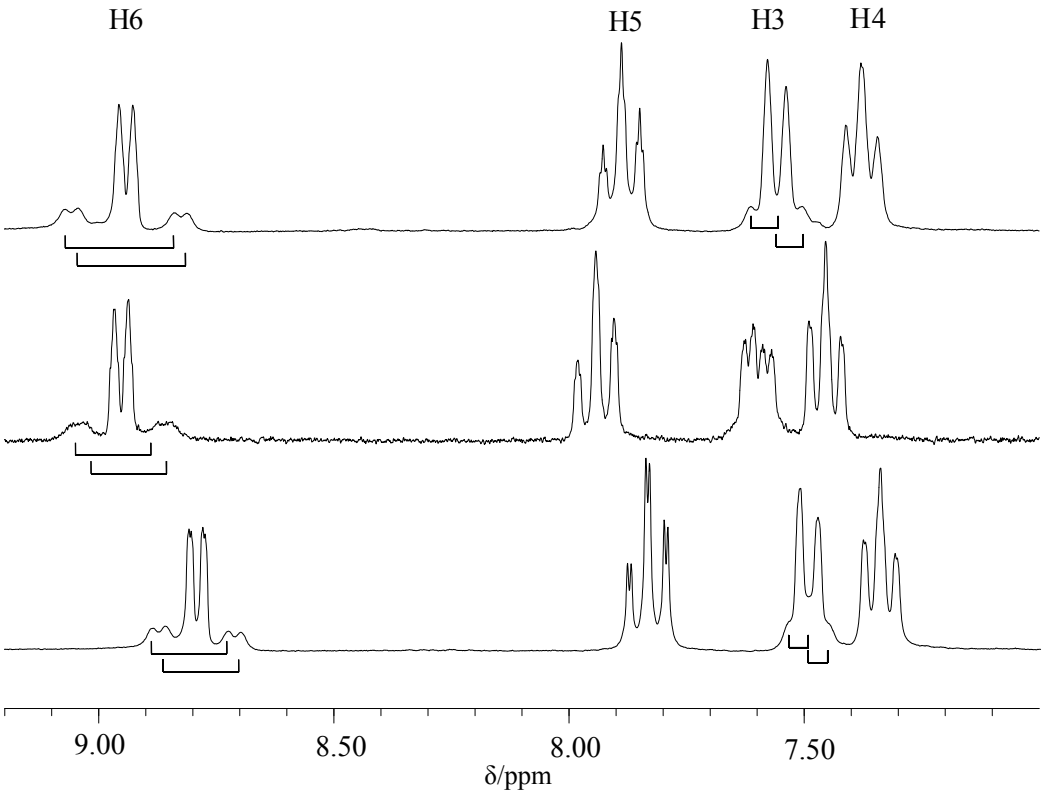

Figure 5.3 Low-field sections of ^{1}H NMR spectra (200 MHz, D_2O) of *trans*-$[Pt(NH_3)_2(2\text{-pic})Cl]NO_3$ (**V-1**) (top), *trans*-$[Pt(NH_3)_2(2\text{-pic})_2](NO_3)_2$ (**V-11**) (middle), and *cis*-$[Pt(NH_3)_2(2\text{-pic})Cl]Cl$ (**V-12**) (bottom). ^{195}Pt satellites of H6 and H3 resonances are indicated.

The ^{1}H NMR spectrum of the bis-ligand complex **V-11** suggests that the reason for two sets of resonances for the methyl protons is due to the presence of rotational isomers. The *ortho* methyl groups can be on the same side (*syn* isomer) or on opposite sides (*anti* isomer). The nearly identical intensities of resonances show that the two rotamers are present in solution in equal amounts.

Solvation of *trans*-$[Pt(NH_3)_2(2\text{-pic})Cl](NO_3)_2$ in DMF and DMSO was monitored by ^{1}H NMR spectroscopy. In is well known that Me_2SO has a large kinetic *trans* effect and as a consequence, ammonia exchange reactions can occur.[125]

5.2.2 X-ray crystal structures of *trans*-$[(NH_3)_2Pt(2\text{-pic})Cl](NO_3)$ (V-1), *trans*-$[(NH_3)_2Pt(2\text{-pic})_2](NO_3)_2$ (V-10) and *cis*-$[(NH_3)_2Pt(2\text{-pic})Cl]Cl$ (V-11)

For compounds **V-1**, **V-11** and **V-12** crystals suitable for X-ray structure determination have been obtained. The average bond distances are comparable to those found in the literature and the average angles are close to the ideal square planar 90° value (Table 5.1).

Complex **V-1** crystallizes as nitrate salt. The dihedral angle between the pyridine ligand and the Pt coordination plane is *ca.* 76°. Each NO_3^- anion makes hydrogen bonds with ammine ligands of Pt, with average bond lengths of 3 Å (O1···N11, 2.99 Å, O1···N12, 3.03 Å, O13···N11, 3.05 Å). Hydrogen bonds between Cl^- and NH_3 ligands are also present (Cl1···N11, 3.32 Å, Cl1···N12, 3.51 Å).

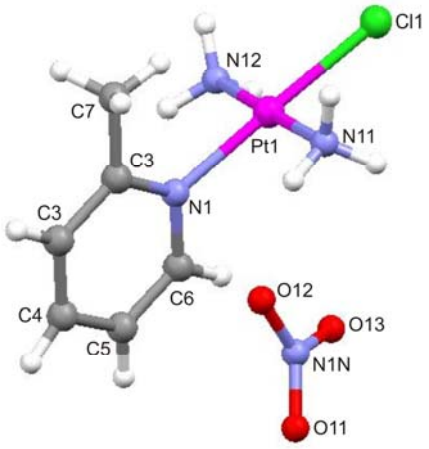

Figure 5.4 Molecular structure of *trans*-$[Pt(NH_3)_2(2\text{-pic})Cl]NO_3$ (**V-1**) and atom numbering scheme.

The 2-pic plane in **V-10** is tilted with respect to the PtN_4 plane with an angle of *ca.* 78°. The crystal structure of **V-10** reveals π-π stacking of aromatic rings of 2-pic ligands, with the shortest intermolecular distance being 3.48 Å. Molecules of **V-10** interact with each other only indirectly through hydrogen bonds between NO_3^- anions and NH_3 ligands (O12···N11, 3.06 Å, O11···N11, 2.97 Å).

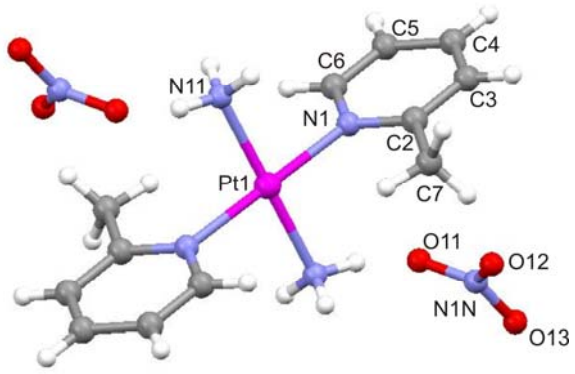

Figure 5.5 Molecular structure of *trans*-$[Pt(NH_3)_2(2\text{-pic})_2](NO_3)_2$ (**V-10**) with atom numbering scheme . In the solid state, the two 2-pic ligands adopt a *head to tail* arrangement.

A view of cation **V-11** is depicted in Figure 5.6. Both coordinated and free Cl^- ions are involved in intermolecular hydrogen bond formation (Cl1(1)···N12, 3.25 Å, Cl1(2)···N12, 3.30 Å, Cl2···N11, 3.29 Å, Cl3···N12, 3.22 Å) No intermolecular π-π stacking interactions are observed between aromatic 2-pic ligands.

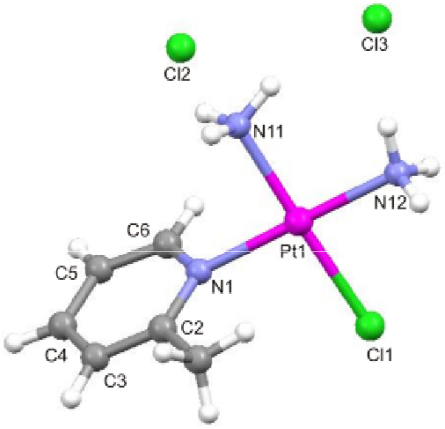

Figure 5.6 Molecular structure of *cis*-$[Pt(NH_3)_2(2\text{-pic})Cl]Cl$ (**V-11**) with atom numbering scheme. The chloride counter ion is distributed over two positions [Cl(2), Cl(3)].

In the *cis* isomer **V-11** the dihedral angle between the metal coordination plane and the 2-pic is *ca.* 74°, hence slightly smaller than in the *trans* isomer.

Table 5.1 Selected bond lengths (Å) and angles (deg.) for **V-1**, **V-10** and **V-11.**

	trans-$[Pt(NH_3)_2(2\text{-pic})Cl]NO_3$ (**V-1**)	*trans*-$[Pt(NH_3)_2(2\text{-pic})_2](NO_3)_2$ (**V-10**)	*cis*-$[Pt(NH_3)_2(2\text{-pic})Cl]Cl$ (**V-11**)
Pt1-N1	2.033(6)	2.028(3)	2.034(6)
Pt1-N12	2.037(8)		2.014(5)
Pt1-N11	2.045(7)	2.049(3)	2.043(5)
Pt1-Cl1	2.2969(19)		2.3000(16)
N1-Pt1-N12	91.2(3)		179.4(3)
N1-Pt1-N11	90.4(3)	89.42(11)/90.58(11)[a]	89.3(2)
N12-Pt1-Cl1	89.75(18)		88.15(15)
N11-Pt1-Cl1	88.64(18)		91.58(18)
2-picoline/ Pt plane	76.11(23)	77.58(10)	73.76(17)

5.2.3 pK_a values of complexes obtained

The pK_a value of a compound is one of its most substantial physicochemical properties and is particularly important for pharmaceutically active molecules. Concerning pK_a determination techniques, numerous methods exist today, which include potentiometry, conductivity, calorimetry, UV-Vis and NMR spectrometry, mass spectrometry, liquid chromatography, capillary zone electrophoresis and software computational predictions.[126] Among these techniques, the NMR titration method[127] has a distinct advantage, since determination of the pK_a value could be done even in the presence of impurities *e. g.* when the 1:1 compound is contaminated with the 1:2 complex, since the latter does not influence the chemical shifts of the monoaqua species. This method was used in present study to determine pK_a values of the complexes prepared.

The monoaqua species were prepared by removal of the chlorido ligand with Ag^+. In case of *trans*-$[Pt(NH_3)_2(4\text{-CNPy})(H_2O)]^{2+}$ measurements have been done right after activating and adjusting pD, since the C ≡ N group is known to undergo hydrolysis with time, leading to the formation of the isonicotineamide ligand (See Chapter 4). Only single sets of NMR resonances are observed during the pH titration, because proton transfer between aqua and hydroxo species is fast on the NMR time scale.

$$trans\text{-}[a_2PtL(H_2O)]^{2+} + H^+ \rightleftharpoons trans\text{-}[a_2PtL(OH)]^{+} + H^+$$

As an example the pH dependence of ^1H NMR shifts of H_3, H_4 and H_5 protons of the 2-pic ligand in complex **V-1** over the pH range 1 – 14 is shown in Figure 5.7. The experimental data were evaluated in a Newton-Gauss non-linear least-squares curve fitting procedure, which gave three pK_a values for the individual resonances. For details of the pK_a calculation, see the experimental section.

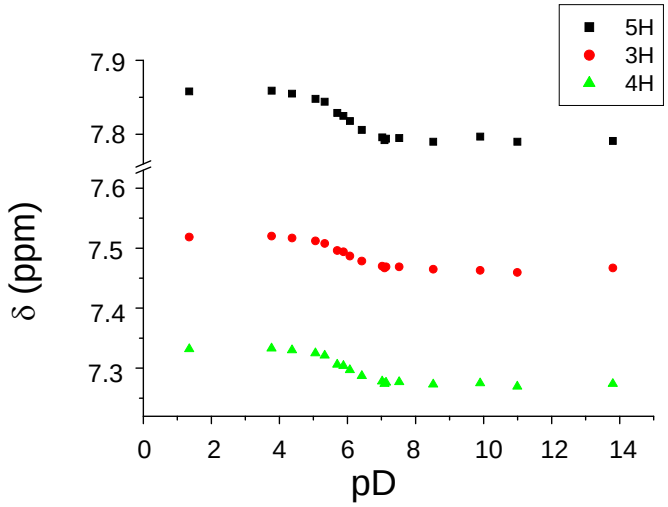

Figure 5.7 pD dependence of chemical shifts (δ) of aromatic proton resonances of 2-pic ligand in *trans*-$[Pt(NH_3)_2(2\text{-pic})(D_2O)]^{2+}$ (**V-1**).

For the other complexes NMR shifts, pK_a values of the monoaqua species, as well as literature data of pK_a values of the free ligands are summarized in Table 5.2. As can be seen from Table 5.2 not all resonances are sensitive to the pH changes. Therefore, for the determination of pK_a values only the most suitable ones were used. Especially *ortho* protons of pyridine ligands are frequently not much affected by pD.

Table 5.2 Chemical shifts of proton resonances of ligand (*L*) in $OH^-(\delta_1)$/ $H_2O(\delta_2)$ species, observed maximum shift (positive value corresponds to upfield shift, negative to downfield), pK_a values of ligand and monoaqua species *trans*-$[(NH_3)_2PtL(aq)]^{n+}$(* taken from literature).

		***trans*-$[(NH_3)_2PtL(aq)]^{n+}$**				
L		$\delta_1(OH^-)$	$\delta_2(H_2O)$	$\Delta\delta$	pK_a (LH^+)	pK_a (H_2O)
2-MePy (2-pic.) **V-1´**	CH_3	3.122	3.073	0.049	5,97*	5,35
	H_3	7.332	7.274	0.058		
	H_4	7,519	7.467	0.052		
	H_5	7.859	7.791	0.068		
	H_6	8.861	8.878	-0.017		

3-MePy (3-pic.) **V-2´**	H_2	8.614	8.624	-0.01	5,68*	5,23
	CH_3	2.354	2.335	0.019		
	H_4	7.820	7.749	0.071		
	H_5	7.395	7.341	0.054		
	H_6	8.532	8.539	-0.007		
Py **V-3´**	H_2	8.749	8.755	-0.006	5,25*	5,30
	H_3	7.997	7.93	0.067		
	H_4	7.534	7.473	0.061		
4-ClPy **V-4´**	H_2	8.713	8.718	-0.005	3,83*	4,97
	H_3	7.633	7.562	0.071		
3-ClPy **V-5´**	H_2	8.936	8.929	0.007	2,81*	4,88
	H_4	8.078	8.00	0.078		
	H_5	7.526	7.466	0.06		
	H_6	8.731	8.727	0.004		
2-ClPy **V-6´**	H_3	7.788	7.729	0.059	0,49*	4,89
	H_4	8.015	7.94	0.075		
	H_5	7.52	7.451	0.069		
	H_6	8.876	8.887	-0.011		
4-CNPy **V-7´**	H_2	9.071	9.063	0.008	1,9*	4,73
	H_3	7.918	7.841	0.077		
$MeNH_2$ **V-8´**	CH_3	2.358	2.368	-0.01	10,62*	5,91
3,5-DiMeAn **V-9´**	CH_3	2.317	2.298	0.019	4,48*	6,26
	H_2	7.05	6.978	0.072		
	H_4	7.01	6.917	0.093		
9-MeG	–	–	–	–	3,11*	5,27*
1-MeC	–	–	–	–	4,6*	5,17*
2-ampy	–	–	–	–	6,86*	5,34*
NH_3	–	–	–	–	9,25*	6,37*

Figure 5.8 shows a plot of the pK_a values of monoaqua complexes *vs.* basicity of free ligand. It is evident that for six complexes data fit excellently on a straight line, giving the following relationship

$$pK_a(H_2O) = (4.52 \pm 0.06) + (0.17 \pm 0.01)\ pK_a(LH^+)$$

Changing pK_a values of the pyridine ligands from 0.49 (4-ClPy) to 5.68 (2-MePy) (Δ = 5.19) affects pK_a values of the complexes obtained little (Δ_{max} = 0.62), and as a consequence, the slope of the straight line is very small.

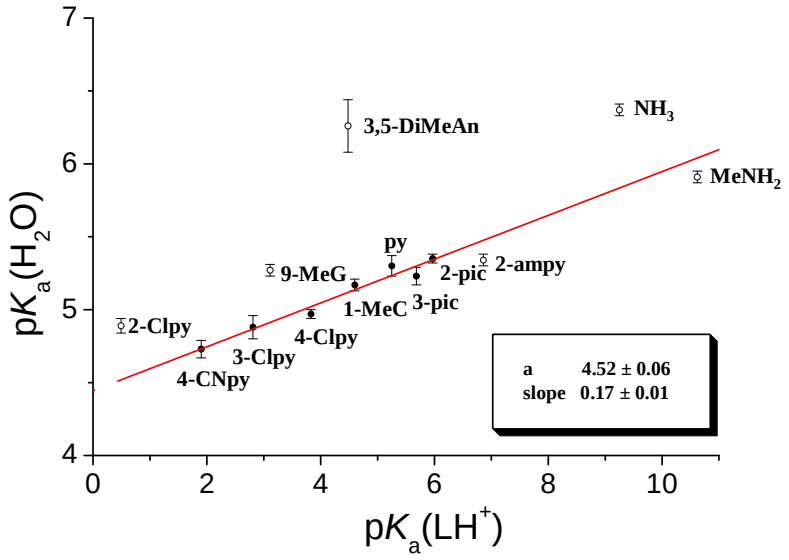

Figure 5.8 Relationship between p*K*a of the H_2O ligand in *trans*-$[Pt(NH_3)_2(L)(H_2O)]^{2+}$ and basicity of *L* [expressed as p*K*a(LH^+)]. The least-squares straight line was calculated for complexes (filled circles) with the following ligands L: 2-pic, 3-pic, py, 4-Clpy, 3-Clpy, and 4-CNpy. Complexes deviating significantly from the straight line (open circles) are discussed in the text. Error bars refer to estimated errors in p*K*a value determinations.

pK_a(H_2O) values of the complexes containing 2-ClPy and 2-ampy ligands deviate from the straight line. Hydrogen bonding interaction between the Cl substituent or a lone electron pair at the exocyclic amino group of 2-ampy ligand and one of the NH_3 groups could be one of the reasons. This property plays a significant role in the complexes of *cis* arrangement, where hydrogen bond donor/acceptor groups are able to stabilize H_2O/OH^- forms selectively.

In case of 3,5-DiMeAn and $MeNH_2$ containing complexes, Pt is bonded to the ligand through a valence saturated *N* atom, hence can not accept π back-donation and is therefore expected to have a dissimilar effect. However, the relatively large error in pK_a value determination in the case of 3,5-DiMeAn and the observed small chemical shift in case of the $MeNH_2$ compound makes it difficult to make a strong point.

5.2.4 Solvation of *trans*-$[(NH_3)_2Pt(2\text{-pic})Cl](NO_3)$ (V-1) in DMF and DMSO

The effect of solvent on the stability of a complex has been studied for *trans*-$[(NH_3)_2Pt(2\text{-pic})Cl](NO_3)$. Different behaviors were observed in DMSO and DMF. ^{1}H NMR spectra of a freshly prepared DMSO-d_6 solution show two major sets of resonances at 8.83 and 8.43 ppm (d), 8.89 and 7.67 ppm (dd), 7.57 and 7.25 ppm (d), 7.38 and 7.17 ppm (dd), indicating that part of the chlorido ligands have been immediately exchanged by solvent molecules with subsequent elimination of the 2-pic ligand. This reflects the well-known strong *trans* labilizing effect of DMSO.

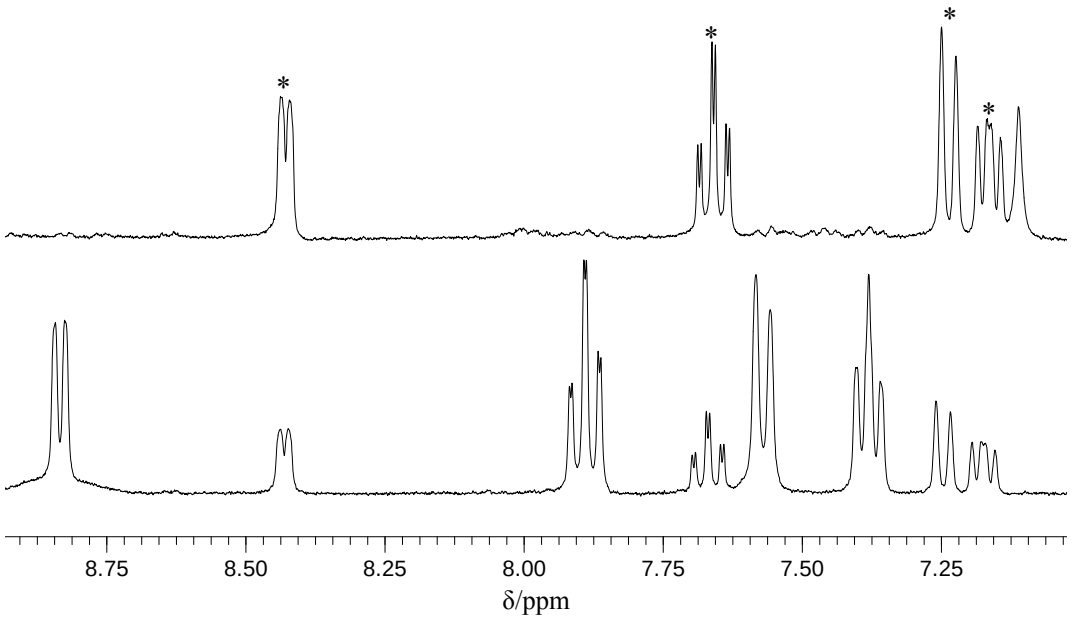

Figure 5.9 Low field section of ^{1}H NMR spectra of bottom: *trans*-$[(NH_3)_2Pt(2\text{-pic})Cl](NO_3)$ (**V-1**) in DMSO-d_6 taken immediately after addition of the solvent; top: previous sample heated at 40°C for 18h. With * marked peaks correspond to free ligand.

Further NMR studies suggest that in DMSO the solvation process is multistep and finally more than one product forms. This can be clearly seen from the NMR peaks of the NH_3 ligands, as shown in Figure 5.10. At an early stage of the reaction only peaks at 4.07 and 4.36 ppm are present which are assigned to the *trans*-$[(NH_3)_2Pt(2\text{-pic})Cl]^{2+}$ (*) and the *trans*-$[(NH_3)_2Pt(DMSO)_2]^{2+}$ (#) respectively. Later on three new peaks (•) at 4.78, 4.60 and 3.89 ppm appear in the spectra, indicating formation of new products. All these products do not longer contain 2-pic. Not only *trans* $\rightarrow$ *cis* isomerization is possible in this instance, but also ammonia exchange reactions can occur. For example, ^{195}Pt NMR spectroscopic studies of *cis*-$Pt(NH_3)_2Cl_2$ in DMSO solution[13] show formation of five additional species: $[Pt(NH_3)_3Cl]^+$,

$[Pt(NH_3)_3(DMSO)]^{2+}$, *cis*-$[Pt(NH_3)(DMSO)Cl_2]$, *trans*-$[Pt(NH_3)(DMSO)Cl_2]$ and *trans*-$[Pt(NH_3)_2(DMSO)Cl_2]^{+}$.

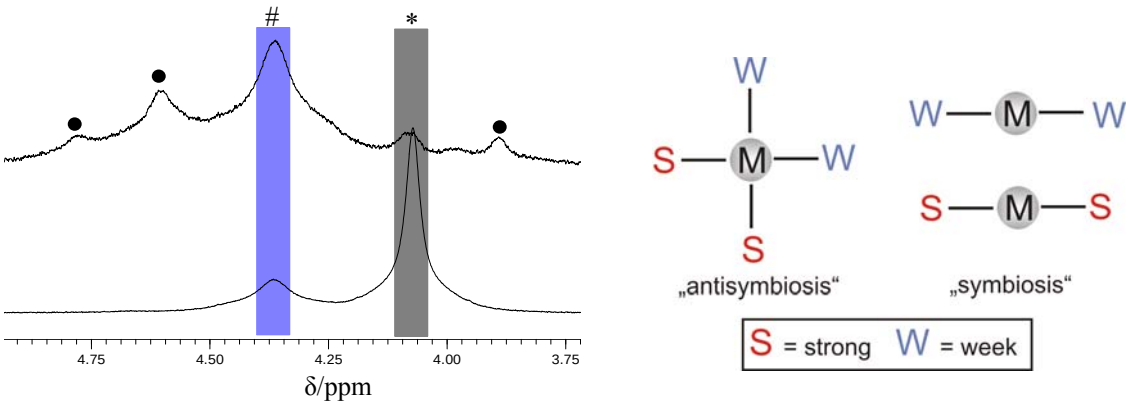

Figure 5.10 ^{1}H NMR spectra of **V-1** in the region corresponding to NH_3 resonances. Bottom: immediately after addition of the solvent. Top: heated at 40°C for 18h. Schematic overview of "symbiosis" and "antisymbiosis" .

According to the concept of chemical symbiosis,[128] when coordinated to a metal, hard bases try to keep their electrons and therefore reduce the positive charge of the metal not efficiently. This forces the metal to act as a hard Lewis acid, which in turn prefers hard bases. Consequently, the soft base will transfer charge to the metal, making it softer. However, in case of soft metals two soft ligands in *trans* position to each other have a destabilizing effect, thus showing antisymbiotic behavior.[129] This is particularly true when ligands are able to participate in π back donation. Taking into account this concept, the observed changes can be explained in the following way: in the initially formed *trans*-$[(NH_3)_2Pt(2\text{-pic})(DMSO)]^{2+}$ complex two ligands *trans* to each other will compete for a single metal-based orbital. The softer DMSO-*S* ligand donates strongly into this orbinal, causing a destabilization of the *trans* Pt–*N* bond. Eventually this leads to breakage of this bond and free 2-pic is detected in the ^{1}H NMR spectra soon after dissolving **V-1** in DMSO. Proton signals corresponding to the original metal complex disappear with time or upon heating, while resonances due to free 2-pic increase in intensity. Typical spectral changes in the aromatic region are shown in Figure 5.9.

In contrast, *trans*-$[(NH_3)_2Pt(2\text{-pic})Cl]^{2+}$ is found to be stable in DMF. Upon aging of the solution no spectral changes occur. Only after removing the chlorido ligand by addition of

one equivalent of $AgNO_3$, coordination of DMF to the platinum center can be detected. The effect of this displacement in chemical shift of the 2-pic ligand is small and detectable only for the H_6 proton, which shifts from 9.05 to 9.01 ppm in the solvent species (Figure 5.11).

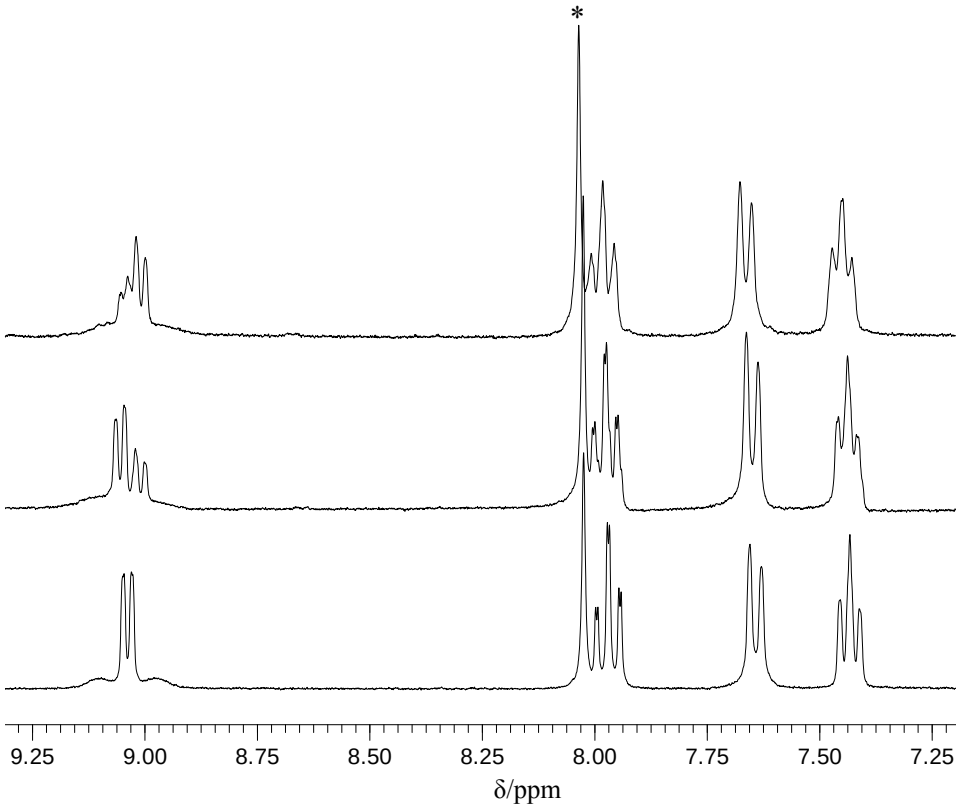

Figure 5.11 Aromatic region of ^{1}H NMR spectra of *trans*-$[(NH_3)_2Pt(2\text{-pic})Cl](NO_3)$ in DMF-d_7. From bottom to top: after dissolving, addition of one equivalent of $AgNO_3$ and stirring at RT for 5h and after 2d, RT.

5.3 Complexes of *trans*-$[(NH_3)_2Pt(L)Cl](NO_3)$ containing S-donor ligands *L*.

In order to gain further information on the behavior of aqua groups in *trans*-$[(NH_3)_2PtL(aq)]^{n+}$ type complexes, we have extended our study to sulphur containing ligands. As has been mentioned before the acidity of the coordinated water molecule in the species *trans*-$[Pt(NH_3)_2(L)(H_2O)]^{2+}$ can be taken as an indirect measure for the M-*L* bond strength and the formal electron density at the metal center. When *L* = DMSO, the formation of the Pt-S bond is preferred. Exceptions are possible in cases of large steric demand, *e. g.* in *cis*-$[Pt(DMSO)_4]^{2+}$ ion, which contains two S-bonded and two O-bonded DMSO ligands.[130] Studies of Rochon *et al.*[131] show that in Pt-sulfoxide bond formation besides σ-donation, π-

back donation has also its contribution and, as ^{195}Pt, ^{13}C, ^{1}H NMR and X-ray crystallographic studies reveal π (Pt → R_2SO) bonding has a significant influence on the structures and properties of these types of compounds.

5.3.1 Preparation of the complexes

Complex *trans*-$[(NH_3)_2Pt(DMSO)Cl](NO_3)$ (**V-12**) has been prepared as described previously.[132] A strong band at 1108 cm^{-1} in its IR spectrum is indicative of M-S(O) bonding.[133] The analogous complex with dimethylsulfid *trans*-$[Pt(NH_3)_2(Me_2S)(H_2O)](NO_3)$ (**V-13**), has been prepared following the same procedure. In the ^{1}H NMR spectra taken in D_2O, the sulfoxide protons are observed at 3.60 ppm with $^{3}J(^{195}Pt\text{-}^{1}H)$ equal to 28.2 Hz and sulfide protons at 2.51 ppm with $^{3}J(^{195}Pt\text{-}^{1}H)$ equal to 57.2 Hz. Contrary to DMSO, DMS has less π-electron acceptor capacity, as has been shown by theoretical calculations.[134]

5.3.2 Crystal structure of {*trans*-$[PtCl(CH_3\text{-}S\text{-}CH_3)(NH_3)_2](NO_3)\}_2 \cdot$ *trans*-$[PtCl_2(NH_3)_2]$ (V-13a)

A single crystal structure determination performed on *trans*-$[PtCl(CH_3\text{-}S\text{-}CH_3)(NH_3)_2](NO_3)$ was not successful because of the poor quality of the crystals. Instead, crystals of a mixed species, {*trans*-$[PtCl(CH_3\text{-}S\text{-}CH_3)(NH_3)_2](NO_3)\}_2 \cdot$ *trans*-$[PtCl_2(NH_3)_2]$, have been isolated in small amounts (< 3%) and were characterized crystallographically.

Figure 5.12 shows the crystal structure of **V-13a**. Both Pt centers have normal square planar geometries. The Pt-S distance of 2.256(3) Å in the *trans*-$[PtCl(CH_3\text{-}S\text{-}CH_3)(NH_3)_2]^+$ unit is in the range of values reported in the literature.[133] In contrast, the Pt-S distance in the same type of complexes bearing DMSO ligand instead of DMS is much shorter. For instance, in the previously reported *trans*-$[(NH_3)_2Pt(DMSO)Cl]Cl$[135] in has a value of 2.204(4) Å. One of the reasons for this difference in bond length is the different oxidation states of the sulfur atom in DMSO and DMS.

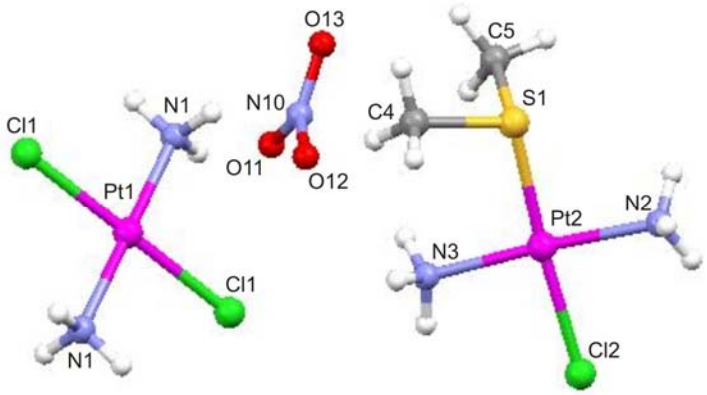

Figure 5.12 Molecular structure of {*trans*-$[PtCl(CH_3\text{-}S\text{-}CH_3)(NH_3)_2](NO_3)\}_2$ · *trans*-$[PtCl_2(NH_3)_2]$ (**V-13a**) with atom numbering scheme.

Table 5.2 Selected bond lengths (Å) and angles (deg.) for **V-13a**.

{*trans*-$[PtCl(CH_3\text{-}S\text{-}CH_3)(NH_3)_2](NO_3)\}_2$ · *trans*-$[PtCl_2(NH_3)_2]$ (**V-13a**)			
Pt1-N1	2.022(9)	N1-Pt1-N1	180(2)
Pt1-Cl1	2.300(3)	N1-Pt1-Cl1	89.0(3)
Pt2-N3	2.047(11)	N1-Pt1-Cl1	91.0(3)
Pt2-N2	2.050(10)	N3-Pt2-N2	176.9(4)
Pt2-S1	2.256(3)	N3-Pt2-S1	95.9(3)
Pt2-Cl2	2.306(3)	N2-Pt2-S1	87.1(2)
		N3-Pt2-Cl2	88.5(3)
		N2-Pt2-Cl2	88.4(3)
		S1-Pt2-Cl2	175.0(13)

5.3.3 pK_a values of the aqua complexes

The pK_a values of the coordinated water molecules in both complexes were determined by the ^{1}H NMR titration method (Figure 5.13) and found to be 3.51 ± 0.03 for *trans*-$[(NH_3)_2Pt(DMSO)(H_2O)]^{2+}$ and 4.76 ± 0.03 for *trans*-$[(NH_3)_2Pt(DMS)(H_2O)]^{2+}$.

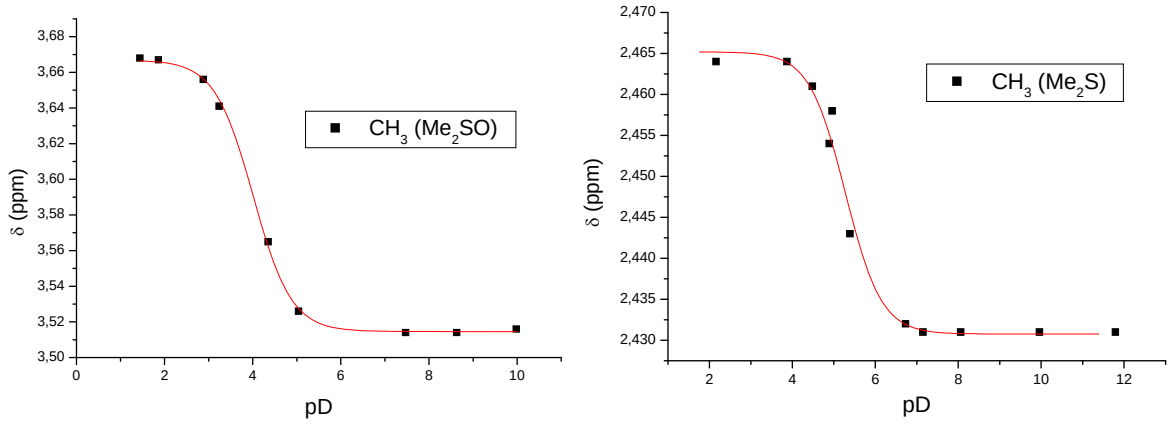

(a) (b)

Figure 5.13 pD dependence of the CH_3 resonance of *trans*-$[(NH_3)_2Pt(DMSO)(aq)]^{2+}$ (a) and *trans*-$[(NH_3)_2Pt(DMS)(aq)]^{2+}$ (b) in ^1H NMR spectra (D_2O, 300 MHz)

The relatively low pK_a values of the aqua ligands were not expected, because *S*-bonded ligands are known to be good σ-donors and hence increase the electron density at the metal center. Consequently, destabilization of the OH^- form might be expected. It is proposed that it is the electron accepting properties of the DMSO ligand in comparison to DMS, which increases the electron density at the DMSO and reduces it at the metal, thereby leading to a relatively high acidity of the aqua ligand.

5.4 Conclusions

The experiments described in this chapter can be summarized as follows:

1) There is a linear relationship between the basicity of substituted pyridine ligands (*L*) and the acidity of the aqua ligand in complexes of type *trans*-$[Pt(NH_3)_2(L)(aq.)]^{2+}$. However, the effect of ligand basicity on the pK_a of the coordinated water is relatively minor.

2) It is well established that the π-acceptor ability of a ligand is a key factor in determining its *trans* effect in substitution reactions involving square-planar complexes.[136] If the *L* ligand is a π-acid, pK_a values of coordinated water molecules in *trans* position are relatively low (3.51 when *L* = DMSO and 4.7–5.4 for substituted pyridines), unlike for amines without π-acceptor ability (6.0 – 6.4 when *L* = NH_2R).

Chapter 6 – Anion complexation by cyclic hosts

6.1 Background

Metal complexes play a significant role in anion receptor chemistry, since metal center, being positively charged, contribute to electrostatic attraction and/or able to act as a Lewis acidic binding site.

This chapter provides an overview of anion binding properties of cyclic homo- and heterometallic complexes containing 2,2´-bpz ligand obtained during this doctoral thesis. These host molecules have different shapes and as a consequence, different propensities to host anionic guests. Association constants for binding processes were established using the NMR titration method.

6.2 Triangular $[\{a_2Pt\}_3(bpz)_3]^{6+}$ hosts

Crystal structures of triangular species consisting of Pt(II) corners linked through 2,2´-bpz ligands reveal that they can serve as hosts for different anions. An advantageous feature of this molecular skeleton is its flexibility and ability to preorganize. Theoretically, ten different isomers are possible, depending on the conformation of bpz ligand. Only two of them have been characterized crystallographically. Previous and present studies show that larger and less hydrophilic anions like PF_6^- ($\Delta G_h < -100$ kJ mol^{-1}), BF_4^- ($\Delta G_h = -190$ kJ mol^{-1}), ClO_4^- ($\Delta G_h = -214$ kJ mol^{-1}), are easily trapped into the cavity. Having a moderate value of hydration energy ($\Delta G_h = -306$ kJ mol^{-1}), NO_3^- anions seem to prefer locations outside of the cavity. Yet, in the presence of additional anions such as in mixed NO_3^-/ClO_4^- and NO_3^-/PF_6^- salts, it can be incorporated in the host, being located at the bottom of the triangle. Structures and anion binding affinities of $[BF_4 \subset cis\text{-}[\{Pt(NH_3)_2(ttt\text{-bpz-}N4,N4')\}_3](BF_4)(SiF_6)_2$, $[(NO_3),(PF_6) \subset cis\text{-}[\{Pt(NH_3)_2(ccc\text{-bpz-}N4,N4')\}_3](PF_6)_4$ and $[NO_3 \subset [\{(en)Pt(ccc\text{-bpz-}N4,N4')\}_3](NO_3)(SO_4)_2$ have been investigated in this study.

The observed structures can be classified in two groups, depending whether the 2,2´-bpz in the host adopts an all-*cis* or an all-*trans* conformation (Scheme 6.1).

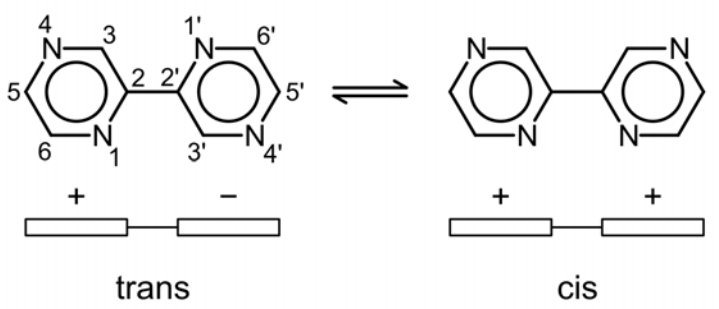

Scheme 6.1

In the all-*trans* conformer (+,–) all three 2,2´-bpz ligands are nearly perpendicular to the Pt_3 plane. In contrast, in the all-*cis* conformer (+,+) 2,2´-bpz ligands are strongly tilted, giving a vase-shape to the molecule.

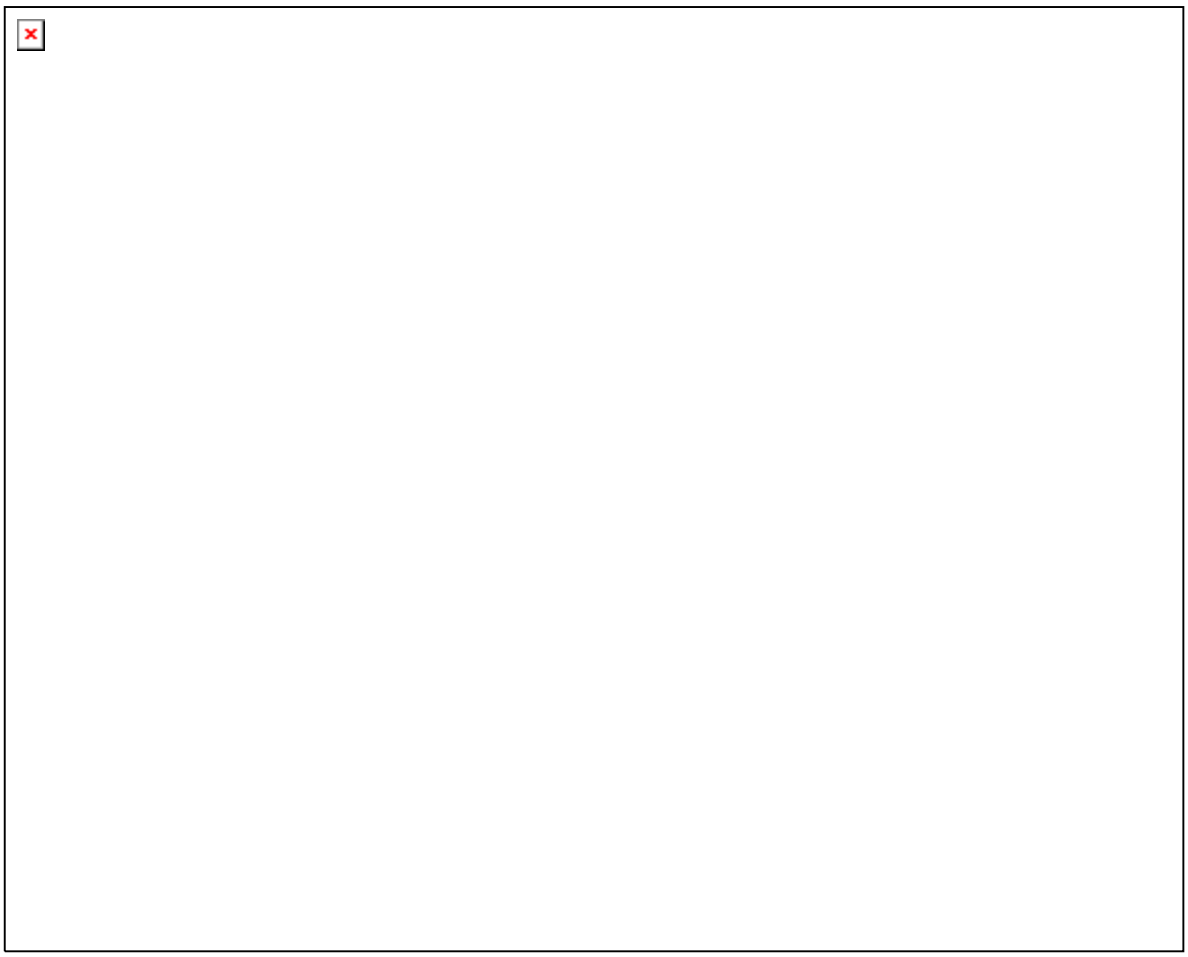

Figure 6.1 Side view of the molecular skeleton with and without encapsulated anion and space filling models of a) $BF_4\subset$*cis*-[{$Pt(NH_3)_2$(*ttt*-bpz-*N4,N4´*)}$_3$]$^{5+}$, b) [NO_3, $PF_6\subset$*cis*-[{$Pt(NH_3)_2$(*ccc*-bpz-*N4,N4´*)}$_3$]$^{4+}$ and c) [$NO_3\subset$[{(en)Pt(*ccc*-bpz-*N4,N4´*)}$_3$]$^{5+}$ (hydrogen atoms and other anions omitted for clarity).

Shapes and dimensions and thus anion binding properties of all three species differ from each other (Figure 6.1). The all-*cis* conformer of the triangle has a larger cavity than the all-*trans* conformer.

cis-[{Pt(NH$_3$)$_2$(*ttt*-bpz-*N4,N4′)*}$_3$]$^{6+}$ (**II-2**) crystallises as mixed BF_4^-/SiF_6^{2-} salt (see Chapter II). The BF_4 ion is located slightly above the Pt_3 plane, with B *ca.* 1.14 Å above the plane (Figure 6.2). The BF_4^- tetrahedron is oriented such that three F atoms are directed exactly toward the metal centers, rather than between them. Therefore, incorporation of BF_4^- into a cavity is assisted by weak Pt···F interactions with long distances of 4.38 – 4.53 Å. SiF_6^- anions are located outside the cavity.

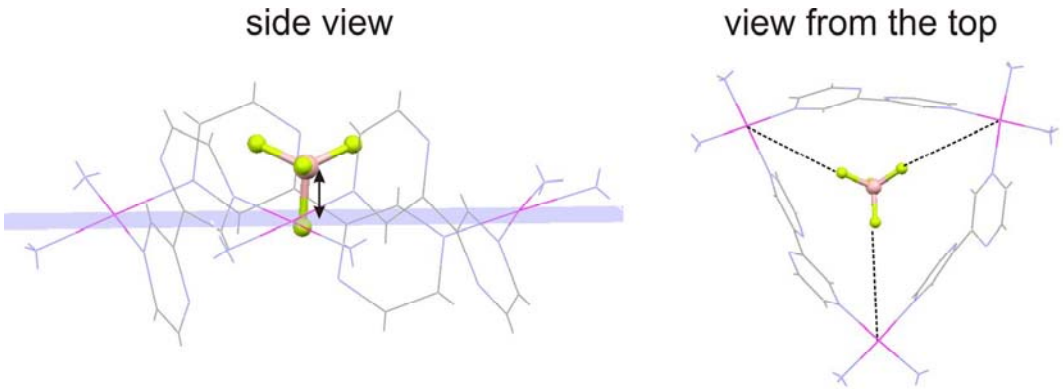

Figure 6.2 Location of BF_4^- anion in **II-2** (side and top views).

The X-ray crystal structure of [NO$_3$,PF$_6$⊂*cis*-[{Pt(NH$_3$)$_2$(*ccc*-bpz-*N4,N4′*)}$_3$](PF$_6$)$_4$ (**II-3**) establishes that encapsulation of the PF_6^- anion is possible. As has previously been shown,[70] cationic cavities of similar triangular species are able to host two anions simultaneously. The mixed PF_6^-/NO_3^- salt of the triangle exists only as all-*cis* conformer. The PF_6^- anion occupies the cavity above the metal coordination plane, with Pt_3-P = 3.79 Å, while NO_3^- anion is positioned almost in the Pt_3 plane (Pt_3-N ≈ 0.5 Å).

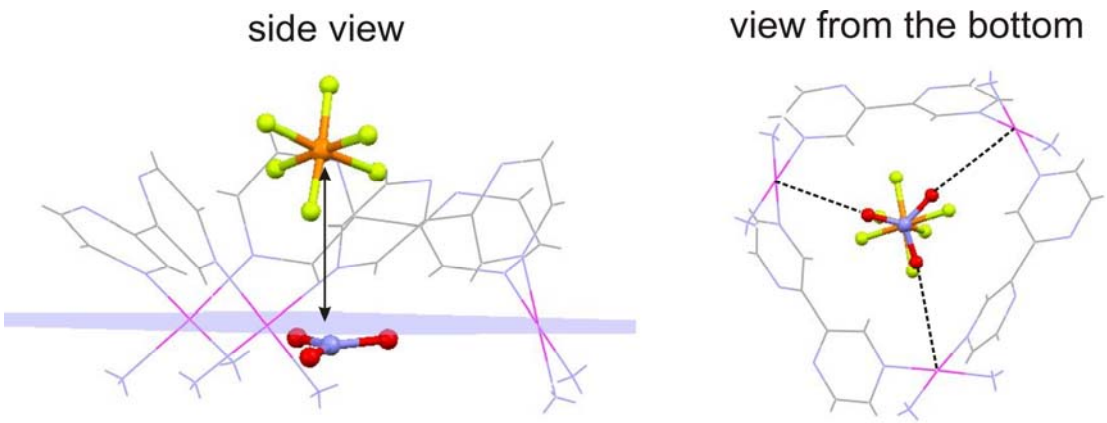

Figure 6.3 Location of PF_6^- and NO_3^- anions in **II-3**.

F atoms of the PF_6^- anion are pointing towards the 2,2′-bpz ligands, with C···F distances ranging from 2.95 – 3.09 Å, which suggest weak CH···F interactions. The oxygen atoms of the trapped NO_3^- anion are directed towards the Pt centers with the following distances: O13···Pt1, 3.25 Å; O12···Pt2, 3.41 Å and O11···Pt3, 3.55 Å. In order to obtain more information about the behavior of the trapped PF_6^- anion in solution, low temperature ^{19}F NMR experiments were performed for $[NO_3,PF_6\subset$*cis*-$[\{Pt(NH_3)_2($*ccc*-bpz-*N4,N4′*$)\}_3](PF_6)_4$ in DMF-d_7 in the temperature range of 216 to 295 K (Figure 6.4). Only a single ^{19}F doublet is observed over the whole temperature range.

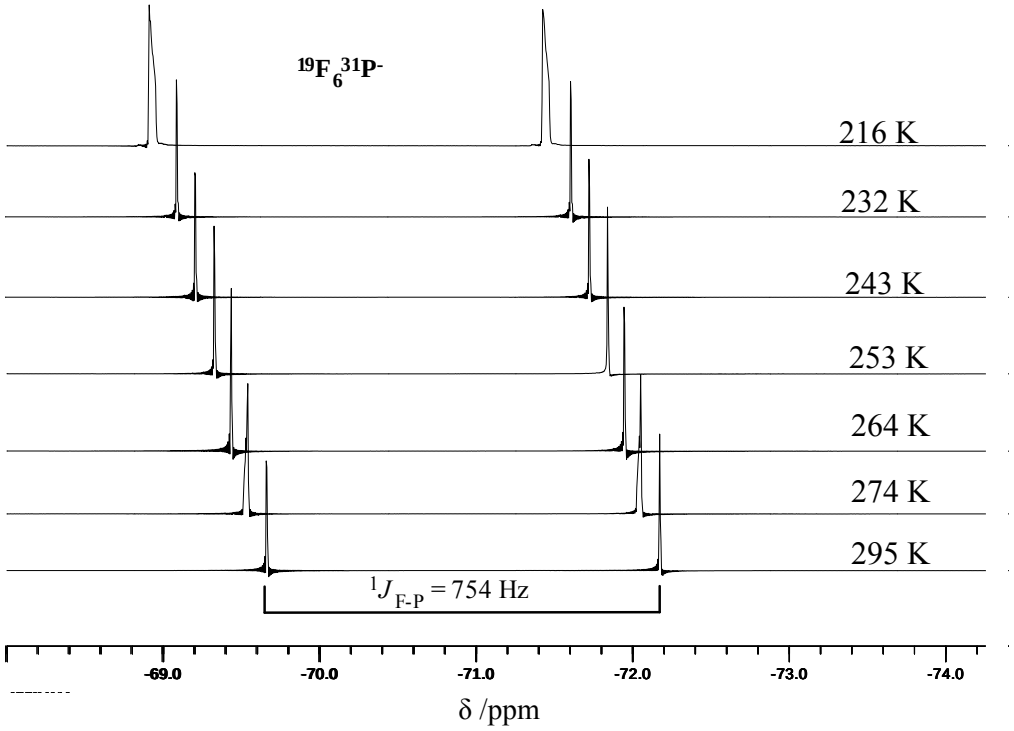

Figure 6.4 Stackplot of the ^{19}F NMR spectra of $[NO_3,PF_6\subset$*cis*-$[\{Pt(NH_3)_2($*ccc*-bpz-*N4,N4′*$)\}_3]^{6+}$ in DMF-d_7 in the temperature range from 295 – 216 K.

This allows the conclusion, that the PF_6^- ion undergoes fast exchange on the NMR time scale between encapsulated and free state, resulting in an equivalence of all PF_6^- anions.

Details of the host-anion interaction in $[NO_3 \subset \{(en)Pt(ccc\text{-bpz-}N4,N4')\}_3](NO_3)(SO_4)_2$ (**II-4**) were investigated by an X-ray crystal structure determination. The results suggest a way how a NO_3^- anion may be taken up by – or expelled from – the host molecule.

Although **II-4** is to be considered a structural variant of the all-*cis* isomer (II), orientations of two 2,2´-bpz ligands are different in it (II´) (Scheme 6.2).

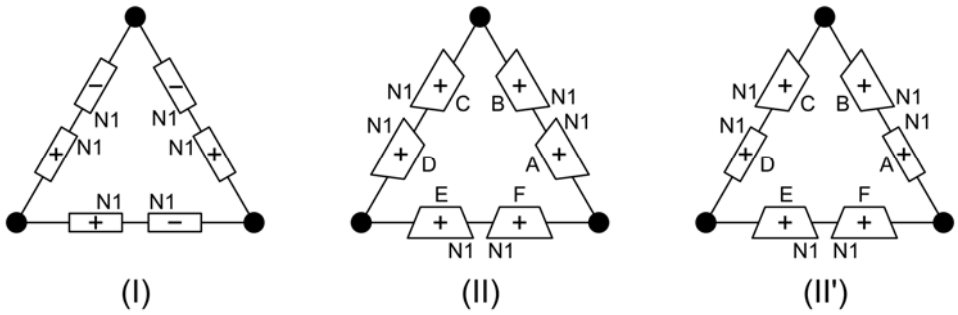

Scheme 6.2

Two pyrazine entities of two 2,2'-bpz ligands are nearly perpendicular to the Pt coordination planes and behave like a pincer for a NO_3^- anion, which is located between two pyrazine rings of the 2,2´-bpz with a $N\cdots Pt_3$ distance of 2.47 Å (Figure 6.5, a). A coplanar arrangement of NO_3^- with the three Pt atoms, would probably allow for a more efficient electrostatic interactions between the oxygen atoms of NO_3^- and the three metals.

Figure 6.5 Molecular representation showing location of nitrate anion (a), nitrate binding through anion-π interactions in **II-4** (b) and hydrogen bonding involving the sulfate anions and water molecules inserted between $enPt^{II}$ entities (c).

Additionally, the anion-π interactions of NO_3^- with pyrazine rings (O33···π(A), 3.28 Å; O32···π(D), 3.58 Å) may account for the structural change in the cavity of C_3-symmetric vase. A pronounced conformational flexibility of the host seems to enable this dynamic process. Hydrogen bonds between SO_4^{2-} and the NH_2 groups at the cage exterior (2.73 – 2.88 Å) are seen in the structure.

6.3 Anion binding by tetranuclear $[\{a_2Pt\}_4(bpz)_4]^{8+}$ host

Due to its biological relevance, recognition of physiologically important anions like nucleotides in water media is of great importance.[137] In this study the molecular tetramer $[\{cis\text{-}Pt(NH_3)_2(tttt\text{-}bpz\text{-}N4,N4')\}_4]^{8+}$ (**II-1**) has been tested as host for adenosine monophosphate (AMP).

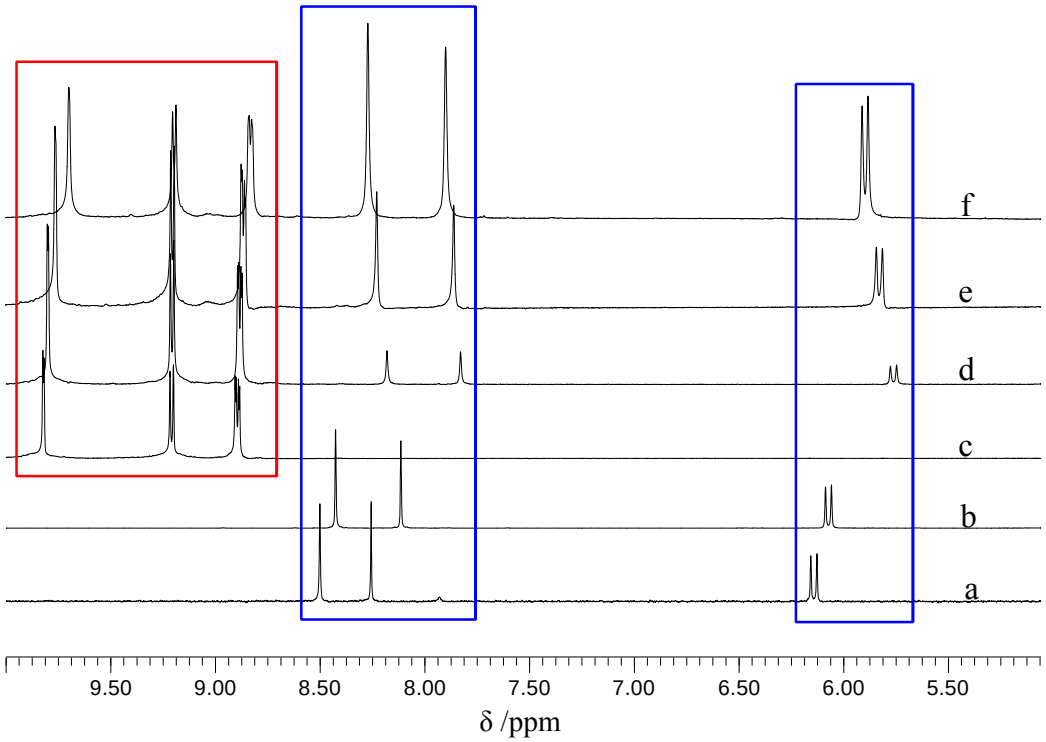

Figure 6.6 ^{1}H NMR spectra (200 MHz, D_2O) of a) 0.005M AMP, b) 0.1M AMP, c)$[\{cis\text{-}Pt(NH_3)_2(tttt\text{-}bpz\text{-}N4,N4')\}_4]^{8+}$, d) solution of tetramer (0.006M) after addition of 1 equivalents of AMP, e) 3 equiv. AMP, f) 7 equiv. AMP.

The Pt_4 anion receptor was titrated with increasing amounts of AMP and ^{1}H NMR spectra were taken after each addition of the nucleotide (Figure 6.6). In was found that the presence of AMP causes small *upfield* shifts of proton signals of the tetramer with the maximum $\Delta\delta$ = 0.13 ppm observed for H3,H3´protons of 2,2´-bpz (0.006 M solution). Proton

signals of AMP undergo *downfield* shifts: Δδ (H8) = Δδ (H2) ≈ 0.1 ppm and Δδ (H2´) = 0.15 ppm. These findings allow the conclusion that π–π and electrostatic interactions between host and guest molecules induce shifts of the proton signals. No detailed picture of this interaction can be derived from these observations, however.

6.4 Anion binding by $[\{a_2Pt\}_3\{a'_2Pd\}_3(bpz)_3]^{12+}$ hosts

$[\{a_2Pt\}_3\{a'_2Pd\}_3(bpz)_3]^{12+}$ hosts are vase-shaped molecules, with a relatively large hydrophobic cavity. The previously reported $[\{(en)Pt(N4,N4'\text{-bpz-}N1,N1')Pd(en)\}_3]^{12+}$ has been crystallized as a mixed salt,[69, 70] with NO_3^- sitting at the bottom of the vase and PF_6^- on top of it. Anion binding studies of it revel stronger binding of SO_4^{2-} in comparison to ClO_4^-, BF_4^-, PF_6^- and $CH_3C_6H_4SO_3^-$. Hereafter an investigation on the anion-binding affinity of the closely related $[\{(NH_3)_2Pt(N4,N4'\text{-bpz-}N1,N1')Pd(en)\}_3]^{12+}$ host is described.

Figure 6.7 shows NO_3^-, SO_4^{2-} and PF_6^- anions encapsulated in the molecular vase. The remaining anions exist outside the cavity and form multiple hydrogen bonds with the cation and water molecules.

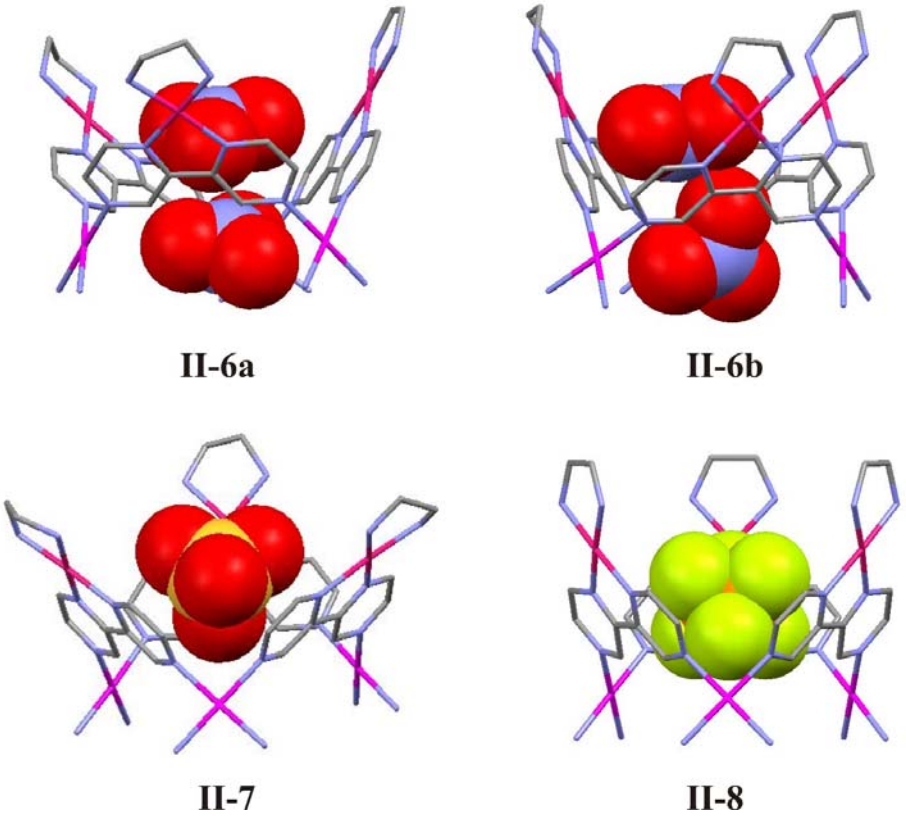

Figure 6.7 Location of encapsulated anions in $[\{a_2Pt\}_3\{a'_2Pd\}_3$2,2´-bpz$)_3]^{12+}$ molecular vases **II-6**, **II-7** and **II-8**.

As mentioned above (Chapter 2), the asymmetric unit of [{$(NH_3)_2$Pt(*N4,N4'*-bpz-*N1,N1'*)Pd(en)}$_3$]$(NO_3)_{12}$ (**II-6**) contains two independent cations: **II-6a** and **II-6b.** In this respect, it is interesting to note that there are significant differences in the way the NO_3^- anions are included in the host interior of both cations.

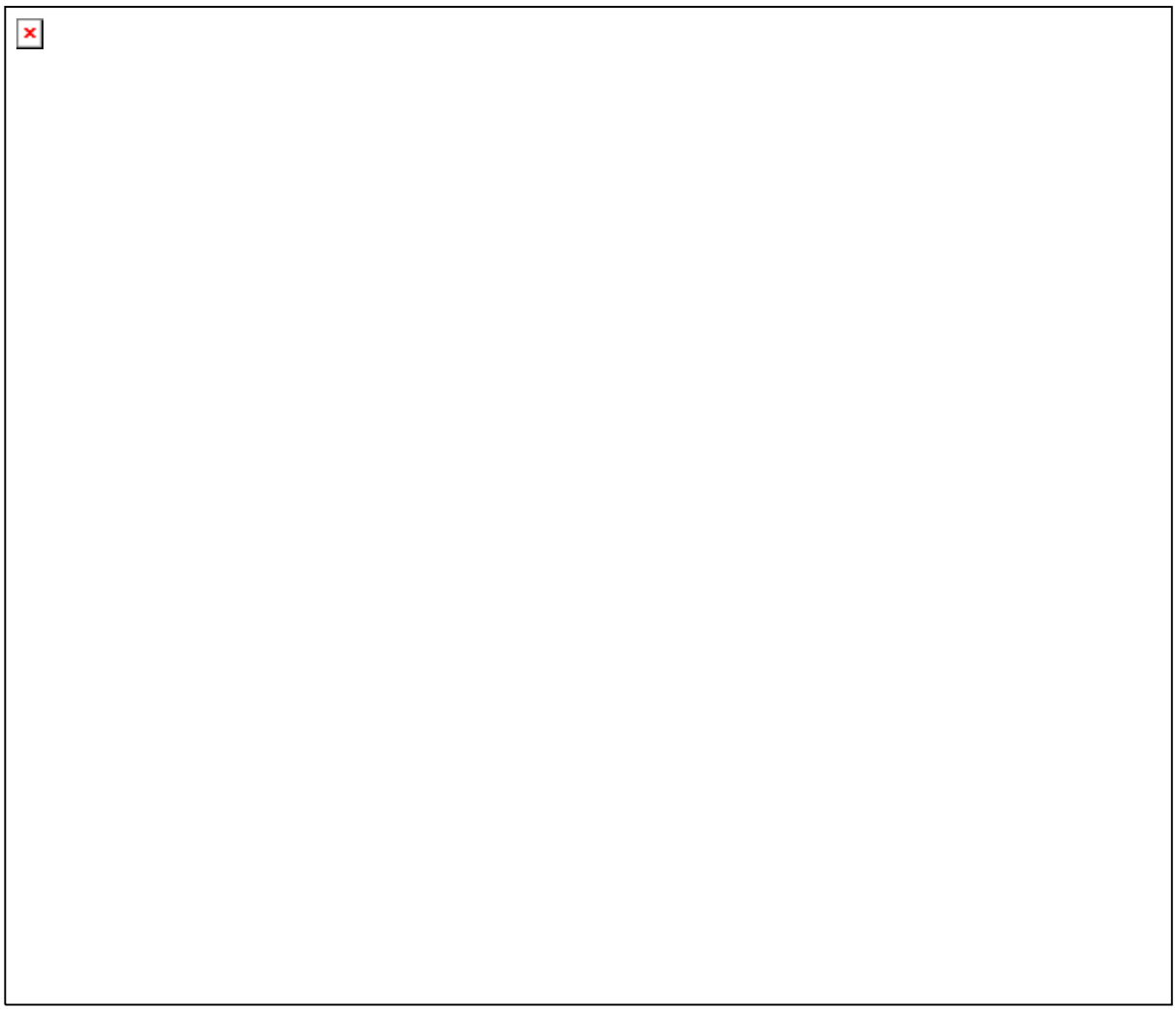

Figure 6.8 Side and top views of molecular vases **II-6a** (a) and **II-6b** (b) showing the locations of the encapsulated nitrate anions and hydrogen bonding interactions within the cavity.

The X-ray crystal structure shows that in **II-6a** one of the nitrate anions is located in the center of the Pt_3 triangle (Figure 6.8, a) with the oxygen atoms pointing towards the Lewis acidic Pt centers (O41···Pt2, 3.51 Å; O42···Pt3, 3.13 Å and O43···Pt1, 3.39 Å). The second nitrate anion is located above the first one, slightly shifted from the center with N40···N190, 3.75 Å and Pt_3···N, 3.56 Å. The electron-poor character of the pyrazine rings, caused by the presence of two endocyclic nitrogen atoms, further increases through coordination to the

metal centers. Consequently, they are prone to lone electron pair···π interactions. Indeed, three water molecules occupy the corners of triangular vase with the following distances: O1W···π(A), 3.60 Å; O1W···π(F), 3.07 Å; O2W···π(B), 3.07 Å; O2W···π(C), 3.61 Å; O3W···π(E), 3.08 Å; O3W···π(D), 3.33 Å. These encapsulated water molecules make strong hydrogen bonding bonding to the NO_3^- anion (O191···O2W, 2.76 Å; O192···O2W, 2.48 Å; O193···O1W, 2.77 Å and O193···O3W, 2.81 Å), holding it in the cavity of the vase.

The cation **II-6b** reveals substantially different orientations of the NO_3^- anions (Figure 6.8, b). The first one is oriented at a large angle (69.5°) to the Pt_3 plane. Its position is supported by hydrogen bonds to the ammine ligands of a neighboring cation (O51···N41, 2.93 Å and O53···N42, 2.94 Å). The second nitrate anion is again located on top of the first one. However, in this case the electrondeficient aromatic rings of 2,2´-bpz contribute to its binding in an π-anion-π contact mode with O232···π(K), 2.95 Å; O232···π(J), 2.92 Å distances. This nitrate anion is disordered over two positions. The third corner is occupied with a water molecule (O4W···π(G), 3.13 Å and O4W···π(L), 3.15 Å). The N230···Pt_3 distance is 3,87 Å.

Binding of the sulfate anion from aqueous solution is especially difficult because of its large free energy of hydration ($\Delta G_h \approx 1090$ kJ mol^{-1}). In order to achieve a selective and efficient binding of sulfate anions, a widely employed strategy is to introduce functional groups capable of forming hydrogen bonds to the molecular skeleton of the receptor molecule.[138] In such hosts, the number of hydrogen bond donor sites can reach twelve.[139] Similarly, the X-ray crystal structure of the sulfate-binding protein reveals, that sulfate is encapsulated deep in the interior of the protein with the help of seven hydrogen bonds.[140]

The molecular vase [{$(NH_3)_2$Pt(*N4,N4′*-bpz-*N1,N1′*)Pd(en)}$_3$]$(SO_4)_6$ (**II-7**) has been crystallized with one SO_4^{2-} anion inside the cavity. The compound represents a unique example of sulfate binding unsupported by hydrogen bonds. As has been shown in previous cases of nitrate binding, O···π interaction can play a significant role in anion complexation by helping to achieve a more efficient receptor-anion interaction. The sulfate anion is disordered over two positions (Figure 6.9), with two of its oxygen atoms oriented towards the faces of two electrondeficient pyrazine rings (O43···π(1), 2.91 Å, O43···π(6), 3.07 Å). It is also bonded to a H_2O molecule, which is likewise involved in O···π interactions (O1w···π(2), 3.00 Å and O1w···π(3); 2.96 Å, distance S···Pt_3 is 3.77 Å). Taking along a water molecule into the host reduces the energy penalty for full dehydration of sulfate.

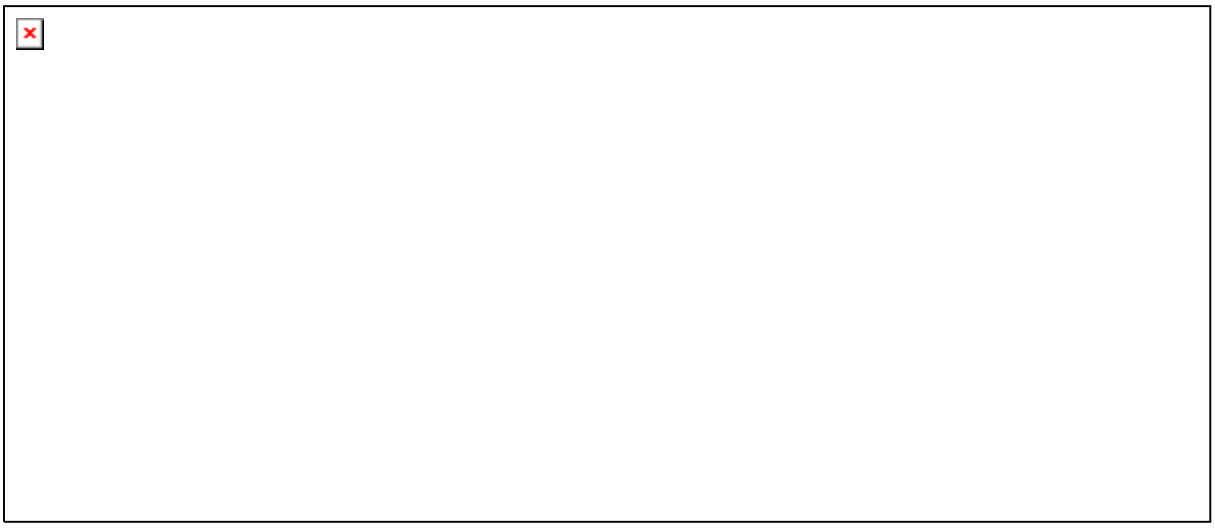

Figure 6.9 Location of SO_4^- anion in **II-7** (side and top views).

The intramolecular encapsulation of SO_4^{2-} anion in the $[Pt_3Pd_3(2,2'\text{-bpz})_3]^{12+}$ compound is confirmed also in solution, as observed by ^1H NMR spectroscopy. The addition of increasing amount of Na_2SO_4 to a solution of $[Pt_3Pd_3(2,2'\text{-bpz})_3](NO_3)_{12}$ (Figure 6.10) induces significant changes in the position of the signals attributed to the H3,H3′ pyrazine protons, which shift downfield by 0.18 ppm. Signals of H5,H5′ and H6,H6′ remain nearly unchanged. Indeed, as the crystal structure suggests, the trapped SO_4^{2-} anion is located close to the hexagon formed by H3,H3′ protons (0.66 Å above the Pt_3 plane), which is responsible for the observed shifts. Other sulfate anions involved in hydrogen bonding interactions with NH_3 ligands are much further away from the H3,H3′ atoms.

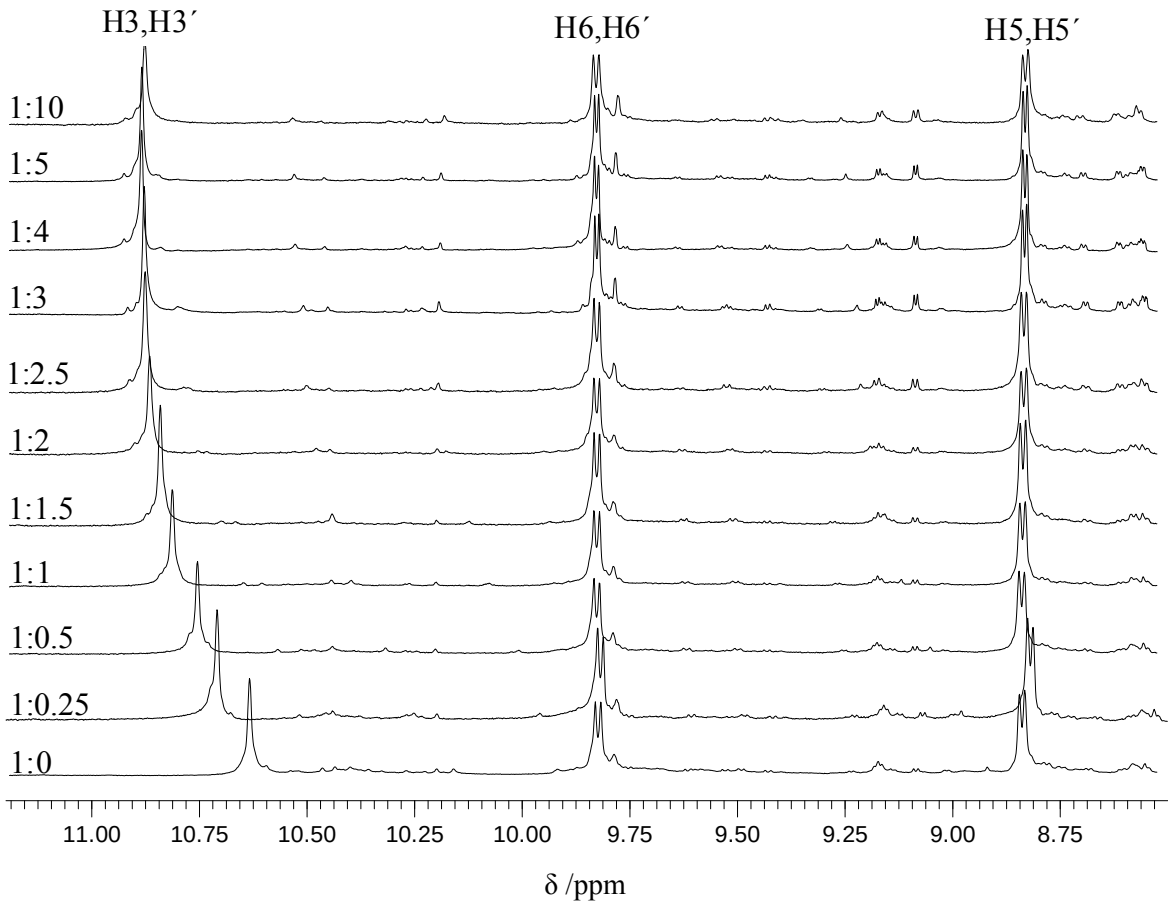

Figure 6.10 Stackplot of ^{1}H NMR spectra showing upfiled shift of H3,H3´proton resonances of bpz in **II-6** upon addition of increasing amounts of Na_2SO_4.

A Job plot analysis carried out for the H3,H3´ resonance of **II-6**/**II-7** revealed a 1:1 stoichiometry between **II-7** and SO_4^{2-}. (Figure 6.11). The association constant was found to be (1.0 ± 0.2) x 10^3 M^{-1} and is somewhat higher than for the previously reported analogue.[70] Although reasons for this difference are not clear yet, slight differences in Lewis acidities of *cis*-$(NH_3)_2Pt^{II}$ and $(en)Pt^{II}$ could be the reason, because they could affect 2,2´-bpz basicity and/or hydrogen bonding properties of the am(m)ine ligands at the three Pt atoms.

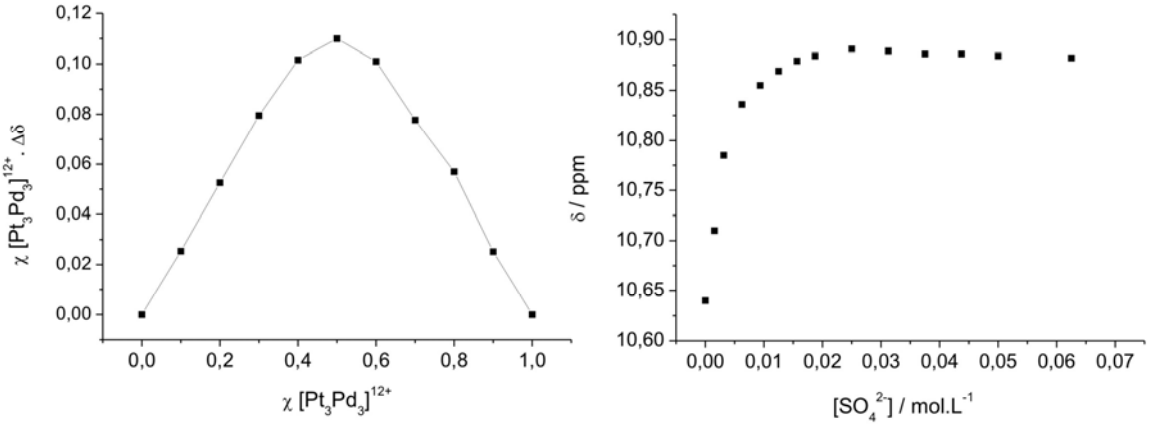

(a) (b)

Figure 6.11 Job plot analysis of H3 resonances (a) and chemical shifts of H3,H3´ 2,2´-bpz resonances in $[Pt_3Pd_3(bpz)_3](NO_3)_{12}$ as a function of the SO_4^{2-} concentration (b).

A preliminary crystal structure analysis of $[\{(NH_3)_2Pt(N4,N4'\text{-bpz-}N1,N1')Pd(en)\}_3](PF_6)_{11}(NO_3)$ (**II-8**) shows that one of the PF_6^- anions is encapsulated in the cavity of the molecular vase (Figure 6.12). It is located above the Pt_3 plane and has a $Pt_3\cdots P$ distance of 2.92 Å.

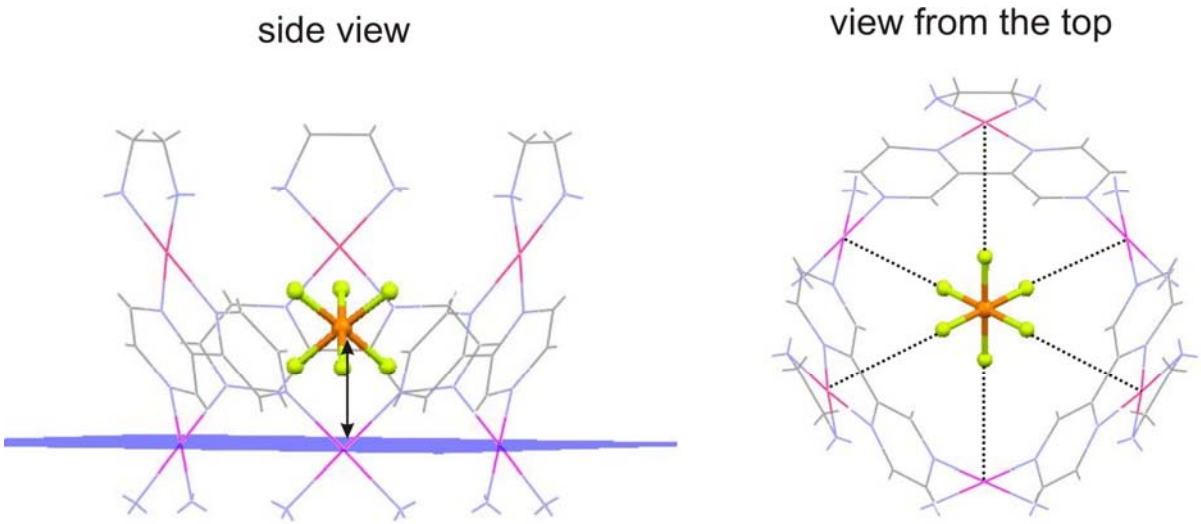

Figure 6.12 Location of PF_6^- anion in **II-8** (side and top views).

The flour atoms of the guest anion are pointed towards the Pt and Pd centers with distances of Pt···F *ca.* 3.75 Å, and Pd···F *ca.* 3.79 Å. The crystal structure determination

demonstrates the excellent size complimentarity of the octahedral PF_6^- anion with the host cation.

6.5 Polycyclic architectures as anion hosts

The cationic charge of the Cu(II) complex $\{[enPt(bpz)]_6Cu_4(H_2O)_6\}^{20+}$ (**II-15**) is neutralized by twenty NO_3^- anions, four of which are encapsulated in the two halves of the paddle wheel (Figure 6.13). A striking feature of this complex is the unusual nitrate binding patterns. One of the NO_3^- anions is within the Pt_3 plane with oxygen atoms oriented towards the Pt centers. Interactions are to be considered weak, with O···Pt distances ranging from 3.25 to 3.43 Å. The second NO_3^- anion is located on top of the first NO_3^-, with N4N···N9N distance to 3.55 Å. There are four additional NO_3^- anions nested inside the cavity, whereas six nitrates are associated via hydrogen bonding interactions with the outside of the macrocyclic cavity. Lengths of these interactions are in the range of 2.82 – 2.98 Å.

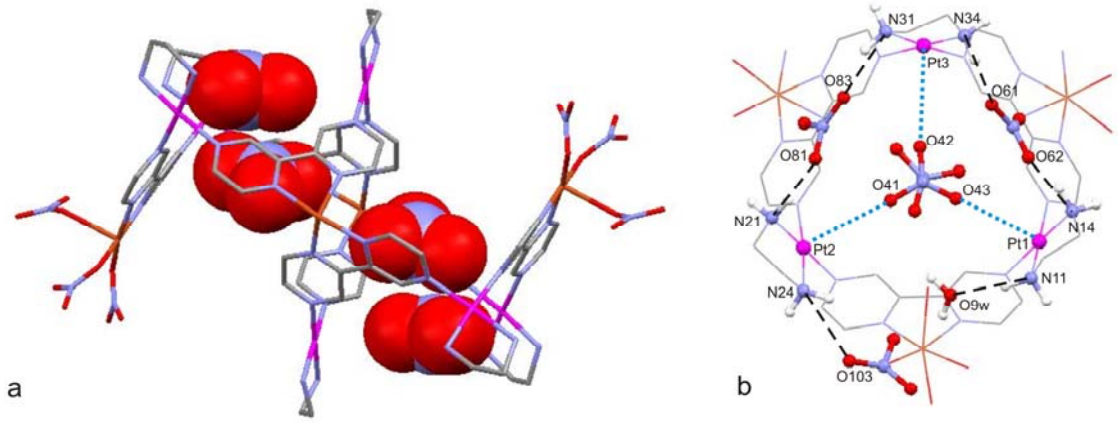

Figure 6.13 Perspective views of compound **II-15,** showing encapsulated NO_3^- anions (a) and hydrogen bonding interactions between the amine ligands and the externaly coordinated nitrates (b) (only one half of the molecule is shown).

More recently, extended anion binding frameworks based on coordination polymers have also become topical.[141] The 1D and 2D structures described in Chapter 2 are composed of $[Pt_3(2,2'\text{-bpz})_3]^{6+}$ units and Cd^{2+} or Ag^+ ions, and they likewise exhibit a high affinity for anions.

As was established by X-ray analysis, the 1D coordination polymer $\{[(en)_2Pt(bpz)]_3[Cd(H_2O)_3][Cd(H_2O)_4](SO_4)_6\ [Cd(H_2O)_6]\}_n$ (**II-15)** contains one encapsulated SO_4^{2-} anion and three water molecules.

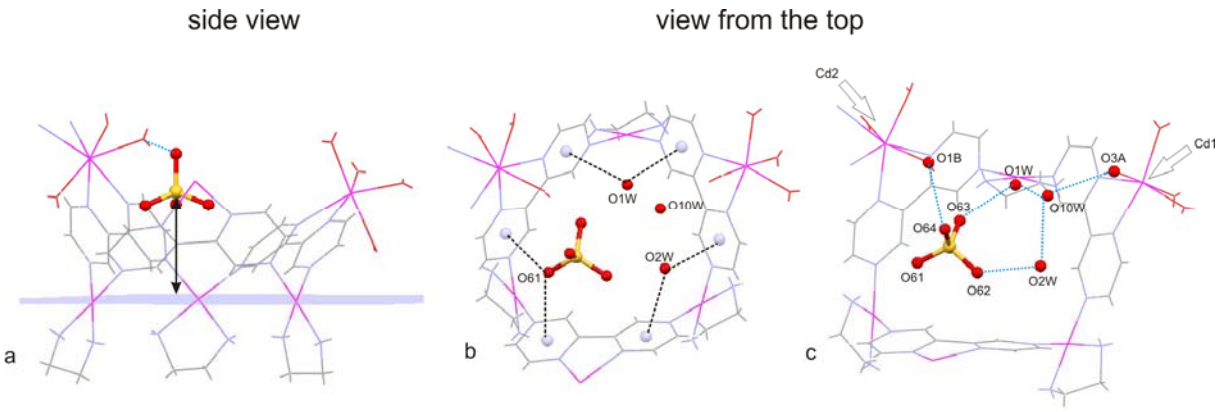

Figure 6.14 Location of the SO_4^- anion in **II-15**. Side view (a), view from the top showing anion···π interactions (b) and view from the top, showing hydrogen bonding interactions (c).

The sulfate anion is located above the Pt_3 plane with an S···Pt_3 distance of 4.20 Å. Very interesting cooperativity effects are present in this complex, where anion-π and hydrogen bonding interactions coexist. As in the previous complex **II-7,** there is a lone pair···π interaction between pyrazine rings and oxygens of the sulfate anion and water molecules (O61···π(E), 3.10 Å; O61···π(D), 2.85 Å; O1W···π(A), 3.19 Å; O1W···π(F), 3.43 Å; O2W···π(B), 3.32 Å; O2W···π(C), 3.62 Å. They are additionally interconnected through hydrogen bonds with the following distances: O62···O1W, 2.63 Å and O63···O2W, 2.58 Å. The hydrogen bond between to the water molecule coorditaned to Cd and the sulfate anion (O64···O1B, 2.80 Å) serves as bridge to hold SO_4^{2-} in place. A similar interaction between water molecules exists on the other side of the molecular unit (O10W···O3A, 2.72 Å) (Figure 6.14).

The 2D porous network $\{[(NH_3)_2Pt(bpz)]_3Ag\ (SiF_6)_3(BF_4)\}_n$ (**II-16**) has been crystallized as mixed SiF_6^{2-}/BF_4^--salt, with one disordered BF_4^- anion encapsulated in the cavity of the structural unit of this polymer, with Pt_3···B distance equal to 2.87 Å. (Figure 6.15, a) The SiF_6^{2-} anions are not included inside the hydrophobic channels of the crystal, but rather are in-between the layers.

The preliminary crystal structure analysis of the $\{[(NH_3)_2Pt(bpz)]_3Ag\ (SO_4)_{3.5}\}_n$ (**II-17**) reveals the existence a 2D porous network structure which has a close similarity to that of **II-16**. One of the SO_4^{2-} anions is located at the bottom of the molecular vase (Figure 6.15, b). The Pt_3···S distance is 0.71 Å.

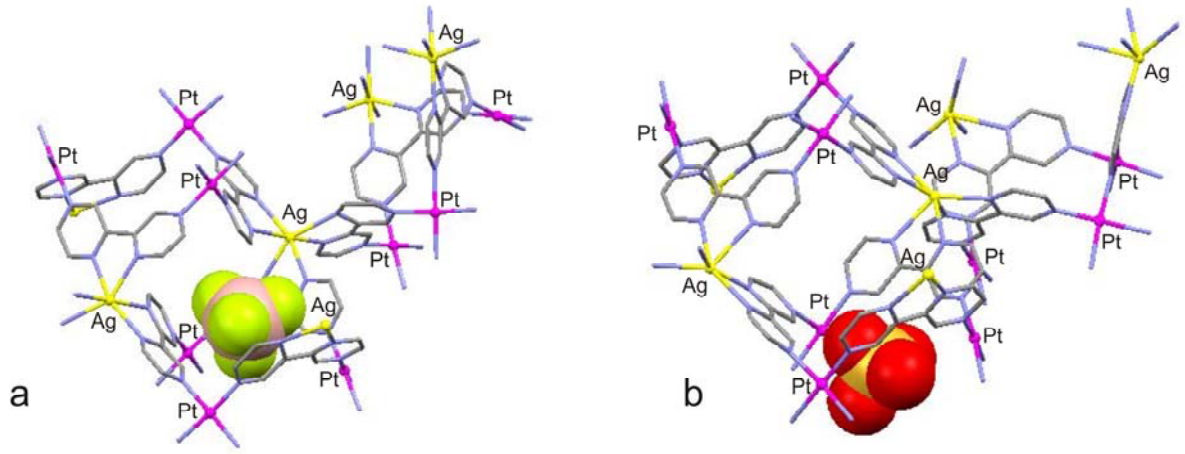

Figure 6.15 Location of BF_4^- anion in **II-16** (a) and SO_4^{2-} anion in **II-17** (b).

6.6 Conclusions

This chapter describes anion binding properties of homo- and heterometallic complexes of 2,2´-bpz. Whereas triangular species are able to encapsulate poorly hydrated BF_4^- and PF_6^- anions, for binding of highly hydrated SO_4^{2-} anion additional features are required. It has been shown that the molecular vases **II-6**, **II-7** and **II-8** behave as very versatile receptors for anions. For instance, owing to the high positive charge (12+) and the presence of electrondeficient aromatic rings, $[Pt_3Pd_3(2,2´\text{-bpz})_3]^{12+}$ molecular vases are able to overcome the solvation-based Hofmeister bias and trap two NO_3^- or one SO_4^{2-} in their cavities. Binding of NO_3^- by triangular species is eased by the conformational flexibility of the host. NMR titration experiments show that there is a weak interaction between the molecular square and AMP. Polymeric 1D and 2D structures also have a range of interesting and potentially useful molecular recognition properties owing to the presence of hydrogen bond donor groups, their positive charge, and the presence of electrondeficient aromatic rings.

The results reported herein stress the importance of anion - π interactions in anion binding and highlight a new noncovalent design principle for their recognition.

Chapter 7 – Studies of metal complex-DNA interactions using AFM

7.1 Background

Different classes of DNA-binding agents with significantly different binding modes have been developed in recent years (see Chapter 1). Molecules, able to bind to DNA and activate or inhibit a particular gene, could open new possibilities in the development of therapeutic and diagnostic agents, as well as serve as models to understand DNA packaging and chromosome folding. Condensation of the DNA molecule, among others, involves overcoming the Coulombic barrier, which arises from the negatively charged phosphates on the DNA, and therefore DNA binding molecules are frequently positively charged. Interaction of them with DNA can be understood as an exchange between naturally occurring mono- and divalent counterions and multiply charged molecules. As have been shown DNA condensation occurs when about 67% of the DNA phosphate charge is neutralized by $[Co(NH_3)_6]^{3+}$ and 87% by protonated spermidine. During condensation, the remaining DNA charge is neutralized.[142]

Positively charged discrete supramolecular structures, which are constructed by using organic ligands and metals centres, have recently attracted curiosity in view of their potential to interact non-covalently with DNA. Cationic metal complexes are promising canditates, since they carry positive charge, which allows them to interact electrostatically with the phosphate groups of DNA. Moreover, the geometries of such molecules can be easily varied applying tools from supramolecular chemistry. For instance, the metallo-supramolecular iron cylinders prepared by M. Hannon *et al.* not only target the major groove of ds-DNA, as observed by NMR, CD and LD studies, but also induce dramatic intramolecular coiling (AFM).[143] A crystal structure determination also shows that such compounds can bind at the heart of Y-shaped DNA junctions.[144] A very similar structure, containing Ru(II) centers instead of Fe, was found to exhibit activity against cancer cell lines. Non-covalent interactions take place also between metallacalix[4]arene containing Pt(II) centers and ct-DNA. While DNA coiling is observed at low concentrations, higher loadings cause formation of inflexible ct-DNA filaments in this case.[145]

For structural analysis of DNA and/or for understanding DNA-substrate interactions, techniques applicable at low concentrations, like electron and scanning probe microscopy, are needed. *A*tomic *F*orce *M*icroscopy (AFM) was invented in 1986[146] and nowadays is one of the most widely used imaging techniques. It enables visualization of biological molecules either in air or in liquid with sub-angstrom (in Z) and nanometer (in XY) resolution. Based on the working principles of *S*canning *T*unneling *M*icroscopy (STM), AFM was developed for nonconducting surfaces. The tip is held several nanometers above the surface, repeatedly scanning across the surface of a sample. Since a laser is pointed at the tip during the measurement, a reflected laser beam measures the variations in tip height and produces a topographic image of the surface (Figure 7.1). There are three commonly used modes, in which AFM can operate: contact mode, non-contact mode and tapping mode. Soft and fragile samples can be successfully imaged using the tapping mode. This mode also gives opportunity to achieve high resolution both in air and in fluid.

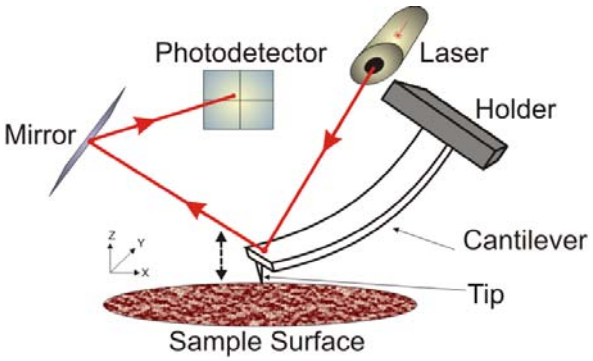

Figure 7.1 Schematic illustration of working principle of AFM

Binding interactions of the cationic, water soluble Pt(II) complex *cis*-[{$Pt(NH_3)_2$(2,2′-bpz)}$_3$]$^{6+}$ (**II-2**) with linearized plasmid pcDNA 3.1 was studied using the AFM technique. Negatively charged $[Pt(CN)_4]^{2-}$ was used as a control.

7.2 Studies on DNA-metal complex interactions

7.2.1 DNA imaging

Freshly cleaved muscovite mica sheets are particularly useful for AFM imaging, due to their clean and flat surface. However, in order to be imaged by AFM, DNA molecules must be immobilized on the surface of the negatively charged mica. This can be achieved by means of electrostatic interactions. One of the most widely used methods is addition of divalent cations to the DNA solution, which serve as a bridge to fix the negatively charged backbone of DNA onto the mica surface.[147] Nickel (Ni^{2+}) and magnesium (Mg^{2+}) ions are often used for

this purpose. (For details of sample preparation, see Chapter 8 – Experimental section.) AFM imaging was performed in tapping mode in an air environment, with a relative humidity of 20-30%.

Figure 7.2 shows the complete population and topography of two different samples of DNA molecules, which differ by the method of drying. While the first one (Figure 7.2, A) was imaged direct after the sample was dried in a stream of nitrogen, the second sample (Figure 7.2, B) was kept under vacuum overnight.

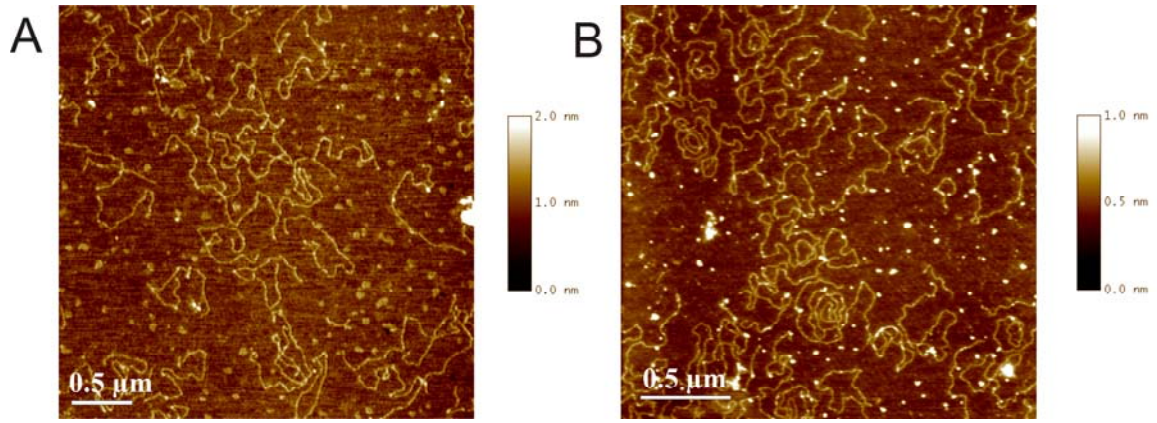

Figure 7.2 Linearized plasmid pc DNA 3.1 adsorbed onto muscovite mica. The image scan area corresponds to (A) 3.4 µm × 3.4 µm (only nitrogen dried) and (B) 2.5 µm × 2.5 µm (additionally dried under vacuum).

The DNA molecules imaged have apparent heights of 0.27 ± 0.20 nm (A) and 0.50 ± 0.24 nm (B), which is similar to heights previously measured with AFM.[151] The heights of dsDNA molecules imaged by AFM are usually smaller than the calculated value of 2 – 2.5 nm for B-forms of dsDNA. Possible reasons for reduced heights of dsDNA molecules are a deformation of DNA under the AFM tip (it often compresses biomaterials during imaging)[148] or the presence of salts in the solution.[149]

The DNA molecule applied in this study adopts the B form with 5428 bp., corresponding to a contour length of 1846 nm by assuming an axial rise of 0.34 nm/bp. Measurements of contour lengths of DNA have been done by using the Image*J* programme (Version 1.43) and by fitting the nominal curve to the tracing of the DNA path as shown in Figure 7.3. Preferably, relaxed molecules are used for these measurements. Measured DNA

lengths correspond to *ca.* 1600 nm, which is within an error of ± 15 % and is in an acceptable range.

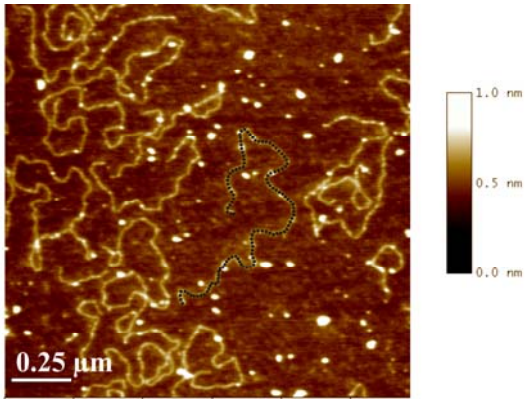

Figure 7.5 Selected DNA contour.

Some of the measured samples are highly oriented and since there is no correlation between the concentration of DNA or Mg^{2+}, most likely the method of drying of samples causes differences in linearly and randomly oriented DNA molecules. In case the surface was not gently dried with compressed nitrogen, but rather a strong stream was applied, DNA molecules tend to arrange in one direction (Figure 7.6).

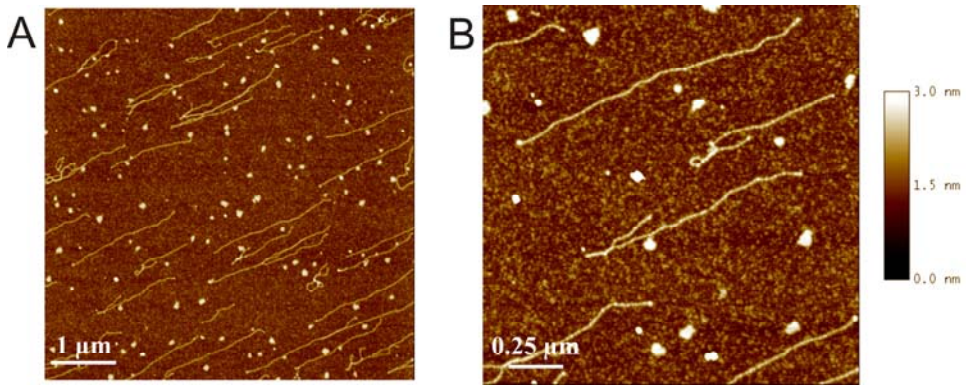

Figure 7.6 Linearized plasmid pc DNA 3.1 adsorbed onto muscovite mica and dried under a strong stream of nitrogen. Image scan area corresponds to 5 µm × 5 µm (A) and 2 µm × 2 µm (B).

In this case, high resolution of the images makes it possible to resolve the helical pitch of the dsDNA. The height of DNA molecules is 0.82 ± 0.22 nm and is nearly the half of the diameter of double helix of DNA *in vivo.*

Increasing amounts of Mg^{2+} ions (up to 100 fold), causes the DNA molecules to adhere densely on the surface and to form an interconnecting network, as shown in Figure 7.7.

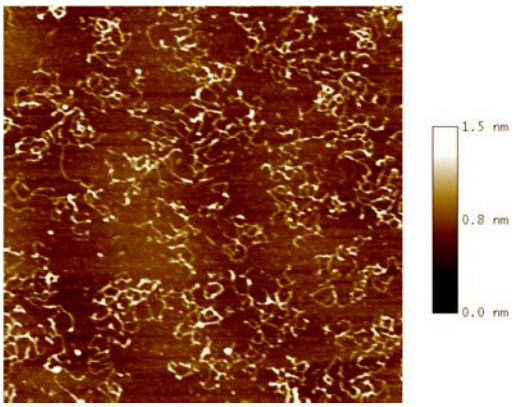

Figure 7.7 Linearized plasmid pc DNA 3.1 adsorbed onto muscovite mica in the presence of 200 mM concentration of $MgCl_2$.

7.3.3 Imaging of metallocomplex-DNA adducts

The images of *cis*-$[\{Pt(NH_3)_2(bpz)\}_3]^{6+}$ (**II-2**) deposited on mica surface does not reveal individual molecules, most likely because the tip of the AFM is not sufficiently small to image the small triangular cations of **II-2**. As can be seen from Figure 7.8 the height of the spots on the mica surface is *ca.* 0.3 nm.

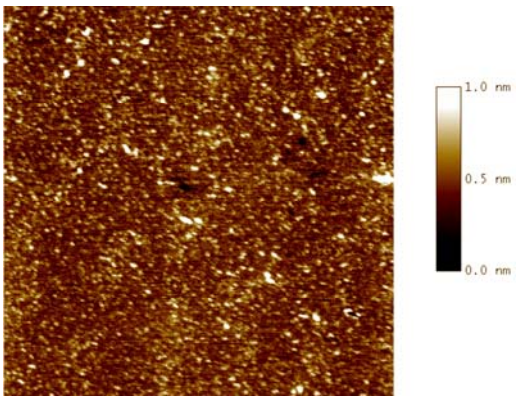

Figure 7.8 AFM image of cations of *cis*-$[\{Pt(NH_3)_2(bpz)\}_3]^{6+}$ deposited on mica surface.

Binding of *cis*-$[\{Pt(NH_3)_2(bpz)\}_3]^{6+}$ to linearized plasmid DNA was accomplished by incubating mixtures of both components at RT for 4 – 5 h. The measurements were done for

mixtures containing DNA base pairs and **II-2** in 10:1 and 10:2 ratios, with the dissolved metal complex added to a solution of fixed concentration of DNA and $MgCl_2$ salt.

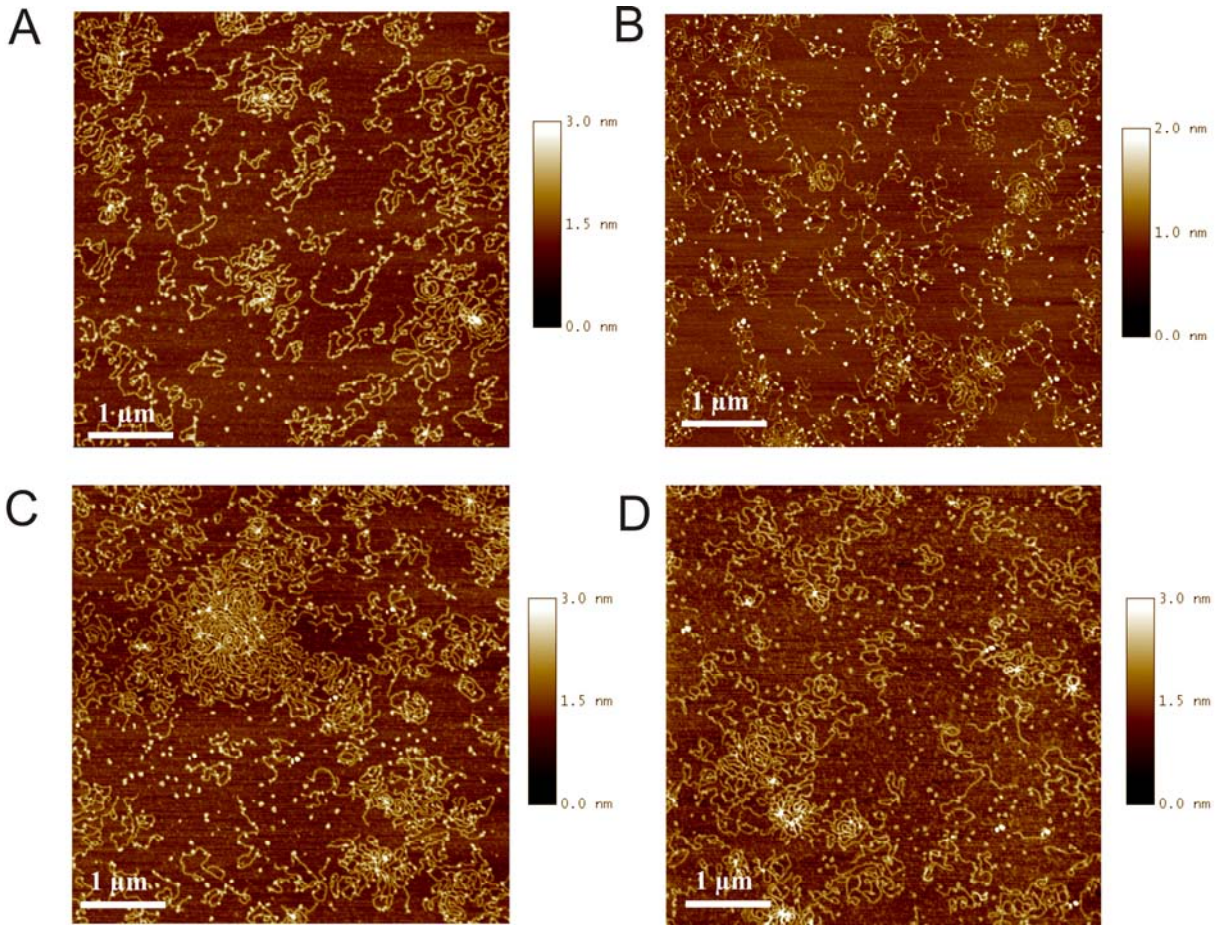

Figure 7.8 AFM images of linearized plasmid pcDNA 3.1 incubated with *cis*-$[\{Pt(NH_3)_2(bpz)\}_3]^{6+}$ (**II-2**) in ratios of base pairs : metal complex of 10:1 (A) and 10:2 (B–D) Image scan areas correspond to 5 µm × 5 µm.

The bright spots in the images are referred to as "knots", formed as a result of DNA-(**II-2**) interactions. The average heights of these "knots" are 0.96 ± 0.36 (A), 1.09 ± 0.23 (B), 0.69 ± 0.28 (C) and 0.70 ±0.19 nm (D), while the height of the DNA strands is only around 0.4 nm. Determination of the height of the DNA serves as a reference, since for AFM measurements carried out in air, the height of a molecule is very sensitive to the imaging conditions.[150]

cis-$[\{Pt(NH_3)_2(bpz)\}_3]^{6+}$ (**II-2**) was found to behave differently as far as interactions with DNA are concerned. In fact, the samples display different topologies. The following main types of modes of condensation products could be identified: cation binding to the individual dsDNA molecules (Figure 7.9, A) and formation of aggregates, composed of

multiple strands of dsDNA, with identification of the individual DNA molecules not possible (Figure 7.9, B).

Condensation and aggregation of DNA are closely related phenomena. The first usually refers to the coiling of a single DNA molecule and is significant in storage and packing of DNA (*e.g.* viral capsids). During aggregation of DNA, multiple chains attract each other and form different complex structures. Formation of daisy-shaped aggregates has been detected in polylysine-DNA complexes imaged by AFM, when the samples in water were diluted with a HEPES, Mg^{2+} solution. (4 kDa PL, lysine : nucleotide 0.5:1).[151] Intermolecular synapsis of DNA molecules are also found at high vTopIB (vaccinia topoisomerase IB) : DNA ratios.[152] In both modes of interactions, the presence of positively charged multivalent molecules/ions is significant for attraction of negatively charged DNA strands.

The effect of sample drying was not investigated, because in was anticipated that weakly condensed/aggregated DNA may have been destroyed upon drying with a stream of nitrogen.

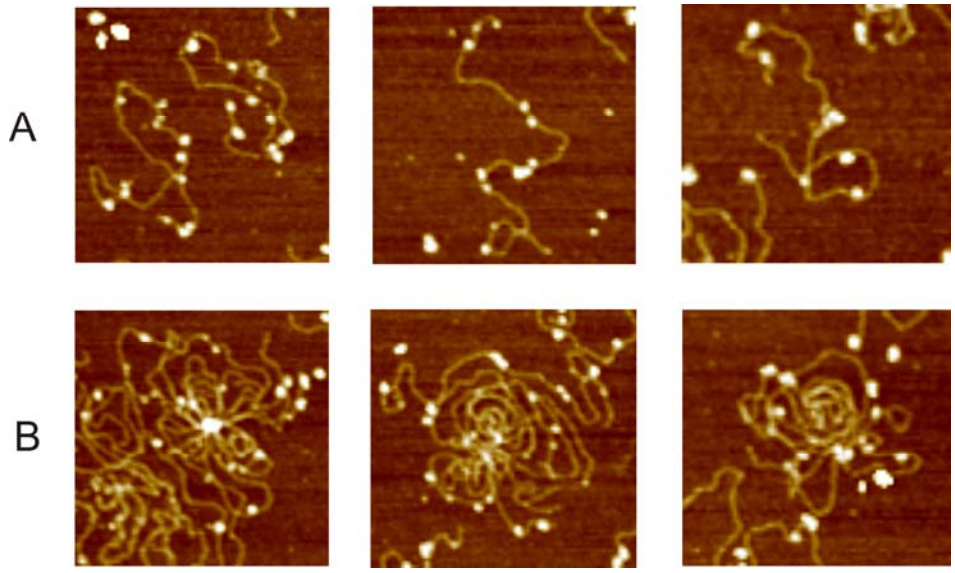

Figure 7.9 AFM images of different 1 × 1 μm areas on mica surface of linearized plasmid pcDNA 3.1 incubated with the complex *cis*-$[\{Pt(NH_3)_2(bpz)\}_3]^{6+}$ (**II-2**) in bp. : molecule ratio of 10:2, displaying condencation (A) and aggregation (B) of dsDNA.

Incubation of DNA with $K_2[Pt(CN)_4]$ was done in the ratio of base pair : metal complex = 10:6. Although, the mica surface is significantly less populated as compared to the other cases, neither condensed nor aggregated DNA molecules are observed. This observation

led as to conclude, that the size and morphology of the dsDNA molecule is not affected upon incubation with the negatively charged tetracyanidoplatinate (II). Figure 7.10 shows zoomed areas (1 µm × 1 µm).

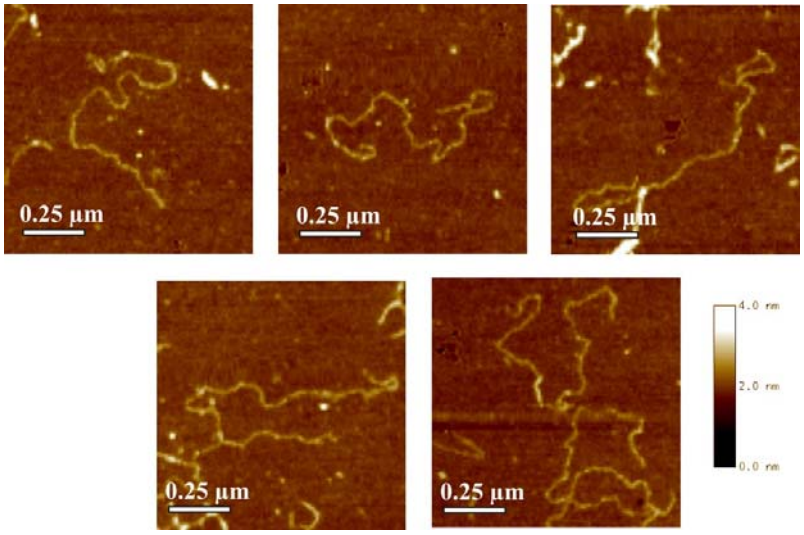

Figure 7.10 The AFM images of linearized pc DNA 3.1, incubated with $K_2[Pt(CN)_4]$ for 4h at RT. Image scan areas correspond to 1 µm × 1 µm.

7.4 Conclusions

The AFM technique was applied to study the interaction between *cis*-$[\{Pt(NH_3)_2(bpz)\}_3]^{6+}$ and linearized plasmid pc DNA 3.1. Although a single experimental technique cannot provide answers to all questions, two distinctly different DNA structural alternations have been observed, namely

I. DNA condensation of individual dsDNA molecules, and

II. DNA aggregation of multiple strands of dsDNA

The negatively charged anion $[Pt(CN)_4]^{2-}$ did not show any effects on the DNA structure. Stil

l the question remains, whether it is the positive charge that induces the condensation of DNA on the basis of electrostatics, or if the 3D-shape of the cation plays a significant role as well.

Chapter 8 – Experimental section

8.1 Instrumentation and methods

8.1.1 NMR spectroscopy

^{1}H NMR spectra were recorded on Varian Mercury 200, on Bruker DPX 300, Bruker DPS 400 or Bruker DRX 500 instruments. In D_2O, TSP (sodium 3-trimethylsilyl-propanesulfonate) (δ = 0 ppm) or TMA (tetramethylammonium salt) (δ = 3.18 ppm) were used as internal standards. Spectra in DMSO-d_6 and DMF-d_7 were recorded without presaturation of the water signal using the resonance of DMSO-d_5 (δ = 2.50 ppm) and DMF-d_7 (δ = 8.03 ppm) as reference. Spectra were processed using MestReC.4.5.6.0, MestReNova 6.03 or ACD/labs softwares.

8.1.2 IR spectroscopy

IR spectra were recorded on a Bruker IFS 28 spectrometer. Measurements (KBr pellets) were carried out from 250 to 4000 cm^{-1}. The spectra were processed with Opus-IR.

8.1.3 Elemental analysis

Elemental analyses were performed on a CHNS-932 Element Analyzer.

8.1.4 X-Ray crystallography

Crystal data were collected on two different diffractometers

I. For compounds **II-5**, **V-1**, **V-11** and **V-12** an Enraf-Nonius Kappa CCD diffractometer with graphite-monochromated MoKα radiation (λ = 0.7107Å) was used. Measurements were done at low temperature (150 K).

II. For the other crystals an Oxford Diffraction Xcalibur diffractometer equipped with an area detector and graphite monochromated MoKα radiation (0.71073Å) was used.

For data reduction and cell refinement, the programs DENZO and SCALEPACK[153] or CrysAlisPro software[154] were used. Corrections for incident and diffracted beam absorption

effects were applied using SADABS.[155] The structures were solved by either standard conventional direct methods or Patterson methods and refined by full-matrix least squares based on F^2 using the SHELXTL-PLUS[156] and SHELXL-97[157] programs. The positions of all non-hydrogen atoms were deduced from difference Fourier maps and were refined anisotropically, except for the disordered atoms. The distances and angles were calculated by using PLATON and the CIF files were generated using the Software WinGX.[158] The graphics were generated using Mercury 2.3.

8.1.5 DNA isolation

For our studies plasmid DNA 3.1 (+) was used. Using its ability to replicate independently in bacterial hosts, it was introduced into *E. coli* cells. The transformed cells obtained are able to produce many copies of the plasmid in large quantities using standard molecular biology procedures. A QIAprep® Spin Miniprep Kit was used as in the operating instructions for isolation of plasmid DNA from bacterial culture. Digestion with restriction endonuclease *Eco*RI was done in order to generate linearized 5428 bp DNA fragments. This procedure was performed under standard conditions. Digested DNA was finally purified by agarose gel electrophoresis, with gel band isolation, using the gel purification kit (Figure 8.1). Concentrations of DNA were estimated by 260-280 nm absorption spectrophotometry.

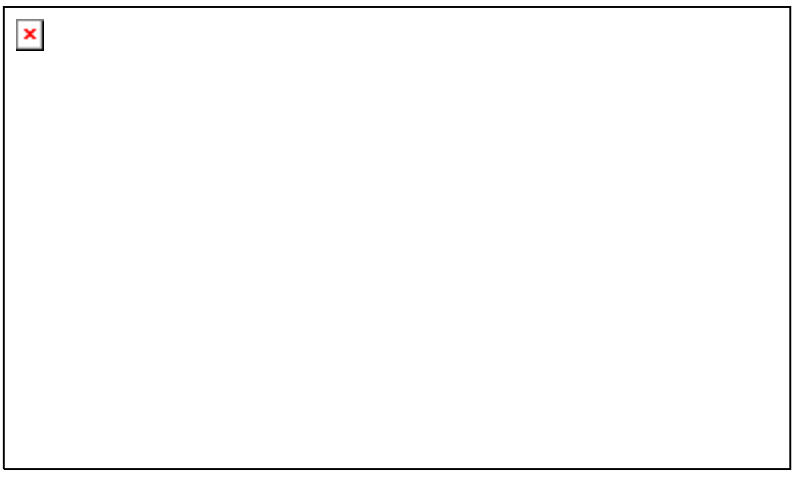

Figure 8.1 Relative positions of different DNA forms of plasmid and of linear fragments on a *tris*-acetate agarose gel.

8.1.6 Atomic Force Microscopy (AFM)

AFM measurements were performed on a MultiMode scanning probe microscope with a NanoScope IIIa controller (Digital Instruments, Santa Barbara, CA, USA) and usage of an E-Scanner (scan size 15 μm; Veeco Instruments, Mannheim, Germany). Images were obtained by applying the Tapping Mode in air with silicon SPM sensors from Nanosensors (PPP-NCHR, NanoAndMore, Wetzlar, Germany) mounted on a MMMC cantilever holder (Veeco Instruments, Wetzlar, Germany). Tips with nominal force constants of 42 $N \cdot m^{-1}$ were used at driving frequencies between 275 and 320 kHz and drive amplitudes between 10 and 63 mV. Height and amplitude images of sample regions were acquired with resolutions of 512 × 512 pixels and scan frequencies between 0.5 and 1.5 Hz. All measurements were carried out at room temperature. The images were analyzed by use of image analysis and processing software NanoScope version 5 (Veeco Instruments, Wetzlar, Germany) and OriginLab 7 (OriginLab, Northampton, MA, USA).

Typically, concentrated stock solutions of a DNA (8 ng/μL) and complexes (2 – 3 ng/μL) were prepared by addition of the corresponding amounts of MQ - H_2O to the DNA solutions of known concentration or by accurately weighing out the dried complex and dissolving it in an accurately measured volume of MQ - H_2O (2.00 ml). Prior to sample preparation the solution was diluted with Milli-Q water to a required concentration. The final Mg^{2+} concentration was 2 – 5 mM.

15 μl sample solutions were prepared in Eppendorf tubes, mixed using a Votex machine, and allowed to incubate at room conditions for 4 – 5 hours to assure sufficient time for complete compound/DNA interactions to take place. Half inch diameter disks of mica (New York Mica Company, New York, NY) were firmly attached to a 15 mm diameter metal shim using an adhesive tab. The metal shim served to mount the sample of the magnetic holder of the AFM piezo stack. Typically, 10 μl of this solution was adsorbed to a freshly cleaved mica surface and allowed to incubate at RT temperature for 2 minutes, then washed with Milli-Q water, and dried under a gentle stream of nitrogen. Before measurement, the samples were further dried under vacuum for ca.18h.

8.1.7 pK_a value determination

The pH* (uncorrected pH) of a D_2O solution was measured by use of a glass electrode type “SenTix Mic” on a pH meter WTW Walheim “Ino-Lab pH Level 1”. The pD values

were obtained by adding 0.4 units to the value displayed on the pH meter.[159] Measurement of the pD dependences were carried out using identical samples, in which the pD of the solutions was modified in small increments by addition of small amounts of DNO_3 and/or NaOD. The p*K*a values of the aqua ligands in the complexes described in the Chapter V were evaluated with a Newton-Gauss non-linear least-squares curve fitting procedure that deals with the chemical shift (δ) data at different pD (equation 1).[160]

$$\delta_{obs} = \frac{\delta_B + \delta_{BH+} + 10^{(pK_{BH+} - pD)}}{1 + 10^{(pK_{BH+} - pD)}} \quad (1)$$

δ_B, δ_{BH+} represent the chemical shifts of complexes, which are not protonated (δ_B) and protonated (δ_{BH+}), respectively. The value pK_{BH+} is the negative logarithms of the acidity constants of BH^+.

The p*K*a values obtained for D_2O were then converted into p*K*a values valid for H_2O by using Equation 2:[161]

$$pK_a(H_2O) = \frac{pK_a(D_2O) - 0.45}{1.015} \quad (2)$$

8.1.8 Association constant determination for host-guest interactions

Host-guest interactions between compound **II-6** and SO_4^{2-} were studied in D_2O solution by means of ^1H NMR spectroscopy. Association constants of the host-guest adduct were established by titration methods. Since a stoichiometry of 1:1 had been determined experimentally by a Job plot analysis (continuous variation method),[162] association constant $K_{a,exp}$ is

$$K_{a,exp} = [HG]/[H][G]$$

and $[HG] = [H]_c = [G]_c$, and $[H] = [H]_{uc}$, $[G] = [G]_{uc}$, ("c" and "uc" denote complexed and uncomplexed species). $K_{a,exp}$ has a unit of M^{-1}. In can also be expressed as log*K*.

The observed chemical shift (δ_{obs}) is

$$\delta_{obs} = \frac{[H]\cdot\delta_H + [HG]\cdot\delta_{HG}}{[H^o]} \quad (3)$$

Here δ_H = the chemical shift of the free host molecule; δ_{HG} = the chemical shift of the host-guest adduct; $[H^o]$ = the initial concentration of the host compound: $[H^o] = [H] + [HG]$ and $[G^o]$ = the initial concentration of the host compound: $[G_0] = [G] + [HG]$.

$$\delta_{obs} = \delta_H + \frac{\left(1 + K[G^o] + K[H^o] - \sqrt{-4K^2[G^o][H^o] + (1+K[G^o] + K[H^o])^2}\right)}{2K[H^o]} (-\delta_H + \delta_{HG}) \quad (4)$$

Equation (4) gives an expression which contains only two unknown parameters, δ_{HG} and *K,* and these were determined by starting an iterative calculation with estimated values, and varying these until the standard deviation reached a minimum (least-squares regression).

8.2 General work descriptions

8.2.1 Starting materials

K_2PtCl_4 and K_2PdCl_4 were purchased from Heraeus and $PdCl_2$ from Sigma. All other chemicals were of commercial origin and used without further purification. Deuterated solvents DMSO-*d6*, DMF-*d7* and D_2O were obtained from Deutero GmbH, Kastellaun (Germany). The following starting compounds were synthesized according to published methods: 2,2´-bpz,[61] *cis*-$PtCl_2(NH_3)_2$,[163] *trans*-$PtCl_2(NH_3)_2$,[164] *trans*-$PtICl(NH_3)_2$,[165] $enPtCl_2$,[163] $enPdCl_2$,[166] $PdCl_2$(bpy),[166] $PdCl_2$(bipzp),[167] $PdCl_2$(dpk),[168] $PdCl_2$(bpz).[70]

8.2.2 Synthesis of compounds

8.2.2.1 Synthesis of [{*cis*-Pt(NH$_3$)$_2$(*tttt*-bpz-*N4,N4´*)}$_4$](SO$_4$)$_4$ (II-1)

An aqueous suspension (40 mL) of *cis*-Pt(NH$_3$)$_2$Cl$_2$ (300 mg, 1.00 mmol) and Ag$_2$SO$_4$ (312 mg, 1.00 mmol) was stirred for 12 h at 40°C with daylight excluded. The resultant AgCl precipitate was filtered off, 2,2´-bpz (156 mg, 1.00 mmol) was added to the clear filtrate and the mixture was heated at 45°C for three days. The resulting solution was concentrated to a volume of 5 mL at 40°C on a rotary evaporator. Cube-shaped brown crystals were obtained after 3–4 weeks at 4°C. The yield was 27 %. – Elemental analysis for C$_{32}$H$_{48}$N$_{24}$S$_4$O$_{16}$Pt$_4$·12H$_2$O: calcd. C 17.88, H 3.38, N 15.64; found C 18.3, H 3.6, N 15.3. – ^{1}H NMR (D$_2$O, TMA, 200 MHz): δ = 9.82 (d, ^3J = 1 Hz, 2H, H$_3$), 9.21 (d, ^3J = 3.4 Hz, 2H, H$_6$), 8.90 (dd, ^3J = 3.4 Hz, ^3J = 1 Hz, 2H, H$_5$).

8.2.2.2 Synthesis of BF$_4$⊂ *cis*-[{Pt(NH$_3$)$_2$(*ttt*-bpz-*N4,N4´*)}$_3$](BF$_4$)(SiF$_6$)$_2$ (II-2)

II-2 was obtained in the same way as described for **II-1** using AgBF$_4$ in the initial step of Cisplatin activation. Formation of SiF_6^{2-} anions in aqueous solution is a result of hydrolysis of the BF_4^- anions and reaction of F^- with glass vessel. Colorless prisms were obtained after *ca.* 6 weeks at 4°C. The yield was 32 %. – Elemental analysis for C$_{24}$H$_{36}$N$_{18}$Si$_2$B$_2$F$_{20}$Pt$_3$·3H$_2$O: calcd. C 17.22, H 2.53, N 15.06; found C 17.1, H 2.7, N 15.06. – ^{1}H NMR (D$_2$O, TMA, 200 MHz): δ = 9.32 (s, 2H, H$_3$), 9.14 (d, ^3J = 3 Hz, 2H, H$_6$), 8.83 ppm (d, ^3J = 3 Hz, 2H, H$_5$**)**.

8.2.2.3 Synthesis of (NO$_3$)(PF$_6$)⊂*cis*-[{Pt(NH$_3$)$_2$(*ccc*-bpz-*N4,N4´*)}$_3$](PF$_6$)$_4$ (II-3)

Orange plates of **II-3** were obtained upon addition of NH$_4$PF$_6$ to aqueous solution of *cis*-[{Pt(NH$_3$)$_2$(*ccc*-bpz-*N4,N4´)*}$_3$](NO$_3$)$_6$ during *ca.* 5 weeks at RT. Yield 44 %. – Elemental analysis for C$_{24}$H$_{36}$N$_{19}$P$_5$F$_{30}$O$_3$Pt$_3$·5H$_2$O: calcd. C 14.21, H 1.79, N 13.12; found C 14.3, H 1.9, N 13.00. – ^{1}H NMR (D$_2$O, TMA, 200 MHz): δ = 9.25 (s, 2H, H$_3$), 9.13 (d, ^3J = 3 Hz, 2H, H$_6$), 8.85 ppm (d, ^3J = 3 Hz, 2H, H$_5$).

8.2.2.4 Synthesis of NO$_3$⊂[{Pt(en)(*ccc*-bpz-*N4,N4´*)}$_3$](SO$_4$)$_2$(NO$_3$) (II-4)

II-4 was prepared as follows: [{enPt(2,2'-bpz-*N4,N4'*)}$_3$](NO$_3$)$_6$ (prepared as described in literature[63]) was dissolved in water and passed over a strongly basic anion exchange

column (Merck) in its SO_4^{2-} form. Per 20 mg of *cis*-[{enPt(2,2'-bpz-*N4,N4′*)}$_3$]$(NO_3)_6$ a volume of 1.4 cm^3 of the anion exchange material was applied. Following washing and lyophylisation of the yellow solution and recrystallization from a small amount of water at 4 °C the title compound was isolated as yellowish crystals in ca 80 % yield. The IR spectrum of **II-4** revealed the presence of both NO_3^- (ca. 1354 cm^{-1}) and SO_4^{2-} (1161 and 637 cm^{-1}), with the latter absorptions dominating in the spectrum. – ^{1}H NMR (D_2O, TMA, 300 MHz): δ = 2.85 (s, 4H, CH_2), 9.37 (s, 2H, H_3), 9.15 (d, ^3J = 3 Hz, 2H, H_6), 8.87 ppm (d, ^3J = 3 Hz, 2H, H_5).

8.2.2.5 Synthesis of *cis*-[Pt$(NH_3)_2$(bpz-*N4*)$_2$]$(NO_3)_2$ (II-5)

cis-$PtCl_2(NH_3)_2$ (300 mg, 1.00 mmol) was suspended in 30 mL of water, $AgNO_3$ (340 mg, 2.00 mmol) was added, and the mixture was stirred overnight at 45°C in dark. After the mixture was cooled, AgCl was removed by filtration and a solution of 2,2´-bpz (636 mg, 4.00 mmol) in 150 mL of water was added to the clear filtrate. The mixture was stirred for three days at 45 °C. Then it was concentrated to 15 mL under vacuum, filtered to remove unreacted 2,2´-bpz and volume reduced to 5 mL. Pale yellow needles crystallized after *ca.* 10 d at 4 °C. The yield was 66 %. Elemental analysis for $C_{16}H_{18}N_{12}O_6Pt \cdot 1.5H_2O$: calcd. C 27.59, H 3.04, N 24.13; found C 27.7, H 3.1, N 24.1. – ^{1}H NMR (D_2O, TMA, 200 MHz): δ = 8.82 (d, ^3J = 2.6 Hz, 1H, $H_{6'}$), 8.86 (dd, ^3J = 1.4 Hz, ^3J = 2.6 Hz, 1H, $H_{5'}$), 8.94 ppm (dd, ^3J = 1.2 Hz, ^3J = 3.2 Hz, 1H, H_5), 9.13 (d, ^3J = 3.4 Hz, 1H, H_6), 9.48 (d, ^3J = 1.4 Hz, 1H, $H_{3'}$), 9.87 (d, ^3J = 1 Hz, 1H, H_3).

8.2.2.6 Synthesis of [{$(NH_3)_2$Pt(*N4,N4′*-bpz-*N1,N1′*)Pd(en)}$_3$]$(NO_3)_{12}$ (II-6) and [{$(NH_3)_2$Pt(*N4,N4′*-bpz-*N1,N1′*)Pd(en)}$_3$]$(SO_4)_6$ (II-7)

For the preparation of **II-6** and **II-7**, respectively, two solutions, A and B, were prepared and subsequently mixed:

(A): *cis*-$PtCl_2(NH_3)_2$ (300 mg, 1 mmol) was suspended in water (30 mL) and stirred at 40 °C over night with $AgNO_3$ (340 mg, 2 mmol) and Ag_2SO_4 (312 mg, 1 mmol), respectively. After filtration of AgCl and addition of 2,2´-bpz (156mg, 0.98 mmol) the mixture was stirred at 80 °C for 3 days.

(B): $PdCl_2$(en) (237 mg, 1 mmol) and the corresponding Ag salt – $AgNO_3$ (340 mg, 2 mmol) or Ag_2SO_4 (312 mg, 1 mmol) – were stirred in water (30 mL) at room temperature for 1h and then filtered from AgCl.

The two solutions (A) and (B) were then mixed and stirred at room temperature over night. The red reaction mixtures were then filtered again, and the volume reduced to 5 mL.

Dark-brown crystals of **II-6** were isolated in 82 % yield within 5 d at 4 °C. – Elemental analysis for $C_{30}N_{36}H_{60}O_{36}Pt_3Pd_3 \cdot 8H_2O$: calcd. C 14.16, H 2.85, N 19.81; found C 14.2, H 3.0, N 19.9. – ^{1}H NMR (D_2O, 300 MHz): δ (ppm) = 2.97 (s, 4H, CH_2), 8.82 (d, ^3J = 3.9 Hz, 2H, H_6), 9.82 (d, ^3J = 3.9 Hz, 2H, H_5), 10.64 (s, 2H, H_3).

Red-brown crystals of **II-7** were isolated in 76 % yield within 10 d at 4°C. – Elemental analysis for $C_{30}N_{24}H_{60}O_{24}S_6Pt_3Pd_3 \cdot 22H_2O$: calcd. C 13.68, H 3.98, N 12.76; found C 13.7, H 3.9, N 12.5. – ^{1}H NMR (D_2O, 300MHz): δ (ppm) = 2.96 (s, 4H, CH_2), 8.81 (d, ^3J = 3.9 Hz, 2H, H_6), 9.81 (d, ^3J = 3.9 Hz, 2H, H_5), 10.88 (s, 2H, H_3).

8.2.2.7 Synthesis of [{$(NH_3)_2$Pt(*N4,N4'*-bpz-*N1,N1'*)Pd(en)}$_3$]$(NO_3)(PF_6)_{11}$ (II-8)

Crystals of **II-8** has been obtained by dissolving **II-6** (100 mg) in water (10 mL) and subsequently recrystallizing it in the presence of excess (10 equiv.) of NH_4PF_6. – Elemental analysis for $C_{30}N_{25}H_{60}O_3P_{11}F_{66}Pt_3Pd_3 \cdot 5H_2O$: calcd. C 10.57, H 2.07, N 10.28; found C 10.2, H 2.2, N 9.9. – ^{1}H NMR (D_2O, 300 MHz): δ (ppm) = 2.95 (s, 4H, CH_2), 8.80 (d, ^3J = 3.9 Hz, 2H, H_6), 9.80 (d, ^3J = 3.9 Hz, 2H, H_5), 10.61 (s, 2H, H_3).

8.2.2.8 Synthesis of [Pd(2,2'-bpz)(*o*-pda)]$(NO_3)_2$ (II-9)

$PdCl_2$(*o*-pda) (143 mg, 0.5 mmol) and $AgNO_3$ (170 mg, 1 mmol) were suspended in 30 mL of water and stirred in the dark for 1 h at RT. After removal of AgCl by filtration, 2,2´-bpz (78 mg, 0.5 mmol) was added and solution was stirred for 1 d at RT. Then the mixture was filtered to remove any precipitate, the volume reduced to 5 mL in vacuum, and allowed to crystallize at RT. After 5 d formation of yellow crystals of **II-9** was observed. The yield was 26 %. – Elemental analysis for $C_{14}N_8H_{14}O_6Pd \cdot H_2O$: calcd. C 32.67, H 3.13, N 21.76; found C 32.6, H 3.2, N 21.4. – ^{1}H NMR (D_2O, 300 MHz): δ (ppm) = 7.40 (s, NH), 7.36 ppm (m, 4H, H3´ and H4´ (*o*-pda)), 8.69 (dd, ^4J = 1.2 Hz, ^3J = 3.2 Hz, 2H, H_5 (bpz)), 9.17 (d, ^3J = 3.3 Hz, 2H, H_6 (bpz)), 9.85 (d, ^4J = 1.2 Hz, 2H, H_3 (bpz)).

8.2.2.9 Synthesis of [Pd(*o*-pda)$_2$](NO$_3$)$_2$ (II-10)

II-10 has been obtained from an NMR-scale reaction. $PdCl_2$(bpz) (30 mg, 0.1 mmol) and $AgNO_3$ (34 mg, 0.2 mmol) were suspended in 700 μL of D_2O and stirred in the dark overnight at RT. After removal of AgCl by centrifugation, *o*-pda (10.8 mg, 0.1 mmol) was added and solution was stirred for 1 d at RT and then centrifuged from any undissolved material. Yellow crystals formed in the NMR tube was characterized crystallographically – ^{1}H NMR (D_2O, 300 MHz): δ (ppm) =7.17 (s, H_3 and H_4 (*o*-pda)).

8.2.2.10 Synthesis of [Pd(2,2'-bpz)(bipzp)](NO$_3$)$_2$ (II-11)

Addition of $AgNO_3$ (170 mg, 0.1 mmol) to the suspension of $PdCl_2$(bipzp) (177 mg, 0.05 mmol) in 30 mL of water resulted to the presipitation of AgCl. The mixture was stirred at RT in the dark for 2h and then filtered from the AgCl. 2,2´-bpz (78 mg, 0.05 mmol) was added to the filtrate, which was stirred for one day at RT. The resulting solution was concentrated in vacuum to a volume of 5 mL. After 3-5 days yellow crystals of **II-11** were obtained in 38% yield. – Elemental analysis for $C_{17}N_{10}H_{18}O_6Pd \cdot 0.5\ H_2O$: calcd. C 35.58, H 3.34, N 24.41; found C 35.7, H 3.4, N 24.4 – ^{1}H NMR (D_2O, 300 MHz): δ (ppm) = 9.92 ppm (d, ^3J = 0.9 Hz 2H, H_3 (bpz)), 9.16 ppm (d, ^3J = 3.3 Hz, 2H, H_6 (bpz)), 8.68 (dd, ^4J = 0.9 Hz, ^3J = 3.3 Hz, 2H, H_5 (bpz)), 8.44 ppm (d, ^3J = 2.7 Hz, 2H, $H_{3'}$(bipzp)), 8.19 ppm (d, ^3J = 2.4 Hz, 2H, $H_{5'}$(bipzp)), 6.80 ppm (dd, ^3J = 2.7 Hz, ^3J = 2.4 Hz, 2H, $H_{4'}$(bipzp)), 3.40 ppm and 2.78 ppm (s, 6H, CH_3).

8.2.2.11 Synthesis of [Pd(2,2'-bpz)(dpk·H$_2$O)](NO$_3$)$_2$ (II-12)

Addition of $AgNO_3$ (170 mg, 0.1 mmol) to a suspension of $PdCl_2$(dpk) (177 mg, 0.05 mmol) in 30 mL of water resulted to the presipitation of AgCl. The mixture was stirred at RT in the dark for 2h and then filtered from AgCl. 2,2´-bpz (78 mg, 0.05 mmol) was added to the filtrate, which was stirred for one day at RT. The resulting solution was concentrated in vacuum to a volume of 5 mL. After 3 days [(dpk·H_2O)$_2$Pd](NO$_3$)$_2$ crystallized as side product from the solution in 8% yield. Light yellow crystals of **II-12** were obtained by further evaporation of the solution at RT. The yield was 42 %. – Elemental analysis for $C_{19}N_8H_{16}O_8Pd$: calcd. C 38.63, H 2.73, N 18.97; found C 38.3, H 2.9, N 18.6. – ^{1}H NMR (D_2O, 300 MHz): δ (ppm) = 9.93 ppm (d, ^3J = 0.6 Hz, 2H, H_3 (bpz)), 9.12 ppm (d, ^3J = 3.3 Hz

2H, H_6 (bpz)), 8.33 (m, 2H, H_5 (bpz) and 2H, $H_{3'}$(dpk)), 8.95 ppm (d, ^3J = 5.4 Hz, 2H, $H_{6'}$(dpk)), 8.39 ppm (dd, ^3J = 7.8 Hz, ^4J = 1.5 Hz, 2H, $H_{4'}$(dpk)), 7.86 ppm (ddd, ^3J = 7.5 Hz; ^3J = 6 Hz; ^4J = 1.8 Hz, 2H, $H_{5'}$(dpk)), 9.60 ppm (s, O1H), 8.90 ppm (s, O2H).

8.2.2.12 Synthesis of {[$(NH_3)_2$Pt(bpz)Pd(*o*-pda)]$_3$}$(NO_3)_{12}$ (II-13)

For the preparation of **II-13**, two solutions, A and B, were prepared and subsequently mixed:

(A): *cis*-$PtCl_2(NH_3)_2$ (150 mg, 0.5 mmol) was suspended in water (20 mL) and stirred at 40 °C over night with $AgNO_3$ (170 mg, 1 mmol) After filtration of AgCl and addition of 2,2´-bpz (78 mg, 0.5 mmol) the mixture was stirred at 80 °C for 3 days.

(B): $PdCl_2$(*o*-pda) (143 mg, 0.5 mmol) and $AgNO_3$ (170 mg, 1 mmol) were stirred in water (20 mL) at room temperature for 2h and then filtered from AgCl.

The two solutions (A) and (B) were then mixed and stirred at RT for 1d. The dark-brown reaction mixture was then filtered again, and the volume reduced to 5 mL. The solution was kept under the argon atmosphere for *ca.* 1 week. Then a black precipitate was filtered off. Yield 42%. – Elemental analysis for $C_{30}N_{36}H_{44}O_{36}Pt_3Pd_3 \cdot 2H_2O$: calcd. C 14.86, H 2.00, N 20.79; found C 14.7, H 2.1, N 20.7. – ^{1}H NMR (D_2O, 300M Hz): δ (ppm) = 7.43 (s, NH), 7.47-7.52 (m, 4H, $H_{3'}$, $H_{4'}$ (*o*-pda)), 9.02 (d, ^3J = 3.9 Hz, 2H, H_5 (bpz)), 9.97 (d, ^3J = 3.9 Hz, 2H, H_6 (bpz)), 10.77 (s, 2H, H_3 (bpz)).

8.2.2.13 Synthesis of [{Pd(en)(2,2´-bpz)}$_2$Ag]$(NO_3)_5$ (II-14)

[Pd(en)(2,2´-bpz)]$(NO_3)_2$ was prepared from $Pd(en)Cl_2$, 2,2´-bpz and $AgNO_3$ as previously described.[63] Yellow crystals of [{Pd(en)(2,2´-bpz)}$_2$Ag]$(NO_3)_5$ were obtained by adding $AgNO_3$ to aqueous solution of [Pd(en)(2,2´-bpz)]$(NO_3)_2$ (1:1, 0.1 mmol, 5 mL), centrifugation from any undissolved material, and slow evaporation of the clear solution at 4^{o}C. The yield was 73 %. – Elemental analysis for $C_{20}N_{17}H_{28}O_{15}AgPd_2$: calcd. C 22.51, H 2.64, N 22.31; found C 23.6, H 3.0, N 22.5. – ^{1}H NMR (D_2O, 400 MHz): δ (ppm) = 2.96 (s, 4H, CH_2), 8.59 (d, ^3J = 3.2 Hz, 2H, H_5), 9.09 (d, ^3J = 3.2 Hz, 2H, H_6), 9.78 (s, 2H, H_3).

8.2.2.14 Synthesis of [Pd(en)(2,2´-bpz)](PF$_6$)$_2$ (II-15)

[Pd(en)(2,2´-bpz)](PF$_6$)$_2$ has been obtained in as yellow crystals by passing aqueous solution of corresponding NO_3^--salt[63] over an anion exchange column conditioned with KPF_6. – Elemental analysis for $C_{10}N_6H_{14}P_2F_{12}Pd \cdot H_2O$: calcd. C 18.99, H 2.55, N 13.28; found C 18.4, H 2.5, N 13.8. – ^{1}H NMR (D_2O, 300 MHz): δ (ppm) = 3.05 (s, 4H, CH_2), 8.59 (d, ^3J = 2.7 Hz, 2H, H_6), 9.10 (d, ^3J = 3 Hz, 2H, H_5), 9.78 (s, 2H, H_3).

8.2.2.15 Synthesis of {[Pd(en)(2,2´-bpz) Ag](PF$_6$)$_3$}$_n$ (II-15a)

Cocrystallization of **II-15** with $AgPF_6$ (1:1 ratio, 0.1 mmol, 5 mL) resulted to the formation of a yellow precipitate of **II-15a** in 87% yield. – Elemental analysis for $C_{10}N_6H_{14}P_3F_{18}Pd \cdot H_2O$: calcd. C 13.56, H 1.82, N 9.49; found C 13.3, H 1.7, N 9.75.

8.2.2.16 Synthesis of *ht*-[Pd(bipzp)$_2$][Ag(NO$_3$)$_3$(H$_2$O)] (II-16)

[Pd(2,2'-bpz)(bipzp)](NO$_3$)$_2$ (**II-11**) (170 mg, 0.3 mmol) was suspended in water (10 mL), $AgNO_3$ (51 mg, 0.3 mmol) added, and the mixture stirred for 1h at RT. Then it was centrifuged to remove any insoluble precipitate and kept for crystallization at 4^{o}C. Colorless prisms of **II-16** were isolated in 26 % yield. – Elemental analysis for $C_{18}N_{11}H_{26}O_{10}AgPd$: calcd. C 28.05, H 3.4, N 19.99; found C 27.6, H 3.8, N 19.3. – ^{1}H NMR (D_2O, 400 MHz): δ (ppm) = 2.80 (s, 3H, CH_2), 3.25 (s, 3H, CH_2), 6.73 (dd, ^3J = 2.4 Hz, ^3J = 2.6 Hz, 2H, H_4), 7.91 (d, ^3J = 2.4 Hz, 2H, H_5), 8.43 (d, ^3J = 2.8 Hz, 2H, H_3).

8.2.2.17 Synthesis of [Cu(2,2´-bpz)(H$_2$O)$_2$SO$_4$] (II-17)

[Pd(2,2'-bpz)(bipzp)](SO$_4$) was prepared as described for **II-11** using Ag_2SO_4 instead of $AgNO_3$. The resulting solution was dried under vacuum and after checking the ^{1}H NMR spectrum of the solid obtained it was used for further synthesis. [Pd(2,2'-bpz)(bipzp)](SO$_4$) (161 mg, 0.3 mmol) was suspended in water (10 mL), $CuSO_4 \cdot 5\ H_2O$ (75 mg, 0.3 mmol) added, and the mixture stirred for 18h at RT. Then it was centrifuged to remove any insoluble precipitate and kept for crystallization. Blue crystals of **II-16** have been isolated in 13% yield and characterized crystallographicaly.

8.2.2.18 Synthesis of $\{[enPt(bpz)]_6Cu_4(H_2O)_6\}(NO_3)_{20}$ (II-18) and $[(en)Pt(2,2´\text{-}bpz)Cu(NO_3)(H_2O)]_3(NO_3)_6\cdot[Cu(NO_3)_3(H_2O)]\cdot[Cu(NO_3)_3(H_2O)_2]\cdot[Cu(NO_3)_2(H_2O)_3]\cdot 1.5H_2O$ (II-19)

$[\{enPt(2,2'\text{-}bpz\text{-}N4,N4')\}_3](NO_3)_6$ (100 mg, 0.06 mmol) was dissolved in water (5 mL), $Cu(NO_3)_2 \cdot 3H_2O$ (28 mg, 0.12 mmol) was added to the solution, and the mixture stirred RT for 1d. Then the violet solution was centrifuged to remove any precipitate and the filtrate kept at 4°C for crystallization. Two different types of crystals have been isolated and characterized crystallographically.

8.2.2.19 Synthesis of $\{[(enPt)_3(bpz)_3Cd_2(H_2O)_7][Cd(H_2O)_6](SO_4)_6\}_n$ (II-20)

$Pt(en)Cl_2$ (325 mg, 1 mmol) was suspended in water (30 mL) and stirred at 40 °C over night with Ag_2SO_4 (312 mg, 1 mmol). After filtration of AgCl and addition of 2,2´-bpz (156 mg, 0.98 mmol) the mixture was stirred at 80°C for 3 days and filtered. To the clear solution $CdSO_4$ (313.5 mg, 1.5 mmol) was added and the mixture was stirred at 45°C for 1d. The resulting solution was concentrated in vacuum to a volume of 5 mL. After 10-15 days crystals of **II-20** were obtained in 68% yield. – Elemental analysis for $C_{30}N_{18}H_{98}O_{52}S_6Cd_3Pt_3$: calcd. C 13.56, H 3.72, N 9.49; found C 13.2, H 4.3, N 9.1. – ^{1}H NMR (D_2O, TMA, 300 MHz): δ = 2.87 (s, 4H, CH_2), 9.43 (s, 2H, H_3), 9.18 (d, ^3J = 3.3 Hz, 2H, H_6), 8.90 ppm (dd, ^3J = 3.3 Hz, ^3J = 0.9 Hz, 2H, H_5).

8.2.2.20 Synthesis of $\{[(NH_3)_2Pt(bpz)]_3Ag\ (SiF_6)_3(BF_4)\}_n$ (II-21)

II-21 was prepared by cocrystalization of $[\{Pt(NH_3)_2(bpz\text{-}N4,N4')\}_3](BF_4)_6$ with one equivalent of $AgBF_4$. Yellow crystals were obtained in 33% yield. – Elemental analysis for $C_{24}N_{18}H_{36}F_{24}B_3Si_2AgPt_3 \cdot 7H_2O$: calcd. C 14.86, H 2.60, N 12.99; found C 14.3, H 2.5, N 12.1. – ^{1}H NMR (D_2O, TSP, 200 MHz): δ = 9.39 (s, 2H, H_3), 9.18 (d, ^3J = 3.2 Hz, 2H, H_6), 8.90 ppm (dd, ^3J = 3.2 Hz, ^3J = 1 Hz 2H, H_5).

8.2.2.21 Synthesis of $\{[(NH_3)_2Pt(bpz)]_3Ag\ (SO_4)_{3.5}\}_n$ (II-22)

II-22 was prepared by cocrystalization of $[\{Pt(NH_3)_2(bpz\text{-}N4,N4')\}_3](SO_4)_3$ with 0.5 equivalent of Ag_2SO_4. The yield was 58% – Elemental analysis for $C_{48}N_{36}H_{72}S_7O_{28}Ag_2Pt_6 \cdot$

$24H_2O$: calcd. C 15.82, H 3.32, N 13.84; found C 16.0, H 3.4, N 13.7. – ^{1}H NMR (D_2O, TMA, 300 MHz): δ = 9.51 (s, 2H, H_3), 9.21 (d, ^3J = 2.7 Hz, 2H, H_6), 8.90 ppm (d, ^3J = 2.7 Hz, 2H, H_5**)**.

8.2.2.22 Synthesis of Pd(en)$(CN)_2$ (III-1)

A solution of enPdCl2 (237 mg, 1 mmol) and AgCN (268 mg, 2 mmol) in water (40 mL), after 10 min ultrasonic treatment, was stirred in dark at 40°C for 18h. AgCl was removed by filtration and the volume of the solution reduced was to 5 ml. Colorless cubic crystals were grown at 4°C. The yield was 58 %. – Elemental analysis for $C_4H_8N_4Pd$ calcd. C 21.98, H 3.69, N 25.6; found C 22.0, H 3.7, N 25.6. – IR (KBr): υ(CN) 2145, 2135 cm^{-1}. – ^{1}H NMR (300 MHz, D_2O): δ = 2.80 ppm (s, CH_2).

8.2.2.23 Synthesis of Pt(en)$(CN)_2$ (III-2) and $[Pt(en)_2][Pt(CN)_4]$ (III-2a)

A solution of $enPtCl_2$ (325 mg, 1 mmol) and AgCN (268 mg, 2 mmol) in water (40 mL) was stirred in dark at 40 °C for ca. 28 h. AgCl that had formed was removed by filtration and the solution containing Pt(en)$(CN)_2$ (**III-2**) was used directly for the synthesis of **III-5**. ^{1}H NMR (300 MHz, D_2O): δ = 2.65 ppm (s, CH_2, $^3J(^{195}Pt\text{-}^1H)$ = 40 Hz).

When the solution was left at RT for 2 – 3 d, white needles of $[Pt(en)_2][Pt(CN)_4]$ (**III-2a**) were isolated in *ca.* 10 % yield. – Elemental analysis for $C_8H_{16}N_8Pt_2 \cdot H_2O$ calcd. C 15.19, H 2.87, N 17.72; found C 15.2, H 2.8, N 17.4. – IR (KBr): υ(CN) 2123 cm^{-1}. – ^{1}H NMR (300 MHz, D_2O): δ = 2.78 ppm (s, CH_2, $^3J(^{195}Pt\text{-}^1H)$ = 32 Hz).

8.2.2.24 Synthesis of *trans*-Pt$(ma)_2(CN)_2$ (III-3)

III-3 was obtained in the same way as described for **III-2,** starting from *trans*-$Pt(ma)_2Cl_2$. *trans*-$Pt(ma)_2(CN)_2$ (**III-3**) was isolated in form of white powder in 62 % yield. – Elemental analysis for $C_4H_{10}N_4Pt \cdot H_2O$: calcd. C 14.68, H 3.69, N 17.12; found C 14.6, H 3.5, N 17.2. – IR (KBr): υ(CN) 2125 cm^{-1}. – ^{1}H NMR (300 MHz, D_2O): δ = 2.57 ppm (s, CH_3).

8.2.2.25 Synthesis of $[Pd(en)(CN)]_4(NO_3)_4$ (III-4)

To a solution of $[enPd(H_2O)_2](NO_3)_2$, obtained by stirring $enPdCl_2$ (237 mg, 1 mmol) and Ag NO_3 (340 mg, 2 mmol) in water (30 mL) for 2 h at RT, followed by filtration of AgCl, was added freshly prepared $Pd(en)(CN)_2$ (**III-1**) (1 mmol in 50 mL water). The bright yellow color of the mixture changed immediately to pale yellow. The volume of the solution was reduced to 5 mL. Within several hours at RT colorless crystals of **III-4** were obtained. The yield was 54%. – Elemental analysis for $C_{12}H_{32}N_{16}O_{12}Pd_4$: calcd. C 14.16, H 3.17, N 22.01; found C 13.9, H 3.2, N 21.8. – IR (KBr): υ(CN) 2190 cm^{-1}. – ^1H NMR (300 MHz, D_2O): δ = 2.63 ppm (s, CH_2-Pd_1), 2.75 ppm (s, CH_2-Pd_2).

8.2.2.26 Synthesis of $[Pt(en)(CN)]_4(NO_3)_4$ (III-5)

To a solution of $[enPt(H_2O)_2](NO_3)_2$ obtained by stirring $enPtCl_2$ (340 mg, 1 mmol) and Ag NO_3 (340 mg, 2 mmol) in water (30 mL) for 2 h at 80 °C, followed by filtration of AgCl, was added freshly prepared (see 8.2.2.23) $Pt(en)(CN)_2$ (1 mmol in 50 mL water). The mixture was stirred at RT for 24 h and the volume of the solution was reduced to 5 mL. The colorless crystals of **III-5** were obtained within 2–3 weeks at RT. The yield was 43%. – Elemental analysis for $C_{12}H_{32}N_{16}O_{12}Pt_4$ (1372.8): calcd. C 10.5, H 2.35, N 16.33; found C 10.3, H 2.5, N 16.3. – IR (KBr): υ(CN) 2192 cm^{-1}. – ^1H NMR (300 MHz, D_2O): δ = 2.54 ppm (s, CH_2-Pt_1), 2.71 ppm (s, CH_2-Pt_2).

8.2.2.27 Synthesis of $[Pt(en)(CN)]_4(C_8H_4O_4)_2 \cdot 10H_2O$ (III-5a)

Few colorless crystals of **III-5a,** suitable for X-ray diffraction studies, were obtained by recrystallization of **III-5** in the presence of a 3-fold excess of the sodium salt of terephthalic acid at RT. – ^1H NMR (300 MHz, D_2O): δ = 2.64 ppm (s, CH_2-Pt_1), 2.81 ppm (s, CH_2-Pt_2).

8.2.2.28 Synthesis of $[Pd_4(bpy)_2(en)_2(CN)_4](NO_3)_4 \cdot H_2O$ (III-6)

For the preparation of **III-6**, two solutions, A and B, were prepared and subsequently mixed:

(A): $Pd(bpy)Cl_2$ (167.5 mg, 0.5 mmol) was suspended in MeOH (30 mL) and stirred at 45°C for 1d with $AgNO_3$ (170 mg, 1 mmol). AgCl was removed by filtration.

(B): $Pd(en)Cl_2$ (118.5 mg, 0.5 mmol) and $AgNO_3$ (170 mg, 1 mmol) were stirred in MeOH (30 ml) at RT overnight and then filtered from AgCl.

The two solutions (A) and (B) were then mixed and stirred at RT for 1d. The white precipitate was filtered and washed with MeOH Yield: 63 %. – Elemental analysis for $C_{14}N_8H_{16}O_6Pd{\cdot}2H_2O$: calcd. C 26.22, H 3.14, N 17.48; found C 26.3, H 3.14, N17.48. – IR (KBr): υ(CN) 2190 cm^{-1}.

8.2.2.29 Synthesis of $[Pd(bpy)(en)](SO_4){\cdot}3H_2O$ (III-7)

III-7 was obtained as described for **III-6** using as solvent H_2O (80 mL for each step) instead of MeOH. $[Pd(bpy)(en)](SO_4){\cdot}3H_2O$ crystallizes in form of colorless blocks in 11% yield. – Elemental analysis for $C_{12}N_4H_{16}O_4SPd \cdot 3H_2O$: calcd. C 30.48, H 4.69, N 11.85; found C 30.0, H 4.7, N 11.9. – ^1H NMR (400 MHz, D_2O): δ = 3.00 ppm (s, CH_2), 7.73 ppm (ddd, 2H, H_5), 8.26 – 8.40 (m, 6H, H_3, H_4 and H_6).

8.2.2.30 Synthesis of *trans*-$[Pd(1\text{-}MeC\text{-}N3)(CN)I_2][(1\text{-}MeC)(1\text{-}MeCH)] \cdot 2H_2O$ (III-8)

III-8 was obtained trying to cocrystallize [Pd(en)(CN)]4(NO3)4 (**III-4**) with [1-MeC]I. **III-8** was obtained in form of orange crystals within 2d at RT. Elemental analysis for $C_{16}N_{10}H_{22}O_3I_2Pd \cdot H_2O$: calcd. C 24.62, H 3.10, N 17.94 found C 25.0, H 3.6, N 18.0.

8.2.2.31 Synthesis of $[(en)Pt(4\text{-}CNpy)_2](NO_3)_2$ (IV-1)

$Pt(en)Cl_2$ (325 mg, 1 mmol) was suspended in water (30 mL), $AgNO_3$ added (340 mg, 2 mmol), and the mixture was stirred for 1 h at 80°C. After the mixture was cooled and AgCl removed by filtration, 4-CNpy (208 mg, 2 mmol) was added and the mixture stirred for 3 days at 45°C. The reaction mixture was filtered and concentrated to 5 mL under vacuum. Colorless crystals of **IV-1** were isolated in 41 % yield after 10-18 d at 4°C. – Elemental analysis for $C_{14}H_{16}N_8O_6Pt \cdot H_2O$: calcd. C 27.77, H 3.00, N 18.51; found C 27.1, H 2.8, N 18.2. – IR (KBr): υ(CN) 2242 cm^{-1}.– ^1H NMR (D_2O, 300 MHz): δ (ppm) = 2.85 (s, 4H, CH_2), 7.99 (d, ^3J = 6.9 Hz, 2H, H_3), 9.04 (d, ^3J = 6.9 Hz, 2H, H_2).

8.2.2.32 Synthesis of [(en)Pt(3-C(O)NH$_2$py)$_2$](NO$_3$)$_2$ (IV-2)

IV-2 was prepared in a similar way as **IV-1,** using 3-CNpy instead of 4-CNpy (see 8.2.2.31). Yellow crystals of **IV-2** were isolated in 65 % yield. – Elemental analysis for $C_{14}H_{16}N_8O_6Pt \cdot H_2O$: calcd. C 26.21, H 3.46, N 17.47; found C 26.5, H 3.4, N 17.7. – IR (KBr): υ(CO) 1672 cm^{-1}.– ^{1}H NMR (D_2O, 300 MHz): δ (ppm) = 2.85 (s, 4H, CH_2), 7.70 (dd, ^3J = 6.0 Hz, ^3J = 8.0 Hz, 1H, H_5), 8.40 (d, ^3J = 8.1 Hz, 1H, H_4), 8.95 (d, ^3J = 5.4 Hz, 1H, H_6), 9.26 (d, ^3J = 1.5 Hz, 1H, H_2).

8.2.2.33 Synthesis of [(en)Pd(4-C(O)NH$_2$py)$_2$](SO$_4$) (IV-3)

Pd(en)Cl_2 (237 mg, 1 mmol) was suspended in water (30 mL) and stirred for 2 h at room temperature with Ag_2SO_4 (312 mg, 1 mmol). After removal of AgCl by filtration and addition of 4-CNpy (208 mg, 2 mmol) to the filtrate, the mixture was stirred for 24 h at RT. The solution was then filtered and concentrated to 5 mL under vacuum. Yellow **IV-3** was obtained in 42% yield within 1 – 2 weeks at 4^{o}C. – Elemental analysis for $C_{14}H_{20}N_6O_6SPd \cdot H_2O$: calcd. C 32.04, H 4.23, N 16.01; found C 30.6, H 4.1, N 15.7. – IR (KBr): υ(CO) 1678 cm^{-1}. – ^{1}H NMR (D_2O, 300 MHz): δ (ppm) = 2.93 (s, 4H, CH_2), 7.92 (d, ^3J = 6.6 Hz, 2H, H_3), 8.94 (d, ^3J = 6.9 Hz, 2H, H_2).

8.2.2.34 Synthesis of [(en)Pd(3-C(O)NH$_2$py)$_2$](ClO$_4$)$_2$ (IV-4)

Pd(en)Cl_2 (237 mg, 1 mmol) was suspended in water (30 mL) and stirred for 2 h at room temperature with $AgNO_3$ (340 mg, 2 mmol). After removal of AgCl by filtration and addition of 3-CNpy (208 mg, 2 mmol) to the filtrate, the mixture was stirred for 24 h at RT. The solution was then filtered and concentrated to 5 mL under vacuum. Colorless crystals of **IV-4** have been obtained upon addition of $NaClO_4$ to the solution. – Elemental analysis for $C_{14}H_{20}N_6O_{10}Cl_2Pd \cdot 2H_2O$: calcd. C 26.04, H 3.75, N 13.02; found C 26.5, H 3.7, N 13.0. – IR (KBr): υ(CO) 1675 cm^{-1}.– ^{1}H NMR (D_2O, 300 MHz): δ (ppm) = 2.91 (s, 4H, CH_2), 7.72 (dd, ^3J = 6.0 Hz, ^3J = 8.0 Hz, 1H, H_5), 8.40 (d, ^3J = 8.1 Hz, 1H, H_4), 8.91 (d, ^3J = 5.1 Hz, 1H, H_6), 9.21 (d, ^3J = 1.8 Hz, 1H, H_2).

8.2.2.35 Synthesis of $[\{(en)Pt\}_6(4\text{-}C(O)NHpy)_4(PF_6)](NO_3)_7$ (IV-5)

$Pt(en)Cl_2$ (97.5 mg, 0.3 mmol) was suspended in water (10 mL), $AgNO_3$ was added (102 mg, 0.6 mmol), and the mixture was stirred for 1 h at 80°C. After the mixture was cooled and AgCl removed by filtration, $[(en)Pt(4\text{-}CNpy)_2](NO_3)_2$ (**IV-1**) (176.4 mg, 0.3 mmol) was added, pH of the solution was adjusted to *ca.* 9 with a solution of NaOH and the mixture was stirred for three days at 45°C. Then the reaction mixture was filtered and concentrated to 5 mL under vacuum. Yellow crystals of **IV-5** were isolated in 19 % yield. – Elemental analysis for $C_{36}H_{72}N_{27}O_{25}PF_6Pt_6 \cdot 10H_2O$: calcd. C 15.56, H 3.34, N 13.61; found C 15.9, H 3.2, N 13.5. – IR (KBr): υ(CO) 1637 cm^{-1}. – ^1H NMR (D_2O, 300 MHz): δ (ppm) = 3.22 (s, 4H, CH_2), 8.05 (m, 2H, H_3), 9.19 (d, ^3J = 5.1 Hz, 2H, H_2).

8.2.2.36 Synthesis of $[(en)Pd(4\text{-}C(O)NH_2py)(NO_3)](NO_3)$ (IV-6)

For the preparation of **IV-6**, two solutions of $[Pd(en)(H_2O)_2](NO_3)_2$ were prepared by following way: $Pd(en)Cl_2$ (118.5 mg, 0.5 mmol) was suspended in water (20 mL) and stirred for 2 h at RT with $AgNO_3$ (170 mg, 1 mmol). After removal of AgCl by filtration, 4-CNpy (104 mg, 1 mmol) was added to the first solution and the mixture was stirred for 24 h at RT. To this mixture a second solution of $[Pd(en)(H_2O)_2](NO_3)_2$ was added and it was stirred for another day at RT. The reaction mixtures was then filtered and concentrated to 5 mL under vacuum. Yellow crystals of **IV-6** were obtained in 18% yield within 2 – 3 weeks at 4°C.

8.2.2.37 Synthesis of *trans*-$[(NH_3)_2Pt(2\text{-}pic)Cl](NO_3)$ (V-1)

V-1 was obtained as follows: *trans*-$PtICl(NH_3)_2$ (10.57 g, 27 mmol) was suspended in water (720 mL), $AgNO_3$ (4.59 g, 27 mmol), dissolved in water (45 mL) was added and the mixture stirred for 2 h in the dark. Yellow AgI was then separated by filtration and washed three times with 50 mL of hot water. To the filtrate 2-picoline (3.19 mL, 32.4 mmol), dissolved in water (45 mL), was added dropwise over a period of 2 h and the solution stirred at 40 °C for 28 h. Concentration of the solution to ca. 80 mL volume produced a white crystalline material, which was recrystallized from water. The yield after recrystallization was 28 %. – Elemental analysis for $C_6H_{13}ClN_4O_3Pt$: calcd. C 17.15, H 3.13, N 13.35; found C 17.2, H 3.1, N 13.4. –^1H NMR (D_2O, 200 MHz): δ = 8.93 (dd, H6, ^3J (^{195}Pt-^1H = 46 Hz), 7.87 (ddd, H5), 7.54 (dd, H3, ^4J (^{195}Pt-^1H) = 11 Hz), 7.36 (ddd, H4), 3.09 (s, CH_3, ^4J (^{195}Pt-^1H) = 11 Hz).

Alternatively **V-1** was obtained as follows: *cis*-$Pt(NH_3)_2Cl_2$ (300 mg, 1 mmol) in DMF (20 mL) was reacted with $AgNO_3$ (169 mg, 1 mmol) for 24 h in the dark, filtered from AgCl, and 2-pic (0.95 mmol), dissolved in DMF (5 mL), was added dropwise during 2 – 3 h. The mixture was then kept at 40 °C for 1 d, concentrated to 5 mL by rotary evaporation and allowed to stay at RT. Colorless crystals of **V-1** appeared within 2 d. ^{1}H NMR spectroscopy proved the trans geometry of the product.

8.2.2.38 Synthesis of *trans*-[$(NH_3)_2$Pt(py)Cl]Cl (V-3)

V-3 was synthesized by slight modification of the method given in the literature.[169] The yield was 76%. – Elemental analysis for $C_5H_{11}Cl_2N_3Pt$: calcd. C 15.84, H 2.92, N 11.08; found C 15.8, H 3.1, N 11.0. – ^{1}H NMR (D_2O, 300 MHz): δ = 8.82 (d, H2), 8.01 (dd, H4), 7.56 (dd, H3).

8.2.2.39 Synthesis of *trans*-[$(NH_3)_2$Pt(4-Clpy)Cl]Cl (V-4)

See 8.2.2.38. The yield was 40%. – Elemental analysis for $C_5H_{10}Cl_3N_3Pt$: calcd. C 14.52, H 2.44, N 10.16; found C 14.4, H 2.6, N 10.2. – ^{1}H NMR (D_2O, 300 MHz): δ = 8.78 (d, H2), 7.65 (d, H3).

8.2.2.40 Synthesis of *trans*-[$(NH_3)_2$Pt(2-Clpy)Cl]Cl (V-6)

See 8.2.2.38. The yield was 56%. – Elemental analysis for $C_5H_{10}Cl_3N_3Pt$: calcd. C 14.52, H 2.44, N 10.16; found C 14.4, H 2.6, N 10.2. – ^{1}H NMR (D_2O, 300 MHz): δ = 8.95 (d, H6), 8.02 (dd, H4), 7.81 (d, H3), 7.54 (dd, H5).

8.2.2.41 Synthesis of *trans*-[$(NH_3)_2$Pt(3,5-DiMeAn)Cl]NO_3 (V-9)

See 8.2.2.38. The yield was 80%. – Elemental analysis for $C_8H_{17}ClN_4O_3Pt$: calcd. C 21.46, H 3.83, N 12.51; found C 21.6, H 4.0, N 12.5. – ^{1}H NMR (D_2O, 300 MHz): δ = 7.01 (s, H4), 6.98 (s, H2), 2.31 (s, CH_3).

8.2.2.42 Synthesis of *trans*-[$(NH_3)_2Pt(2\text{-pic})_2$]$(NO_3)_2$ (V-10)

V-10 has been isolated at a later stage of the reaction carried out for the synthesis of *trans*-[$(NH_3)_2Pt(2\text{-pic})Cl$]$(NO_3)$ (**V-1**) (8.2.2.37). Upon further concentration of the final solution, *trans*-[$(NH_3)_2Pt(2\text{-pic})_2$]$(NO_3)_2$ was isolated in 32% yield. Characterization was achieved by X-ray crystallography. – ^{1}H NMR (D_2O, 200 MHz): δ = 8.95 (dd, H6, ^3J (^{195}Pt-^{1}H = 36 Hz), 7.94 (ddd, H5), 7.62 (dd, H3), 7.58 (dd, H3_), 7.45 (ddd, H4), 3.2 (s, CH_3, ^4J (^{195}Pt-^{1}H ca. 10 Hz), 3.19 (s, CH_3, ^3J (^{195}Pt-^{1}H ca. 10 Hz).

8.2.2.43 Synthesis of *cis*-[$(NH_3)_2Pt(2\text{-pic})Cl$]Cl (V-11)

cis-[$(NH_3)_2Pt(2\text{-pic})Cl$]Cl was prepared as follows: *cis*-$(NH_3)_2PtCl_2$ (3.0 g, 10 mmol) was dissolved in H_2O (500 mL), and 2-picoline (10 mmol) was added. The solution was stirred for 2 d at 55 ^{o}C. The solution was then reduced in volume (rotavapor, 45 ^{o}C) to 5 mL and filtered. The filtrate was brought to dryness, yielding a viscous material, which within several days gave a crystalline material, admixed with viscous [2-picH]Cl. Following treatment with EtOH (5 mL), a white solid was obtained, which was filtered off. According to ^{1}H NMR spectroscopy it consisted of a mixture of **V-11** and *cis*-[$(NH_3)_2Pt(2\text{-pic})_2$]$Cl_2$. The mixture was recrystalized twice from EtOH. The yield of **V-11** was 38%. – Elemental analysis for $C_6H_{13}Cl_2N_3Pt$: calcd. C 18.32, H 3.3, N 10.69; found C 18.4, H 3.3, N 10.8. – ^{1}H NMR (D_2O, 200 MHz): δ = 8.79 (dd, H6, ^3J (^{195}Pt-^{1}H = 32 Hz), 7.83 (ddd, H5), 7.49 (d, H3, ^4J (^{195}Pt-^{1}H) = 9 Hz), 7.34 (ddd, H4), 3.09 (s, CH_3, ^4J (^{195}Pt-^{1}H) =10 Hz).

8.2.2.44 ^{1}H NMR chemical shifts of *trans*-[$(NH_3)_2Pt(L)Cl]^+$ complexes not isolated in pure form:

trans-[$(NH_3)_2Pt(3\text{-pic})Cl$]Cl (**V-2**). – ^{1}H NMR (D_2O, 300 MHz): δ = 8.69 (s, H2), 8.60 (d, H6), 7.83 (d, H4), 7.42 (dd, H5), 2.37 (s, CH_3).

trans-[$(NH_3)_2Pt(3\text{-Clpy})Cl$]Cl (**V-5**). – ^{1}H NMR (D_2O, 200 MHz): δ =9.01 (d, H2), 8.82 (d, H6), 8.16 (d, H4), 7.65 (dd, H5).

trans-[$(NH_3)_2Pt(4\text{-CNpy})Cl$]Cl (**V-7**). – ^{1}H NMR (D_2O, 300 MHz): δ = 9.15 (d, H2), 7.94 (d, H3).

trans-[$(NH_3)_2Pt(MeNH_2)Cl$]Cl (**V-8**). – ^{1}H NMR (D_2O, 400 MHz): δ = 2.45 (s, CH_3).

8.2.2.45 Synthesis of *trans*-[$(NH_3)_2Pt(Me_2SO)Cl](NO_3)$ (V-12)

The complex **V-12** was prepared in a slight modification of the method previously described in the literature.[170] To the suspension of *trans*-$Pt(NH_3)_2Cl_2$ (150 mg, 0.5 mmol) in MeOH (30 mL) $AgNO_3$ (170 mg, 1 mmol) and Me_2SO (35.46 μL, 0.5 mmol) was added. The reaction mixture was stirred overnight at 80°C (Me_2SO). The insoluble AgCl precipitate was filtered off and the filtrate evaporated to dryness and then dissolved in ethanol. Ether was added until the solution became cloudy. Upon cooling, the white solid was filtered off and dried. Yield: 82% for **V-12** Colourless crystals of **V-12** has been obtained upon evaporation of the reaction mixture at 4°C. – Elemental analysis for $C_2H_{12}N_3SO_4ClPt$: calcd. C 5.94, H 2.99, N 10.38; found C 5.8, H 2.8, N 10.2. – IR (KBr): υ(M-S(O)) 1108 cm^{-1}. – ^1H NMR (D_2O, 300 MHz): δ (ppm) = 3.60 (s, $^3J(^{195}Pt\text{-}^1H)$ = 28.2 Hz).

8.2.2.46 Synthesis of *trans*-[$(NH_3)_2Pt(Me_2S)Cl](NO_3)$ (V-13)

V-13 was prepared in the similar way as **V-12** using Me_2S (36.98 μL, 0.5 mmol) instead of Me_2SO and carrying out the reaction at 55 °C. Yield: 57 %. Colorless crystals of composition {*trans*-$[PtCl(CH_3\text{-}S\text{-}CH_3)(NH_3)_2](NO_3)\}_2$ · *trans*-$[PtCl_2(NH_3)_2]$ (**V-13a**) were obtained upon slow evaporation of the methanol solution at 4°C. – Elemental analysis for $C_2H_{12}N_3O_3SClPt$: calcd. C 6.18, H 3.11, N 10.81; found C 6.1, H 3.3, N 10.5. – ^1H NMR (D_2O, 300 MHz): δ (ppm) = 2.51 (s, $^3J(^{195}Pt\text{-}^1H)$ = 57.2 Hz).

Appendix I – List of compounds isolated or studied in solution

(Compounds studied by X-ray crystallography are indicated by #)

1. # [{*cis*-Pt$(NH_3)_2$(*tttt*-bpz-N4,N4′)}$_4$]$(SO_4)_4$ (**II-1**)

2. # $BF_4\subset$ *cis*-[{Pt$(NH_3)_2$(*ttt*-bpz-N4,N4′)}$_3$]$(BF_4)(SiF_6)_2$ (**II-2**)

3. # $(NO_3)(PF_6)\subset$*cis*-[{Pt$(NH_3)_2$(*ccc*-bpz-N4,N4′)}$_3$]$(PF_6)_4$ (**II-3**)

4. # $NO_3\subset$[{Pt$(en)_2$(*ccc*-bpz-N4,N4′)}$_3$]$(SO_4)_2(NO_3)$ (**II-4**)

5. # *cis*-[Pt$(NH_3)_2$(bpz-N*4*)$_2$]$(NO_3)_2$ (**II-5**)

6. # [{$(NH_3)_2$Pt(*N4,N4′*-bpz-*N1,N1′*)Pd(en)}$_3$]$(NO_3)_{12}$ (**II-6**)

7. # [{$(NH_3)_2$Pt(*N4,N4′*-bpz-*N1,N1′*)Pd(en)}$_3$]$(SO_4)_6$ (**II-7**)

8. # [{$(NH_3)_2$Pt(*N4,N4′*-bpz-*N1,N1′*)Pd(en)}$_3$]$(NO_3)(PF_6)_{11}$ (**II-8**)

9. # [Pd(2,2'-bpz)(*o*-pda)]$(NO_3)_2$ (**II-9**)

10. # [Pd(*o*-pda)$_2$]$(NO_3)_2$ (**II-10**)

11. # [Pd(2,2'-bpz)(bipzp)]$(NO_3)_2$ (**II-11**)

12. # [Pd(2,2'-bpz)(dpk·H_2O)]$(NO_3)_2$ (**II-12**)

13. {[$(NH_3)_2$Pt(bpz)Pd(*o*-pda)]$_3$}$(NO_3)_{12}$ (**II-13**)

14. # [{Pd(en)(2,2′-bpz)}$_2$Ag]$(NO_3)_5$ (**II-14**)

15. # [Pd(en)(2,2′-bpz)]$(PF_6)_2$ (**II-15**)

16. {[Pd(en)(2,2′-bpz) Ag]$(PF_6)_3$}$_n$(**II-15a**)

17. # *ht*-[Pd(bipzp)$_2$][Ag$(NO_3)_3(H_2O)$] (**II-16**)

18. # [Cu(2,2′-bpz)$(H_2O)_2SO_4$] (**II-17**)

19. # {[(en)Pt(bpz)]$_6$Cu$_4(H_2O)_6$}$(NO_3)_{20}$ (**II-18**)

20. # [(en)Pt(2,2′-bpz)Cu$(NO_3)(H_2O)$]$_3(NO_3)_6$·
[Cu$(NO_3)_3(H_2O)$]·[Cu$(NO_3)_3(H_2O)_2$]·[Cu$(NO_3)_2(H_2O)_3$]·1.5H_2O (**II-19**)

21. # {[((en)Pt)$_3$(bpz)$_3$Cd$_2(H_2O)_7$][Cd$(H_2O)_6$]$(SO_4)_6$}$_n$ (**II-20**)

22. # {[$(NH_3)_2$Pt(bpz)]$_3$Ag $(SiF_6)_3(BF_4)$}$_n$ (**II-21**)

23. # {[$(NH_3)_2$Pt(bpz)]$_3$Ag $(SO_4)_{3.5}$}$_n$ (**II-22**)

24. # Pd(en)$(CN)_2$ (**III-1**)

25. Pt(en)$(CN)_2$ (**III-2**)

26. # [Pt$(en)_2$][Pt$(CN)_4$] (**III-2a**)

27. *trans*-$Pt(ma)_2(CN)_2$ (**III-3**)

28. # $[Pd(en)(CN)]_4(NO_3)_4$ (**III-4**)

29. # $[Pt(en)(CN)]_4(NO_3)_4$ (**III-5**)

30. # $[Pt(en)(CN)]_4(C_8H_4O_4)_2 \cdot 10H_2O$ (**III-5a**)

31. $[Pd(bpy)(en)(CN)_2(NO_3)_2]\cdot H_2O$ (**III-6**)

32. # $[Pd(bpy)(en)](SO_4)\cdot 3H_2O$ (**III-7**)

33. # *trans*-[Pd(1-MeC-*N3*)(CN)I_2](1-MeC)(1-MeCH)$\cdot 2H_2O$ (**III-8**)

34. # $[(en)Pt(4\text{-}CNpy)_2](NO_3)_2$ (**IV-1**)

35. # $[(en)Pt(3\text{-}C(O)NH_2py)_2](NO_3)_2$ (**IV-2**)

36. # $[(en)Pd(4\text{-}C(O)NH_2py)_2](SO_4)$ (**IV-3**)

37. # $[(en)Pd(3\text{-}C(O)NH_2py)_2](ClO_4)_2$ (**IV-4**)

40. # $[\{(en)Pt\}_6(4\text{-}C(O)NH_2py)_4(PF_6)](NO_3)_7$ (**IV-5**)

41. # $[(en)Pd(4\text{-}C(O)NH_2py)(NO_3)](NO_3)$ (**IV-6**)

42. # *trans*-$[(NH_3)_2Pt(2\text{-}pic)Cl](NO_3)$ (**V-1**)

43. *trans*-$[(NH_3)_2Pt(3\text{-}pic)Cl]Cl$ (**V-2**)

44. *trans*-$[(NH_3)_2Pt(py)Cl]Cl$ (**V-3**)

45. *trans*-$[(NH_3)_2Pt(4\text{-}Clpy)Cl]Cl$ (**V-4**)

46. *trans*-$[(NH_3)_2Pt(3\text{-}Clpy)Cl]Cl$ (**V-5**)

47. *trans*-$[(NH_3)_2Pt(2\text{-}Clpy)Cl]Cl$ (**V-6**)

48. *trans*-$[(NH_3)_2Pt(2\text{-}CNpy)Cl]Cl$ (**V-7**)

49. *trans*-$[(NH_3)_2Pt(MeNH_2)Cl]Cl$ (**V-8**)

50. *trans*-$[(NH_3)_2Pt(3,5\text{-}DiMeAn)Cl](NO_3)_2$ (**V-9**)

51. # *trans*-$[(NH_3)_2Pt(2\text{-}pic)_2](NO_3)_2$ (**V-10**)

52. # *cis*-$[(NH_3)_2Pt(2\text{-}pic)Cl]Cl$ (**V-11**)

53. *trans*-$[(NH_3)_2Pt(DMSO)Cl](NO_3)$ (**V-12**)

54. *trans*-$[Pt(NH_3)_2(Me_2S)Cl](NO_3)$ (**V-13**)

55. # $\{$*trans*-$[PtCl(CH_3\text{-}S\text{-}CH_3)(NH_3)_2](NO_3)\}_2 \cdot$ *trans*-$[PtCl_2(NH_3)_2]$ (**V-13a**)

Appendix II – Abbreviations

Å	angstroms ($1x10^{-10}$ m)
AFM	Atomic Force Microscopy
bpy	2,2´-bipyridine
bipzp	bis(pyrazol-1-yl)propane
bp	base pair
2,2´-bpz	2,2´-bipyrzine or bpz
ccc	*cis-cis-cis*
CD	circular dichroism
Clpy	chlorpyridine
d	NMR-doublet
dd	NMR-doublet-of-doublet
ddd	NMR-doublet-of-doublet-of-doublet
3,5-DiMeAn	3,5-dimethylaniline
DMS	dimethylsulfid
DMSO	dimethylsulfoxide
d_6-DMSO	deuterated dimethylsulfoxide
DNA	deoxyribonucleic acid
ctDNA	calf-thymus DNA
dsDNA	double-stranded DNA
δ	chemical shift
9-EtA	9-ethyladenine
en	enthylenediamine
h	hours
hh	*head-head*
ht	*head-tail*
LD	linear dichroism
m	multiplet
M	molar (mol dm^{-3})
$MeNH_2$	methylamine

mM	milli-molar concentration ($1x10^{-3}$ mol dm^{-3})
μM	micro-molar concentration ($1x10^{-6}$ mol dm^{-3})
nm	nanometer (10^{-9}m)
1-MeC	1-methylcytosine
1-MeC^{-}	1-methylcytosine anion (deprotonated at N4)
Mepy (pic)	methylpyridine
1-MeU	1-methyluracil
NMR	Nuclear Magnetic Resonance
pD	negative logarithm of the deuterium concentration
pH	negative logarithm of the proton concentration
pK_a	negative logarithm of the acidity constant
ppm	parts per million
py	pyridine
RNA	ribonucleic acid
RT	room temperature
s	NMR-singlet
STM	Scanning Tunneling Microscopy
t	NMR-triplet
ttt	*trans-trans-trans*
tttt	*trans-trans-trans-trans*
TSP	sodium 3-trimethylsilyl-propanesulfonate
^3J	spin-spin coupling constant (here via three bonds)

Summary

The main objective of the present dissertation was to study discrete supramolecular metal complexes generated by self-assembly of transition metals and *N*-donor ligands. Two aspects of such complexes were of specific interest: anion binding properties and interactions with double-stranded DNA.

In **Chapter II** the design, synthesis and characterization of metal-supramolecular complexes of different topologies are described. Coordination driven self-assembly of *cis*-$[(NH_3)_2Pt(H_2O)_2]^{2+}$ and 2,2′-bpz leads to the simultaneous formation of molecular squares and triangles, which exist in an equilibrium mixture. In the molecular square *cis*-$[\{Pt(NH_3)_2(tttt\text{-bpz-}N4,N4')\}_4]^{8+}$ (**II-1**), all four 2,2′-bpz ligands adopt *trans* conformations of the two pyrazine entities. The X-ray analyses of triangular species *cis*-$[\{Pt(NH_3)_2(ttt\text{-bpz-}N4,N4')\}_3]^{6+}$ (**II-2**) and *cis*-$[\{Pt(NH_3)_2(ccc\text{-bpz-}N4,N4')\}_3]^{6+}$ (**II-3**) reveal that all three 2,2′-bpz ligands adopt the identical all-*trans* or all-*cis* orientations. Formation of these structures is controlled by the preference of Pt^{II} for coordinating to the 2,2′-bpz ligand in a bridging mode through the N4,N4′ nitrogen atoms under the reaction conditions applied.

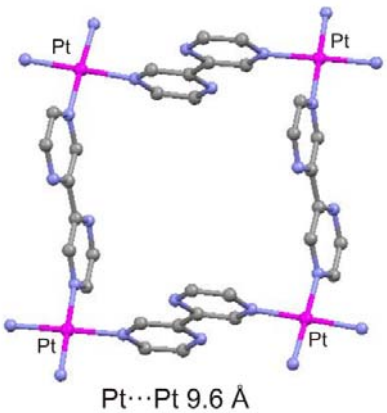

Pt···Pt 9.6 Å

II-1

Pt···Pt 9.5 Å

II-2

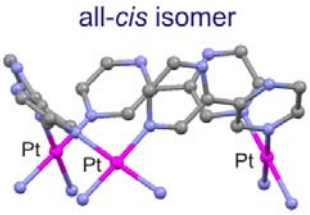

Pt···Pt 7.9 Å

II-3

Isolation of the molecular square from the reaction mixture becomes possible by using appropriate reaction and crystallization conditions. By increasing the temperature of the reaction mixtures, the equilibrium can be completely shifted towards formation of the entropy-favored triangles.

The synthesis and crystal structures of a fragment of squares and triangles, *cis*-$[Pt(NH_3)_2(bpz\text{-}N4)_2]^{2+}$ (**II-5**) is also presented. In this compound, the 2,2´-bpz ligands act in a monodentante fashion.

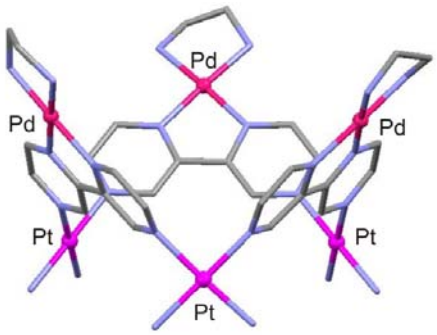

II-6

Binding of (en)Pd^{II} to the available N1,N1´sites in the molecular triangles **II-3** leads to hexanuclear, vase-shaped constructs, which display deeper cavities. The X-ray crystal structures of three different salts **II-6** (NO_3^-), **II-7** (SO_4^{2-}) and **II-8** (PF_6^-) are described. In all cases, anions are encapsulated in the cavities.

Attempts were made to obtain analogues of **II-6**, **II-7** and **II-8** with still deeper cavities by replacing the en ligands at Pd by larger ligands such as *o*-pda, bipzp, and dpk·H_2O. The synthetic pathway leading to such putative vases was different from that described above in that chelates of type [Pd(2,2'-bpz-*N1,N1´*)(*o*-pda)]$(NO_3)_2$ (**II-9**), [Pd(2,2'-bpz-*N1,N1´*)(bipzp)]$(NO_3)_2$ (**II-11**) and [Pd(2,2'-bpz-*N1,N1´*)(dpk·H_2O)]$(NO_3)_2$ (**II-12**) were initially prepared, to be subsequently cross-linked to the cycle via the still available N4 and N4´ sites. Attempts to achieve this via Ag^+ or Cu^{2+} ions failed, however.

Coordinatively "naked" transition metal ions (Cu^{2+}, Cd^{2+}, Ag^+) binding to [{*cis*-$Pt(a)_2$(2,2´-bpz-*N4,N4´*}$_3$]$^{6+}$ ((a)$_2$ = $(NH_3)_2$ or en) instead of *cis*-$(a)_2Pd^{II}$ (*c. f.* **II-6** – **II-8**) leads to a multitude of different structural motifs, the structures of which could only be revealed by the help of X-ray crystallography. Reasons for these different binding modes are the various coordination numbers and geometries that can be adopted by these metal ions.

Coordination of Cu^{2+} to [{(en)Pt(2,2´-bpz-*N4,N4´*}$_3$]$^{6+}$ results in the formation of a mixture of products, two of which were structurally characterized. Thus, cation {[(en)Pt(bpz)]$_6$$Cu_4$$(H_2O)_6$}$^{20+}$ (**II-18**) has the appearance of a "paddle wheel" as a consequence of coordination of Cu^{2+} ions to the two N1,N1´ nitrogen atoms of two 2,2´-bpz ligands from two different triangles. The remaining to N1,N1´ sites likewise chelate Cu^{2+} ions, but do not cross-link in an intermolecular fashion. The second mixed Pt,Cu complex characterized is of composition [(en)Pt(2,2´-bpz)Cu$(NO_3)(H_2O)$]$_3$$(NO_3)_6$·[Cu$(NO_3)_3(H_2O)$] [Cu$(NO_3)_3(H_2O)_2$]· [Cu$(NO_3)_2(H_2O)_3$]·1.5$H_2O$ (**II-19**). The structure has the appearance of a double cone consisting of two Pt_3 triangles, cross-linked by Cu^{2+} ions and stabilized by a complicated network of additional Cu^{2+} cations, NO_3^- anions, and H_2O molecules.

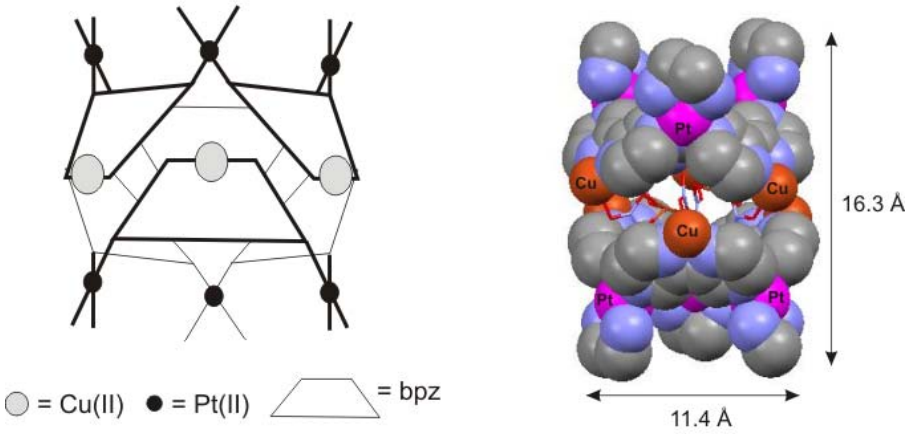

II-19

Coordination polymers, as opposed to discrete heteronuclear complexes, are obtained upon reaction of $[\{(en)Pt(2,2'\text{-bpz-}N4,N4'\}_3]^{6+}$ or $[\{cis\text{-}(NH_3)_2Pt(2,2'\text{-bpz-}N4,N4'\}_3]^{6+}$ with Cd^{2+} and Ag^{+} salts, respectively: $\{[((en)Pt)_3(bpz)_3Cd_2(H_2O)_7]\ [Cd(H_2O)_6](SO_4)_6\}_n$ (**II-20**), $\{[(NH_3)_2Pt(bpz)]_3Ag\ (SiF_6)_3(BF_4)\}_n$ (**II-21**), and $\{[(NH_3)_2Pt(bpz)]_3Ag\ (SO_4)_{3.5}\}_n$ (**II-22**). In aqueous solution these species dissociate into Pt_3 triangles and the transition metal ions, according to ^1H NMR spectroscopy.

The **Chapters III** and **IV** deal with the coordination chemistry of cyanide as well as 3- and 4-cyanopyridines with *cis*-$(a)_2M^{II}$ (M = Pt, Pd). These ligands are non-symmetrical and hence are expected to form more complicated mixtures of cyclic or open structures. In order to limit the number of possible isomers, preformed building blocks were employed (Chapter III). For example, by starting out from $Pd(en)(CN)_2$ (**III-1**) and reacting it with $(en)Pd^{II}$, the molecular square $[Pd(en)(CN)]_4(NO_3)_4$ (**III-4**) is obtained.

The analogous Pt complex **III-5** was prepared in a similar way. Only the latter proved suitable for non-covalent interaction with a nucleobase (9-methyladenine) in aqueous solution, but details could not be revealed.

As outlined in **Chapter IV**, 3- and 4-cyanopyridine ligands are subject to facile hydrolysis to amides in the presence of $(en)M^{II}$ (M = Pt, Pd). Only in one case, with $[(en)Pt(4\text{-}CNpy)_2](NO_3)_2$ (**IV-1**), were the cyanopyridine ligands not hydrolysed. Of the compounds characterized crystallographically (**IV-2** – **IV-6**), the hexanuclear square $[\{(en)Pt\}_6(4\text{-}C(O)NH_2py)_4(PF_6)](NO_3)_7$ (**IV-5**) is the most interesting one, as it displays monofunctional Pt coordination via the pyridine-*N* site and *head-tail* bridging of the amide functions.

Chapter V deals with the effects of *trans*-positioned ligands *L* in complexes of type *trans*-$[Pt(NH_3)_2(L)(H_2O)]^{2+}$ on the acidity of the aqua ligand. A linear relationship between the basicity of the substituted pyridine ligand L and the pK_a of the coordinated water is observed. If the *L* ligand is a π-acid, pK_a values of coordinated water molecules in *trans* position are relatively low (3.5 when *L* = DMSO, and 4.7–5.4 for substituted pyridines), unlike for ligands without π-acceptor ability (4.8 when *L* = DMS, and 6.0 – 6.4 when *L* = NH_2R).

Chapter VI summarizes X-ray structural as well as solution studies concerning the interactions of anions with cyclic homo- and heterometallic complexes containing 2,2′-bpz ligands. Both the high positive charges of trinuclear (+6) and hexanuclear (+12) complexes and the presence of the π-electron deficient 2,2′-bpz heterocyclic rings facilitate anion binding.

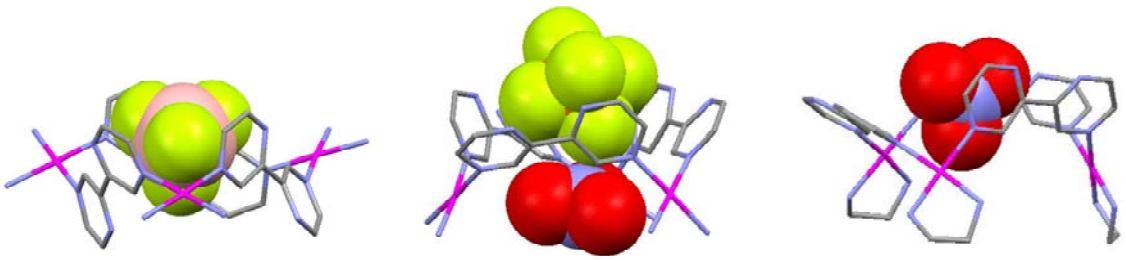

II-2 II-3 II-4

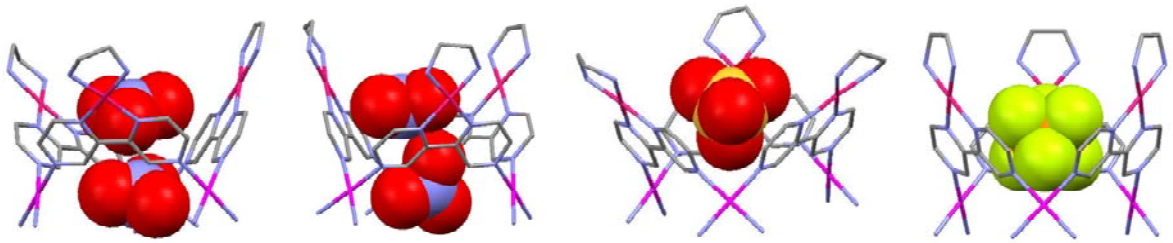

II-6a **II-6b** **II-7** **II-8**

Among these findings, incorporation of SO_4^{2-} anion (**II-7**) is particularly noteworthy. ^{1}H NMR experiments in many cases permit such interactions to be also detected in solution.

The research described in **Chapter VII** report on non-covalent binding interactions of trinuclear *cis*-$[\{Pt(NH_3)_2(bpz)\}_3]^{6+}$ with linearized plasmid DNA 3.1 (5428 bp) using the AFM technique. Upon interaction with the molecular triangle **II-2**, dsDNA starts to bend and coil and the long fibres of free DNA are no longer visible.

Two distinctly different DNA structural alternations have been observed, namely DNA condensation of individual dsDNA molecules (A), and DNA aggregation of multiple strands of dsDNA (B).

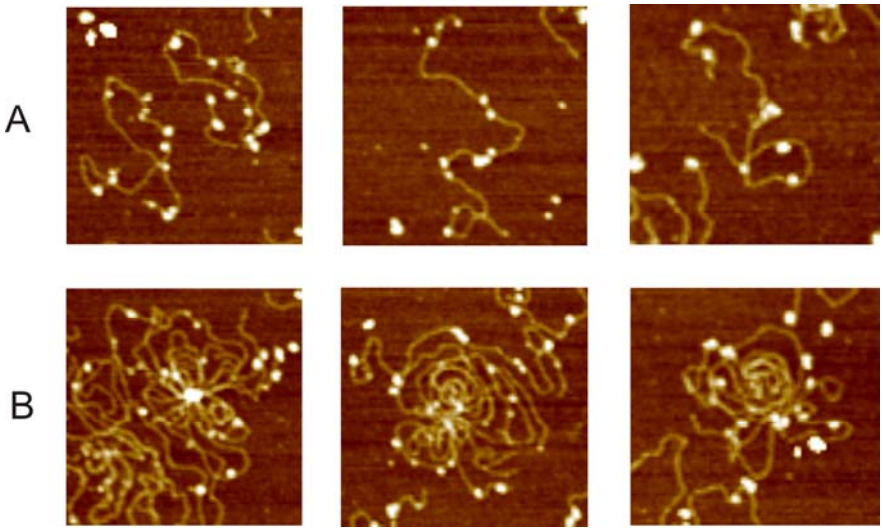

The question remains, whether it is the positive charge that induces the condensation of DNA based on electrostatics, or if the 3D-shape of the molecule plays a significant role as well.

Parts of the results of these investigations have been summarized in the following papers:

Galstyan, Anzhela; Shen, Wei-Zheng; Freisinger, Eva; Alkam, Hussein; Sanz Miguel, Pablo J.; Schürmann, Markus; Lippert, Bernhard.

Supramolecular Isomerism of 2,2´-Bipyrazine Complexes with *cis*-$(NH_3)_2Pt^{II}$ *(in preparation).*

Galstyan Anzhela; Sanz Miguel, Pablo J.; Lippert, Bernhard.

A "directed" approach toward a cationic molecular square containing four isonicotinamidate ligands and (4+2) $(en)Pt^{II}$ metal entities *(submitted).*

Galstyan Anzhela; Sanz Miguel, Pablo J.; Wolf, Jacqueline; Freisinger, Eva; Lippert, Bernhard.

Discrete Molecular Squares $[(en)M(CN)]_4^{4+}$ Derived from $[(en)M(CN)_2]$ (with M = Pt^{II}, Pd^{II}) *(in press).*

Galstyan, Anzhela; Sanz Miguel, Pablo J.; Lippert, Bernhard.

$[NO_3\subset\{(en)Pt(2,2'\text{-bpz})\}_3]NO_3(SO_4)_2$: Snapshot of nitrate insertion into a cationic Pt_3 metallacycle or simply a packing effect?

Dalton Transactions (**2010**), *39(28)*, 6386–6388.

Galstyan, Anzhela; Sanz Miguel, Pablo J.; Lippert, Bernhard.

Electrostatics Plus O-π Interactions Rather Than "Directed" Hydrogen Bonding Keep SO_4^{2-} in a Triangular Pt_3Pd_3-Tris(2,2'-bipyrazine) Host.

Chemistry--A European Journal (**2010**), *16(19)*, 5577–5580.

Galstyan, Anzhela; Shen, Wei-Zheng; Lippert, Bernhard.

Aqua group acidity in complexes of the type *trans*-$[Pt(NH_3)_2(L)(H_2O)]^{2+}$ (with *L* = substituted pyridines). Linear, yet weak dependence of pK_a of the aqua ligand from L basicity.

Zeitschrift fuer Naturforschung, B: A Journal of Chemical Sciences (**2009**), 64(11/12), 1653–1661.

Zusammenfasung

Das Hauptziel der vorliegenden Dissertation war die Synthese diskreter supramolekularer Metallkomplexe durch Selbstorganisation von Übergangsmetallen und *N*-Donorliganden. Zwei Aspekte dieser Komplexe waren von besonderem Interesse: die Möglichkeit der Anionenbindung und Wechselwirkungen mit doppelsträngiger DNA.

In **Kapitel II** werden Design, Synthese und Charakterisierung von supramolekularen Metallkomplexen unterschiedlicher Form beschrieben. Durch gesteuerte Selbstorganisation Koordination von *cis*-$[(NH_3)_2Pt(H_2O)_2]^{2+}$ und 2,2'-bpz werden gleichzeitig molekulare Quadrate und Dreiecke ausgebildet, die im Gleichgewicht vorliegen. Im molekularen Quadrat *cis*-$[\{Pt(NH_3)_2(tttt\text{-bpz-}N4,N4')\}_4]^{8+}$ (**II-1**) liegen alle vier 2,2'-bpz Liganden in *trans*-Konformation vor. Die Röntgenstrukturanalysen der dreieckigen Spezies *cis*-$[\{Pt(NH_3)_2(ttt\text{-bpz-}N4,N4')\}_3]^{6+}$ (**II-2**) und *cis*-$[\{Pt(NH_3)_2(ccc\text{-bpz-}N4,N4')\}_3]^{6+}$ (**II-3**) zeigen, dass alle drei 2,2'-bpz Liganden die identische all-*trans* oder all-*cis* Orientierung annehmen. Die Bildung dieser Strukturen wird durch die verbrückende Koordination der N4- und N4' - Stickstoffatome der 2,2'-bpz Liganden an Pt^{II} bedingt.

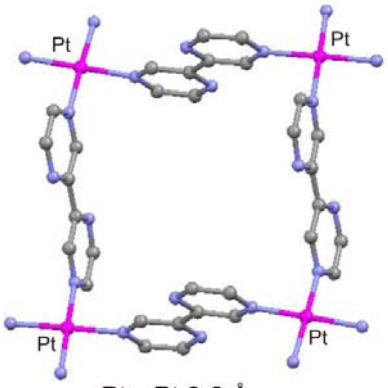

II-1

Pt···Pt 9.5 Å

II-2

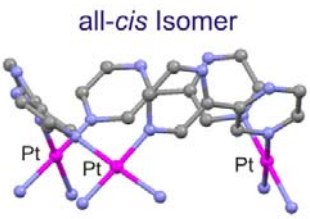

Pt···Pt 7.9 Å

II-3

Die Isolierung des molekularen Quadrats aus dem Reaktionsgemisch gelingt unter geeigneten Reaktions- und Kristallisationsbedingungen. Durch Erhöhung der Temperatur des Reaktionsgemischs kann das Gleichgewicht ganz auf die Seite der Bildung der entropisch begünstigten Dreiecke verschoben werden.

Die Synthese und Kristallstruktur eines Fragments von Quadraten und Dreiecken, *cis*-$[Pt(NH_3)_2(bpz\text{-}N4)_2]^{2+}$ (**II-5**) wird ebenfalls vorgestellt. In dieser Verbindung sind die 2,2'-bpz Liganden monodentat koordiniert.

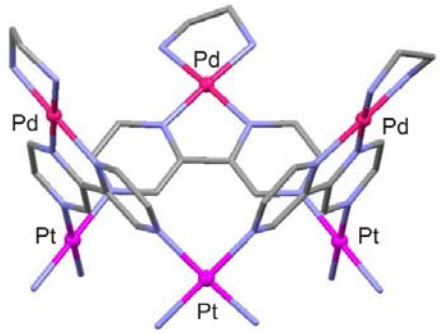

II-6

Die Bindung von (en)Pd^{II} über die verfügbaren N1, N1' Stickstoffatome im molekularen Dreieck **II-3** führt zu sechskernigen, vasenförmigen Konstrukten, die tiefe Kavitäten besitzen. Die Kristallstrukturen von drei verschiedenen Salzen **II-6** (NO_3^-), **II-7** (SO_4^{2-}) und **II-8** (PF_6^-) werden beschrieben. In allen Fällen sind die Anionen in den Hohlräumen eingeschlossen.

Es wurden Versuche unternommen, Analoga von **II-6**, **II-7** und **II-8** mit noch tieferen Hohlräumen durch Ersetzen des en-Liganden am Palladium durch sterisch anspruchsvollere Liganden wie *o*-pda, bipzp und dpk · H_2O zu erhalten. Der Syntheseweg zu den angestrebten vermeintlichen Vasen unterscheidet sich vom zuvor beschriebenen: Chelate des Typs [Pd(2,2'-bpz-*N1,N1´*)(*o*-pda)]$(NO_3)_2$ (**II-9**), [Pd(2,2'-bpz-*N1,N1´*)(bipzp)]$(NO_3)_2$ (**II-11**) und [Pd(2,2'-bpz-*N1,N1´*)(dpk·H_2O)]$(NO_3)_2$ (**II-12**) wurden nämlich zunächst hergestellt, um anschließend über die noch verfügbaren N4 und N4´ Stellen zyklisiert zu werden. Versuche, dies über Ag^+ oder Cu^{2+}-Ionen zu bewerkstelligen, scheiterten jedoch.

Die Bindung koordinativ "nackter" Übergangsmetallionen (Cu^{2+}, Cd^{2+}, Ag^+) an [{*cis*-Pt(a)$_2$(2,2´-bpz-*N4,N4´*}$_3$]$^{6+}$ ((a)$_2$ = $(NH_3)_2$ oder en) anstelle von *cis*-(a)$_2$$Pd^{II}$ (vgl. **II-6** – **II-8**) führt zu einer Vielzahl unterschiedlicher Strukturmotive, die nur mit Hilfe der Röntgenstrukturanalyse aufgeklärt werden konnten. Gründe für diese verschiedenen Bindungsarten sind die unterschiedlichen Koordinationszahlen und Geometrien der eingesetzten Metallionen.

Koordination von Cu^{2+} an [{(en)Pt(2,2´-bpz-*N4,N4´*}$_3$]$^{6+}$ führte zur Bildung eines Gemischs von Produkten, von denen zwei strukturell charakterisiert wurden. So hat das Kation {[(en)Pt(bpz)]$_6$$Cu_4$($H_2O$)$_6$}$^{20+}$ (**II-18**) das Aussehen eines "Schaufelrads" als Folge der Koordination von Cu^{2+}-Ionen an die beiden N1, N1´ Stickstoffatome von zwei 2,2'-bpz Liganden aus zwei verschiedenen Dreiecken. Die restlichen N1, N1' Stickstoffatome sind ebenfalls an Cu^{2+}-Ionen koordiniert, jedoch nicht intermolekular. Der zweite erhaltene, gemischte Pt,Cu-Komplex hat die Zusammensetzung [(en)Pt(2,2´-bpz)Cu(NO_3)(H_2O)]$_3$(NO_3)$_6$·[Cu(NO_3)$_3$(H_2O)][Cu(NO_3)$_3$(H_2O)$_2$]· [Cu(NO_3)$_2$(H_2O)$_3$]·1.5H_2O (**II-19**). Die Struktur hat das Aussehen eines Doppelkonus, bestehend aus zwei Pt_3-Dreiecken, die über Cu^{2+}-Ionen verbunden sind und durch ein kompliziertes Netz von zusätzlichen Cu^{2+}-Kationen und NO_3^- -Anionen stabilisiert werden.

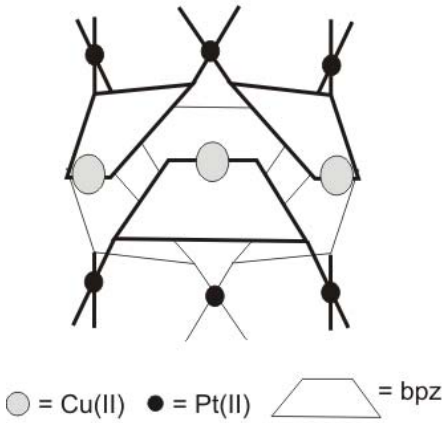

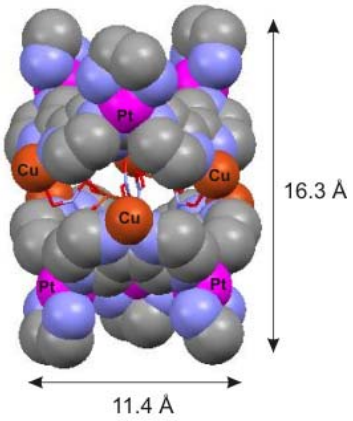

II-19

Im Gegensatz zu diskreten heteronuklearen Komplexen entstehen bei der Reaktion von $[\{(en)Pt(2,2'\text{-bpz-}N4,N4'\}_3]^{6+}$ oder $[\{cis\text{-}(NH_3)_2Pt(2,2'\text{-bpz-}N4,N4'\}_3]^{6+}$ mit Cd^{2+}- und Ag^{+}-Salzen die Koordinationspolymere $\{[((en)Pt)_3(bpz)_3Cd_2(H_2O)_7][Cd(H_2O)_6](SO_4)_6\}_n$ (**II-20**), $\{[(NH_3)_2Pt(bpz)]_3Ag(SiF_6)_3(BF_4)\}_n$ (**II-21**), und $\{[(NH_3)_2Pt(bpz)]_3Ag\ (SO_4)_{3.5}\}_n$ (**II-22**). ^{1}H-NMR-Spektroskopie zeigt, dass diese Strukturen in wässriger Lösung in Pt_3-Dreiecke und Übergangsmetallionen dissoziieren.

Kapitel III und **IV** befassen sich mit der Koordinationschemie von Cyanid sowie 3- und 4-Cyanopyridin mit *cis*-$(a)_2M^{II}$ (M = Pt, Pd). Diese Liganden sind nicht symmetrisch und daher konnte erwartet werden, dass sie kompliziertere Gemische von zyklischen und offenen Strukturen bilden. Zur Begrenzung der Anzahl der möglichen Isomere wurden vorgeformte Bausteine eingesetzt (Kapitel III). Als Beispiel wurde ausgehend von $Pd(en)(CN)_2$ (**III-1**) durch Umsetzung mit $(en)Pd^{II}$ das molekulare Quadrat $[Pd(en)(CN)]_4(NO_3)_4$ (**III-4**) erhalten.

Der analoge Pt-Komplex **III-5** wurde in ähnlicher Weise hergestellt. Lediglich letzterer erwies sich als geeignet für das Studium nicht-kovalenter Wechselwirkungen mit

einer Modellnucleobase (9-Methyladenin) in wässriger Lösung. Details dieser Wechselwirkungen konnten jedoch noch nicht aufgeklärt werden.

Wie in **Kapitel IV** angedeutet, hydrolysieren 3- und 4-Cyanopyridinliganden leicht zu entsprechenden Amiden in Gegenwart von $(en)M^{II}$ (M = Pt, Pd). Nur in einem Fall, dem $[(en)Pt(4\text{-}CNpy)_2](NO_3)_2$ (**IV-1**), wurden die Cyanopyridinliganden nicht hydrolysiert. Von den kristallographisch charakterisierten Verbindungen (**IV-2** – **IV-6**), ist das sechskernige Quadrat $[\{(en)Pt\}_6(4\text{-}C(O)NH_2py)_4(PF_6)](NO_3)_7$ (**IV-5**) besonders interessant, da es sowohl monofunktionelle Platinkoordination über den Pyridin-Stickstoff als auch Kopf-Schwanz-Verbrückung über die Amid-Funktionen aufweist.

Kapitel V befasst sich mit den Auswirkungen der *trans*-positionierten Liganden *L* in Komplexen des Typs *trans*-$[Pt(NH_3)_2(L)(H_2O)]^{2+}$ auf die Acidität des Aqua-Liganden. Es wird ein linearer Zusammenhang zwischen der Basizität der substituierten Pyridin-Liganden *L* und dem pK_S -Wert des koordinierten Wasser beobachtet. Wenn der Ligand *L* eine π-Säure ist, sind die pK_S-Werte von koordinierten Wassermolekülen in *trans*-Stellung relativ niedrig (3.5 bei *L* = DMSO im Vergleich zu 4.7 – 5.4 für substituierte Pyridine), im Gegensatz zu Liganden ohne π-Akzeptor-Fähigkeit (4.8 wenn *L*= DMS und 6.0 – 6.4 bei *L* = NH_2R).

Kapitel VI befasst sich mit der Untersuchung von Wechselwirkungen zwischen Anionen und zyklischen homo- und heteronuclearen Komplexen mit 2,2´-bpz Liganden mit Hilfe von Rötgenstrukturanalyse und Lösungsuntersuchungen. Sowohl die hohe positive Ladung der dreikernigen (+6) und sechskernigen (+12) Komplexe und die Anwesenheit der π-elektronenarmen, heterocyclischen 2,2´-bpz-Ringe erleichtern die Anionenbindung.

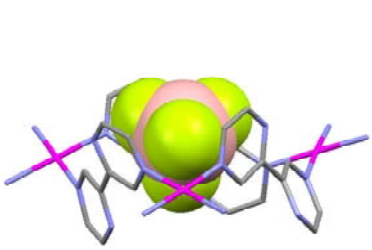

II-2

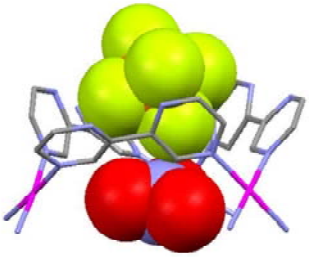

II-3

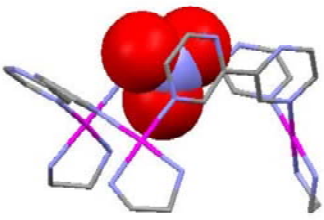

II-4

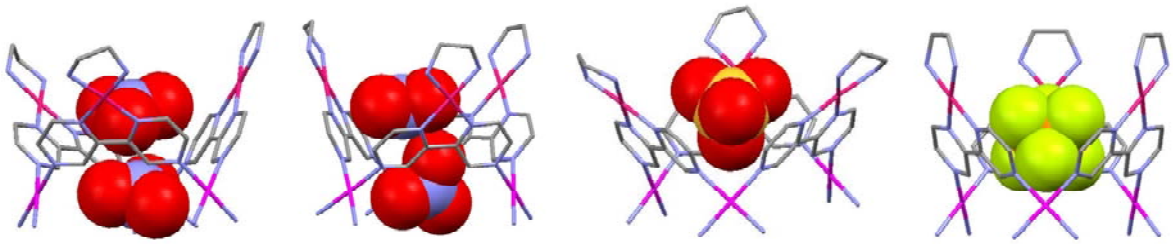

II-6a **II-6b** **II-7** **II-8**

Zu erwähnen ist in diesem Zusammenhang die Einlagerung des SO_4^{2-} Anions (**II-7**). ^{1}H-NMR-Experimente ermöglichte in vielen Fällen der Nachweis entsprechender Interaktionen auch in Lösung.

Die in **Kapitel VII** beschriebenen Ergebnisse beziehen sich auf nicht-kovalente Wechselwirkungen von dreikernigem *cis*-$[\{Pt(NH_3)_2(bpz)\}_3]^{6+}$ mit linearisierter Plasmid-DNA 3.1 (5428 bp) mit Hilfe von AFM. Infolge der Wechselwirkungen mit dem molekularen Dreieck **II-2** beginnt dsDNA sich zu biegen und aufzuwickeln, bis die ursprüngliche Faserstuktur der DNA nicht mehr erkennbar ist. Zwei deutlich unterschiedliche DNA-Strukturwechsel sind zu beobachten, nämlich DNA-Kondensation einzelner doppelsträngiger DNA-Moleküle (A), und DNA-Aggregation mehrerer Stränge der dsDNA (B).

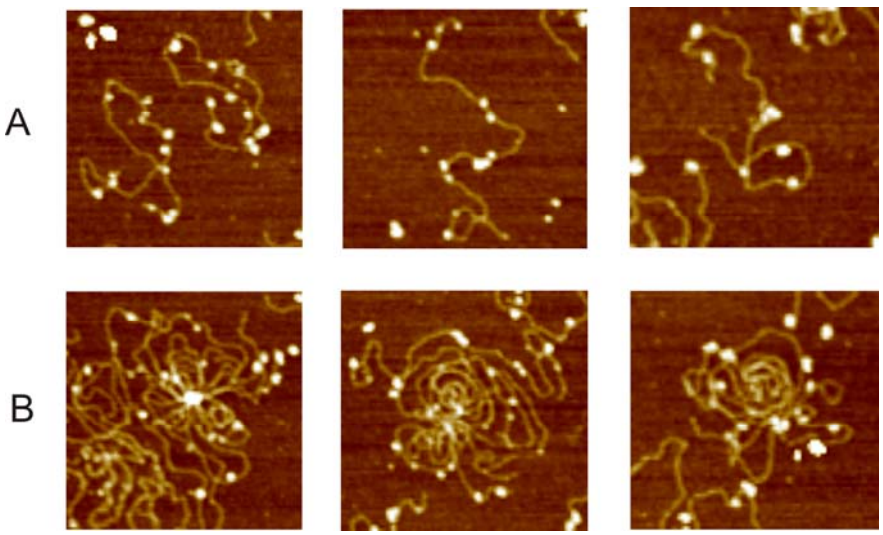

Die Frage, ob lediglich die positive Ladung des eingesetzten Metalladreiecks die Kondensation der DNA induziert, oder ob auch die dreidimensionale Form des Molekülkations eine wichtige Rolle spielt, konnte bisher nicht beantwortet werden.

Ein Teil der Ergebnisse der oben angeführten Untersuchungen wurden in den folgenden Veröffentlichungen zusammengefasst:

Galstyan, Anzhela; Shen, Wei-Zheng; Freisinger, Eva; Alkam, Hussein; Sanz Miguel, Pablo J.; Schürmann, Markus; Lippert, Bernhard.

Supramolecular Isomerism of 2,2´-Bipyrazine Complexes with *cis*-$(NH_3)_2Pt^{II}$ *(in preparation).*

Galstyan Anzhela; Sanz Miguel, Pablo J.; Lippert, Bernhard.

A "directed" approach toward a cationic molecular square containing four isonicotinamidate ligands and (4+2) $(en)Pt^{II}$ metal entities *(submitted).*

Galstyan Anzhela; Sanz Miguel, Pablo J.; Wolf, Jacqueline; Freisinger, Eva; Lippert, Bernhard.

Discrete Molecular Squares $[(en)M(CN)]_4^{4+}$ Derived from $[(en)M(CN)_2]$ (with M = Pt^{II}, Pd^{II}) *(in press).*

Galstyan, Anzhela; Sanz Miguel, Pablo J.; Lippert, Bernhard.

$[NO_3\subset\{(en)Pt(2,2'\text{-bpz})\}_3]NO_3(SO_4)_2$: Snapshot of nitrate insertion into a cationic Pt_3 metallacycle or simply a packing effect?

Dalton Transactions (**2010**), *39(28)*, 6386–6388.

Galstyan, Anzhela; Sanz Miguel, Pablo J.; Lippert, Bernhard.

Electrostatics Plus O-π Interactions Rather Than "Directed" Hydrogen Bonding Keep SO_4^{2-} in a Triangular Pt_3Pd_3-Tris(2,2'-bipyrazine) Host.

Chemistry--A European Journal (**2010**), *16(19)*, 5577–5580.

Galstyan, Anzhela; Shen, Wei-Zheng; Lippert, Bernhard.

Aqua group acidity in complexes of the type *trans*-$[Pt(NH_3)_2(L)(H_2O)]^{2+}$ (with *L* = substituted pyridines). Linear, yet weak dependence of pK_a of the aqua ligand from L basicity.

Zeitschrift fuer Naturforschung, B: A Journal of Chemical Sciences (**2009**), 64(11/12), 1653–1661.

References

[1] See, e. g. S. B. Howerton, C. C. Sines, D. Van Derveer, L. D. Williams *Biochemistry* **2001,** *40,* 10023.

[2] J. N. Parkinson, M. P. H. Lee, S. Neidle, *Nature*, **2002**, *417*, 876.

[3] L. D. Williams, L. J. Maher III, *Annu. Rev. Biophys. Biomol. Struct.,* **2000**, *29*, 497.

[4] J. Anastassopoulou, T. Theophanides, *Critical Reviews in Oncology/Hematology*, **2002**, *42*, 79.

[5] E. C. Theil, K. N. Raymond, *Transition-Metal Storage, Transport, and Biomineralization*. In *Bioinorganic Chemistry* (Ed. I. Bertini, H. B. Gray, S. Lippard, J. Valentine), **1994**, Mill Valley, California.

[6] J. Miller, A. D. McLachlan, A. Klug, *EMBO J.* **1985**, *4*, 1609.

[7] G.-R. Burmester, *Z Rheumatol*, **2001**, *60*:167; S. J. Berners-Pricem, R. J. Bowen, M. J. McKeage, P. Galettis, L. Ding, C. Baguley, W. Brouwer., *J. Inorg. Biochem.,* **1997**, *67*, 154.

[8] J. Cade, *Med. J. Australia* **1949**, *36*, 349.

[9] B.Rosenberg, L. VanCamp, T. Krigas, *Nature*, **1965**, *205*, 698.

[10] C. G. Hartinger, S. Zorbas-Seifried, M. A. Jacupec, B. Kynast, H. Zorbas, B. K. Keppler, *J. Inorg. Biochem.,* **2006**, *100*, 891; W. H. Ang, P. J. Dyson, *Eur. J. Inorg. Chem.*, **2006**, *20*, 4003.

[11] A. Bergamo, A. Masi, P. J. Dyson, G. Sava*, Int. J. Oncol.*, **2008**, *33(6)*, 1281.

[12] J. D. Watson, F. H. C. Crick, *Nature*, **1953**, *171*, 964.

[13] E. Chargaff, *Experientia*, **1950**, *6*, 201.

[14] a) R.R. Sinden, *DNA Structure and Function*; Academic Press: New York, **1994**, b) A. A. Travers *Annu. Rev. Biochem*. **1989**, *58*, 427. c) N. R. Cozzarelli, J. C. Wang, *DNA Topology and its Biological Effects*; Cold Spring Harbor Laboratory Press: New York, **1990**.

[15] D. Flatters, M. Young, D. L. Beveridge et al. *J Biomol Struct Dyn.* **1997,** *14*, 757, V. I. Ivanov, L. E. Minchenkova, B. K. Chernov. et al. *J Mol Biol.* **1995**, *245*, 228.

[16] X. J. Lu, Z. Shakked, W. K. Olson, *J Mol Biol.* 2000, 300, 819; A. Jacobo-Molina, J. Ding, R.G. Nanni et. al., *Proc Natl Acad Sci.*, **1993,** *90*, 6320.

[17] B. F. Eichman, J. M. Vargason, B. H. M. Mooers, P. S. Ho, *Proc Natl Acad Sci*., **2000**, *97*, 3971.

[18] B. Eichman, J. M. Vargason, B. H. M. Mooers, P. S. Ho, *Proc.Natl. AS*, **2000**, *97*, 397

[19] Y. Wang, D. J. Patel, *J. Mol. Biol.* **1995**, *251*, 76.

[20] K. Luger, A. Mäder, R Richmond, D. Sargent, T Richmond, *Nature,* **1997**, *389,* 251.

[21] S. T. Garcia, A. McQuillan, L. Panasci, *Biochem.Pharmacol.,* **1988***, 37,* 3 189.

[22] a) P. M. Takahara, A. C. Rosenzweig, C. A. Frederick and S. J. Lippard, *Nature*, **1995**, *377*, 649; b) U. M. Ohndorf, M. A. Rould, Q. He, C. O. Pabo and S. J. Lippard, *Nature*, **1999**, *399*, 708.

[23] S. Komeda, T. Moulaei, K. Kruger Woods, M. Chikuma, N. P. Farrell, L. D. Williams *J. Am. Chem.Soc.*, **2006**, *128*, 16092.

[24] B. P. Casey, P. M. Glazer, *Prog Neucleic Acid Res Mol Biol,* **2001**; *67*: 163; R. Gambari, *Curr Pharm Des*, **2001**; *7*, 1839.

[25] A. Olesky, A. G.Blanco, R. Boer, I. Uson, J. Aymami, A. Rodger, M. J. Hannon, M. Coll, *Angew. Chem. Int. Ed.* **2006**, *45*, 1227

[26] L.S. Lerman, *J. Mol. Biol*., **1961**, *3,* 18.

[27] See e.g a) P. B. Glover, P. R. Ashton, L. J. Childs, A. Rodger, M. Kercher, R. M. Williams, L.D. Cola, Z. Pikramenou, *J. Am. Chem. So*c., **2003**, *125*, 9918; b) L. A. Levine, C. M. Morgan,K. Ohr andM. E.Williams, *J. Am. Chem.Soc.*, **2005**, *127*, 16764; c) K.W. Jennette, S. J. Lippard, G. A. Vassiliades, W. R. Bauer, *Proc. Natl. Acad. Sci*., **1974**, *71*, 3839.

[28] C. L. Kielkopf, K. E. Erkkila, B. P. Hudson, J. K. Barton D. C. Rees, *Nat. Struct. Biol*., **2000**, *7*, 117.

[29] D. R. Boer, A. Canals, M. Coll, *Dalton Trans.*, **2009**, 399.

[30] S. Neidle, S. Balasubramanian *Quadruplex Nucleic Acids*, RSC Publishing, Royal Society of Chemistry, Cambridge, **2006**.

[31] J. Deng, B. Pan and M. Sundaralingam, *Acta Crystallogr. D. Biol.Crystallogr.*, **2003**, *59*, 2342; L. Martino, A. Virno, B. Pagano, A. Virgilio, S. DiMicco, A. Galeone, C. Giancola, G. Bifulco, L. Mayol and A. Randazzo, *J. Am. Chem.Soc.*, **2007**, *129*, 16048.

[32] H. Yu, X. Wang, M. Fu, J. Ren, X. Qu, *Nuc. Ac. Res.*, **2008**, 36, 5695.

[33] J. Müller, B. Lippert, *Angew. Chem. Int. Ed*. **2006**, *45*, 2503.

[34] A. L. Brogden, N. H. Hopcroft, M. Searcey, C. J. Cardin, *Angew. Chem. Int. Ed.*, **2007**, *46*, 3850.

[35] Recently published books on supramolecular chemistry: a) J. W. Steed, J. L. Atwood, *Supramolecular Chemistry*, **2009**, Wiley; b) J. W. Steed, D. R. Turner, K. J. Wallace, *Core Concepts Supramolecular Chemistry and Nanochemistry*, **2007**, Wiley, c) P. J. Cragg, *A Practical Guide to Supramolecular Chemistry*, **2005**, Wiley

[36] J.-M. Lehn, *Supramolecular Chemistry: Concepts and Perspectives*, **1995**, VCH, Weinheim.

[37] E. Fischer *Ber. Dt. Chem. Ges.*, **1894**, *27*, 2985.

[38] a) S. Leininger, B, Olenyuk, P. J. Stang, *Chem Rev*. **2000**, *100*, 853; b) J. A. R. Navarro, B. Lippert, *Coord. Chem Rev*. **1999**, *653*,185.

[39] K. J. C. Van Bommel, A. Friggeri, S. Shinkai, *Angew. Chem. Int. Ed.* **2003**, *42*, 980.

[40] J.-M. Lehn, *Chem. Soc. Rev.,* **2007**, 36, 151.

[41] B. Moulton, M. J. Zaworotko, *Chem. Rev.*, **2001**, *101*, 1629.

[42] J.-P. Zhang, X.-C. Huang, X.-M. Chen, *Chem. Soc. Rev.*, **2009**, *38*, 2385.

[43] P. J. Steel, *Coord. Chem. Rev.***1990**, *106*, 227. C. Kaes, A. Katz,M. W. Hosseini, *Chem. Rev*. **2000**, *100*, 3553.

[44] M. Fujita, J. Yazaki, K. Ogura, *J. Am. Chem. Soc.***1990**, 112, 5645.

[45] P. J. Stang. D. H. Cao, *J. Am. Chem. Soc.***1994**, 116, 4981.

[46] C. J. Pedersen, *J. Am. Chem. Soc.,* **1967**, *89*, 7017.

[47] M. Yoshizawa, J. K. Klosterman, M. Fujita, *Angew. Chem. Int. Ed.,* **2009***, 48,* 3418*,* A. C. Schulze, K. Föcker, I. M. Oppel, *Nachrichten aus der Chemie*, **2009**, *57*, 507.

[48] M. D. Pluth, K. N. Raymond, *Chem. Soc. Rev.*, **2007**, *36*, 161.

[49] A. Bianchi, K. Bowman-James, E. Garcia-Espana, *Supramolecular Chemistry of Anions*; **1997**, Wiley-VCH: New York.

[50] V. Kral, O. Rusin, T. Shishkanova, R. Volf, P. Matejka, K. Volka, *Chem. Listy*, **1999**, *93,* 546.

[51] J. P. Gallivan,D. A. Dougherty, *Org. Lett.* **1999**, *1*, 103.

[52] Y. Danten, T. Tassaing, M. Besnard, *J. Phys. Chem. A* **1999**, *103*, 3530.

[53] I. Alkorta, I. Rozas, J. Elguero, *J. Org. Chem.* **1997**, *62*, 4687.

[54] B. L. Schottel, H. T. Chifotides, K. R. Dunbar, *Chem. Soc. Rev*., **2008**, *37*, 68.

[55] See, e. g. a) P. Gamez, T. J. Mooibroek, S. J. Teat, J. Reedijk, *Acc. Chem. Res.* **2007**, *40*, 435; b) S. Demeshko, S. Dechert, F. Meyer *J. Am. Chem. Soc.*, **2004**, *126*, 4508, P. de Hoog, P. Gamez, I. Mutikainen, U. Turpeinen, J. Reedijk, *Angew. Chem. Int. Ed.*, **2004**, *43*, 5815.

[56] a) A. Sautter, D. G. Schmid,G. Jung, F. Würthner, *J. Am. Chem. Soc.,* **2001**, *123*, 5424; b) K. Uehara, K. Kasai, N. Mizuno, *Inorg. Chem*., **2007**, *46*, 2363; c) T. Weilandt, R. W. Troff, H. Saxell, K. Rissanen, C. Schalley, *Inorg. Chem*., **2008**, *47*, 7588; d) A. Gutierrez, M. Mounir, O. Rossell, E. Ruiz, A. Rang, M. Engesser, *Inorg. Chem*., **2007**, *46*, 3395; e) M. Ferrer, M. Mounir, O. Rossell, E. Ruiz, M. A. Maestro, *Inorg. Chem*., **2003**, *42*, 5890.

[57] S. Ghosh, P. S. Mukherjee, *Inorg. Chem*. **2009**, *48*, 2605.

[58] a) Z. Huang, M. Du, H.-B. Song, X.-H. Bu, *Cryst. Growth Des.,* **2004**, *4*, 71; b) Y.-B. Dong, J.-P. Ma, R.-Q. Huang, M. D. Smith, H.-C. zur Loye, *Inorg. Chem.,* **2003**, *42*, 294; c) Y.-B. Dong, J.-Y. Cheng, R.-Q. Huang, M. D. Smith, H.-C. zur Loye, *Inorg. Chem.,* **2003**, *42*, 5699; d) N. Gimeno, R. Vilar, *Coord. Chem Rev.,* **2006**, *250(23-24),* 3161.

[59] M. Schweiger, S. R. Seidel, A. M. Arif, P. J. Stang. *Inorg. Chem*., **2002**, *41(9)*, 2556.

[60] G. M. Whitesides, J. P. Mathias, C. T. Seto, *Science,* **1991**, *254*, 1312.

[61] R. I. Crutchley, A. B. P. Lever, *Inorg. Chem*., **1982**, *21*, 2276

[62] N. Neto, M. Muniz-Miranda, *Spectrochem. Acta* **1994**, *50 A*, 357.

[63] R.-D. Schnebeck, L. Randaccio, E. Zangrando, B. Lippert, *Angew. Chem.* **1998**, *110*, 128; *Angew. Chem. Int. Ed. Engl.* **1998**, *37*, 119.

[64] W.-Z. Shen, *Dissertation*, **2007**, Dortmund.

[65] Y. K. Kryschenko, S. R. Seidel, A. M. Arif, P. J. Stang, *J. Am. Chem. Soc.,* **2003**, 125, 5193.

[66] See e. g., a) S. Ghosh, D. R. Turner, S. R. Batten, P. S. Mukherjee, *DaltonTrans.*, **2007**, 1869; b) H. Piotrowski, K. Polborn,G. Hilt, K. Severin, *J. Am. Chem. Soc.* **2001**, *123*, 2699; c) T. Habereder, M. Warchhold, H. Noth, K. Severin, *Angew. Chem., Int. Ed.* **1999**, *38*, 3225; d) S.-W. Lai, M. C.-W. Chan, S.-M. Peng, C.-M. Che, *Angew. Chem., Int. Ed.* **1999**, *38*, 669.

[67] M. Schweiger, S. R. Seidel, A. M. Arif, P. J. Stang, *Angew. Chem., Int. Ed.* **2001**, *40*, 3467.

[68] See,e.g.; a) H. Schöllhorn, U. Thewalt, B. Lippert, *J. Chem. Soc., Chem. Comm.*, **1986**, 258; b) H. Casellas, A. Pevec, B. Kozlevˇcar, P. Gamez , J. Reedijk, *Polyhedron*, **2005**, *24*, 1549; c) T. F. Mastropietro, D. Armentano, E. Grisolia, C. Zanchini, F. Lloret, M. Julve, G. De Munno, *Dalton. Trans*., **2007**, 514.

[69] R.-D. Schnebeck, E. Freisinger, B. Lippert, *Angew. Chem. Int. Ed. Engl.* **1999**, *38*, 168; *Angew. Chem.* **1999**, *111*, 235.

[70] R.-D. Schnebeck, E. Freisinger, F. Glahé, B. Lippert, *J. Am. Chem. Soc.,* **2000**, *122*, 1381.

[71] R.-D. Schnebeck, E. Freisinger, B. Lippert, *Chem. Commun.* **1999**, 675.

[72] R.-D. Schnebeck, E. Freisinger, B.Lippert, *Eur. J. Inorg. Chem.*, **2000**, 1193.

[73]M. C. Miles, J. D. Wilson, *Inorg. Chem.,* **1975***, 14,* 2357.

[74] A. L. Balch, R. H. Holm, *J. Am. Chem. Soc*, **1966**, *88*, 5201.

[75] F. Ullmann, F. Mauthner, *Ber. Dtsch. Chem. Ges.,* **1903***, 35*,4302.

[76] R. Kockerbauer, P.J. Bednarski, *J. Inorg. Biochem.*, **1996**, *62*, 281.

[77] D. Herebian, E. Bothe, F. Neese, T. Weyhermüller, K. Wieghardt, *J. Am. Chem. Soc***., 2003**, *125*, 9116.

[78] G. Annibale, L. Canovese, L. Cattalini, G. Natile, M. Biagini-Cingi, A.-M. Manotti-Lanfredi, A. Tiripicchio, *J. Chem. Soc., Dalton Trans.*, **1981**, 2280.

[79] A. Khutia, P.J. Sanz Miguel, B. Lippert, submitted.

[80] See. e. g.: a) C.-Q. Wan, L. Zhao, T. C. W. Mak, *Inorg. Chem.,* **2010**, *49*, 97. b) D.Pocic, J.-M. Planeix, N. Kyritsakas, A. Jouaiti, M.W. Hosseini, *Cryst. Eng Comm.,* **2005**, *7*, 624; c) O.-S. Jung, Y. J. Kim, Y.-A. Lee, J. K. Park, H. K. Chae, *J. Am. Chem. Soc*., **2000**, *122*, 9921.

[81] C. B. Aakeröy, N. Schultheiss, J. Desper, *Dalton Trans.*, **2006**, 1627.

[82] W. Bauer, F. Hampel, H. Maid, *Z. Naturforsch.,* **2010**, *65b,* 273; G. Mezei, P. Baran, R. G. Raptis, *Angew. Chem. Int. Ed.,* **2004**, *43*, 574.

[83]For recent reviews, see: a) A. Phan, C. J. Doonan, F. J. Uribe-Romo,C. B. Knobler, M. O'Keeffe, O. M. Yaghi, *Acc. Chem. Res.,***2010**, *43*, 58; b) T. Uemura, N. Yanai, S. Kitagawa, *Chem. Soc. Rev.,***2009**, *38*, 1228, c) X. D. Zheng, T. B. Lu, *CrystEngComm*, **2010**, *12*, 324; d) L. J. Murray, M. Dinca, J. R. Long, *Chem. Soc. Rev.,* **2009**, *38*, 1294.

[84] See e. g., a) E. Lee, J. Kim, J. Heo, D. Whang, K. Kim, *Angew. Chem., Int. Ed.*, **2001**, *40*, 399; b) O. M. Yaghi, H. Li, *J. Am. Chem. Soc.,* **1995**, *117*, 10401; c) O. S. Jung, Y. J. Kim, K. M. Kim, Y. A. Lee, *J. Am. Chem. Soc.*, **2002**, *124*, 7906.

[85] See e. g., a) V. P. Fedin, K. Kim, *Angew. Chem., Int. Ed.*, **2006**, *45*, 916; b) M. Fujita, Y. J. Kwon, S. Washizu, K. Ogura, *J. Am. Chem. Soc.*, **1994**, *116*, 1151; c) T. Sawaki, Y. Aoyama, *J. Am. Chem. Soc.*, **1999**, *121*, 4793.

[86] See e. g.; a) D. Mircea, J. R. Long, *Angew. Chem., Int. Ed.*, **2008**, *47*, 6766; b) B. L. Chen, N. W. Ockwig, A. R. Millward, D. S. Contreras, O. M. Yaghi, *Angew. Chem., Int. Ed.*, **2005**, *44*, 4745; c) H. Chun, D. N. Dybtsev, H. Kim, K. Kim, *Chem-Eur. J.*, **2005**, *11*, 3521; d) N. L. Rosi, J. Eckert, M. Eddaoudi, D. T. Vodak, J. Kim, M. O'Keeffe, O. M. Yaghi, *Science*, **2003**, *300*, 1127.

[87] A. K. Cheetham, C. N. R. Rao, R. K. Feller, *Chem. Commun.,* **2006**, 4780.

[88] See, e. g.: a) A. Arola and R. Vilar, *Curr. Top. Med. Chem.* **2008**, *8*, 1405, b) S. M. Haider and S. Neidle, *Biochem. Soc. Trans.* **2009**, *37*, 583, c) M. Gunaratnam, S. Swank, S. M. Haider, K. Galesa, A. P. Reszka, M. Beltran, F. Cuenca, J. A. Fletcher and S. Neidle, *J. Med. Chem.* **2009**, *52*, 3774, d) L. Guittat, P. Alberti, D. Gomez, A. De Cian, G. Pennarun, T. Lemarteleur, C. Belmokhtar, R. Paterski, H. Morjani, C. Trentesaux, E. Mandine, F. Boussin, P. Mailliet, L. Lacroix, J.-F. Riou and J.-L. Mergny, *Cytotechnology* **2004**, *45*, 75.

[89] See, e. g.: a) K. M. Rahman, A. P. Reszka, M. Gunaratnam, S. M. Haider, P. W. Howard, K. R. Fox, S. Neidle and D. E. Thurston, *Chem. Comm.* **2009**, 4097, b) M. Read, R. J. Harrison, B. Romagnoli, F. A. Tanious, S. H. Gowan, A. P. Reszka, W. D. Wilson, L. R. Kelland and S. Neidle, *Proc Natl Acad Sci* **2001**, *98*, 4844, c) R. T. Wheelhouse, D. Sun, H. Han, F. X. Han and L. H. Hurley, *J. Am. Chem. Soc.*, **1998**, *120*, 3261.

[90] See, e. g.: a) F. X. Han, R. T. Wheelhouse and L. H. Hurley, *J. Am. Chem. Soc.* **1999**, *121*, 3561, b) A. Arola-Arnal, J. Benet-Buchholz, S. Neidle and R. Vilar, *Inorg. Chem.* **2008**, *47*, 11910, c) L. Ren, A. Zhang, J. Huang, P. Wang, X. Weng, L. Zhang, F. Liang, Z. Tan and X. Zhou, *ChemBioChem* **2007**, *8*, 775, d) D. P. N. Goncalves, R. Rodriguez, S. Balasubramanian, J. K. M. Sanders, *Chem. Comm.* **2006**, 4685.

[91] J. Woodward, *Philos. Trans. R. Soc. London*, **1724**, *33*, 15.; C. Brown, *Philos. Trans. R. Soc. London,* **1724**, *33*, 17.

[92] S. Tanase, J. Reedijk, *Coord. Chem. Rev.*, **2006**, *250*, 2501

[93] V. Balzani, A. Juris, M. Venturi, S. Campagna, S. Serroni, *Chem.Rev.* **1996**, *96*, 759.

[94] J. A. Davies, F. R. Hartley, S. G. Murray, M. A. Pierce-Butler, *J. Chem. Soc. Dalton Trans*., **1983** , 1305.

[95] I. Ara, N. Chaouche, J. Forniés, C. Fortuño, A. Kribii, A. Martín, *Eur. J. Inorg. Chem.* **2005**, 3894.

[96] S-W. Lai, K-K. Cheung, M. C.-W. Chan, C-M. Che, *Angew. Chem. Int. Ed.,* **1998**, *37*, 184.

[97] L. R. Falvello, M. Tomas, *Chem. Comm*., **1998**, 273.

[98] P. Terech, R. G. Weiss, *Chem. Rev.,* **1997**, *97*, 3133.

[99] G. Magnus, *Ann. Phys. Chem.,* **1828**, *14*, 239; M. Atoji, J. W. Richardson, R. E. Rundle, *J. Am. Chem. Soc.*, **1957**, *79*, 3017.

[100] R. E. Clarke, P. C. Ford, *Inorg. Chem.*, **1970**, *9*, 495.

[101] a) R. E. Clarke, P. C. Ford, *Inorg. Chem*., **1970,** *9*, 495; b) A. E. Almaraz, L. A. Gentil, L. M. Baraldo, J. A. Olabe, *Inorg. Chem*., **1996**, *35*, 7718, c) M. Ketterle, W. Kaim, J. A. Olabe,

A. R. Parise, J. Fiedler, *Inorg. Chim. Acta*, **1999**, *291*, 66; d) A. Maiboroda, H. Lang, *New J. Chem.*, **2001**, *25*, 642.

[102] a) W. Zhang, J. R. Jeitler, M. M. Turnbull, C. P. Landee, M. Wei, R. D. Willett, *Inorg. Chim. Acta* **1997**, *256* (2), 183; b) M. K. Bhattacharya, S. J. Bora, B. K. Das, *J. Chem. Cryst.,* **2008**, *38*, 195; c) B. K. Das, S. J. Bora, M. K. Bhattacharya, R. Barman, *Acta Crystallogr., Sect. B* **2009**, *65 (4),* 467.

[103] H. Y. Huang, W. J. Chen, C. C. Hang, A. Yeh, *Inorg. Chem.* **1991**, *30*, 1862.

[104] J. A. Kovacs, *Chem. Rev*., **2004**, *104*, 825.

[105] V. Yu. Kukushkin, A. J. L. Pombeiro, *Inorg. Chim. Acta*, **2005**, *358*, 1, and references theirin.

[106] See e. g. a) A. Erxleben, I. Mutikainen, B. Lippert, *Dalton Trans.*, **1994,** 3667, b) J. Ruiz, N. Cutillas, V. Rodrıguez, J. Sampedro, G. Lo´pez, P. A. Chaloner, P. Hitchcock, *Dalton Trans.*, **1999**, 2939; c) G. Sanchez, J. L. Serrano, M. C. Ramirez de Arellano, J. Perez, G. Lopez, *Polyhedron*, **2000**, *19*, 1395; d) R. Cini, A. Cavaglioni, F. P. Intini, F. P. Fanizzi, C. Pacifico, G. Natile, *Polyhedron*, **1999**, *18*, 1863; e) R. Cini, F. P. Fanizzi, F.P. Intini, L. Maresca, G. Natile, *J. Am. Chem. Soc.*, **1993**, *115*, 5123; f) F. D. Rochon, P. C. Kong, R. Melanson, *Inorg. Chem.*, **1990**, *29*, 1352; g) L. Maresca, G. Natile, F. P. Intini, F. Gasparrini, A. Tiripicchio, M. Tiripicchio-Camellini, *J. Am. Chem. Soc.*, **1986**, *108*, 1180; h) M. L. Kuznetsov, N. A. Bokach, V. Y. Kukushkin, T. Pakkanen, G. Wagner, A. J. L. Pombeiro, *Dalton Trans.,* **2000**, 4683.

[107] See, e. g., a) K. Matsumoto, J. Matsunami, K. Mizuno, H. Uemura, *J. Am. Chem. Soc.*, **1996**, *118*, 8959; b) Y. Lin, H. Misawa, J. Yamada, K. Matsumoto, *J. Am. Chem. Soc.*, **2001**, *123*, 569; c) G. Bandoli, A. Dolmella, F. P. Intini, C. Pacifico, G. Natile, *Inorg.Chim. Acta*, **2003**, *346*, 143; d) T. Abe, H. Moriyama and K. Matsumoto, *Inorg. Chem.*, **1991**, *30*, 4198.

[108] K. A. Hofmann, G. Bugge, *Ber. Dtsch. Chem. Ges.*, **1908**, *41*, 312.

[109] J. Ruiz, N. Cutillas, V. Rodriguez, J. Sampedro,G. Lopez, P. A.Chaloner, P. B. Hitchcock, *J. Chem. Soc., Dalton Trans.*, **1999**, 2939.

[110] R. A. Adrian, S. Zhu, D. R. Powell, G. A. Broker, E. R. T. Tiekink, J. A. Walmsley, *Dalton Trans.*, **2007**, 4399.

[111] J. K. Bera, B. W. Smucker, R. A. Walton, K. R. Dunbar, *Chem. Commun.*, **2001**, 2562.

[112] a) T. R. Cech, *Science* **1987**, *236*, 1532; b) T. R. Cech, B. L. Bass, *Annu. Rev. Biochem.* **1986**, *55*, 599.

[113] C. Guerrier-Takada, K. Gardiner, T. Marsh, N. Pace, S. Altman, *Cell,* **1983**, *35*, 849.

[114] a) R. K. O. Sigel, A. M Pyle, *Chem. Rev.*, **2007,** *107*, 97,b) A. M. Pyle, *J. Biol. Inorg. Chem.,* **2002**, *7*, 679, and ref. therein;

[115] See e. g. a) E. Kimura, *Pure & Appl. Chem.,* **1993**, *65*, 355, b) D.E., Wilcox, *Chem. Rev***. 1996**, *96*, 2435; c) R. Blakely, B. Zerner, *J. Mol. Catal,* **1984**. *23*, 263.

[116] See e.g. a) H. Schöllhorn, U. Thewalt, B. Lippert, *J. Am. Chem. Soc.*, **1989**, *111*, 7213, b) H. Sigel, *J. Am. Chem. Soc.*, **1975**, *97*, 3209.

[117] B. Lippert in *Prog. Inorg. Chem.* **2005**, *54*, 385.

[118] P. M. Lax, M. Garijo Anorbe, B. Müller, E. Y. Bivian-Castro, B. Lippert, *Inorg. Chem.* **2007**, 46, 4036.

[119] J. Arpalahti, P. Lehikoinen, *Inorg. Chem.* **1990**, *29*, 2564.

[120] J. K. Burdett, *Inorg.Chem*. **1977**, *16*, 3013.

[121] D. Jaganyi, A. Hofmann, R. van Eldik, *Angew. Chem. Int. Ed.* **2001**, *40*, 1680.

[122] a) P. Colamarino, P.L. Orioli. *J. Chem. Soc. Dalton Trans.,* **1975,** 1656; b) F. Caruso, R. Spagna, L. Zambonelli. *Acta Crystallogr.Sect. B: Struct. Crystallogr. Cryst. Chem.***, 1980,** *B36*, 713; c) F. Caruso, R. Spagna, L. Zambonelli. *J. Cryst. Mol. Struct.,* **1978***, 8*, 46; d) V. Y. Kukushkin, V. K. Bel'skii, E. A. A. Aleksandrova, E. Y. Pan'kova, V. E. Konovalov, V. N. Yakovlev, A. I. Moiseev, *Zh. Obshch. Khim.,* **1991**, *61*, 318.

[123] L.S. Hollis, A. R. Amundsen, E. W. Stern, *J. Med. Chem.*, **1989**, *32*, 128.

[124] a)W. J. Louw, R. van Eldik, *Inorg. Chem.*, **1981**, *20*, 1939; b) D. Cornacchia, L. Cerasino, C. Pacifico, G. Natile, *Eur. J. Inorg. Chem.,* **2008**, 1822.

[125] S. J. S. Kerrison, P.J. Sadler, *Chem. Soc., Chem. Comm.*, **1977**, 861.

[126] a) R.Wrobel, L. Chmurzynski, *Anal. Chim. Acta*, **2000**, *405*, 303; b) A. E. Martell, R. J. Motekaitis, *Determination and Use of Stability Constants*, 2nd ed., VCH Publishers: New York, **1992**; J. Barbosa, D. Barron, J. L. Beltran, V. Sanz-Nebot, *Anal. Chim. Acta*, **1995**, *317*, 75;. R. Kaliszan, P. Wiczling, M. J. Markuszewski, *J. Chromatogr.*, *A* **2004**, *1060*, 165.

[127] See, e.g. R. K. O. Sigel, S. M. Tompson, E. Freisinger, F. Glahe, B. Lippert, *Chem. Eur. J.,* **2001**, *7*, 1968.

[128] C. K. Jorgensen*, Inorg. Chem.,* **1964**, *3*, 1201.

[129] R. G. Pearson, *Inorg. Chem.* **1973**, *12*, 712.

[130] L. I. Elding, A. Oskarsson, *Inorg. Chim. Acta,* **1987**, *130*, 209.

[131] F. D. Rochon, C. Bensimon, C. Tessier, *Inorg. Chem. Acta*, **2007**, *361*, 16.

[132] A. P. S. Fontes, A. Oskarsson, K. Lovqvist, N. Farrell, *Inorg. Chem.* **2001,** *40,* 1745.

[133] F. A. Cotton, R. Francis, J. W. D. Horrocks, *J. Phys. Chem.* **1960**, *64*, 1534.

[134] F. P. Fanizzi, N. Margiotta, M. Lanfranchi, A. Tiripicchio, G. Pacchioni, G. Natile, *Eur. J. Inorg. Chem.,* **2004**, 1705.

[135] W. I. Sundquist, K. J. Ahmed, L. S. Hollis, S. J. Lippard, *Inorg. Chem.* **1987**, *26,* 1524.

[136] F. Basolo, *Coord. Chem. Rev.* **1996**, *154*, 151, and references cited therein.

[137] C. Bazzicalupi, A. Bencini, A. Bianchi, V. Fusi, C. Giorgi, A. Granchi, P. Paoletti, B. Valtancoli, *J. Chem. Soc, Perkin Trans.*, **1997**, *2*, 775.

[138] See, e. g. a) L. R. Eller, M. Stepien, C. J. Fowler, J. T. Lee, J. L. Sessler, B. A. Moyer, *J. Am. Chem. Soc.* **2007**, *129*, 11020; b) J. L. Sessler, E. Katayev, G. D. Pantos, P. Scherbakov, M. D. Reshetova, V. N. Khrustalev, V. M. Lynch, Y. A. Ustynyuk, *J. Am. Chem. Soc.* **2005**, *127*, 11442; c) B. Wu, J. Liang, J. Yang, C. Jia, X.-J. Yang, H. Zhang, N. Tang, C. Janiak, *Chem. Commun.* **2008**, 1762; d) F. Zhuge, B. Wu, J. Liang, J. Yang, Y. Liu, C. Jia, C. Janiak, N. Tang, X.-J. Yang, *Inorg. Chem*. **2009**, *48*, 10249; e) S. O. Kang, Md. A. Hossain, D. Powell, K. Bowman-Jones, *Chem. Commun.* **2005**, 328; f) R. Prohens, G. Martorell, P. Ballester, A. Costa, *Chem. Commun.* **2001**, 1456.

[139] R. Custelcean, P. Remi, P. V. Bonnesen, D.-e. Jiang, B. A. Moyer, *Angew. Chem.* **2008**, *120*, 1892, *Angew. Chem. Int. Ed.* **2008**, 47, 1866 and references cited therein.

[140] J. W. Pflugrath, F. A. Quiocho, *Nature,* **1985**, *314*, 257; J. J. He, F. A. Quiocho, *Science,* **1991**, *251*, 1479.

[141] R. Custelcean, B. A. Moyer, *Eur. J. Inorg. Chem*., **2007**, 1321.

[142] D. Matulis, I. Rouzina, V. A. Bloomfield, *J. Mol. Biol.* **2000**, *296*, 1053.

[143] M. J. Hannon, V. Moreno, M. J. Prieto, E. Moldrheim, E. Sletten, I. Meistermann, C. J. Isaac, K. J. Sanders, A. Rodger, *Angew. Chem. Int. Ed.,* **2001**, *40*, 879.

[144] A. Oleksi, A. G. Blanco, R. Boer, I. Usòn, J. Aymami, A. Rodger, M. J. Hannon, M. Coll, *Angew. Chem.* **2006**, *118*, 1249; *Angew. Chem. Int. Ed.* **2006**, *45*, 1227.

[145] M. A. Galindo, D. Olea, M. A. Romero, J. Gómez, P. del Castillo, M. J. Hannon, A. Roger, F. Zamora, J. A. R. Navarro, *Chem. Eur. J.,* **2007,** 13, 5075.

[146] G. Binnig, C. F. Quate, C. Gerber, *Phys. Rev. Lett.,* **1986**, *56*, 930.

[147] H. Cheng, K. Zhang, J. A. Libera, M. O. de la Cruz, M. J. Bedzyk, *Biophys. Journal,* **2006**, *90*, 1164.

[148] J. Vesenka, S. Manne, G. Yang, C. Bustamante, E. Henderson, *Scanning Microsc.,* **1993**, *7,* 781.

[149] Y. L. Lyubehenko, P. I. Oden, D. Lampner, S. M. Lindsay, K. A. Dunker, *Nucleic Acids Res.* **1993**, *21,* 1117.

[150] Y. Jiao, T. E. Schaffer, *Langmuir*, **2004**, *20*, 10038.

[151] H. G. Hansma, R. Golan, W. Hsieh, C. P. Lollo, P. Mullen-Ley, D. Kwoh, *Nucleic Acids Research,* **1998,** *Vol. 26, No. 10,* 2481.

[152] F. Moreno-Herrero, L. Holtzer, D. A. Koster, S. Shuman, C. Dekker, N. H. Dekker, *Nucleic Acids Research*, **2005**, *Vol. 33, No. 18*, 5945.

[153] Z. Otwinowski, W. Minor in *Methods in Enzymology*, Vol. 276, *Macromolecular Crystallography*, Part A (Eds.: C.W. Carter, Jr., R.M. Sweet), Academic Press, New York, **1997**, pp. 307.

[154] CrysAlisPro, Oxford Difraction (Poland), **2009**.

[155] G. M. Sheldrick, SADABS, Program for Empirical Absorption Correction of Area Detector Data, University of Göttingen, Göttingen (Germany) **2002**.

[156] G. M. Sheldrick, SHELXTL-PLUS (VMS), Siemens Analytical X-ray Instruments Inc., Madison, Wisconsin (USA) **1990**.

[157] G. M. Sheldrick, SHELXL-97, Program for the Refinement of Crystal Structures, University of Göttingen, Göttingen (Germany) **1997**. See also: G.M. Sheldrick, *Acta Crystallogr.* **2008**, *A64*, 112.

[158] L. J. Farrugia, WINGX, A MS-Windows System of Programs for Solving, Refining and Analysing Single Crystal X-ray Diffraction Data for Small Molecules, University of Glasgow, Glasgow, Scotland (U.K.) **2005**. See also: L. J. Farrugia, *J. Appl. Crystallogr.* **1999**, *32*, 837.

[159] R. Lumry, E. L. Smitz, R. R. Glantz, *J. Am. Chem. Soc*., **1951**, *73*, 4335.

[160] R. Tribolet, H. Sigel *Eur. J. Biochem*., **1987**, *163*, 353.

[161] R. B. Martin, *Science,* **1963**, 1198.

[162] P. Job, *Ann Chim* **1925**, *9*, 113.

[163] a) S. C. Dhara, *Indian. J. Chem.,* **1970**, *8*, 193. b) G. Raudaschl-Sieber, B. Lippert, J. D Hoeschele, *Inorg. Chim. Acta* **1983**, *78*, L43.

[164] G. B. Kauffmann, D. O. Cowan *Inorg. Synth.,* **1963**, *7*, 239.

[165] H. Morita, J.C. Bailar, Jr., *Inorg. Synth.* **1983**, *22*, 124.

[166] J. Mc Cormick, E. N. Jaynes, Jr, R. I. Kaplan, *Inorg. Synth.,* **1972**, *13*, 216.

[167] G. Minghetti, M. A. Cinellu, *J. Organomet. Chem.* **1986**, *315*, 387.

[168] M. J. Rauterkus, B. Krebs, *Angew. Chem. Int. Ed.* **2004**, *43*, 1300.

[169] L. S. Hollis, A.R. Amundsen, E.W. Stern, *J. Med. Chem.* **1989**, *32*, 128.

[170] a) J.-M. Delafontaine, P. Khodadad, P. Toffoli, N. Rodier, *Acta Crystallogr. C* **1985**, *41*, 702., b) W. I. Sundquist, K. J. Ahmed, L. S. Hollis, S. J. Lippard, *Inorg. Chem.* **1987**, *26*, 1524.